

Polyazamacrocycles as Potential Positron Emission Tomography (PET) Agents

Stephen Hughes

A thesis submitted to Cardiff University in accordance with the requirements for the
degree of Doctor of Philosophy in the Faculty of Science, Department of Chemistry,
Cardiff University

Oct. 2012

Declarations

This work has not been submitted in substance for any other degree or award at this or any other university or place of learning, nor is being submitted concurrently in candidature for any degree or other award.

Signed (candidate)

Date

STATEMENT 1

This thesis is being submitted in partial fulfillment of the requirements for the degree of PhD

Signed (candidate)

Date

STATEMENT 2

This thesis is the result of my own independent work/investigation, except where otherwise stated. Other sources are acknowledged by explicit references. The views expressed are my own.

Signed (candidate)

Date

STATEMENT 3

I hereby give consent for my thesis, if accepted, to be available for photocopying and for inter-library loan, and for the title and summary to be made available to outside organisations.

Signed (candidate)

Date

STATEMENT 4: PREVIOUSLY APPROVED BAR ON ACCESS

I hereby give consent for my thesis, if accepted, to be available for photocopying and for inter-library loans after expiry of a bar on access previously approved by the Academic Standards & Quality Committee.

Signed (candidate)

Date

Abstract

The synthesis of ligand systems and complexes thereof suitable for use as positron emission tomography (PET) agents is studied herein. The ligands 6,6'-(1,4-diazepane-1,4-diyl)bis(3-aminobenzoate) (HP^R), 6,6'-(piperazine-1,4-diyl)bis(3-aminobenzoate) ($\text{Pip}^{R.2HCl}$), 6,6',6''-(1,4,7-triazonane-1,4,7-triyl)tris(3-aminobenzoate) (TACN^R), 1,4-bis(2-amino-4-tolyl)-1,4-diazepane (HP^{Tol}), 1,4-bis(2-amino-4-trifluoromethylphenyl)-1,4-diazepane (HP^{CF_3}), di-tert-butyl 4,4'-(1,4-diazepane-1,4-diyl)bis(3-aminobenzoate) (HP^{tButyl}), 1,3-bis(2-amino-4-tolyl)-1,3-diazacyclohexane (Pip^{Tol}), 1,4,7-tris(2-amino-4-trifluoromethylphenyl)-1,4,7-triazacyclononane (TACN^{CF_3}), have been studied. Ni(II), Cu(II), and Zn(II) complexes of these ligands have been synthesised, DFT calculations have elucidated structural configuration, whilst x-ray crystal structures of NiHP^{tButyl} , and CuTACN^{CF_3} have been determined. EPR measurements of CuHP^R have been taken.

A series of triazine core compounds have been prepared for use as model compounds for targeting molecules. The compound $\text{Tz}(\text{EtGly})(\text{BocGuan})\text{Cl}$ has been synthesised with the required arms to selectively bind to the integrin $\alpha_v\beta_3$. DO3A moieties have been added to these ligands, and mass spectra analysis of the coordination products with a series of metals has been determined.

NO2A derived compounds 2,2'-(7-tosyl-1,4,7-triazonane-1,4-diyl)diacetic acid (TsTACNA_2) and 2,2'-(7-(4-nitrophenyl)-1,4,7-triazonane-1,4-diyl)diacetic acid (NPhTACNA_2) have been studied, with the x-ray crystallography of the copper complexes completed. Positron emission tomography (PET) studies of the complexes have also been undertaken and show high levels of complexation at ng scales, with moderate stability in human serum.

Glutaric acid functionalised compounds (2S,2'S)-2,2'-(1,4-diazepane-1,4-diyl)dipentanedioic acid (HPGlut), 2,2',2''-(1,4,7-triazonane-1,4,7-triyl)tripentanedioic acid (TACNGlut), and 2,2'-(4,11-dimethyl-1,4,8,11-tetraazacyclotetradecane-1,8-diyl)dipentanedioic acid (DM -

CGLut) have been synthesised, with the copper complex of DMCClut affording structural determination. The Mn(II) and Gd(III) complexes of the DMCClut ligand system have been studied by xylenol orange UV titration for their metal-ligand binding ratio, with the Mn(II) system showing a 1:1 binding ratio, whilst the Gd(III) complex showed no binding at all.

Synthesis of the trispyrazylborate analogue, tris(4-methyl-2-(2-pyridine)pyrazyl)borate (MeTpPy), was unsuccessful, however, the bis- (MeDpPy) and tetra- (MeQpPy) substituted analogues were successfully synthesised.

Acknowledgements

I would like to thank Prof. Peter Edwards for allowing me to be part of his research group for the last 5 years. His help and advice throughout my MChem and PhD studies has been invaluable, and I am very grateful for the opportunities he has afforded me.

I would also like to thank Dr. Ian Fallis for the great faith he has shown in me, and his ability to look past the occasional hic-cup. It has been a pleasure working as part of his research group, with a constant stream of new ideas and ways around problems, I have learnt so much from him.

I will be indebted to Dr. Ian Morgan forever. He has helped (forced) me to learn so much, both in chemistry terms and in the wider world of life. He has always been a friend when I needed it, and also the scary post-doc with immense strength and knowledge when that was required.

I am also grateful to Dr Ben Ward for the time he spent teaching me the basics of DFT and crystallography, as well as being a sounding board for some of my more quirky ideas. Dr. Nancy Dervisi and Dr. Angelo Amoroso have also been a massive help, with suggestions in group meetings and being there for general chats about chemistry. Dr. Tom Tatchell's help has been invaluable with advice on the rigid arm ligand synthesis, general day-to-day chemistry, and also for correcting (very) early versions of this work.

I would like to thank the whole of the inorganic section, for their friendship and ability to make the worst situations slightly more bearable. In particular I must mention Dr (?!) James Wixey with whom I have shared the entirety of my PhD experience. He has helped me through the rough and the smooth, and kept me going through everything. Our friendly competition has helped push me on, and I would like to think he feels the same. A massive thank you to everyone else from lab 1.124, past and present, including Stacey, Owen, Tom (T-Mob), Mark (Gerbs), Schnee and Tracey. The laughs you have all

given me, both intentional and not, will not be forgotten. Thanks to Stacey in particular for listening to me complain constantly, and to Schnee for being the best Erasmus student anyone could wish to meet. Thanks also go out to Tim (Tiny) and Brendan, I have very much enjoyed being your conference buddy and estranged lab mate, and have loved pretty much every minute (with the exception of maybe the mornings) of our trips away. Cambridge in particular will not be forgotten.

Of course I would like to thank all the people who have helped me out in my time at Cardiff, including the stores boys – Gaz, Jamie, Mal, and Simon – Robin and Dave in the mass spec department for putting up with my strange requests, and Dr. Rob Jenkins for his support with NMR and friendly chat around the department. I greatly appreciate the time and effort of Drs. Kariuki (Cardiff), Tizzard and Pitak (Southampton) have put into determining and solving the crystal structures.

I reserve my greatest thanks for my family. My parents have been nothing but supportive throughout my education, and I hope this goes some way to repaying and thanking you for all the time and energy you have put into helping reach this point, I love you all very much. Finally I must thank Kat for all the support she has given me. Without her I would not have had a decent meal in the last couple of months and probably never have finished writing this thesis, you've kept me on the straight and narrow.

List of Abbreviations

AcOH - acetic acid	KBr - potassium bromide
Å - angstroms	$L^{x,y}$ - Fallis group ligand nomenclature for ligands with x nitrogens and y nitrobenzenes
Ar - aromatic	LR - low resolution
^{11}B - boron eleven isotope	m - multiplet
boc - <i>t</i> -butyl carbamate	mg - milligram
br - broad	MHz - mega Hertz
^{13}C - carbon thirteen isotope	mmol - millimole
cm^{-1} - wavenumbers	mol - mole
cyclam - 1,4,8,11-tetraazacyclotetradecane	ml - millilitre
cyclen - 1,4,7,10-tetraazacyclododecane	MRI - magnetic resonance imaging
δ - NMR chemical shift	m/z - mass/charge ratio
d - doublet	NMR - nuclear magnetic resonance
D - deuterium	ppm - parts per million
DCM - dichloromethane	SPECT - single photon emission computed tomography
DMAC - dimethylacetamide	TACN - 1,4,7-triazacyclononane
DMAP - <i>N,N'</i> -dimethylaminopyridine	TFA - trifluoroacetic acid
DMF - dimethylformamide	THF - tetrahydrofuran
DMSO - dimethylsulphoxide	TLC - thin layer chromatography
DMSO- d_6 - deuterated dimethylsulphoxide	Ts - tosyl
Et - ethyl	pTSA - para-tosyl sulphonic acid
^1H - proton	UV/Vis - ultra violet/visible
HR - high resolution	w - weak
IR - infra red	

Contents

1	Introduction	1
1.1	Macrocycles	1
1.1.1	Introduction To Macrocycles	1
1.1.2	Azamacrocycles	2
1.1.3	Chelate and Macrocyclic Effect	3
1.1.4	Jahn-Teller Distortion	5
1.2	Positron Emission Tomography	6
1.2.1	Positron Emission Tomography	6
1.2.2	The Science of PET	8
1.2.3	PET Detectors	10
1.2.4	Synthesis of PET isotopes	13
1.3	Potential Ligands in Copper and Gallium PET Agents	14
1.3.1	Acyclic ligands	15
1.3.2	Macrocyclic ligands	17
1.4	Aims	22
2	Rigid Arm Polyazamacrocycles	23
2.1	Introduction	23
2.2	Anilino ligand synthesis	29
2.3	Metal complexes of HP ^{Tol}	33
2.3.1	Nickel(II) complex	34
2.3.2	Copper(II) complex	36
2.4	Metal complexes of HP ^{CF₃}	38
2.4.1	Nickel(II) complex	38

2.4.2	Copper(II) complex	40
2.4.3	Zinc(II) complex	40
2.5	Metal complexes of TACN ^{CF₃}	43
2.5.1	Copper(II) complex	44
2.6	Metal complexes of HP ^{tButyl}	44
2.6.1	Nickel(II) complex	44
2.6.2	Copper(II) complex	46
2.6.3	Zinc(II) complex	49
2.7	Carboxy ligand synthesis	51
2.8	Metal complex of carboxyl ligands	54
2.8.1	Copper(II) Complexes	55
2.8.2	Nickel(II) Complex	58
3	Triazine Core Derived PET Agents	59
3.1	Introduction	59
3.2	Synthesis of Dipyridamole Analogues	63
3.3	Dendrimeric Triazines	71
3.4	Synthesis of RGD nonpeptidic mimic	76
4	Acetate Functionalised TACNs as PET Agents	81
4.1	Introduction	81
4.2	NO ₂ A derivatives	83
4.3	PET Data	90
5	Other Work	94
5.1	Glutamate Chemistry	94
5.1.1	Introduction	94
5.1.2	Amino acid type bis-acid interconversion	95
5.1.3	Synthesis of Glutaric Macrocycles	96
5.1.4	Potential application as an MRI contrast agent	99
5.2	Functionalisation of fluorobenzene substituted homopiperazines	101
5.3	Synthesis of trispyrazylborate analogues for potential PET imaging	104
6	Conclusions	109

7 Experimental	113
7.1 Experimental conditions	113
7.2 DFT calculations	113
7.3 EPR Measurements	114
7.4 X-Ray data	114
7.5 Radiolabelling	114
7.6 Rigid Arm Polyazamacrocycles	115
7.6.1 Pendant arms	115
7.6.2 Sythesis of Carboxy Ligands	121
7.6.3 Metal Complexes of Carboxyl Ligands	126
7.6.4 Synthesis of Anilino Ligands	128
7.6.5 Metal Complexes of Anilino Ligands	137
7.7 Triazine Core Derived Compounds	143
7.7.1 Dipyridamole type complexes	143
7.7.2 DO3A Ligands	147
7.7.3 DO3A Complexes	151
7.7.4 Dendrimers	152
7.7.5 RGD type ligands	156
7.7.6 RGD type complexes	163
7.8 Acetate and Alcohol Functionalised TACNs and Homopiperazines	164
7.8.1 Functionalised TACNs	164
7.8.2 TACN Complexes	168
7.9 Other Work	170
7.9.1 Glutamate Chemistry	170
7.9.2 Trispyrazyborate analogues	174
7.10 PET experiments	176
7.10.1 ^{64}Cu radiolabelling	176
7.10.2 Determination of $\log P$ values	177
7.10.3 Stability in human serum	177
A Crystal structures of ligands and ligand precursors	186
A.1 Crystal structure of $\text{HP}^{1-\text{NO}_2}$	186
A.2 Crystal structure of $\text{TACN}^{1-\text{NO}_2}$	187

<i>CONTENTS</i>	xii
A.3 Crystal structure of $\text{DMC}^{1-\text{NO}_2}$	187
A.4 Crystal structure of $\text{HP}^{3-\text{NO}_2}$	188
A.5 Crystal structure of $\text{HP}^{\text{Sang}-\text{NO}_2}$	189
A.6 Crystal structure of HP^{CF_3}	190
A.7 Crystal structure of $\text{Pip}^{3-\text{NH}_2}$	190
A.8 Crystal structure of Pip^{Tol}	191
B Amino Acids	192
C X-Ray crystal structure data	194

Chapter 1

Introduction

1.1 Macrocycles

1.1.1 Introduction To Macrocycles

Macrocyclic chemistry is a vast, varied, and extremely active area of research even though it originates from the early 1960s. A macrocycle is defined by IUPAC as a cyclic macromolecule or a macromolecular cyclic portion of a molecule, and is more generally associated with rings of greater than 9 atoms, and in the context of ligands for metals, a minimum of 3 donor atoms. Synthetic chemists usually restrict this definition further so as it includes only cyclic molecules with three or greater hetero atoms. Macrocycles have found use in many areas of medical research such as contrast agents, biological tracers, anti AIDS/HIV drugs, tumour therapy, enzyme modelling, and protein labelling, which may account for their presence naturally in biological systems. Macrocycles have also been used in surfactant chemistry, metal extraction/recognition, and more recently in liquid crystals.

Naturally occurring macrocycles include porphyrin rings (1) found in hemoglobin, chlorin (2) rings found in chlorophyll, and corrin (3) rings in vitamin B12. More synthetic examples of macrocycles include, crown ethers (4), cryptands (5), calixarenes (6), polyamines (7), phthalocyanines (8), and mixed donor macrocycles (9) (fig. 1.1). Macrocycles have found an extended use in systems such as catenanes, rotaxanes, and molec-

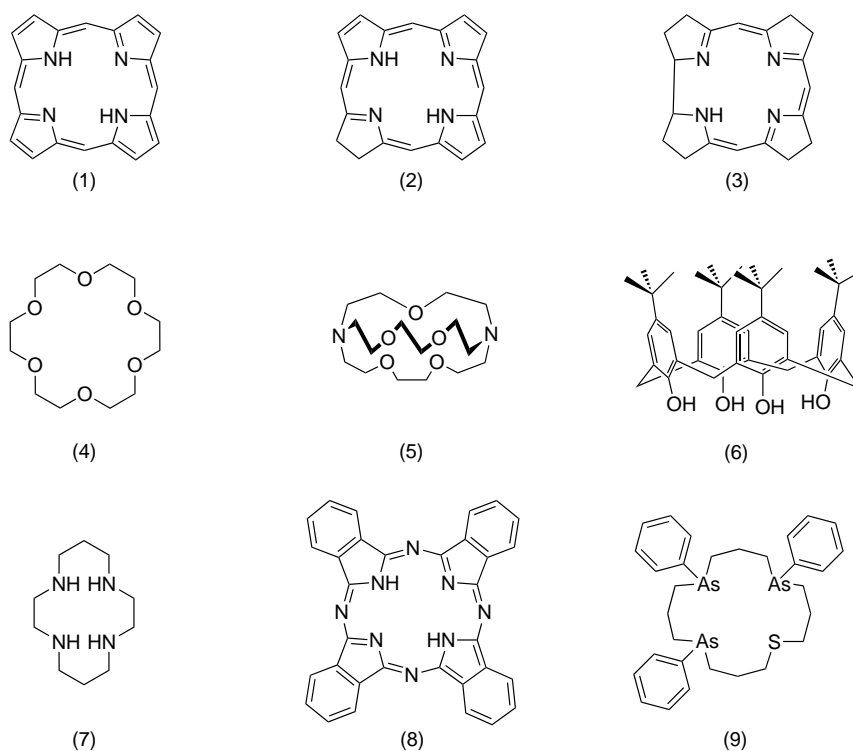


Figure 1.1: Examples of macrocycles

ular knots (knotanes) that involve interlocked macrocyclic molecules.

1.1.2 Azamacrocycles

Polyazamacrocycles are an extremely important area of modern medical research, with derivatives of 1,4,7,10-tetrazacyclododecane-1,4,7,10-tetraacetic acid (DOTA) finding use in many areas including cancer treatment and diagnosis. The ability to functionalise the amine moieties of these macrocycles allows easy access to 'tuned' ligands suitable for binding most metal ions. Polyazamacrocycles come in many sizes, however, most research is currently based on 1,4,9-triazacyclononane (TACN), 1,4,7,10-tetraazacyclododecane (cyclen), and 1,4,8,11-tetrazatetradecane (cyclam) (fig. 1.2).

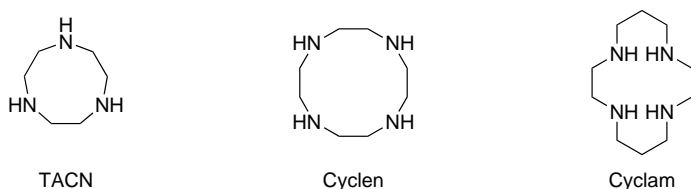


Figure 1.2: Polyazamacrocycles

The concentration on these macrocycles in particular is due to the size of the cavity

hole created by the amines being the correct size to comfortably bind metals of medical interest. Complexes of TACN usually form with the TACN occupying one face of the coordination sphere, leading to 'piano-stool' like complexes, whilst complexes of cyclam usually occur with the metal ion in the centre of the macrocycle (fig. 1.3).

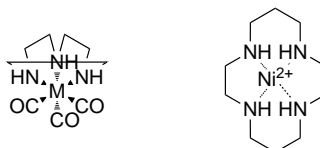


Figure 1.3: TACN piano stool, and cyclam complex
M = Mo, W

1.1.3 Chelate and Macrocyclic Effect

Chelate Effect

The chelate effect is defined as the greater stability of chelated complexes compared with their non-chelated analogues. An example of the chelate effect can be seen in the stability constants of the complexes $[\text{Cd}(\text{MeNH}_2)_4]^{2+}$ and $[\text{Cd}(\text{en})_2]^{2+}$. [1]

$$-RT \ln K = \Delta G^\circ = \Delta H^\circ - T\Delta S^\circ \quad (1.1)$$

Equilibrium	$\log \beta$	ΔG	ΔH	$-T\Delta S$
$\text{Cd}^{2+} + 4 \text{MeNH}_2 \rightleftharpoons [\text{Cd}(\text{MeNH}_2)_4]^{2+}$	6.55	-37.4	-57.3	19.9
$\text{Cd}^{2+} + 2 \text{en} \rightleftharpoons [\text{Cd}(\text{en})_2]^{2+}$	10.62	-60.67	-56.48	-4.19

R = gas constant, T = temperature (kelvin), K = equilibrium constant, G° = Gibb's free energy, H° = standard enthalpy, S° = standard entropy

The free energy is related to the equilibrium constant K through equation 1.1, with a larger equilibrium constant meaning a more stable complex. As would be expected, the enthalpy of the complexes is very similar due to the bond formation being very similar for both complexes – both are Cd-NH bonds. The largest difference between the two complexes is a result of a greater entropy of the chelated system. This in its simplest form is due to the fact that in the chelate complex three molecules join to form one, whilst in the monodentate complex five molecules become one, so there is less loss of disorder in the chelate system. This is further compounded when the molecules

of solvation are accounted for, with four solvation molecules replacing two chelating molecules, increasing entropy further.

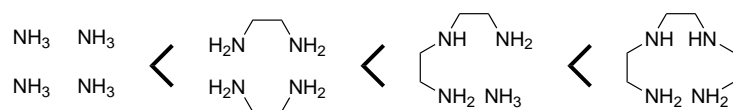


Figure 1.4: Increasing stability of chelate complexes

Another factor involved in the chelate effect is well described by Schwarzenbach.[2] If the chelate and its monodentate analogue are in competition with each other, both have an equal chance of coordination the first time. After that, the pendant arm of the chelate is more likely to coordinate in another position due to the fact that it is in much closer proximity to the metal centre. The proximity argument also helps to explain the greater stability of large chelates over multiple smaller ones, such as two ethylenediamine molecules are less stable than one triethylenetetraamine ligand (fig. 1.4).

Macrocyclic Effect

The macrocyclic effect is an expansion of the chelate effect and describes the increased stability of macrocyclic complexes over their open chain analogues when there are no steric influences on the complex. The cause of increased stability is two-fold in the macrocyclic effect, there are favourable enthalpic and entropic effects upon coordination of a macrocycle. The entropic effects are similar to those in the chelate effect, with the addition macrocycles have a lower rotational freedom than linear chelates and so upon coordination less rotational freedom is lost from the macrocycle than the chelate. The larger effect comes from enthalpy. If the macrocycle has the correct cavity size for the metal ion it is coordinating the metal-donor bonds will be significantly stronger than those that are strained. This is best shown in the stability constants of Ni(cyclam) and Cu(cyclen) complexes (fig. 1.5).

The increase in stability ($\log \beta$) of Ni(cyclam) over its acyclic analogue is 6.9, whilst the increase for Cu(cyclen) over its acyclic analogue is only 3.7. The cavity size of the cyclam macrocycle is the correct size for the Ni^{2+} ion, where it sits in the plane of the macrocycle, whilst the cavity in cyclen is too small for the Cu^{2+} ion and it sits above

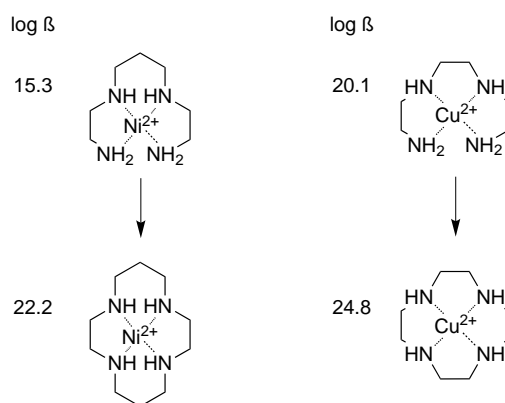
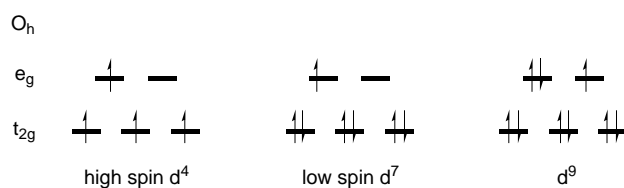


Figure 1.5: Macrocyclic effect

the ring, causing the macrocycle to twist so the nitrogen lone pairs point up toward the metal ion. Not only has the cavity hole been shown to affect the macrocyclic effect, but also a number of other factors such as pH, and solvation of the macrocycle. It is therefore hard to define exactly and must be taken as a sum of all these factors.

1.1.4 Jahn-Teller Distortion

The Jahn-Teller distortion is an electronic effect describing the distortion of non-linear electronic states in molecules. [3] The effect is most noticeable in d^9 octahedral copper complexes, due to the unequal occupancy of a degenerate molecular orbital, but is also easily seen in complexes where a doubly degenerate orbital (eg. e_g) is unequally occupied (low spin d^7 , and high spin d^4) (fig. 1.6).

Figure 1.6: Unequally occupied e_g orbitals

The effect is most noticed in e_g orbitals as they are orientated toward the ligands and so distortion results in large changes in the relative energies, whereas t_{2g} orbitals are orientated between the ligands and so any distortion results in smaller energy changes. The same is true of tetrahedral complexes where the distortion is less obvious as the orbitals do not align with the ligands. The Jahn-Teller distortion can manifest itself as either a lengthening or shortening of bonds, however, longer bonds are most common.

The effect is easily seen when viewing the crystal structure of $\text{Cu}(\text{H}_2\text{O})_6^{2+}$. The axial Cu-O bonds are found to be $\sim 2.38 \text{ \AA}$, whilst the equatorial bonds are $\sim 1.95 \text{ \AA}$ (fig. 1.7).

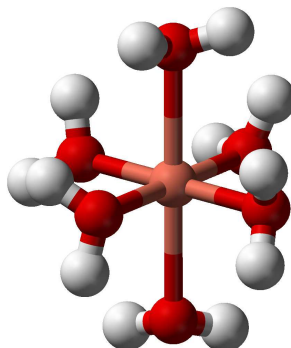


Figure 1.7: Crystal structure of $[\text{Cu}(\text{H}_2\text{O})_6]^{2+}$

1.2 Positron Emission Tomography

1.2.1 Positron Emission Tomography

Positron emission tomography (PET) is currently the fastest growing area of research in nuclear medicine. This is due to the ability of PET to be used in both diagnostic and therapeutic medicine as well as study of metabolic pathways through the use of ^{18}F -fluorodeoxyglucose (FDG). PET is currently used extensively in the US by oncological specialists who have found PET results have altered the management of patients in up to 30 % of cases (based on study of 5,062 patients).[4] An example of these alterations is the case of a patient with known lung cancer but no other symptoms. After an FDG-PET examination it was found the patient had extensive metastatic disease in their brain, and so a different treatment was administered. (fig. 1.8) This was only possible due to the metabolic nature of the FDG probe, and would most likely have been missed by older techniques. PET is not only useful in oncology, but also cardiology and neuropsychiatry. The ability of PET imaging to alter treatment in such large ways it can no longer be thought of as optional, and should be considered a key diagnostic tool even in health care systems at the lower end of gross national product investment (i.e. the NHS), and to this end must be an area of chemical and biological research to expand rapidly. This expansion has already started in engineering terms, with more and more sensitive de-

tectors being designed and implemented almost daily, allowing patients to be scanned with a higher resolution and at a higher turn over. Modern PET scanners are combining imaging modalities to allow fusion of different imaging techniques, such as MRI/PET and CT/PET. This allows the spatial resolution of PET overlaying a more general image of the body offered by the other modalities.

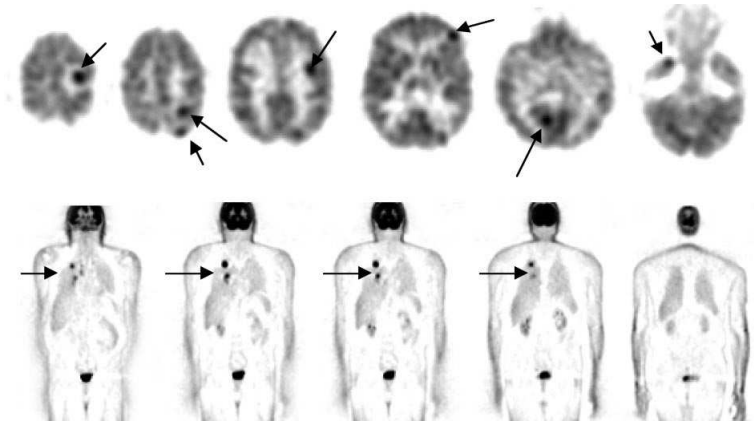


Figure 1.8: PET scan of patient with lung and brain cancer

Currently there are three main areas in which PET imaging is used; Cancer diagnosis and treatment, cardiac surgery, and neurology. The oncological use of PET has been well established in the USA for a decade with the first approval of PET imaging in diagnostic tests coming as early as 01.01.1998. (Medicaid/Medicare) Oncological PET is used for a wide variety of reasons including; diagnosis of scarring versus active tumours, how aggressive a tumour is (based on degree of FDG uptake), how widespread the cancer is (staging), measuring the response to therapy, and identification of the cancer site itself. Use of PET in cardiac surgery is mainly aimed at measuring myocardial perfusion (how the heart functions currently through blood flow studies) using ^{13}N -ammonia, and myocardial viability (whether the heart can recover from dysfunctions, or can be used in a transplant) using FDG. In neurology PET is used for management of brain tumours (especially those causing para-neoplastic symptoms), and has been shown to give earlier diagnosis and determination of dementia than current methods.

One of the main criticisms (unfairly) aimed at PET imaging is its cost. PET imaging requires use of a cyclotron and specialised laboratory facilities that are expensive to set up. However, the use of PET to change treatments and diagnose problems reduces the overall cost of the treatment of a patient. Cost effectiveness studies by Bailey *et al.*

show that PET imaging is 'cost-neutral' in most cases and some times 'cost-saving' over non PET techniques (table 1.1).[5] They argue that the long term effects cannot yet be evaluated as the technique is still relatively young, but the early results suggest that we should not wait another 10 years before using PET widely as its short term benefits (unnecessary surgery avoided, necessary surgery sped up etc.) massively out-way the negatives.

Procedure	Cost/Year saved (\$)
Liver Transplant	43,000 - 250,000
Renal Dialysis	116,000
Chemotherapy (breast)	46,200
Cardiac Transplant	27,200

Table 1.1: Money per life-year saved through differential treatment after PET scan

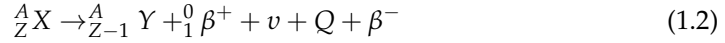
1.2.2 The Science of PET

Positron Emission Tomography is based on the ability of a positron to annihilate an electron with the resulting emission of two equal energy photons in opposite directions. The positron (same mass but opposite charge to an electron) was first postulated by Dirac in 1928, but wasn't observed until 1932 during cosmic ray research by Anderson, and both were awarded the Nobel Prize in physics for the discovery.

In PET the emission of a positron from the radionuclide results in an annihilation event with a nearby electron. This emission is the result of radioactive decay, whereby the radioactive nucleus is trying to lower its energy and reach a stable nuclear configuration. Radiation can be classified into two general forms; electromagnetic, and particulate. Electromagnetic radiation results in the production of pure energy in the form of x-ray and γ -ray photons. Positrons are particulate radiation. Particulate radiation includes α -decay, β^- -decay, and β^+ -decay.¹ Positrons are produced in two ways: pair production, and nuclear transmutation. Nuclear transmutation is when an element spontaneously converts into another through long term radioactive decay. Pair production results in the production of a positron and neutrino as by-products of the decay of a proton into a neutron. This process requires a proton rich nucleus, and after conversion

¹ α -decay is the loss of ${}^4_2\text{He}^{2+}$, β^- -decay is the loss of an electron and antineutrino ($\bar{\nu}$), β^+ -decay is the loss of a positron and neutrino (ν).

into a neutron, the remaining charge is released as a positron. The resultant neutrino production is the result of a need to conserve energy, and was postulated by Pauli in 1931. As the resultant nucleus has a charge of one less than the starting element, an electron is also released, which leaves the resultant nucleus and a neutral species. The general equation for positron decay is given below. (eq. 1.2)



After decay, the positron emitted can have any energy up to a given maximum. This energy is then reduced through collision and scattering interactions with the surrounding environment. When the positron has reached a low enough energy (energy of positron and electron must be similar) a collision with an electron will lead to the formation of a new particle called a positronium. Positronium is a metastable element and has a half life of around 10^{-7} s. In human tissue the probability of formation of a positronium is much lower, and direct annihilation is much more likely. The distance the positron travels after emission is given the value Z and is a major contributor to the maximum theoretical resolution possible. Higher energy positrons will have a higher Z value than low energy positrons, and results in differing resolutions depending on the positron emitting element used. (table 1.2) If Z can be lowered, then the resolution of PET can be greatly increased.

Nuclide	E_{max} (MeV)	Z_{mean} (mm) (in water)
${}^{11}\text{C}$	0.959	1.1
${}^{13}\text{N}$	1.197	1.5
${}^{15}\text{O}$	1.738	2.5
${}^{18}\text{F}$	0.633	0.6
${}^{68}\text{Ga}$	1.898	2.9
${}^{82}\text{Rb}$	3.400	5.9

Table 1.2: Different Z values (in water) shown as function of initial positron energy

When the positron and electron finally annihilate, the resulting energy is released in the form of photons (usually two, but three is possibly - <1% probability). If there is no momentum of the positron at the point of annihilation, the resultant photons are released at exactly 180° to each other, however if there is not zero-energy momentum at the point of annihilation, then the photons are released within $\pm 0.5^\circ$ of this value. This also adds to the error in resolution by up to 1.5 mm depending on the distance of the

detectors from the annihilation site. The photons emitted have an energy of 511 KeV, which can be easily calculated using Einstein's energy-mass equivalence. (eq. 1.3)

$$\begin{aligned}
 E &= mc^2 \\
 &= (9.11 \times 10^{-31} \text{Kg}) \cdot (3 \times 10^8 \text{ms}^{-1})^2 \\
 &= 8.2 \times 10^{-14} \text{J} \\
 &= \frac{8.2 \times 10^{-14} \text{J}}{1.6 \times 10^{-19} \text{J eV}^{-1}} \\
 &= 511 \text{KeV}
 \end{aligned} \tag{1.3}$$

1.2.3 PET Detectors

The type of detectors used in PET imaging are scintillation detectors, and consist of an inorganic crystal layer, which upon interaction with an external photon releases visible light photons *via* excitation and relaxation of an electron to the conduction band, which are then themselves detected by a photo-detector. The photo-detector measures the number of photons that interact with it, and this value is proportional to the original energy of the external photon. Scintillation detectors also have a very good stopping efficiency for the PET photons due to their composition (heavy inorganic elements, and high density).

The sensitivity of the detector is dependent on a number of factors; the stopping power of PET photons, signal decay time, light output, and intrinsic energy resolution. The stopping power is measured by the attenuation length of a photon in the scintillator. A low attenuation value signifies a highly efficient stopping power of the crystal, and is dependent on its density and effective atomic number. A short decay time is important as it allows each pulse to be processed independently and at a faster rate. Good light output is vital as it helps achieve good spatial and energy resolutions. Good energy resolution is needed to process the difference between a legitimate PET photon signal, and one which has been Compton scattered² in the subject. Intrinsic energy resolution also affects the energy resolution of the system, and arises from inhomogeneities in the

²Compton scattering occurs when the photon interacts with electrons in atoms in the tissue and causes a deflection of the photon and drop in the energy.

crystal, which can lead to non-uniform light output.

Common crystals used in scintillators include; NaI(Tl), BGO (bismuth germanate - $\text{Bi}_4\text{Ge}_3\text{O}_{12}$), LSO (lutetium oxyorthosilicate doped with cerium - $\text{Lu}_2\text{SiO}_5:\text{Ce}$), YSO (Yttrium oxyorthosilicate doped with cerium - $\text{Y}_2\text{SiO}_5:\text{Ce}$), GSO (Gadolinium oxyorthosilicate doped with cerium - $\text{Gd}_2\text{SiO}_5:\text{Ce}$), BaF_2 . (fig. 1.9) Each crystal system has advantages and disadvantages, but most current whole body scanners use BGO due to their excellent stopping power and high sensitivity of photon detection, the major drawback being a low light emission that requires the addition of photo-multipliers to achieve a good spatial resolution. This increases the cost and complexity of the machine somewhat. LSO looks like a possible candidate to replace the BGO systems, as it has very good light output and a high stopping power. Its major drawback is the presence of naturally occurring ^{176}Lu (2.6 % abundance, $\tau_{1/2} = 3.8 \times 10^{10}$ yrs) which is a β^- emitter and therefore releases γ -rays in the energy range 88-400KeV. This intrinsic radiation means it is not suitable for low energy application.

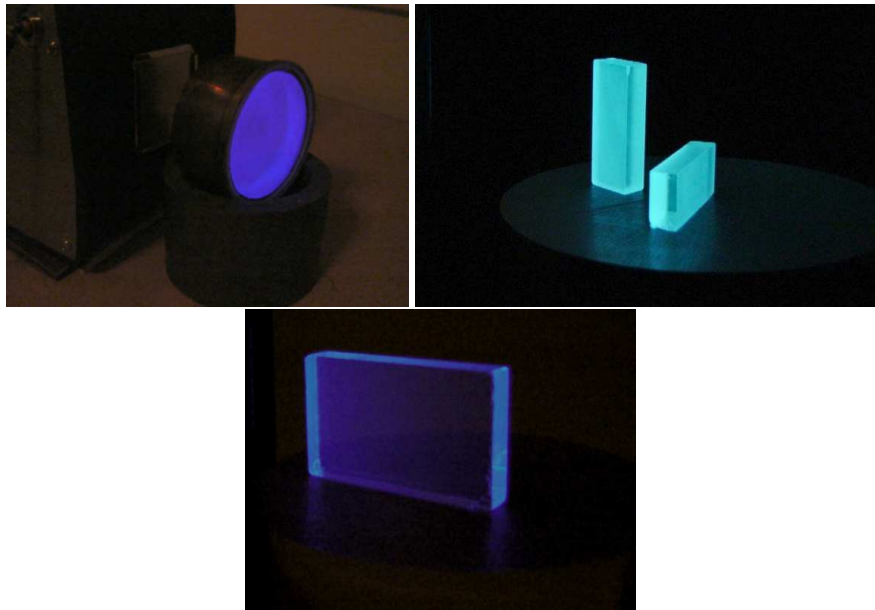


Figure 1.9: Scintillator crystals exposed to X-rays: NaI(Tl), BGO, and BaF_2 (left to right)

Due to the difference in distance a photon needs to travel, and slight differences in the scanner surfaces, an uncertainty in coincidence will occur. It is therefore necessary for the detector to take this possibility into account when dismissing random coincidences. After detection of photon one, the detector sends a signal. If another signal is detected within 2τ of the first, then it is counted as a potential signal. If it is outside

of this time, then the signals are ignored. In this case 2τ is any time, but must be more than the time taken for a photon to travel from one side of the scanner to the other, as not all events occur in the centre. For a 1m wide scanner this means 2τ must be more than 3.3 ns. Ultra-fast scintillators such as BaF₂ require little more than 3.3 ns to accept coincidence, whereas slower detectors such as NaI(Tl) would require a slightly longer time. The problem with having a coincidence window is the occurrence of random coincidences, and the larger the window the larger the opportunity for random coincidences to occur. This increases the noise in the measurement, as well as flagging up potentially false positives. The level of random coincidences increases proportionally with the square of the activity, whilst the true coincidences only increase linearly. This means that at high activity levels, random coincidence can overtake true levels. There is no really successful method for removal of these random levels so the best way to lower the random noise is to have a small timing window, and hence an ultra-fast scintillator.

Good timing resolution is not only good for reducing the noise levels in data, but is key to working out where the annihilation reaction took place. The difference in arrival time between two photons can be used to work out the exact space in which the annihilation took place. This calculation requires an ultra-fast scintillator for a decent resolution (~ 6 mm), currently the only scintillator quick enough is BaF₂.

As with the timing of the detection, the energy of detection must also be within a predefined window. This prevents Compton scattered pairs registering on the detector and giving false data on the position of the annihilation events. As in a scintillator the energy is detected as a function of light, a good light emitting source is required for accurate definition of the photon energies. Even the best (of the common crystals) detection systems have a low end energy value of 450 KeV. This means that a deviation of up to 30° from the true response line will be detected as a hit. This requires additional layers of computer software to estimate the distribution of scattered photons and remove them from the signal, hence improving the image contrast.

The sensitivity of a scanner is dependent on two main properties; the shape of the scanner, and the stopping efficiency of the scintillator. The ideal geometry of a scanner is a thin ring in which the patient lies. (fig. 1.10) This allows complete 360° detection of annihilation events, whilst keeping longitudinal scattering coincidences low. The high stopping efficiency, as mentioned earlier, allows for more coincident events to be



Figure 1.10: A Siemens TruePoint PET-CT multimodal scanner

recorded in a set time, which in turn reduces the signal to noise ratio and gives better resolution images. A high stopping power also reduces the parallax error in images. The parallax error is caused by a lack of adjustment for the depth the photon travels in the detector before being detected. (fig. 1.11) This can cause some blurring of images, but can be avoided by having thinner films of crystals, with higher stopping powers.

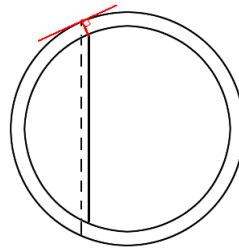


Figure 1.11: Representation of parallax error

Dotted line = Actual photon path
Solid line = Interpreted path

1.2.4 Synthesis of PET isotopes

The nuclear reactions involved in synthesising the PET isotopes are of major importance. It must be possible to successfully separate the desired PET element from its starting material, and so has been a source of heavy research. There are many different methods for synthesising PET isotopes, but the major methods for the synthesis of ^{60}Cu , ^{64}Cu , ^{68}Ga , ^{86}Y , and ^{89}Zr are described.

^{60}Cu Production

^{60}Cu ($\tau_{1/2} = 24 \text{ min.}$, β^+ 93 %) is prepared using a targeting system in which the reaction $^{60}\text{Ni}(p,n)^{60}\text{Cu}$ takes place and ^{60}Cu is isolated via ion exchange chromatography.[6]

A ^{60}Ni enriched target is sometimes used, but increases the cost.

^{64}Cu Production

^{64}Cu ($\tau_{1/2} = 12.7$ hrs, β^+ 19 %) is prepared using a similar method to ^{60}Cu , through either $^{64}\text{Ni}(p,n)^{64}\text{Cu}$ or $^{64}\text{Ni}(d,2n)^{64}\text{Cu}$ reactions.[6] Both use enriched ^{64}Ni targets that must be irradiated before use to increase production of ^{64}Cu . [7] The difficulty in recovering the ^{64}Ni has led to recent developments including the use of ^{64}NiO .

^{68}Ga Production

^{68}Ga ($\tau_{1/2} = 68$ min., β^+ 89 %) is produced naturally by the electron capture decay of ^{68}Ge ($\tau_{1/2} = 271$ days). ^{68}Ga is isolated by elution with 0.1M HCl forming the salt $^{68}\text{GaCl}_3$. Complications arise due to the presence of some impurities (Ti^{4+} , Fe^{3+} , Zn^{2+} from the initial Ge source), high volumes of eluate, and high concentrations of HCl. This has led to recent work into chromatographic methods of purification.[8]

^{86}Y Production

^{86}Y ($\tau_{1/2} = 14.7$ hrs, β^+ 34 %) is produced through the bombardment of Sr targets with high energy protons, although reaction of Ge targets with heavy ion particles ($^{16}\text{O}^{6+}$) has also been used. Isolation of the ^{86}Y has been achieved through many methods, but ion exchange chromatography is the most common.[9]

^{89}Zr Production

^{89}Zr ($\tau_{1/2} = 78$ hrs, β^+ 23 %) is prepared via a $^{89}\text{Y}(p,n)^{89}\text{Zr}$ reaction, and purified using a double extraction protocol, followed by anion exchange, resulting in 99.999% purity. Other methods have recently been published, but have major problems particularly in the production of YCl_3 by-products. [10]

1.3 Potential Ligands in Copper and Gallium PET Agents

Whilst the use of metal ions in PET agents is still a relatively new area of interest, there are a number of popular motifs that allow facile coordination of a metal to a functionalisable generic core. The ligands used in copper PET chemistry tend to have coordination number between 4 and 6, with those tetradentate ligands using copper(II)'s preference for square planar geometry over tetrahedral (see the Jahn-Teller distortion). Current tetradentate copper ligands commonly contain two neutral nitrogen donors (amino or imino) and two charged species such as amido, oxo, or thiolato moieties to neutralise

the complex. Due to the added stability gained by filling the coordination sphere of the copper ion, hexadentate ligands have become the focus of much research. These hexadentate ligands are generally based on polyazamacrocyclic cores such as TACN, cyclen, and cyclam. Methods of functionalisation of the macrocycles by addition of pendant arms to the amine nitrogens and the carbon backbone have been developed. Commonly anionic groups are added to these macrocycles so as neutral complexes are formed. Gallium chelators generally include hard donors such as anionic oxygens, and thiolates, due to the hard acidic nature of the Ga^{3+} ion. There are therefore some ligands that can be used for both Cu(II) and Ga(III) chemistry.

1.3.1 Acyclic ligands

The most researched acyclic copper ligands are based around the bis(thiosemicarbazonato) motif (fig. 1.12). These ligands have a rigid planar structure, forcing the copper centre into its favoured square planar geometry. The terminal sulphur moieties deprotonate upon coordination forming neutral complexes. The square planar geometry has been proven by a series of x-ray crystal structures, and it has been found that alkylation of the carbon backbone caused a lengthening of the C-C bond, and hence a bigger cavity hole in which the copper can sit.[11] These molecules have been investigated for hypoxia imaging, as reduction of the copper centre from Cu(II) to Cu(I) causes the metal to become uncoordinated, and stay in the hypoxic tissue.

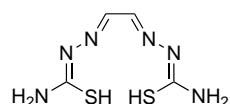


Figure 1.12: Bis(thiosemicarbazonato) ligand system

Many generic chelators have also been tested and derivatised for use in PET. Cu-EDTA complexes form a distorted N_2O_4 octahedron, whilst CuDTPA forms an N_3O_3 complex (fig. 1.13).[12] 1,3,5-triaminocyclohexane with three N-substituted methylpyridines has been tested with radio copper, and the crystal structure shows a distorted octahedral environment (fig. 1.14).[13]

Ligands designed for gallium chemistry include derivatives of *o*-hydroxybenzyl iminodiacetic acid, forming an NO_3 coordination geometry, where it was found that substituents in the *para* positions had a substantial effect on the stability constants of the complexes (fig. 1.15).[14] The more electron withdrawing the *para* group the lower the

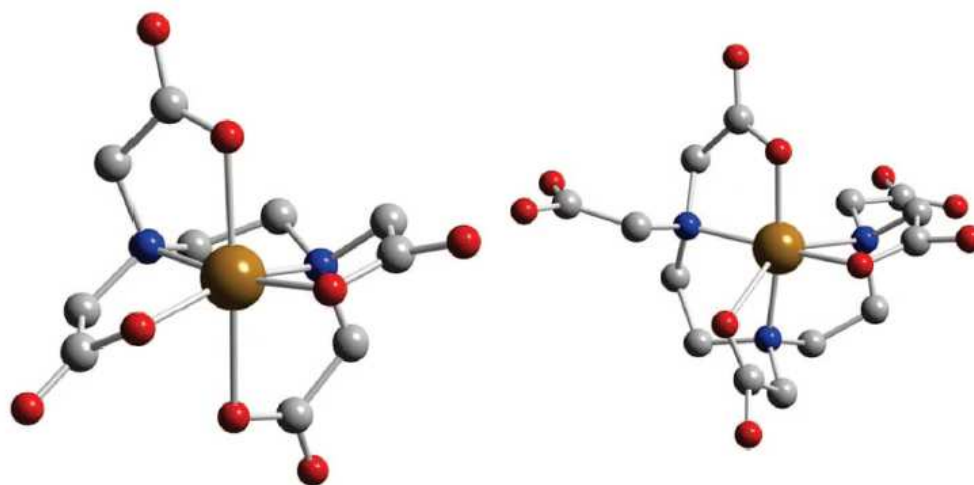


Figure 1.13: X-ray crystal structures of CuEDTA and CuDTPA [12]

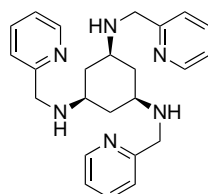
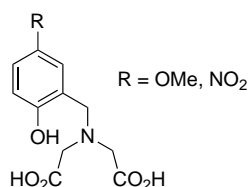


Figure 1.14: Substituted 1,3,5-triaminocyclohexane [13]

stability, due to the presence of lower electron density on the hydroxyl oxygen.

Figure 1.15: *o*-hydroxybenzyl iminodiacetic acid [14]

Another tetradentate gallium chelate is a tripodal tris(2-mercaptobenzyl)amine, which forms a stable tetrahedral NS_3 Ga(III) complex, whereas the indium analogue requires additional solvent coordination.[15] The EDTA derived ligand *N,N'*-bis(2-hydroxybenzyl)-ethylenediamine-*N,N'*-diacetic acid (HBED) has been shown to have an exceptionally high stability constant (37.7) in the Ga(III) complex, and derivatives (HBED-CC) have been synthesised that allow coupling to antibody fragments (diabodies).[16] Whilst EDTA and DTPA complexes of Ga(III) are known, these ligands favour In(III) coordination (fig. 1.16).[17]

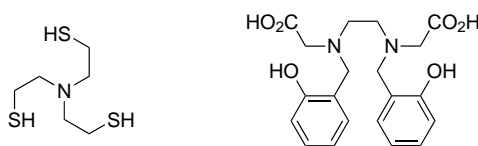


Figure 1.16: Tripodal tris(2-mercaptobenzyl)amine (left) and HBED (right) ligands [15, 16]

1.3.2 Macrocyclic ligands

TACN derived NO₂A and NOTA are TACN macrocycles with 2 or 3 carboxymethyl pendant arms respectively. They have been shown to have a good affinity to copper, and take square-pyramidal and octahedral geometries respectively (fig. 1.17).[18, 19] The stability of NO₂A is not significantly less than for NOTA complexes, and as such allows access to further functionalisation through the unsubstituted third amine nitrogen. Oddly, the crystal structure of CuNO₂A shows that only one acetate is coordinating to copper, with both oxygen atoms bound to separate copper atoms. The remaining acetate arm remains protonated, and is involved in hydrogen bonding to the perchlorate counter ion. Ga complexes of NOTA have been shown to have a very high tolerance to acid decomplexation, with a sample reportedly surviving 6 months in 5 M HNO₃. [20] The stability of the GaNOTA complex is attributed to the full encapsulation of the Ga(III) ion within the macrocyclic cavity. Nucleophilic attack is also negated in this complex due to the acetate arms, hence increasing its stability both in vitro and in vivo. The tris(2-mercaptoethyl) substituted ligand, TACN-TM, was found to form a distorted octahedron, with similarly impressive stability (fig. 1.17).[21]

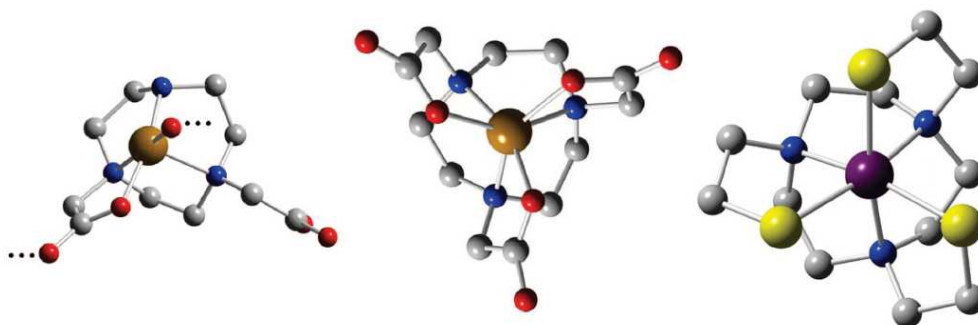


Figure 1.17: X-ray crystal structures of CuNO₂A (left), CuNOTA (centre), and GaTACN-TM (right) [18, 19, 20]

DO₃A and DOTA – the cyclen analogues of NO₂A and NOTA – have been synthe-

sised and their copper binding investigated.[22, 23] Both DO3A and DOTA form octahedral copper complexes, with N_4O_2 donor groups (fig. 1.18). The coordinated carboxyl moieties are found to be *trans* each other and coordinate on the same face.

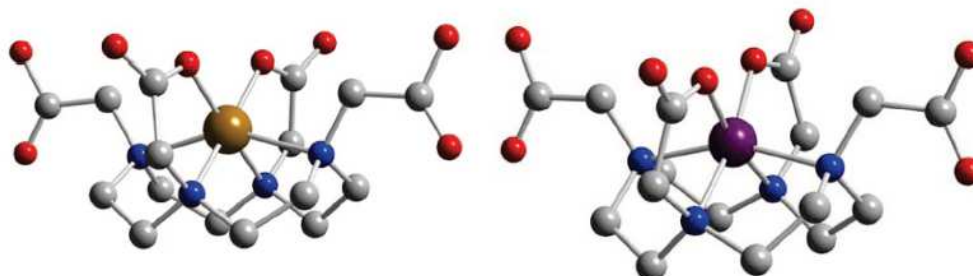


Figure 1.18: X-ray crystal structures of CuDOTA (left), and GaDOTA (right) [22, 24]

A cross bridged DO2A complex was developed to envelop the copper ion into its centre (Cu-CB-DO2A).[25] X-ray data showed that the copper ion sat out of the plane of the cyclen ring in a severely distorted octahedral geometry, believed to be due to a shrunken cavity hole (fig. 1.19). Ga complexes of DOTA has been studied, as the potentially octadentate ligand can successfully fill the required six coordination sites of octahedral gallium complexes. Simple complexes of Ga and DOTA show a similar structure to those afforded by the copper complex, with two binding acetate arms, and two free (fig. 1.18).[24]

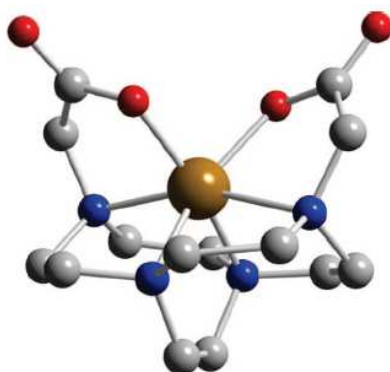


Figure 1.19: X-ray crystal structure of Cu-CB-DO2A [25]

These free acetate arms are advantageous and can be used for conjugation to targeting molecules, and indeed many such molecules have been described. Ga-DOTA-*D*-PheNH₂ forms an octahedral complex with one free acetate arm and one free amide arm, and has been used to explain the better kidney clearance of the octapeptide la-

belled Ga-DOTA-TOC when compared with the Y^{3+} analogue (fig. 1.20).[26] The Y^{3+} complex is likely to make use of the full octadentate potential of the ligand, although no structural evidence exists to defend the assumption. However, DOTA and its derivatives are not ideal chelators of Ga(III) as the cavity size of the macrocycle is much too large for the metal and so stabilities of the complexes are significantly lower than those of the NOTA analogues (GaNOTA $\log K = 31.0$, whilst GaDOTA $\log K = 21.3$).[27, 28]

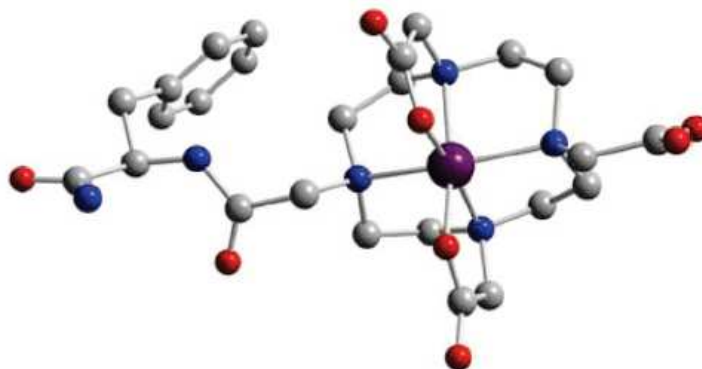


Figure 1.20: Ga-DOTA-*D*-PheNH₂ [26]

Copper cyclam complexes have been studied due to the larger cavity size of the macrocycle. This cavity is larger than that of cyclen, and therefore accommodates the copper(II) ion better. Ligands involving at least one pendant acetate arm have been studied, with the hexamethyl mono carboxyl arm (CuMe₆TE1A) forming the expected square pyramidal complexes (fig. 1.21).[29]

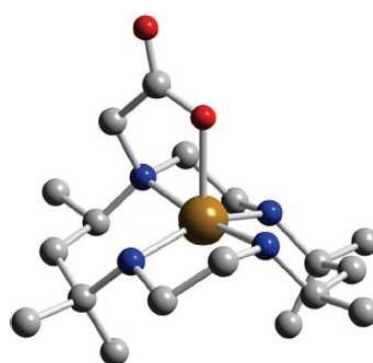


Figure 1.21: X-ray structure of CuMe₆TE1A [29]

Addition of two arms leads to two possible situations, the arms adjacent or opposite each other. In both cases the acetate arms assume the axial positions above and below the copper centre that sits in the plane of the cyclam ring (fig. 1.22).

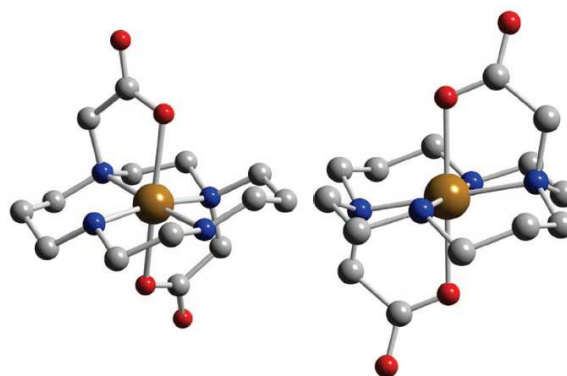


Figure 1.22: X-ray structures of both CuTE2A complexes - cis (left) and trans (right)

X-ray structures of the tetrasubstituted Cu-TETA complexes show the possibility of distortion along either the acetate axial, or across two of the cyclam nitrogens.[30] Functionalisation of the carbon backbone of a TETA complex with a *p*-nitrobenzyl moiety, shows the formation of the expected octahedral complex (fig. 1.23).[31] As would be expected, given the larger cavity size than found in cyclen derivative, no structural data has been obtained for GaTETA complexes, and it should also be noted that the stability of these complexes is still lower with $\log K = 19.7$. [28]

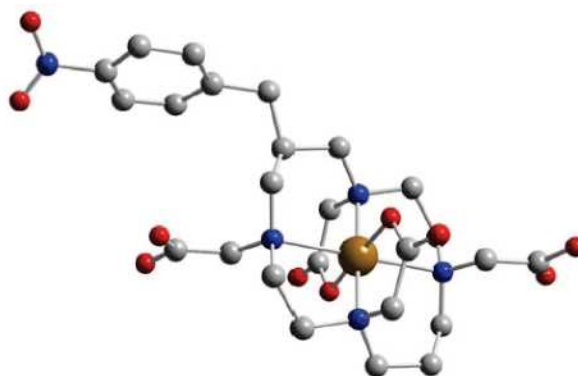


Figure 1.23: X-ray structure of C-functionalised CuTETA complex [31]

Bridged cyclam complexes of copper(II) have also been investigated, with the synthesis of a diacetate ligand (CB-TE2A) and a monoacetate-monoacetamide ligand (CB-TEAMA) accessed for investigation into their *in vivo* behaviour (fig. 1.24).[32] It was found that while both complexes formed the expected enveloped octahedral complexes, the Cu-O_{amide} bond was weaker than that of the Cu-O_{acetate} bond. More interestingly, the Cu-CB-TE2A complex is shown to have remarkable stability toward acid decomplexation, with a half-life of a week in 5 M HCl at 90°C.[33] The ligand has since been further

C-functionalised with a *p*-isothiocyanatobenzyl group, which was subsequently coupled to biotin.[34] Adjacently bridged cyclam complexes have also been synthesised, and are found to form square planar complexes, with any pendant arm coordination occurring axially forming square based pyramidal complexes.[30] Ga-CB-TE2A complexes also show inertness toward demetallation, with a sample reportedly more than 80 % intact after 6 months in 5 M DCl (fig. 1.24).[35]

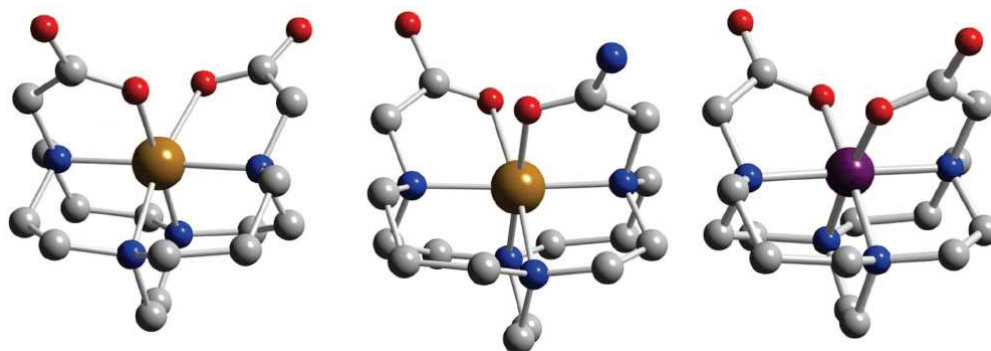


Figure 1.24: X-ray structures of Cu-CB-TE2A (left), Cu-CB-TEAMA (centre), and Ga-CB-TE2A (right) [32, 35]

Cryptand ligands have been researched for their ability to act as ligands for ^{64}Cu due to the well-known strong binding and inertness of sarcophagine complexes DIAMSAR and SARAR have both received recent attention (fig. 1.25).[36, 37, 38] Doubly protonated DIAMSAR is found to have a coordination geometry between octahedral and trigonal prismatic, with elongation of two trans Cu-N bonds. A glutaric acid derived DIAMSAR ligand has recently been synthesised, forming distorted octahedral copper complexes, with the ability to conjugate peptides to the glutaric arms.[39]

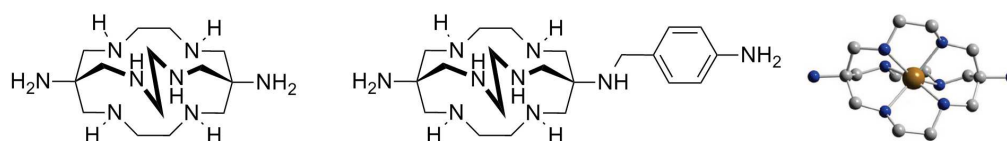


Figure 1.25: DIAMSAR (left), SARAR (centre), and x-ray structure of CuDIAMSAR (right)

1.4 Aims

In this thesis we aim to develop novel PET imaging agents that have the ability to target specific anatomical or biological functions. The suitability of these ligands for PET will also be tested.

Development of previous work in the Fallis group on homopiperazine based ligands with a view to use in PET will also be undertaken, whilst also assessing the coordination chemistry of these ligands.

Chapter 2

Rigid Arm Polyazamacrocycles

2.1 Introduction

Functionalisation of macrocycles has been extensively researched in the last decade. The ability to selectively tune the metal-ligand interaction by the addition of different pendant arms has become both academically and commercially important, for instance in the formation of exceptionally stable biologically active metal complexes. Nitrogen containing azamacrocycles are amongst the most commonly studied, and are the focus of our work. The amine in these macrocycles has the advantage of being a relatively hard donor, and therefore suitable for complexation to PET active metals, such as copper, yttrium, and gallium. Azamacrocycles can be functionalised in one of two general ways; first, through derivatisation of the carbon backbone, and secondly through functionalisation of the nitrogen atoms. The major disadvantage of derivatisation of the carbon backbone is that each variation requires total synthesis of the molecule, whereas functionalisation of the nitrogen atom has a standard carbon backbone and addition of separate specialised pendant arms for each variation. Large scale synthesis of the main framework is therefore possible and reduces the amount of steps needed to make each derivative. The drawback of functionalisation of the nitrogen ring only, is that the number of substituents possible is dictated by the number of nitrogen atoms in the ring (small) compared to the number of carbons in the framework (large). Addition of functionality to a C₂ carbon backbone can most easily be added through use of an amino acid derivative, as exemplified by the synthesis of the TACN and cyclen derivatives

from (2S)-lysine by Parker *et al.* and from *p*-nitrophenylalanine by Meares, Moi, and DeNardo (fig. 2.1).[40, 41] It is interesting to note that in the formation of the TACN derivative, the diethylenetriamine nitrogens are protected by coordination to copper before protection of the terminal amine, and then deprotected with H₂S and cyclised in the normal manner. In all the complexes detosylation was best achieved through cleavage with conc. H₂SO₄, although other methods such as reductive cleavage in Li/NH₃(l) were attempted.

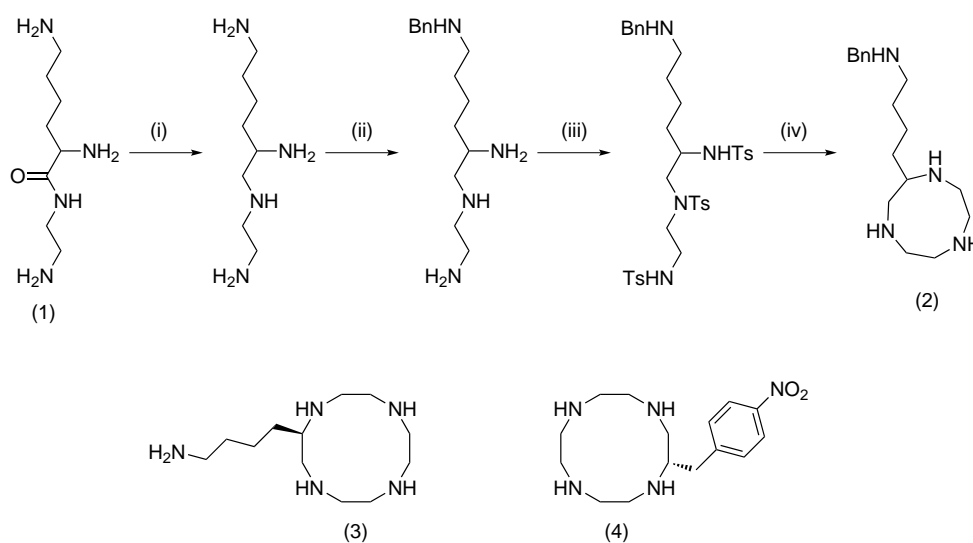


Figure 2.1: C-Functionalised macrocycles

- (1) Lysine functionalised ethylenediamine
 (2) C-functionalised TACN from lysine
 (3) C-functionalised cyclen from lysine
 (4) C-functionalised cyclen from nitrophenylalanine
 i) BH₃.THF ii) CuCO₃, Benzoyl chloride, H₂S iii) TsCl iv) Ethyleneglycol ditosylate

When there is a C₃ backbone, e.g. cyclam and 12N₃, use of a β-amino acid could take the place of the amino-acids as described above, however an alternative is to perform a condensation reaction of a diamine with a C-substituted malonate to form an amide, followed by reduction with BH₃.THF as shown by Parker (fig. 2.2).[42]

Our focus, however, was on functionalisation of the nitrogen. Substitution of the nitrogen has been well documented, and has included (but are not limited to) anilines (1), phenols (2), thiophenols (3), phosphonates (4), amides (5), carboxylic acids (6), alcohols (7), amines (8), thiols (9), alkyl (10), vinyl (11), and alkynyl (12) groups (fig. 2.3).[43, 44, 45, 46, 47, 48, 49, 50, 51, 52, 53]

Previous work in the Fallis group has shown that synthesis of a more rigid arm

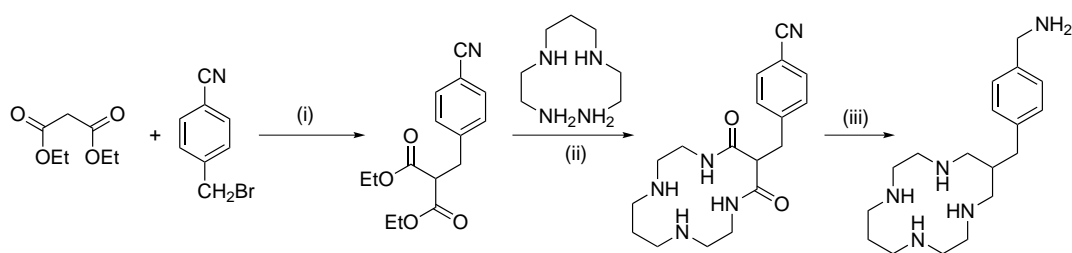


Figure 2.2: Malonate synthesis of c-functionalised macrocycles
 i) NaOEt iii) BH_3 .THF

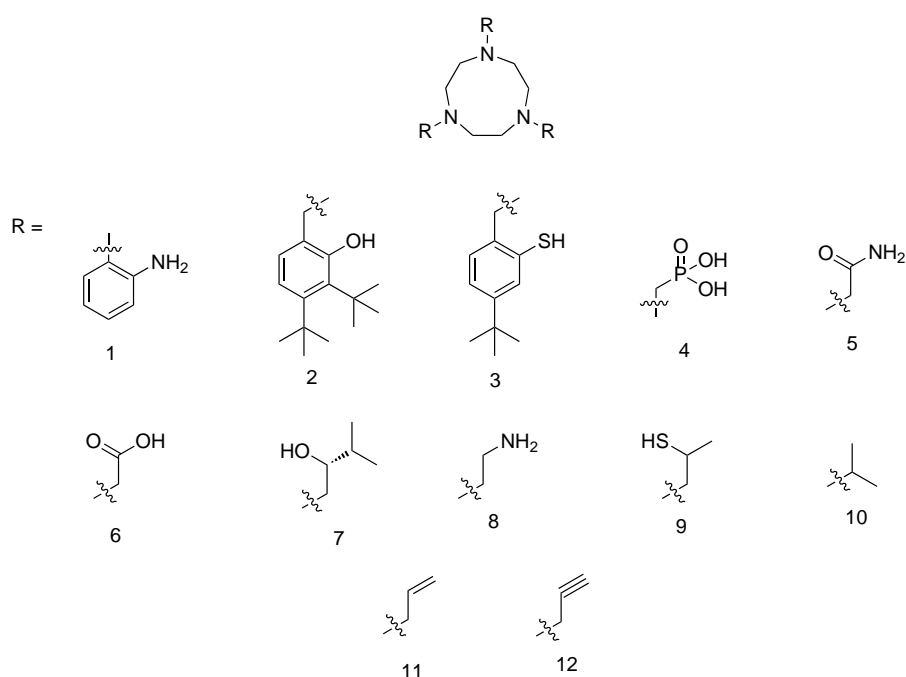


Figure 2.3: TACN with pendant donors

macrocycle increases the metal-ligand interaction, compared to the 6 member chelate analogue (L^1).^[54] Synthesis of the rigid arm macrocycle was through an $\text{S}_{\text{N}}\text{Ar}$ type reaction of 2-fluoronitrobenzene with TACN in acetonitrile, giving the desired product in good yield (72 %). Hydrogenation of the nitro group to an aniline by hydrogen gas over Pd/C gave the free oxygen sensitive 1,4,7-tris(2-aminophenyl)-1,4,7-triazacyclononane (L^{33}) ligand. Complete hydrogenation was indicated by a colour change from orange to colourless due to the conversion of the nitro group to an aniline. Coordination of L^{33} to a series of first-row transition metals (Fe – Zn) was completed by addition of the ligand in ethanol to the metal perchlorate (fig. 2.4). X-ray crystal structure data showed average metal-nitrogen bond lengths were considerably shorter than previously reported

hexaaza-metal complexes, and EPR studies indicated that there was a much greater torsional strain upon these complexes than their L^1 equivalents.

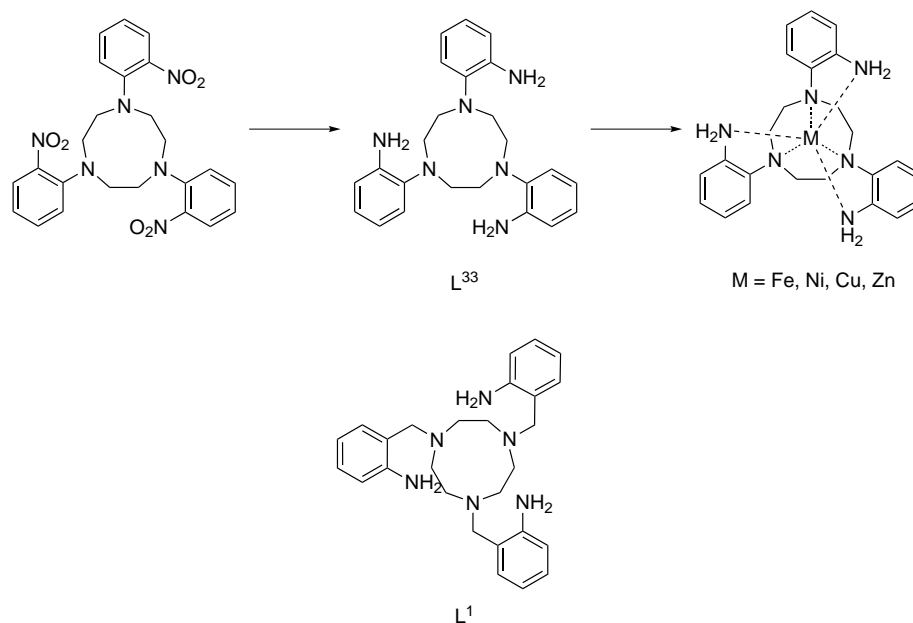


Figure 2.4: L^{33} and L^1

This work was expanded upon, by Fallis and Tatchell, with further functionalisation of the benzene rings.[55] Addition of difluoronitrobenzenes resulted in the formation of ligands with a free fluorine upon the benzene ring which could potentially be further substituted in a similar reaction to that of the initial reaction (fig. 2.5). Mis-insertion products could be removed by recrystallisation, yielding the desired symmetrically substituted products. These compounds were then hydrogenated as before to yield the free oxygen-sensitive ligands. Coordination to a wide range of metals was possible (Mn – Zn, Cd, Hg, and Pb) and x-ray structure analysis for most of the complexes obtained. It was found that the average bond length for all of the complexes was comparable with other common MN_6 complexes, and that therefore functionalisation of the benzene ring had little effect on the strength of the metal-ligand bond. It was also noted that ^{19}F NMR shifts could be used as an indication of coordination and successful hydrogenation of the nitro moiety in some cases, with a shift from c. -100 ppm to c. -125 ppm upon hydrogenation, then to c. -110 ppm upon Zn coordination, in the case of the *para*-fluoro ligand.

It was shown that sequentially substituted TACN rings were accessible by control-

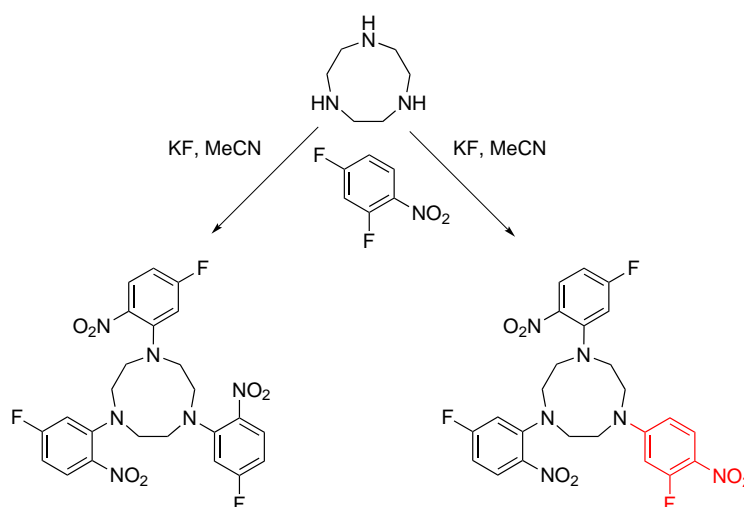


Figure 2.5: Mis-insertion product

ling the number of equivalents of pendant arm added (fig. 2.6). Addition of 1 equivalent led to the formation of the mono-substituted compound. Addition of a second equivalent of a different pendant arm lead to the asymmetrically substituted compound, and addition of a third equivalent of a further pendant arm yielded the triply substituted compound. The order of pendant arm addition was said to be important in minimising the chances of mis-insertion products, but this would only be the case in the addition of fluoro derivatives.

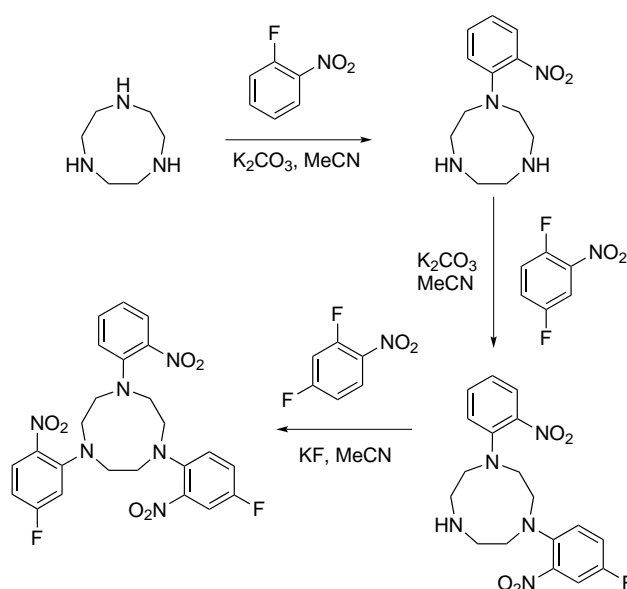


Figure 2.6: Mixed fluoro TACN synthesis

Homopiperazine can be thought of as a pseudo-macrocycle, in that its chemistry is similar to TACN – it can be functionalised through the carbon backbone and the nitrogens in the ring – although it only forms chelates, rather than capping a metal centre as TACN would. Little chemistry has been done on the formation of rigid arm homopiperazine complexes, with unpublished work from the Fallis group being the only compounds we are aware of.[55, 56] Synthesis of homopiperazine analogues of the fluoro-functionalised L^{33} has been reported by Fallis and Tatchell (fig. 2.7). Coordination of metal species was achieved by addition of the metal perchlorate to an ethanolic solution of the ligand under anaerobic conditions, with x-ray crystal structure data of the Ni complex obtained. The bond lengths for the fluoro-functionalised complexes were found to be slightly different from that of the parent compound, with an increase of 0.012 \AA in the Ni-N_{ring} distance and a shortening of the Ni-N_{aniline} distance by 0.013 \AA . It is suggested that this is due to the electron withdrawing effect of the fluorine on the *para* ring amine, causing a lengthening of the bond distance. Functionalisation of the aniline was also investigated with the addition of tosyl chloride to form a sulfonamide, with the aim of forming charge neutral square planar complexes (fig. 2.7). After reduction of the nitro moiety to an aniline, tosyl chloride in basic conditions was added, forming the sulfonamides. Reaction with various metal salts was attempted, but only the nickel complex was obtained, although fortunately yielding crystals of x-ray quality. X-ray data showed the presence of a neutral nickel complex, with no coordinating solvent. The nickel was in a square planar environment, with a slight distortion of 11° , which was suggested to be caused by the tight bite angle due to the small ring system.

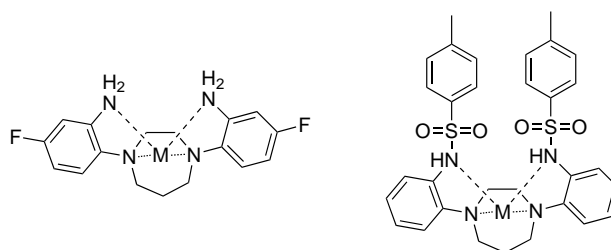


Figure 2.7: Homopiperazine analogues, and tosylated L^{22}

2.2 Anilino ligand synthesis

Given that previous evidence supported the fact that functionalisation of the benzene ring had little effect on the strength of the metal-ligand bond, we believed that functionalisation of these rings could lead to potential peptide binding sites, and thus a method of using these chelates in PET studies. In order to understand further how the functionalisation of the benzene pendant arm would affect the metal-ligand bond strength a series of 5-functionalised-2-fluoronitrobenzenes with electron withdrawing and electron donating groups were chosen for use as the pendant arms. Synthesis of the homopiperazine compounds was analogous to that described previously for L²², with 2 equivalents of the fluoronitrobenzene added to a solution of homopiperazine and 2 equivalents of potassium carbonate in acetonitrile under an inert atmosphere. The compounds were formed in moderate to high yields (47 - 99 %), as yellow to dark red solids (table 2.1).

Synthesis of the more complicated amide (HP^{Amide-NO₂}) (fig. 2.8) was achieved through the reaction of 4-fluoro-3-nitrobenzoic acid with oxalyl chloride to give the acid chloride, followed by addition of the desired amine, this was then reacted with homopiperazine under the aforementioned conditions.

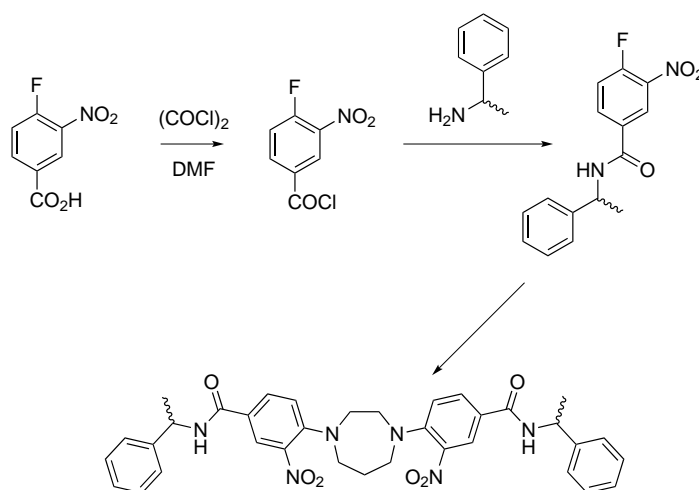


Figure 2.8: Synthesis of HP^{Amide}

Both the racemic and chiral compounds were synthesised. The ¹H NMR of the racemic compound showed only one set of signals, so it was hypothesised that there was some kind of intermolecular influence between the pendant arms, resulting in only

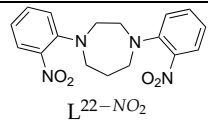
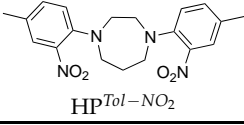
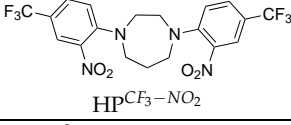
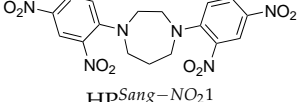
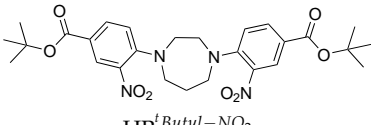
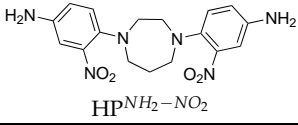
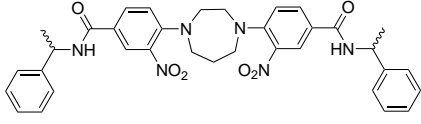
Ligand	Yield (%)	Colour	λ_{max} (nm) (ϵ (mol ⁻¹ cm ⁻¹))
 L ²² -NO ₂	90	Bright orange	384 (2706)
 HP ^{Tol} -NO ₂	97	Dull orange	422 (4506)
 HP ^{CF₃} -NO ₂	47	Orange	404 (4651)
 HP ^{Sang} -NO ₂ 1	49	Yellow	369 (27549)
 HP ^{tButyl} -NO ₂	90	Yellow	407 (4992)
 HP ^{NH₂} -NO ₂	91	Red-Brown	458 (2937)
 HP ^{Amide} -NO ₂	76	Yellow	417 (5632)

Table 2.1: Homopiperazine ligands

one stereoisomer being formed. The hypothesis was tested by performing a 'doped' experiment, in which 20 % of the pendant arm added was known to be pure (R-), whilst the remaining 80 % was racemic. This should have resulted in a larger proportion of the (R, R-) compound being formed and so the difference in shift would have been observable in the ¹H NMR, however, only one set of signal was observed, meaning that the racemic and chiral molecules were not distinguishable by ¹H NMR. As in the previous examples we then attempted to reduce the nitro group to an aniline. Successful reduction is indicated by a colour change from orange to colourless, associated with the conversion of the nitro group to an aniline. 2 different methods were deployed for the functional group interconversion, both being successful. Reduction of the nitro-compounds to their aniline counterparts with tin chloride in acidic ethanol under nitrogen gave the desired colour change, however, attempts to isolate the aniline based inter-

mediates were unsuccessful due to the highly oxygen sensitive nature of these ligands. Instead the interconversion was completed using the previously described hydrogenation method, involving Pd/C and methanolic solutions. It was found that pre-washing the Pd/C catalyst media with methanol gave faster reaction times, which has been attributed to impurities being present in the commercially purchased compounds. The hydrogenation was usually complete overnight, and as before was indicated by a colour change from orange to colourless. After completion the ligand was isolated by filtration under nitrogen and the solvent removed under reduced pressure yielding the desired product as a white/off-white solid. The free aniline ligands were found to be oxygen sensitive and went off irreversibly within a few hours in the presence of air, indicated by a browning of the solid, and so were stored under a nitrogen atmosphere. Due to the oxygen sensitive nature of these ligands they were used without further purification or characterisation. However, during attempts to grow crystals of complexes of the HP^{CF_3} ligands, crystals of the free ligand were obtained, of which the structure is given in appendix A.

Synthesis of the TACN analogue of $\text{HP}^{\text{CF}_3-\text{NO}_2}$ was also successful, using the same general conditions as for the homopiperazine compound, whilst the piperazine analogue of $\text{HP}^{\text{Tol}-\text{NO}_2}$ was also synthesised again yielding the desired compound. Hydrogenation of the piperazine compound gave the desired colour change from orange to colourless; however attempts to form complexes did not give the desired mass although colour changes were noted. Attempts to grow crystals of the copper complex yielded the free ligand, and the structure is given in appendix A. It is thought that the complexes exist in equilibrium in solution due to the large strain that would be exerted in the structure, however it was decided not follow up on this. The $\text{TACN}^{\text{CF}_3-\text{NO}_2}$ was also hydrogenated as before, giving the colour change of orange to colourless.

We hypothesise that the use of diazacyclooctane (DACO) in the place of piperazine or homopiperazine would afford more stable complexes. This is due to the larger ring size lowering the ring strain in the complexes. This has not been tested in this thesis, but would be interesting to follow up in future.

A comparison of the UV-Vis data for the ligands shows the influence the *para* group has on the electronics of the system (fig. 2.9). Using the parent compound $\text{L}^{22-\text{NO}_2}$ as a comparison, it would be expected that there would be a shift to lower wavelengths

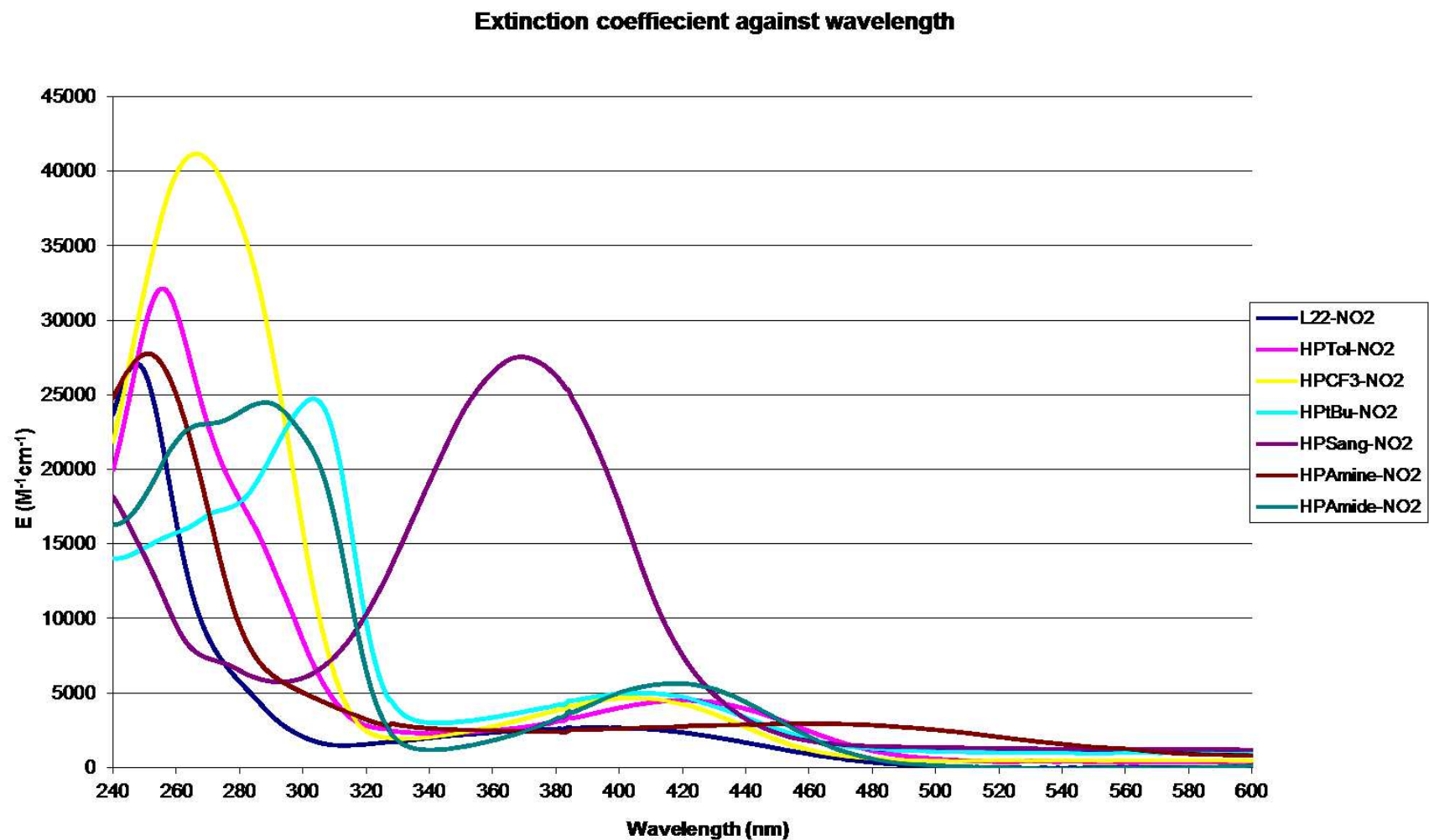


Figure 2.9: UV-Vis comparison of ligands
Artifacts at 382 nm are a machine error during bulb changeover

of those compounds with electron withdrawing groups in the *para* position, whilst an increase in wavelength for those compounds with electron donating groups would be expected. The Hammett parameters give a numerical value to the electronic effect of the substituent in both *para*- and *ortho*- positions (see table 2.2), with positive numbers meaning electron withdrawing, and negative numbers being electron donating. The Hammett parameter (σ_p) is the summation of the relative inductive and resonance effects of the group. It is important to remember that these effects are in addition to

Group	σ_p
H	0.00
Me	-0.17
CF ₃	0.54
CO ₂ Me	0.45
NO ₂	0.78
NH ₂	-0.66
CO ₂ NH ₂	0.36

Table 2.2: Hammett Parameters

that of the *ortho* nitro group, which is exerting an effect on the electronics of this system, therefore the order of electron withdrawing strength should be considered to be $\text{HP}^{\text{Sang-NO}_2} > \text{L}^{22\text{-NO}_2} > \text{HP}^{\text{CF}_3\text{-NO}_2} > \text{HP}^{\text{tButyl-NO}_2} > \text{HP}^{\text{Amide-NO}_2} > \text{HP}^{\text{Tol-NO}_2} > \text{HP}^{\text{Amine-NO}_2}$. This order is found to be present in the lambda max values of these compounds. The other striking difference in these values is the extinction coefficients (ϵ). By far the largest value is that of the $\text{HP}^{\text{Sang-NO}_2}$ compound ($\epsilon = 27549 \text{ M}^{-1}\text{cm}^{-1}$), which is due to the chromophoric nature of the nitro groups. The parent compound has the lowest extinction coefficient due to it being the least conjugated, and an increase in extinction coefficient is noted for the $\text{HP}^{\text{Amide-NO}_2}$ compound which contains additional chromophores in the presence of phenyl rings.

2.3 Metal complexes of HP^{Tol}

Metal complexes of the HP^{Tol} ligand were prepared by addition of a degassed ethanolic solution of the desired metal perchlorate to solid ligand under an inert atmosphere. Gentle heat was applied for 2-3 minutes with stirring, and then the solution allowed to cool, and stirred at room temperature for at least one hour. Addition of diethyl ether to

the solution resulted in the precipitation of the metal complexes, which were found to be air stable.

2.3.1 Nickel(II) complex

The nickel complex was found to be a cream solid. UV-Vis spectroscopy, run in acetone, shows the presence of 3 distinct absorptions at 435 ($\epsilon = 75.7 \text{ mol}^{-1}\text{cm}^{-1}$), 583 ($\epsilon = 7.2 \text{ mol}^{-1}\text{cm}^{-1}$), and 630 ($\epsilon = 1.9 \text{ mol}^{-1}\text{cm}^{-1}$) nm, indicating a mixture of square planar and octahedral species in solution.¹H NMR, also in acetone, show a slight broadening of all signals, with the sharpest being that of the methyl group on the ring, which would be explained by its distance through space from the paramagnetic centre. This paramagnetism could be attributed to coordination of acetone to the metal centre, even though acetone is generally regarded as a weakly coordinating solvent. The IR spectrum shows a signal at 3226 cm^{-1} and 3186 cm^{-1} assigned as the symmetrical and asymmetrical stretches of a coordinated aniline. The mass spectra showed the required isotope pattern for this complex.

Attempts to grow crystals of x-ray quality was unsuccessful, so DFT calculations were undertaken to gain more insight into the likely structure and bonding found in the molecule (fig. 2.10).² The calculations assumed square planar geometry, without the presence of coordinating solvent. The nickel atom sits in the middle of the amine and aniline atoms, in a slightly distorted square with angles found to be 86.3° and 93.7° . The N_{ring} -Ni bond lengths are found to be 1.899 \AA , whilst the $N_{aniline}$ -Ni bond lengths are calculated as 1.931 \AA , these values are comparable to those found by Perkins for the parent L²² ligand (N_{ring} -Ni 1.898 \AA and $N_{aniline}$ -Ni 1.911 \AA), indicating the methyl groups has little effect on the electronics of the delocalised system.[56] The average Ni-N bond length of 1.915 \AA is almost exactly that of a strain free NiN_4 square planar complex (1.91 \AA), however the large difference between the two nitrogen environments indicate that there is significant strain on the molecule.[57] The benzene rings are bent slightly from linearity, which can be attributed to the unsymmetrical nature of the homopiperazine ring, causing this molecule to lose a high degree of symmetry and join the C_s point group, only having a mirror plane.

²B3LYP / 6-31G (B3LYP / 6-31G(d,p) for metal atom and bound atoms) - input and output files on attached CD

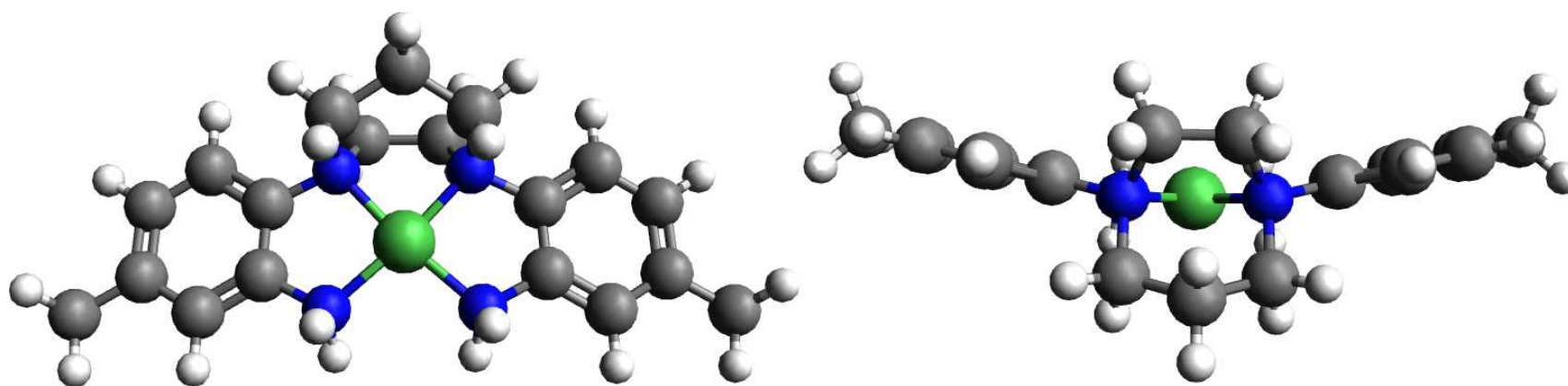


Figure 2.10: DFT calculated structure of NiHPTol
Selected Bond Lengths: Ni-N(34) 1.931 Å, Ni-N(37) 1.898 Å, Ni-N(38) 1.899 Å, Ni-N(39) 1.931 Å

2.3.2 Copper(II) complex

The copper complex was synthesised in an analogous method to that of the Ni complex. UV-Vis data shows a peak at 565 nm ($\epsilon = 292.2 \text{ mol}^{-1} \text{ cm}^{-1}$) in acetone, assigned to the ${}^2T_{2g} \leftarrow {}^2E_g$ transition. The IR data shows signals at 3522 and 3243 cm^{-1} , which have been assigned as the symmetrical and asymmetrical stretching frequencies of a coordinated aniline. The mass spectra showed the required isotope pattern for this complex.

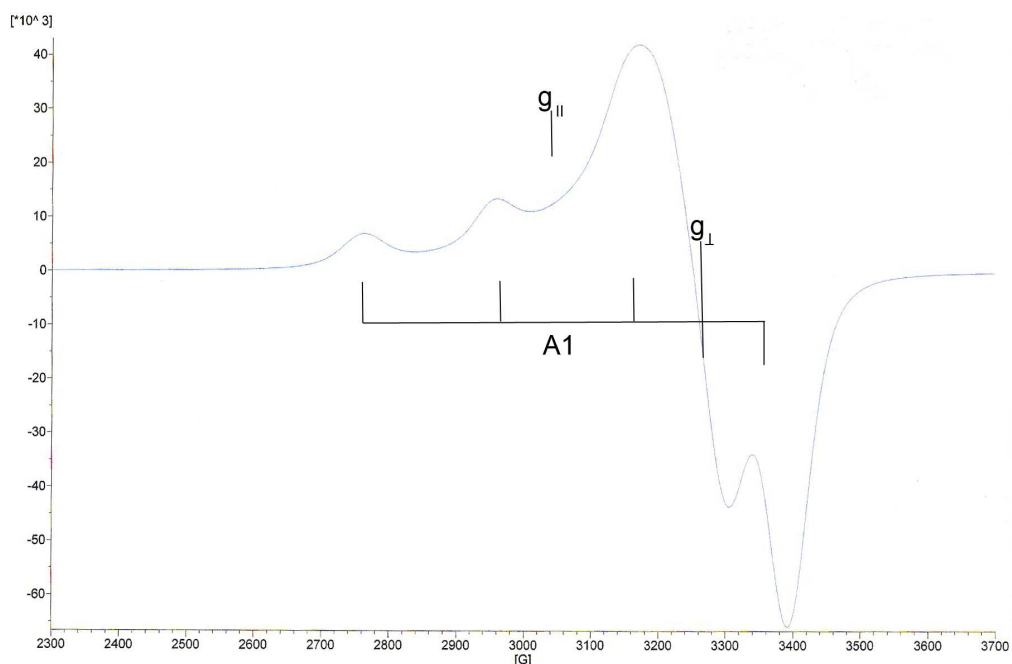


Figure 2.11: EPR of CuHP^{Tol} in DMF/MeCN

An EPR spectrum of the compound was collected by members of Dr. D. Murphy's group from a frozen glass MeCN-toluene solution of the sample (fig. 2.11). The spectrum shows the presence of 4 distinct peaks as would be expected from a d^9 copper(II) complex with four coordinated nitrogens. Hyperfine coupling constants of $A_{||} = 200 \text{ G}$ are noted, with $g_{||} = 2.195$ and $g_{\perp} = 2.041$. Compounds with $g_{||} < 2.3$ are considered to be covalent in nature, whilst $g_{||} \geq 2.3$ are ionic, therefore the complex CuHP^{Tol} is to be considered highly covalent in nature.[58] The values for $g_{||}$ and $A_{||}$ are also close to those reported for other CuN_4 complexes such as $[\text{Cu}(\text{AMH})_2](\text{OH})_2$ - $g_{||} = 2.171$ and $A_{||} = 210 \text{ G}$.[58]

Again, growth of suitable crystals was unsuccessful, so DFT calculations were used to probe the structure of the complex in a square planar geometry (fig. 2.12). As in the Ni

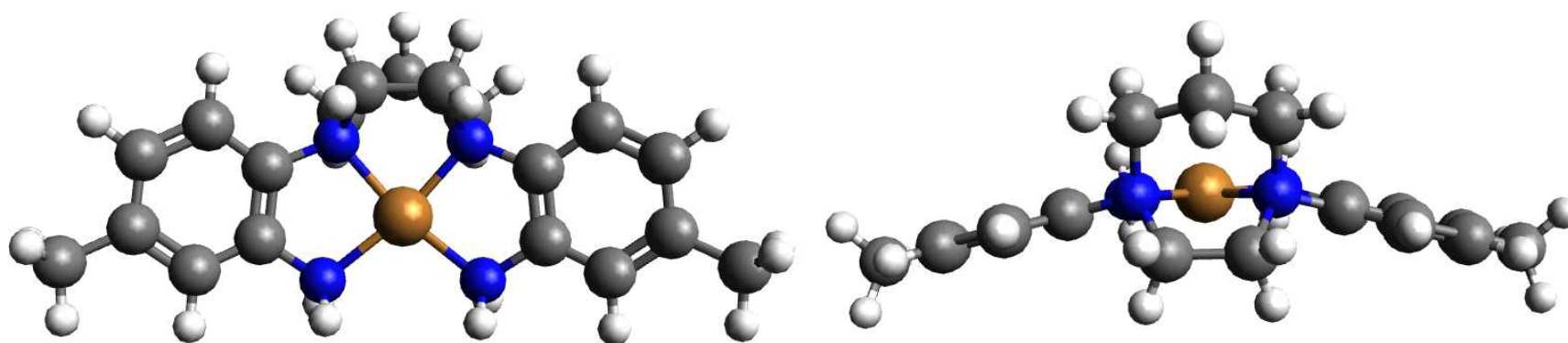


Figure 2.12: DFT calculate structure of CuHP^{Tol}
Selected Bond Lengths: Cu-N(34) 2.014 Å, Cu-N(37) 1.987 Å, Cu-N(38) 1.987 Å, Cu-N(39) 2.013 Å

complex the Cu atom sits slightly above the centre (2.4°) of a distorted square formed by the amine and aniline nitrogen atoms, where the angles are found to average 84.5° and 95.5° . The N_{ring} -Cu bond lengths are found to be 1.987 \AA , whilst the $N_{aniline}$ -Cu bond lengths are calculated as 2.013 \AA , which is comparable to those found by Perkins in L^{22} (N_{ring} -Cu 1.992 \AA and $N_{aniline}$ -Ni 2.008 \AA). As in the nickel complex, the benzene rings are bent out of linearity, which is caused by the lack of flexibility in the homopiperazine ring. The molecule has only a mirror plane and no other symmetry operators and thus is also part of the C_S point group.

2.4 Metal complexes of HP^{CF_3}

Metal complexes of the HP^{CF_3} ligand were prepared by addition of a degassed ethanolic solution of the desired metal perchlorate to solid ligand under an inert atmosphere. Gentle heat was applied for 2-3 minutes with stirring, and then the solution allowed to cool, and stirred at room temperature for at least one hour. Addition of ether to the solution resulted in the precipitation of the metal complexes, which were found to be air stable.

2.4.1 Nickel(II) complex

UV data for the nickel complex shows 3 peaks as found for the HP^{Tol} complex, 391 ($\epsilon = 40.2 \text{ mol}^{-1} \text{ cm}^{-1}$), 507 ($\epsilon = 19.8 \text{ mol}^{-1} \text{ cm}^{-1}$), and 803 ($\epsilon = 11.2 \text{ mol}^{-1} \text{ cm}^{-1}$) nm, this again indicates a mixture of square planar and octahedral species in solution. This was also shown in the ^1H NMR spectra, where the peaks were very broad, and therefore not analysed or reported. Peaks in the IR spectra at 3419 and 3344 cm^{-1} are assigned to the symmetrical and asymmetrical stretches of aniline coordination, and the sharp peak at 1332 cm^{-1} is assigned to the C-F bond.

DFT calculations show that the nickel atom sits very slightly above the plane (0.8°) in a distorted square planar arrangement, with angles of 86.2° and 93.8° , similar to that calculated for the $NiHP^{Tol}$ complex (fig. 2.13). The N_{ring} -Ni bond lengths are found to be 1.898 \AA , whilst the $N_{aniline}$ -Ni bond lengths are 1.934 \AA . The N_{ring} -Ni bond length is the same as that of the parent L^{22} ligand, the $N_{aniline}$ -Ni bond is slightly longer. The CF_3 group is sufficiently electron withdrawing (c.f. Hammett parameters 2.2) that one

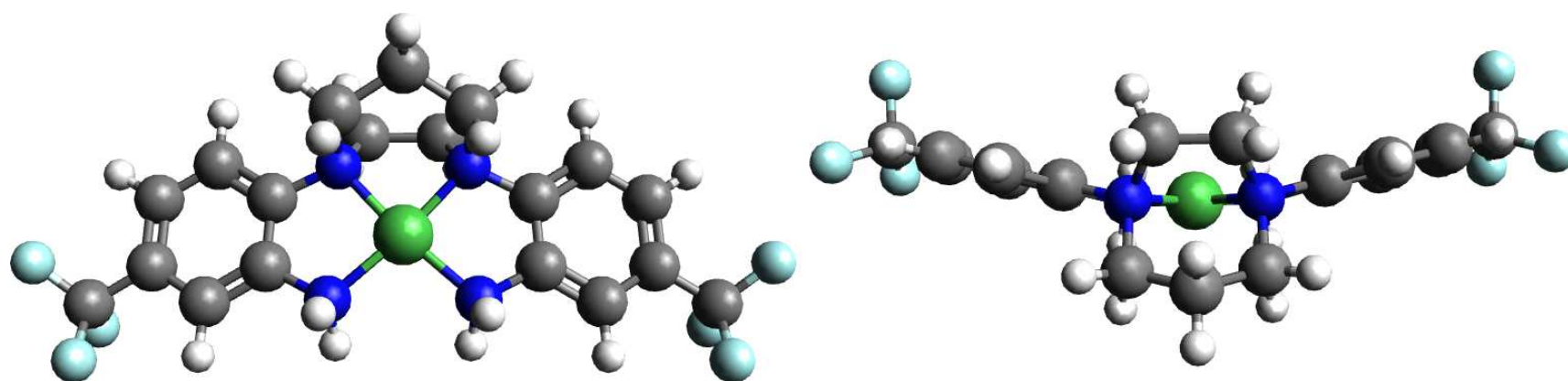


Figure 2.13: DFT calculated structure of $\text{NiHP}^{\text{CF}_3}$
Selected Bond Lengths: Ni-N(34) 1.934 Å, Ni-N(37) 1.898 Å, Ni-N(38) 1.898 Å, Ni-N(39) 1.934 Å

would assume therefore, that there would be a lengthening of the N_{ring} -Ni bond length as opposed to the $N_{aniline}$ -Ni bond length as that is *para* to the CF_3 group. This is probably just an anomaly in the calculation method, and real data would be needed to assess this properly. The large difference in the N_{ring} -Ni and $N_{aniline}$ -Ni bond lengths shows significant strain in the system, as in the analogous HP^{Tol} complex. Once again, the benzene rings are bent from linearity, giving the molecule C_5 symmetry, with the presence of only a single mirror plane.

2.4.2 Copper(II) complex

The purple copper complex gave a single peak in the UV spectrum at 572 ($\epsilon = 142.8 \text{ mol}^{-1}\text{cm}^{-1}$) nm, which is assigned the ${}^2T_{2g} \leftarrow {}^2E_g$ transition, although is a very long tail starting from beyond 1100 nm that may be hiding other peaks. As with the nickel complex there were peaks at 3519 and 3433 cm^{-1} in the IR spectrum associated with the symmetrical and asymmetrical stretches of the coordinated aniline, and a peak at 1332 cm^{-1} due to the C-F bond.

Like the Ni complex, DFT studies show that the copper atom sits very slightly out of the plane (0.8°) in a distorted square planar geometry, with angles of 84.3° and 95.7° (fig. 2.14). The larger distortion than in the nickel complex is due to the larger size of the copper ion than its nickel partner. At 1.987 Å, the N_{ring} -Cu bond lengths are the same as the $CuHP^{Tol}$ complex, whilst the $N_{aniline}$ -Cu bond lengths are also similar at 2.017 Å. As in the nickel complex, it is slightly surprising that the N_{ring} -Cu bond lengths are not slightly longer, but again these lengths are from an idealised gas calculation and may not be exactly as found in reality. Again, there is a large strain in the molecule as evidenced by the fact there is a large discrepancy between the N_{ring} -Cu and $N_{aniline}$ -Cu bond lengths. The molecule is in the C_5 point group, due to the presence of only one mirror plane.

2.4.3 Zinc(II) complex

The zinc complex was analysed using IR spectroscopy, a peak at 3287 cm^{-1} is assigned to the aniline, whilst the presence of a peak at 1334 cm^{-1} is indicative of the C-F bond.

DFT calculations of the Zn complex show the molecule is highly distorted, with the Zn atom trying to force a tetrahedral geometry and causing a large twist in the molecule (fig. 2.15). This is understandable as Zn has no preference for its geometry and tends

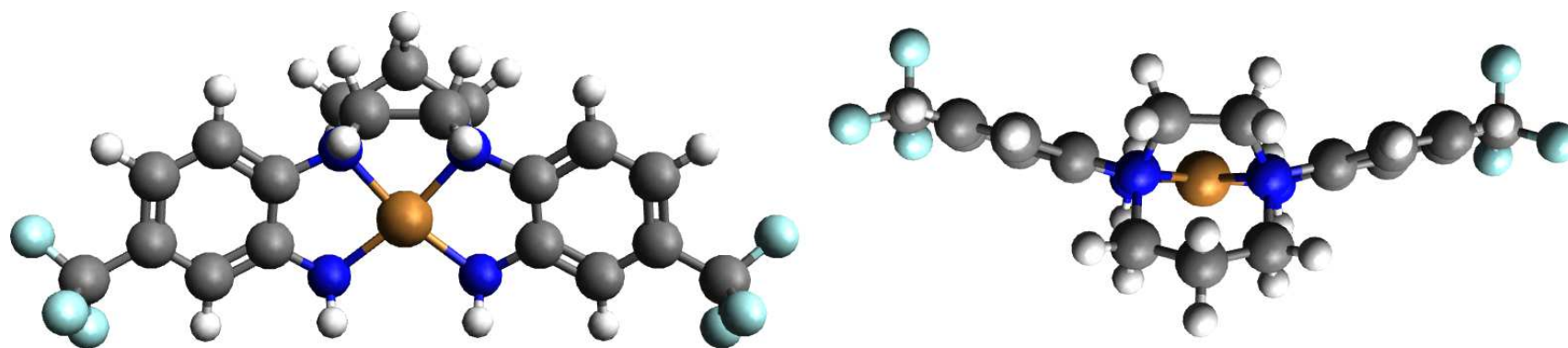


Figure 2.14: DFT calculated structure of $\text{CuHP}^{\text{CF}_3}$
Selected Bond Lengths: Cu-N(34) 2.017 Å, Cu-N(37) 1.987 Å, Cu-N(38) 1.987 Å, Cu-N(39) 2.017 Å

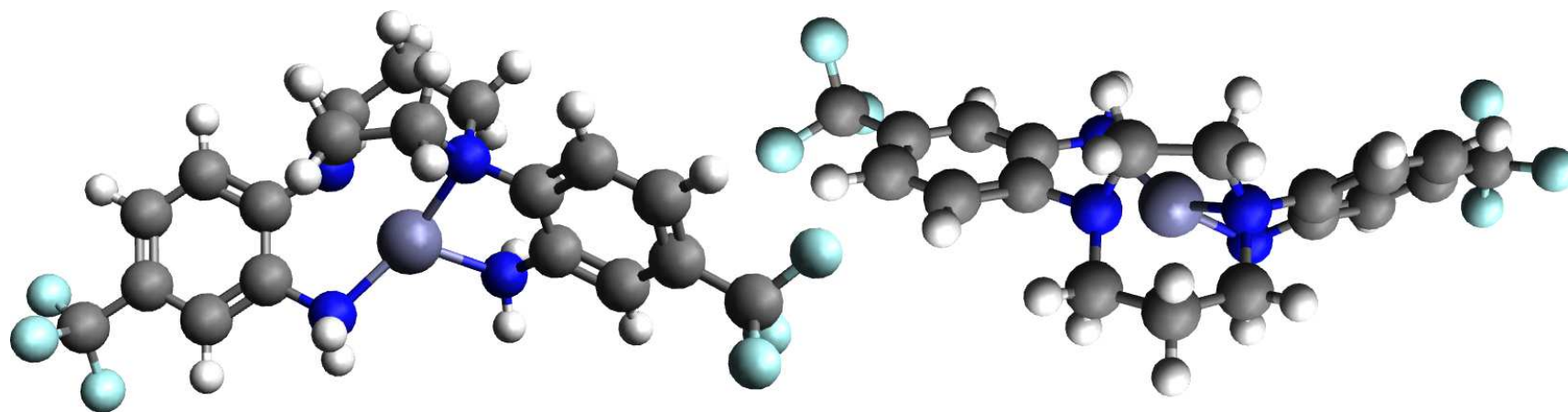


Figure 2.15: DFT calculated structure of $\text{ZnHP}^{\text{CF}_3}$
Selected Bond Lengths: Zn-N(34) 2.056 Å, Zn-N(37) 2.052 Å, Zn-N(38) 2.069 Å, Zn-N(39) 2.044 Å

to form tetrahedral complexes over square planar ones due to the lower energy of the system. If a plane is drawn through the line of the ring nitrogens and the Zn centre, there is a twist of 57.8° , and 71.5° from the plane to the $N_{aniline}$ atoms (fig. 2.16).

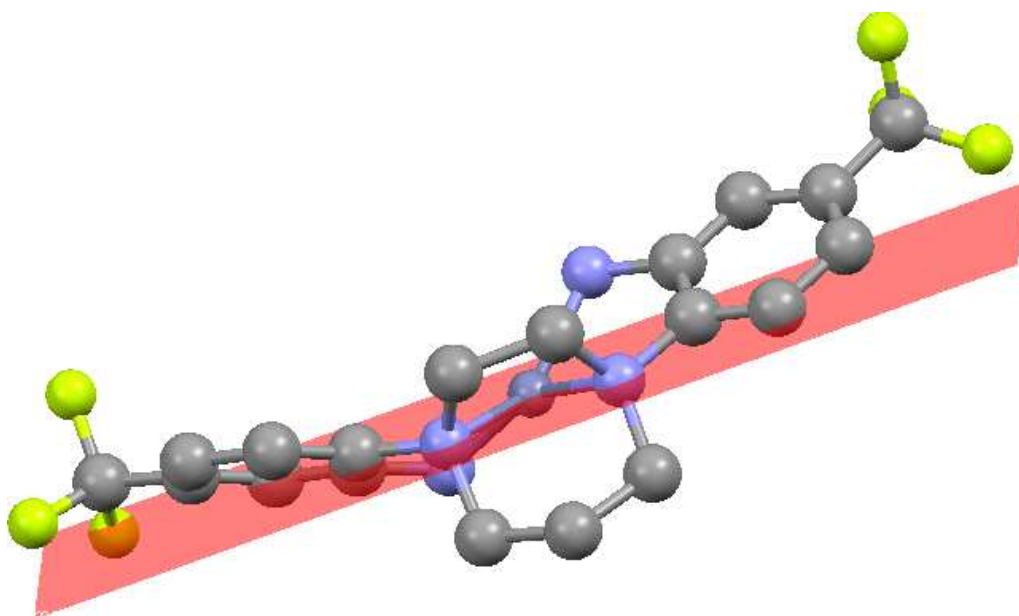


Figure 2.16: Plane in the Zn structure

The N-Zn bond distances are all different, with the two $N_{aniline}$ -Zn bond lengths being 2.044 \AA and 2.056 \AA , whilst the two N_{ring} -Zn lengths are 2.052 \AA and 2.069 \AA . It is interesting to note that the longest and shortest bonds are both on the same side of the molecule, (fig. 2.15(left) left hand side). There are currently no pure ZnN_4 complexes reported in the Cambridge Crystal Database, all complexes involve at least one more coordinating ligand. It is therefore unwise to compare these bond lengths to any other reported distance. This indicates that the likely structure obtained, if crystals of this complex ever come to light, would have at least coordinating solvent, and may not be as strained as this structure is.

2.5 Metal complexes of $TACN^{CF_3}$

Metal coordination was attempted by addition of metal perchlorate in degassed ethanol to the free ligand under an inert atmosphere. Gentle heat was applied, and the solution stirred at room temperature over night. After filtration the solvent was removed *in vacuo*, and the complex found to be stable to air.

2.5.1 Copper(II) complex

Crystals suitable for x-ray diffraction of the copper complex were grown by vapour diffusion of diethyl ether into acetonitrile. The acquired structure was not as expected, but showed the loss of one pendant arm, and the formation of a 5 coordinate MN_5 species. It is believed that this structure is of a small impurity in the sample and not reflective of the bulk species. The crystals were sent off for analysis before any further data was accumulated. We were unable to repeat the synthesis so no further data has been recorded.

2.6 Metal complexes of HP^{tButyl}

Metal complexes of the HP^{tButyl} ligand were prepared as for the HP^{Tol} complexes, by addition of a degassed ethanolic solution of the desired metal perchlorate to solid ligand under an inert atmosphere. Gentle heat was applied for 2-3 minutes with stirring, and then the solution allowed to cool, and stirred at room temperature for at least one hour. Addition of ether to the solution resulted in the precipitation of the metal complexes, which were found to be air stable.

2.6.1 Nickel(II) complex

High resolution mass spectrometry revealed the correct m/z and isotopic pattern for the formation of the complex, whilst also visible in the spectra was a signal for the demetallated compound. IR spectra showed a broad signal at 3399 cm^{-1} , which indicates the presence of water in the sample. This peak has covered the area of the spectrum where aniline stretches are usually visible, and so they are unassignable. The sample had been dried under vacuum prior to the IR analysis, and therefore hints at the presence of water in the solid structure. The peak at 1635 cm^{-1} has been assigned to the ester function. This value is significantly lower than usually expected for an ester ($\sim 1740\text{ cm}^{-1}$) and this is due to the large amount of delocalisation throughout the molecule. This has the result of greatly lowering the double bond nature of the C=O bond, and in turn lowering the expected frequency of the moiety in the IR spectrum. The UV-Vis spectrum was dominated by the chromophoric ligand, however, 2 shoulders relating to d-d transitions were visible, these lie at 487 and 623 nm, and indicate a square planar geometry in the complex. The transitions are tentatively assigned the ${}^2B_{1g} \leftarrow {}^1B_{2g}$ and

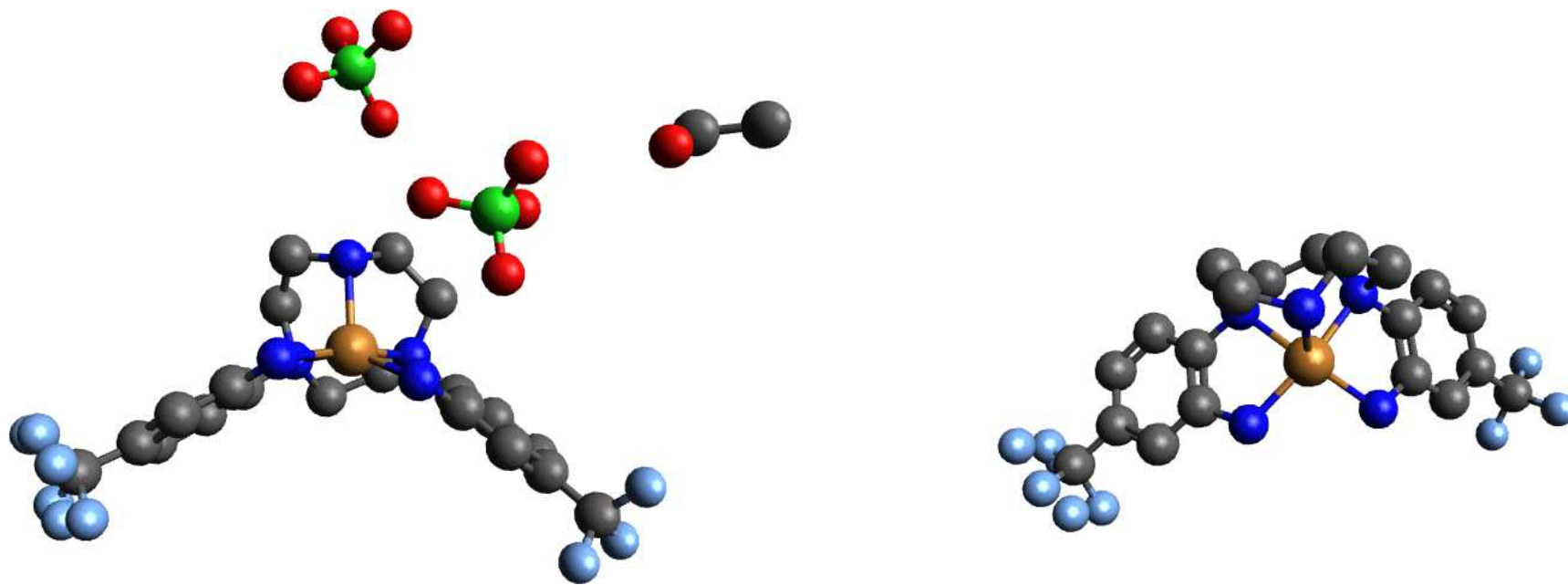


Figure 2.17: X-ray structure of $\text{CuTACN}^{\text{CF}_3}$ (left with perchlorate anions and solvent, right without)
Selected Bond Lengths: Cu-N(22) 1.995(3) Å, Cu-N(12) 2.008(3) Å, Cu-N(11) 2.039(3) Å, Cu-N(21) 2.060(3) Å, Cu-N(31) 2.188(3) Å

${}^2A_{1g} \leftarrow {}^1B_{2g}$ transition respectively, although there may be more signals hidden by the large ligand signal as found for the other NiHP^x complexes.

Crystals suitable for x-ray diffraction were able to be grown by vapour diffusion of diethyl ether into acetonitrile (fig. 2.18). The colourless needle-like crystals were orthorhombic and occupied the Pbc_a space group.³ The nickel atom sits slightly above the middle of a distorted square planar geometry (1.5°), with angles of 85.8°, 86.4°, 93.8°, 94.0° for the aniline nitrogens and ring nitrogens respectively. The N_{ring}-Ni bond lengths are found to be 1.905(5) Å, whilst the N_{aniline}-Ni bond lengths are 1.905(4) Å and 1.916(4) Å. These lengths are very similar to those quoted for a strain free NiN₄ complex (see above), although the bond angles show that there is some steric strain on the system. There is no difference in the bond lengths found in this complex when compared with those of the parent L²² complex, showing that (at least in the solid state) there is no effect on the nitrogen-metal bond strengths with a change in the electron withdrawing nature of the *para* substituent. As seen in the DFT calculated structures there is a bend from linearity for the benzene rings, leading to a C₅ symmetrical molecule. There is also a NiCl₄ moiety in the crystal lattice to give the molecule overall charge neutrality.

2.6.2 Copper(II) complex

IR spectra for the copper complex showed similar features to the Ni complex. A low frequency C=O stretch was observed at 1635 cm⁻¹, with aniline stretches present at 3245 and 3382 cm⁻¹. The low frequency of the C=O stretch is again believed to be caused by the large delocalisation of charge throughout the molecule, lowering the double bond character of the bond. UV-Vis spectroscopy showed the presence of 3 distinct peaks lying at 410, 612, and 813 cm⁻¹. This indicates the presence of a number of coordination geometries in solution. High resolution mass spectrometry shows the required mass and isotope pattern for the formed complex, whilst the demetallated compound is also visible in the low resolution spectrum.

Crystals suitable for x-ray analysis were not obtainable, and so DFT calculations were undertaken to afford information on the structure of the molecule (fig. 2.19). Once again the copper atom sits in the centre of a distorted square (0.5° out of the plane), with angles of 84.5° and 95.5°. The N_{ring}-Cu bond lengths of 1.988 Å are the same as for the HP^{Tol} and HP^{CF₃} complexes. The N_{aniline}-Cu bond lengths are 2.010 Å and 2.012 Å,

³Full crystal data is available in Appendix X

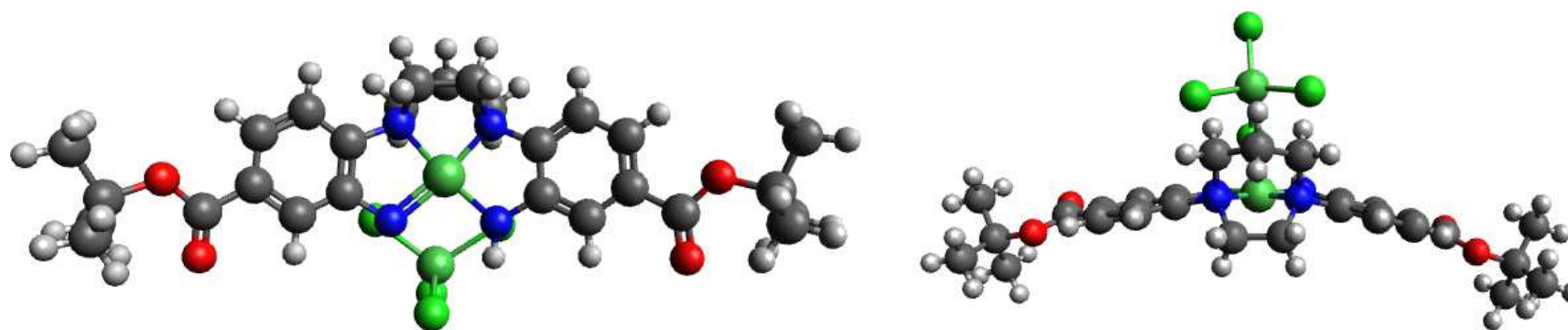


Figure 2.18: X-ray structure of $\text{NiHP}^{\text{Butyl}}$ with NiCl_4 counter ion
Selected Bond Lengths: Ni-N(1) 1.916(4) Å, Ni-N(2) 1.905(5) Å, Ni-N(3) 1.905(5) Å, Ni-N(4) 1.905(4) Å

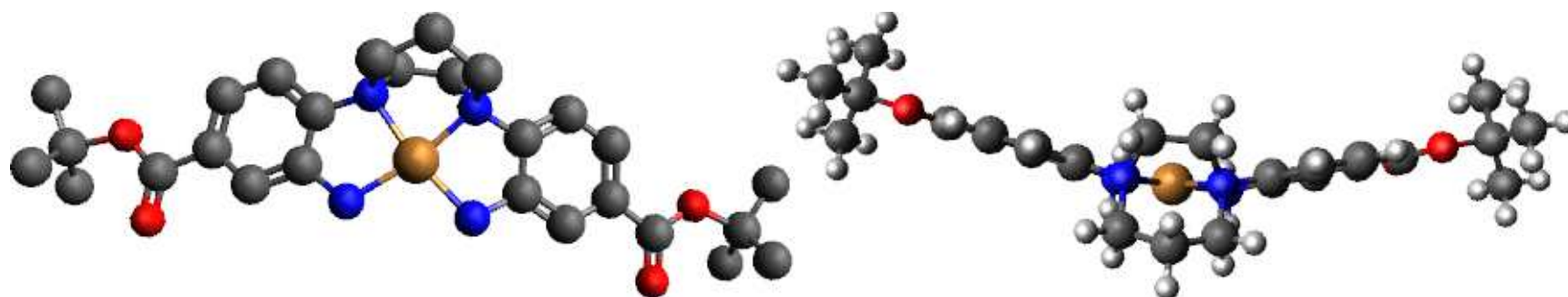


Figure 2.19: DFT Structure of CuHP^{tButyl}
Selected Bond Lengths: Cu-N(62) 2.012 Å, Cu-N(65) 1.988 Å, Cu-N(66) 1.987 Å, Cu-N(67) 2.010 Å

which is the same as those in the HP^{CF_3} complexes. Again the molecule is displaying a C_5 symmetry, having only one mirror plane and no axis of rotation.

2.6.3 Zinc(II) complex

The zinc complex was also synthesised, and was analysed using IR and mass spectrometry. A high resolution mass spectrum was not accessible for the complex, with values outside the allowed range found. However, a low resolution spectrum gave a signal at the desired mass. IR analysis showed the 2 signals for aniline coordination as in other complexes, at 3466 and 3260 cm^{-1} , with the C=O stretch at a higher frequency than for the other $\text{HP}^{\text{tButyl}}$ complexes at 1714 cm^{-1} . DFT shows geometrical distortion and therefore a loss of conjugation relative to the other metal complexes and this would account for a higher frequency than seen before (although still lower than a typical ester signal).

DFT calculations show that the zinc complex is, again, highly distorted, with the aniline nitrogens twisted by 58.6° and 71.9° , which is very similar to the $\text{ZnHP}^{\text{CF}_3}$ complex (fig. 2.20 and 2.21).

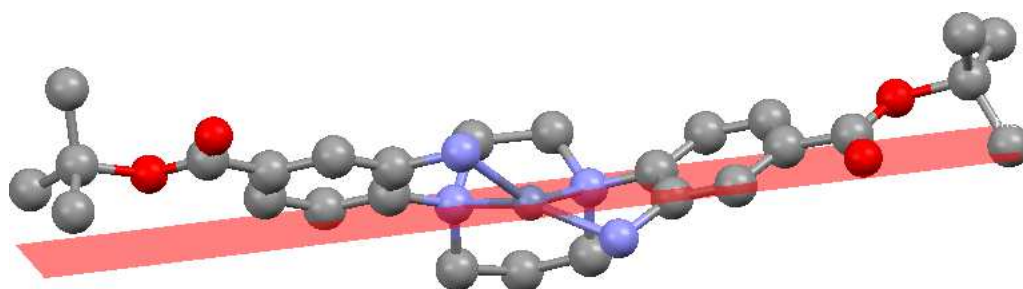


Figure 2.21: Plane in Zn structure

The $N_{\text{ring}}\text{-Zn}$ bond lengths of 2.052 Å and 2.068 Å are very similar to the $\text{ZnHP}^{\text{CF}_3}$ complex, whilst the $N_{\text{aniline}}\text{-Zn}$ bond lengths of 2.048 Å and 2.038 Å are considerably shorter. This is a continuation of the pattern noticed for the $\text{CuHP}^{\text{tButyl}}$ complex. Again, it can be assumed that there will be some form of coordinating ligand in experimentally formed crystals, and so little conclusions should be drawn from these calculations.

It can be seen from the x-ray and DFT structures that substitution of the benzene ring *para*- to the ring nitrogen has only a small effect on the metal bond strength. Therefore functionalisation of these areas is an option when trying to synthesise a targeting molecule. We have also shown that it is possible to form amide bonds at the *para* posi-



Figure 2.20: DFT structure of $\text{ZnHP}^{\text{tButyl}}$
Selected Bond Lengths: Zn-N(62) 2.048 Å, Zn-N(65) 2.052 Å, Zn-N(66) 2.068 Å, Zn-N(67) 2.038 Å

tion, and it is therefore a route to peptide conjugation.

2.7 Carboxy ligand synthesis

Having shown that functionalisation of the benzene *para* to the ring nitrogens had little effect we became interested in synthesising neutral complexes. It is desirable clinically to have neutral drugs, as this lowers the chance of patients suffering drug-induced shock. As the *ortho*-nitro group activates the fluorine of the benzene ring towards nucleophilic substitution we needed to find a suitably electron withdrawing group to match its activating power. The carboxyl group was chosen, but due to the ability of this to also react with an amine to form an amide, we needed to protect it in the form of an ester.

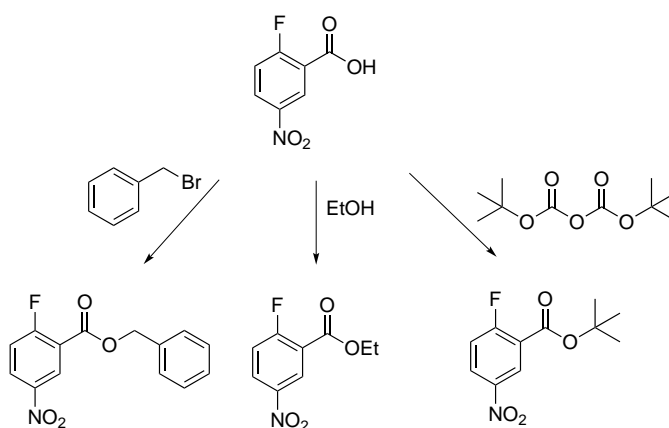


Figure 2.22: Pendant arm synthesis

Synthesis of the benzyl, ethyl, and ^tbutyl esters was performed on both 2-halobenzoic acid, and 2-halo-5-nitrobenzoic acid. Benzyl protection of the carboxylic acid was achieved through reaction of benzyl bromide with the acid in DMF in the presence of a phase transfer catalyst yielding the desired ester as yellow/orange powders in moderate to high yields (68 % - 92 %) (fig. 2.22). Both the fluoro- and chloro-nitrobenzoic acids were used as we wished to see if the presence of two electron withdrawing groups was enough to activate the chlorine towards substitution. Fluorobenzoic acid and iodobenzoic acid were chosen to see whether the ester was activating enough to activate the fluorine towards substitution, with the option of a Buchwald-Hartig amination using the iodide if the former was not possible.

The ethyl esters were synthesised from the acid in ethanol with sulfuric acid as the

catalyst, whilst the *t*-butyl esters were formed by reaction of the acid with boc-anhydride in the presence of DMAP⁴ (fig. 2.22). Addition of the carboxyl pendant arms 1-NO₂, 2-NO₂, and 3-NO₂ to homopiperazine proceeded as with the nitro compounds. It was found there was no difference in reactivity between the fluoro- and chloro- derivatives, and so the chloro- compound was used preferentially on economic grounds. Addition of the non-nitro derivatives by this method failed, and Buchwald-Hartig amination was not attempted due to problems found later in the complex synthesis.

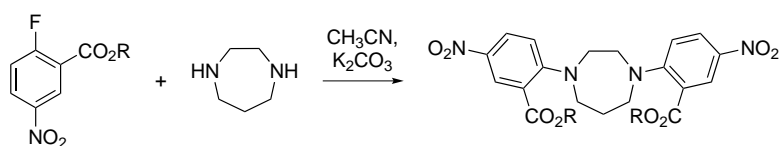


Figure 2.23: HP^{LX-NO₂}

In addition to homopiperazine compounds, we also produced piperazine, TACN, and dimethylcyclen based ligands. This was to prove that the reaction conditions were the same for similar macrocycles as well as giving a route to related complexes. Crystal structures for the ligand precursors Pip^{3-NO₂}, HP^{1-NO₂}, HP^{3-NO₂}, TACN^{1-NO₂} and DMC^{1-NO₂} were obtained and are given in Appendix A.

⁴DMAP = N,N-dimethyl-4-aminopyridine

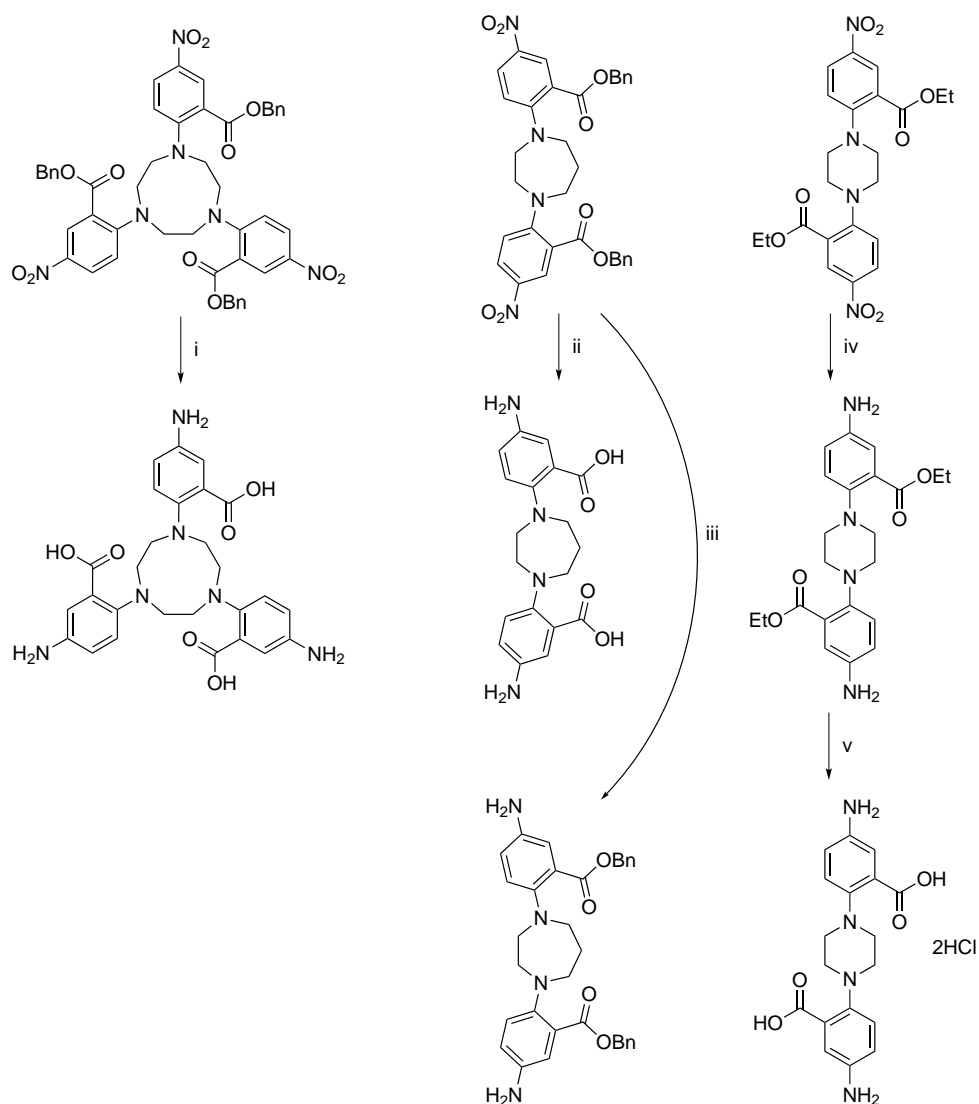


Figure 2.24: Synthesis of free carboxyl ligands

(i) Pd/C, THF:MeOH, H₂ (ii) Pd/C, THF, acetic acid, H₂ (iii) SnCl₂, EtOH (iv) Pd/C, MeOH, H₂ (v) HCl (2 M)

The free ligand was accessed through various means depending upon the protecting group of the ester (fig. 2.24).

The TACN^{1-NO₂} pro-ligand was deprotected in a one step protocol using Pd/C in a THF:MeOH solution under an atmosphere of hydrogen (i). The hydrogenation of the nitro group to an aniline and deprotection of the benzylic ester occur simultaneously. Reduction of the nitro group to an aniline results in a colour change from orange to colourless, however, this is not indicative of the benzylic ester cleavage, and so the hydrogenation was performed over 2 days. It was also noted that the colour change in

this compound occurred much slower than the time taken for similar reductions for the $\text{HP}^{\text{Anilino}}$ ligands described previously. This resulted in a highly air sensitive compound that had to be stored under an inert atmosphere.

The sensitivity of the $\text{HP}^{1-\text{NO}_2}$ compounds to this method was found to be equally as challenging, and the hydrogenation needed stronger conditions with the addition of a drop of acetic acid to lead it to completion (ii).

We also attempted selective reduction of the nitro-group to an aniline, leaving the ester function in place (iii). This was due to the possibility of a method of tagging a protein or amino acid type group to the ligand through amide bond formation. To this end reduction of $\text{HP}^{1-\text{NO}_2}$ by SnCl_2 in ethanol was undertaken. After reflux for 18 hours a colour change was noted, from bright orange to an off white-orange. After extraction with chloroform and removal of solvents *in vacuo*, the product was found as a brown-orange oil. ^1H NMR data showed the presence of the compound, but also many other signals, and mass spectra showed the desired m/z peak, as well as a plethora of other values. It was therefore concluded that the sample was air sensitive in this form as well, and no further work was attempted.

The HCl salt of the free ligand Pip^{R} was accessed from the pro-ligand $\text{Pip}^{3-\text{NO}_2}$. Hydrogenation of the pro-ligand gave the expected reduction of the nitro to an aniline, as evidenced through loss of colour from orange to colourless (iv). To this was then added degassed HCl (2 M) and stirred at room temperature under an inert atmosphere for 18 hours (v). After removal of the solvent *in vacuo* a colourless white solid remained that was very hygroscopic. ^1H NMR whilst broad showed the loss of the ethyl group, as well as a shift in aromatic protons as would be expected from reduction of the nitro-group.

2.8 Metal complex of carboxyl ligands

Metal complexes of the free ligand were accessed through addition of an alcoholic solution of the desired metal salt to a solution of free ligand. It was found that the complexes had very limited solubility and so samples strong enough to give useful UV data were unable to be accessed, resulting in analysis by MS, IR, and EPR only.

2.8.1 Copper(II) Complexes

Complex of Pip^R

Neutralisation of the free ligand salt with triethylamine under inert conditions followed by addition of copper(II) chloride in a degassed methanol solution resulted in a colour change from colourless to deep blue. Removal of the solvents *in vacuo* followed by precipitation of a chloroform solution in hexane resulted in a blue solid. IR spectra of the solid showed the expected peaks for a free aniline 3446 and 3356 cm⁻¹ as well as an unexplained signal at 3221 cm⁻¹. The later signal could identify the presence of a protonated aniline species, either from the complex, or from triethylamine that has not been successfully removed during work up. The coordinated carboxylate is seen with stretches at 1597 and 1377 cm⁻¹.

Complex of HP^R

Addition of an ethanolic solution of copper acetate to a THF solution of the free ligand afforded a colour change from colourless to blue then green. High resolution mass spectrum of the resulting solid showed presence of the desired compound as the Na⁺ salt. IR data show the desired 2 signals for the presence of an aniline at 3437 and 3217 cm⁻¹, with bound carboxylate signals at 1596 and 1398 cm⁻¹.

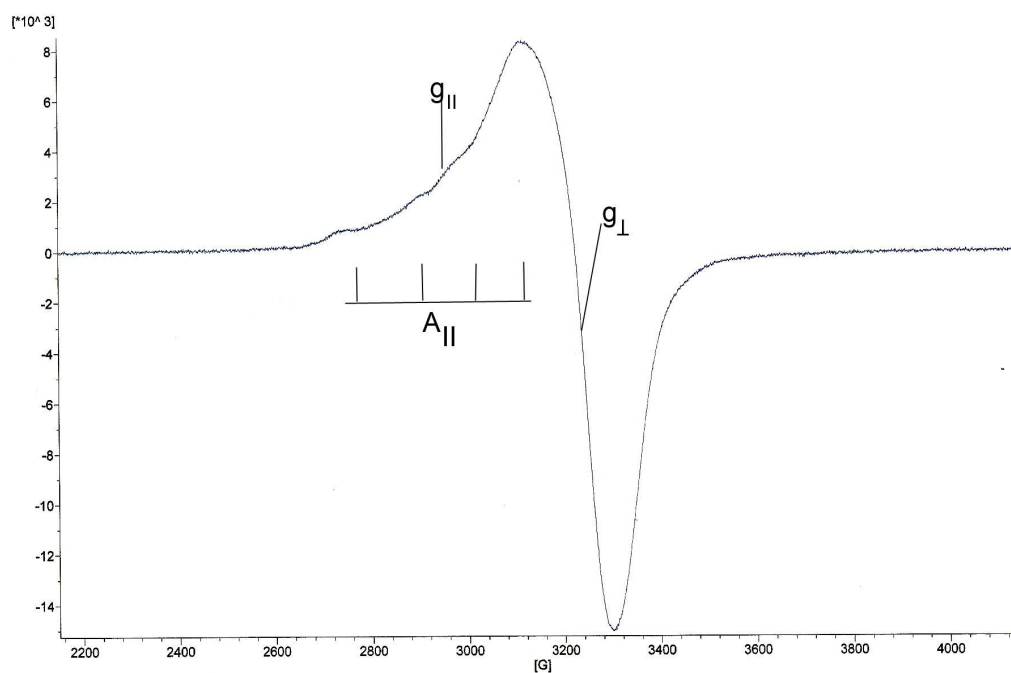


Figure 2.25: EPR spectra of CuHP^R

A sample was handed in for EPR analysis as a blue frozen glass solution of DMSO:EtOH (fig. 2.25). The spectrum shows the presence of only one species but others are potentially hidden by the broadness of the peak. To identify if there are hidden species, further analysis at a greater frequency would be required in order to pull the peaks apart. A value of $A_{||} = 110$ G is found with $g_{||} = 2.250$ and $g_{\perp} = 2.083$. The larger $g_{||}$ value found here than for the CuHP^{Tot} complex shows the greater degree of ionic bonding between the carboxylate and copper, than that of the aniline copper bond.

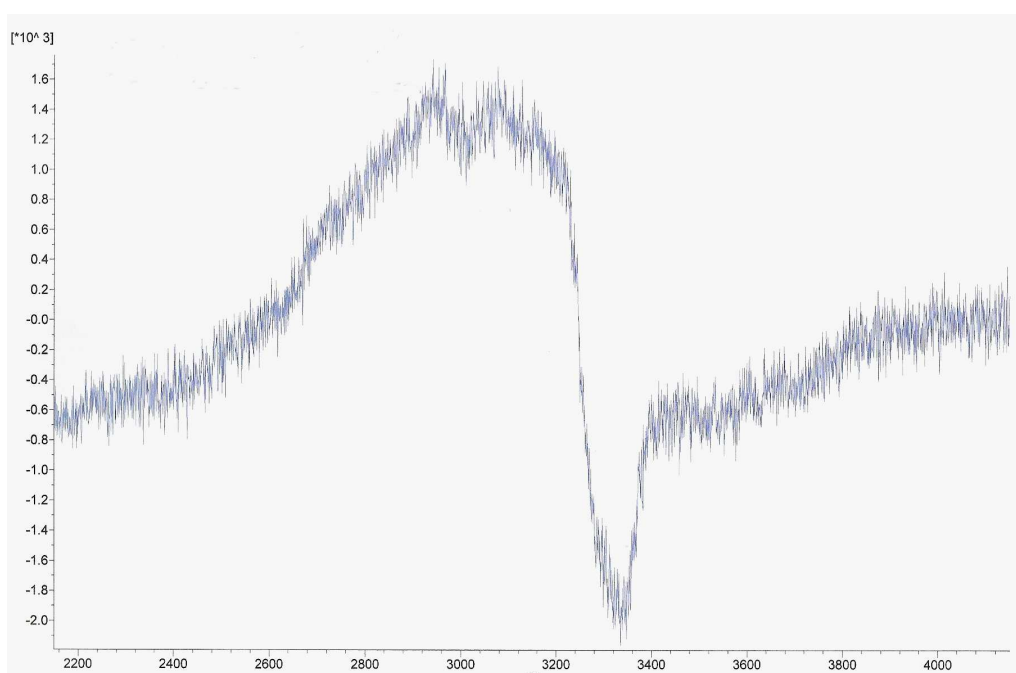


Figure 2.26: EPR spectra of CuHP^{R} with excess DMSO

It was noted that when additional DMSO was added to the EPR sample there was a colour change from blue to red. A further EPR spectra of the red solution was taken, and a vast difference in output was seen (fig. 2.26). A complete loss of peak definition is noted, and is believed to be caused by an overlap of both octahedral and square planar complexes due to coordination of DMSO to the copper centre. Again, higher frequency analysis of the sample may shed some light on this, but was not available at the time these results were acquired.

Complex of TACN^{R}

Addition of an ethanolic solution of copper(II) nitrate to a THF solution of the free

ligand under inert conditions afforded a colour change from colourless to purple. After work up, the product was isolated as a deep purple/black solid.

IR analysis showed the 2 expected peaks for the presence of an aniline group at 3353 and 3216 cm^{-1} , with coordinated carboxyl signals at 1560 and 1374 cm^{-1} . High resolution mass spectrometry of the solid gave the required mass and isotope pattern predicted for the complex.

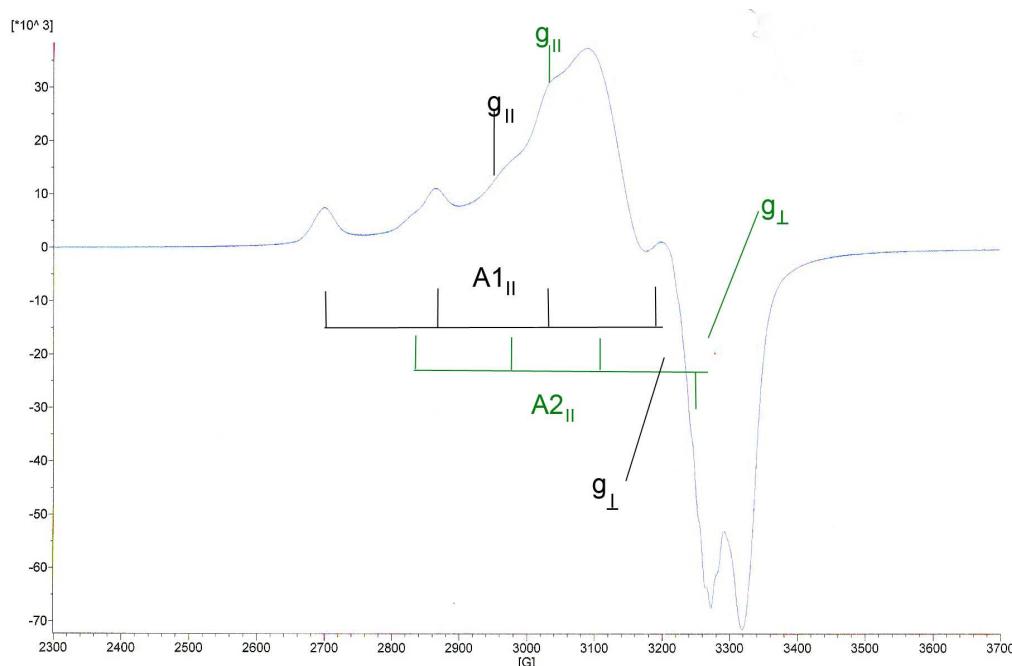
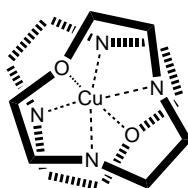


Figure 2.27: EPR spectra of CuTACN^R

Once again EPR studies were undertaken of the complex using a DMSO:MeOH frozen glass. Two distinct patterns are observed in the EPR spectrum indicating the presence of 2 species in the solution (fig. 2.27). Species 1 has $A_{||} = 170$ G with $g_{||} = 2.202$ and $g_{\perp} = 2.119$. Species 2 has $A_{||} = 143$ G with $g_{||} = 2.156$ and $g_{\perp} = 2.041$. The values for species 1 compare well with those reported for a bis-[9]ane N_2O copper complex $\text{Cu}([\text{9}]\text{aneN}_2\text{O})_2^{2+}$, which contains a similar CuN_4O_2 ligand framework, at $g_z = 2.202$ and $A_z = 193.5$ G.[59]

It is also stated in Kavana's paper that a minor signal is seen and is attributed to the conformational isomers possible. This could explain the presence of 2 discrete signals in the acquired spectrum for this complex, with the isomers being an octahedral and trigonal bipyramidal geometry. Further EPR studies, and structural data - either X-ray data, or computational - would be needed to add weight to this theory.

Figure 2.28: $\text{Cu}([\text{9}] \text{aneN}_2\text{O})_2^{2+}$ [59]

2.8.2 Nickel(II) Complex

Complex of HP^R

The nickel(II) complex of HP^R was also synthesised in the same manner as the copper complex. A high resolution mass spectrum was unobtainable due to values outside of the allowed range, however, the low resolution spectra showed the desired m/z and isotopic pattern for the complex, with an aqua adduct also seen. IR spectroscopy revealed a broad peak at 3429 cm^{-1} assigned to a water molecule and indicates that water is trapped in the solid lattice, which is therefore covering any signals that would be seen for the anilines. The signals for the carboxylate occur slightly higher than for the copper complex at 1634 and 1384 cm^{-1} indicating a slightly weaker bond to the metal centre.

Chapter 3

Triazine Core Derived PET

Agents

3.1 Introduction

Cyanuric chloride (2,4,6-trichloro-1,3,5-triazine) and its fluorine analogue have long been used as building blocks for polymers and herbicides, however more recently they have been shown to exhibit biological functionality, specifically in tumour inhibition.[60, 61] Current chemotherapeutic agents that contain the 1,3,5-triazine moiety include hexamethylmelamine (HMM, Altretamine©), and 2-amino-4-morpholino-s-triazine both of which are used to treat ovarian and breast cancers (fig. 3.1).

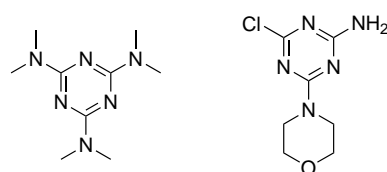


Figure 3.1: HMM (left) and 2-amino-4-morpholino-s-triazine (right)

The ability to progressively substitute the chlorine atoms of cyanuric chloride with nucleophiles allows facile access to a vast library of compounds with the same core structure, but also the ability to tune the substituents to fit a desired purpose, e.g. addition of hydrophilic side arms to increase water solubility.

Previous work has shown that imidazolyl moieties attached to the triazine core ex-

hibit inhibition of aromatase of the human placental microsomes, which are expressed excessively in breast cancers.[62] These compounds also include the presence of morpholino-, and thiomorpholino- moieties, with the most inhibitory compound being the bis(thiomorpholino)-imidazolyl-triazine, which has a 15x inhibitory affect when compared to the reference compound CGS-16949A (Fadrozole hydrochloride) (fig. 3.2).

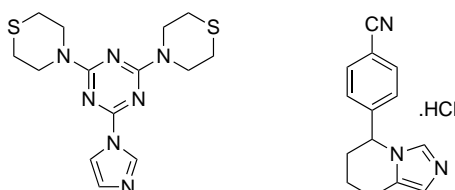


Figure 3.2: Bis(thiomorpholino)-imidazolyl-s-triazine (left), fadrozole hydrochloride (right)

Sulphonamide inhibition of carbonic anhydrases (CAs) has been known for a long time, with many different compounds currently being used clinically as antiglaucoma agents, antiepileptics and diuretics. However, some CAs are found more regularly in cancer cells than in normal cells, as they convert CO_2 into bicarbonate and allow the tumour cells to regulate their pH more effectively.[63] Acetazolamide (AAZ, Diamox[®]) was primarily used to treat glaucoma and epilepsy, but its ability to interfere with the mode of action of CAs (and hence reducing the pH) in tumour cells has allowed it to be used alongside existing cytotoxic agents as part of anticancer therapies. Further studies showed that other effective antiglaucoma agents have significant anticancer properties, these include methazolamide (MZA, Neptazane), and ethoxzolamide (EZA) (fig. 3.3).[64]

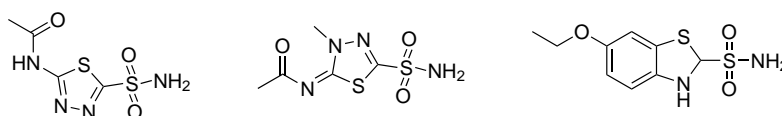


Figure 3.3: AAZ (left), MZA, EZA (right)

Work by Garaj has shown that triazines with attached sulphonamide show good inhibition of the tumour associated CAs I, II, and IX. Synthesis involved the 1:1 addition of sulphanilamide to cyanuric chloride followed by further functionalisation by addition of a series of amines, amides, and phenols, in a 1:2 ratio, affording the fully substituted triazine (fig. 3.4).[65] Higher levels of inhibition were noted for those compounds with

smaller moieties at the triazine core, whilst there was also high selectivity shown by those with acidic moieties towards CA IX which could be used as a methodology to target hypoxic tumours.

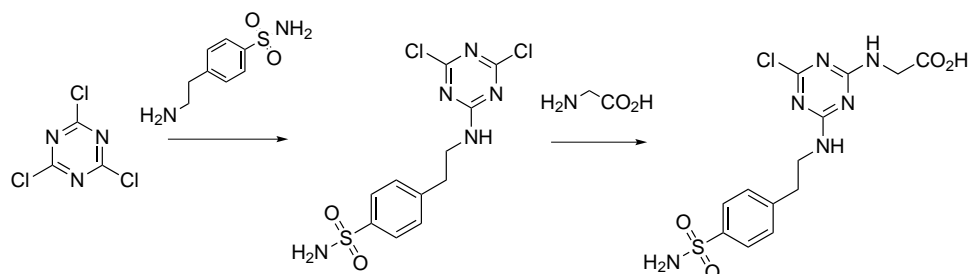


Figure 3.4: Synthesis of Garaj's most successful CA IX inhibitor

Dipyridamole (Persantine) has a similar core structure to that of cyanuric chloride, with a tetrasubstituted pyrimidopyrimidine core. The drug (fig. 5), used as a treatment for prevention of strokes, inhibits thrombus formation and is also a vasodilator, making it an attractive target for a PET active tracer. We believe that a similarly substituted triazine ring would be an interesting target as the interactive moieties would be the same, but there would be position left on the ring that would allow further functionalisation e.g. addition of a metal binding site.

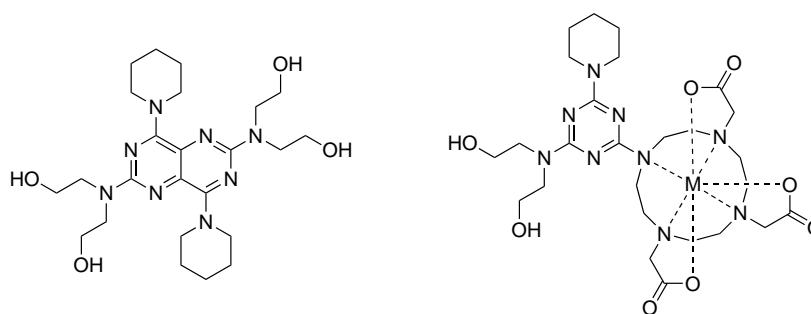


Figure 3.5: Dipyridamole (left), our target (right)

Integrins are heterodimeric glycoproteins containing *alpha* and *beta* subunits, which have, in mammals, been characterised into combinations of 18 *alpha* units, and 8 *beta* units. Integrins are important in biological mechanisms for cell-cell and cell-matrix interactions, and as such have been studied extensively. Tumour metastasis involves many cell-cell and cell-matrix interactions, for example transfer from one site to another through the blood or lymph systems and so inhibition of the protein is therefore

important in the treatment and diagnosis of cancers, oestoporosis, renal failure, and retinopathy.[66] The integrin $\alpha_V\beta_3$ is responsible for cells binding to proteins in the extracellular matrix (ECM), and has been found to be over expressed in many tumour cells, including osteosarcomas, neuroblastomas, lung/breast/prostate/bladder carcinomas, and melanomas.[67, 68, 69, 70] It is also important to consider that many diseases are caused by the misregulation of blood vessel growth for example rheumatoid arthritis, and so could also be diagnosed or treated if the over expression of these proteins could be traced.[71] The crystal structure of the integrin complexed with an arg-gly-asp (RGD) ligand was first published in 2002 by Arnaout, Shang, et.al, and showed inhibition of the molecule occurred through an RGD cyclic peptide.[72] The distance between the terminal ends of this cyclic peptide is around 14 Å, with one terminus being a glycidic acid moiety and the other being the guanidnyl moiety of arginine (fig. 3.6).

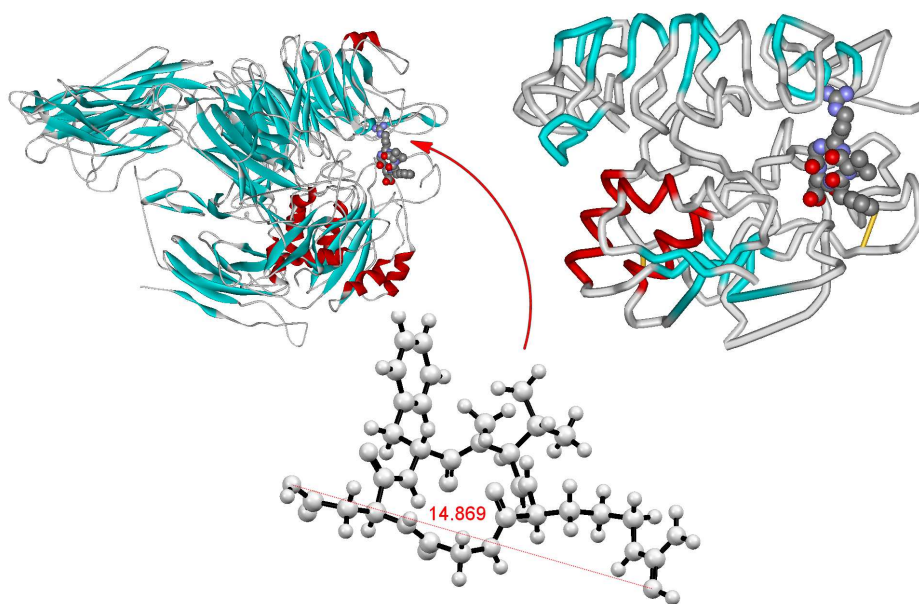


Figure 3.6: Integrin-RGD crystal structure (above), cyclic RGD peptide distance (below)

The RGD sequence is known as the "universal cell recognition site" as it is frequently found as the binding sequence for ligands to integrins (table 3.1), however there is a high selectivity for differing proteins all containing the RGD sequence for each integrin.[73] This selectivity is not fully understood yet, however the conformation of the peptide can alter the receptor selectivity and affinity.[66] It has also been shown that small changes to the sequence i.e. substitution of Asp with Glu, can result in a total loss of binding

affinity.[74]

Integrin	Ligand	Binding Sequence
$\alpha_2\beta_1$	Collagen Laminin	DGEA/ RGD <i>Unknown</i>
$\alpha_3\beta_1$	Laminin Collagen; Epiligrin Fibronectin	KQNCLSSRASFRGCVRNLRSLR <i>Unknown</i> RGD
$\alpha_4\beta_1$	Fibronectin VCAM-1	IDAPS/LDV/REDV/X-D-Y <i>Unknown</i>
$\alpha_5\beta_1$	Fibronectin	RGD
$\alpha_V\beta_1$	Fibronectin, Vitronectin	RGD
$\alpha_L\beta_2$	ICAM-1 ICAM-2, ICAM-3	KELLPLGNRNV <i>Unknown</i>
$\alpha_M\beta_2$	Fibrinogen Compliment 3bi	GGAKQAGDV <i>Unknown</i>
$\alpha_X\beta_2$	Fibrinogen	GPRP
$\alpha_{IIb}\beta_3$	Fibrinogen Fibronectin, Vitronectin, vWF, Thrombospondin	GGAKQAGDV/ RGD RGD
$\alpha_V\beta_3$	Vitronectin, Fibronectin, Fibrinogen, Collagen, Thrombospondin, Thrombin, Osteopontin, Bone Sialoprotein, Tenascin	RGD
$\alpha_{LRI}\beta_3$	Entactin	RGD
$\alpha_V\beta_5$	Vitronectin	RGD
$\alpha_V\beta_6$	Fibronectin	RGD

Table 3.1: Binding sites of selected integrins[73]

The distance between the active moieties (pharmacophors) of the RGD sequence has been shown to be important in the activity and specificity in inhibition of the integrin $\alpha_{IIb}\beta_3$, and can therefore be assumed that this also an important factor when designing integrin inhibitors.[75] Given that the distance between pharmacophors in the crystallised $\alpha_V\beta_3$ structure is 12 Å, any nonpeptidic target molecule must also be of this length.

3.2 Synthesis of Dipyridamole Analogues

As previously described, the use of cyanuric chloride as a model for the dipyridamole core affords the ability to add extra functionality to the molecule through substitution at the 3rd chloride. Addition of a DO3A moiety here allows facile access to metal complexes and therefore adds potential as a Cu, Ga or Y PET agent. Before synthesising the target compound, it was important to understand the conditions needed to add a

DO3A moiety to a triazine ring. Synthesis of symmetrically and asymmetrically substituted aminochlorotriazines with morpholino-, piperidino-, and thiomorpholino- side chains has been known for a long time and are simple one-pot reactions (fig. 3.7).[76] The reaction proceeds as an S_NAr type reaction with substitution of the chlorine atoms by the chosen amine.

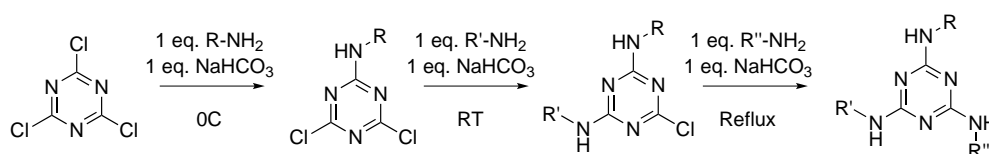


Figure 3.7: General synthesis of mono, bis, and tri substituted s-triazines

We prepared a sequence of symmetrically and asymmetrically substituted triazines to explore new reaction conditions (table 3.2). It was found that stirring at room temperature was sufficient for substitution of the second chlorine in moderate yield, where as in the previous literature, heating to around 40°C was required.[76] 1H NMR identification of the products can be difficult due to the lack of aromatic protons for integration, however, ^{13}C NMR gives a much better understanding of whether the reaction has given the mono- or bis- substituted products. Relative integration of the triazinyl quaternary carbons shows the carbon environment that is more populated, with the peak around 170 ppm representing the chlorocarbon and the lower peak being that of the substituted carbon.

R	R'	Yield (%)
Piperidine	Cl	66
Morpholine	Cl	61
Diethanolamine	Cl	77
Thiomorpholine	Cl	61
Piperidine	Piperidine	64
Piperidine	Diethanolamine	62
Piperidine	Morpholine	57
Morpholine	Morpholine	65
Diethanolamine	Diethanolamine	90

Table 3.2: Symmetrically and asymmetrically substituted triazines and yields

2,4-Dimorpholino-s-triazine was reacted with DO3A.HBr in acetonitrile in an inert atmosphere under reflux for 5 days to yield the trisubstituted s-triazine (TzMorph₂DO3A). A lack of unreacted DO3A was noted in the 1H NMR spectrum by a loss of a broad resonance above 10 ppm characteristic of DO3A.HBr, which is the result of proton co-

ordination to the DO3A core itself. Deprotection using TFA, followed by addition of metal acetate gave the desired metal complex (fig. 3.8). The addition of metal salt and its subsequent coordination was achieved in milligram scale, and complex formation was shown by high resolution mass spectrometry. The extremely long reaction time in comparison to that of mono- and bis- substituted triazines is believed to be due to a combination of the much less activated 3rd chlorine substitution along with the lower reactivity of the 4th amine in the macrocyclic ring.

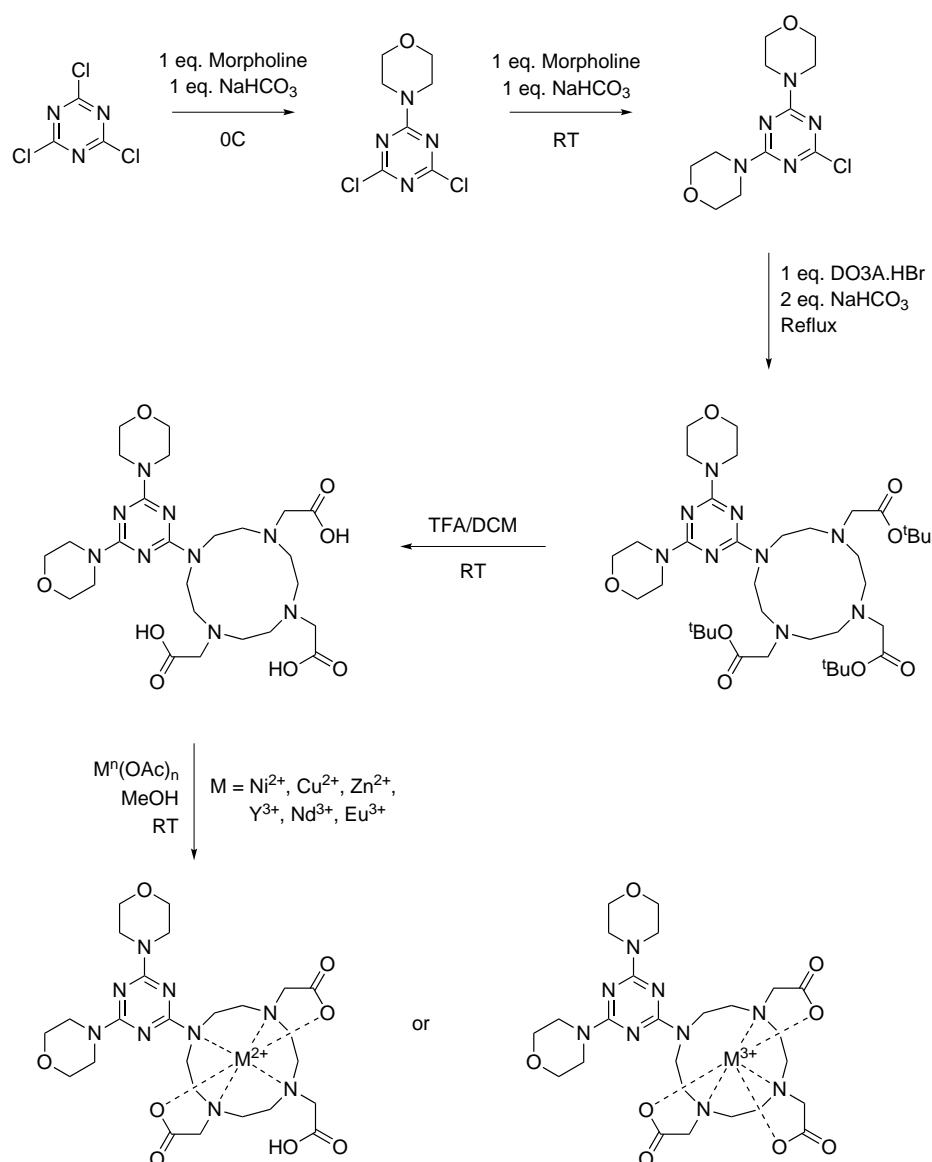


Figure 3.8: Synthesis of $\text{TzM}_2\text{DO3A}$ complexes

Attempts to grow crystals of these structures have so far failed. It was believed that

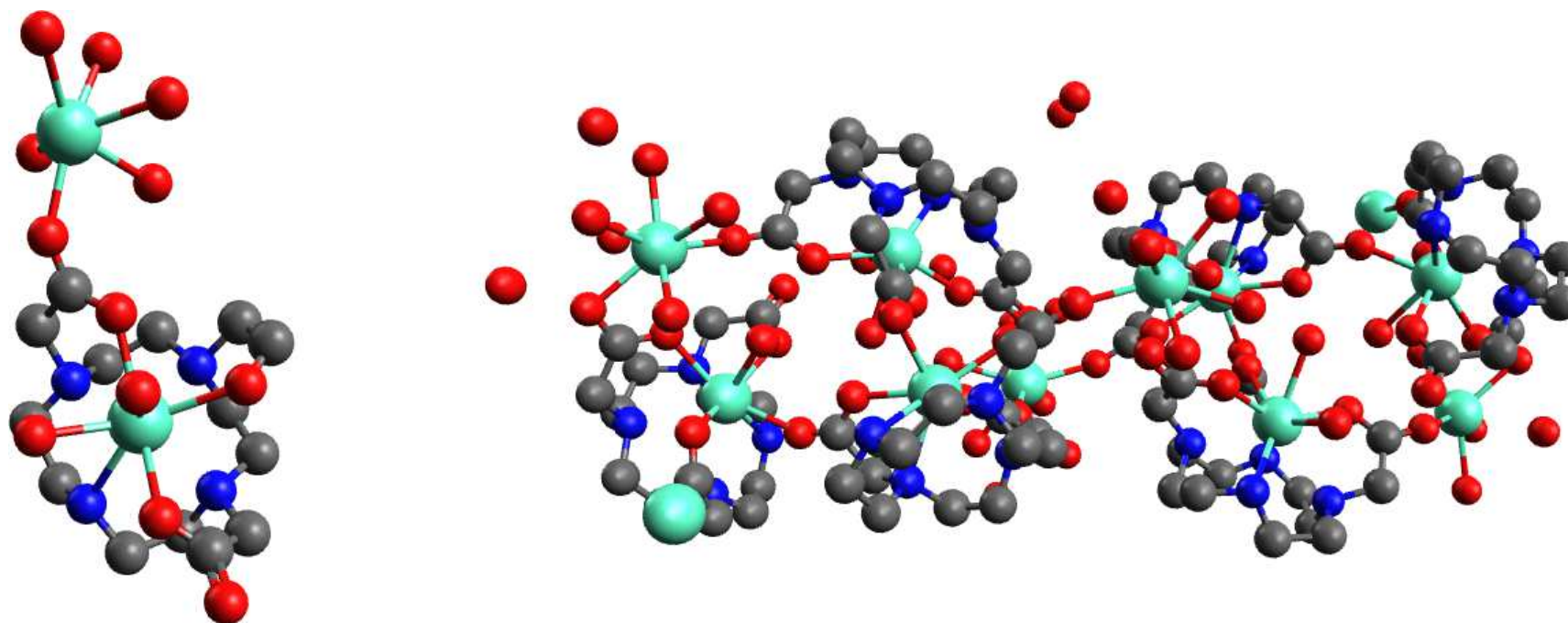


Figure 3.9: X-Ray structure of crystals from $\text{EuTzM}_2\text{DO}_3\text{A}$ coordination attempts simplified to show the 2 Eu environments (left), full (right)

crystals of a Eu complex had formed, however, the X-ray diffraction data shows the formation of a large ordered structure of Eu and DO3A (fig. 3.9) with the asymmetric fragment containing 5 Eu atoms in 2 environments (one environment being coordinated by DO3As and the other being an aqua-acetate coordination sphere) and a large amount of disordered water. This is believed to have formed by metal promoted cleavage of the N-triazine bond due to the lewis acidity of the metal chosen. As the triazine core is very electron deficient, addition of a lewis acidic metal to the DO3A moiety would make it an excellent candidate to act as a leaving group, and this we believe is what is seen in this crystal structure. A less lewis acidic metal such as lanthanum would most likely not cause this cleavage, and would be an interesting avenue to follow up.

DFT studies of the Ni, Cu, and Zn complexes show an interesting bend in the molecular structure, giving the molecules have a perceived boat formation (fig. 3.10). The DO3A fragment is bent back toward the triazine core, so as the metal centre is level with the triazine core. Bond lengths from the DFT have not been analysed, as with no real data to compare it against for accuracy.

The zinc(II) complex is a 5 coordinate N_3O_2 donor set species, with N_2O_2 forming a perfect square planar cavity (fig. 3.11). The amine furthest from the triazine ring also coordinates to the metal centre, whilst its acetate arm does not due to the charge neutrality of the complex. It is interesting to note that there is no bonding between the metal and the amine attached to the triazine, which is most likely due to the lone pair being withdrawn into the delocalised ring.

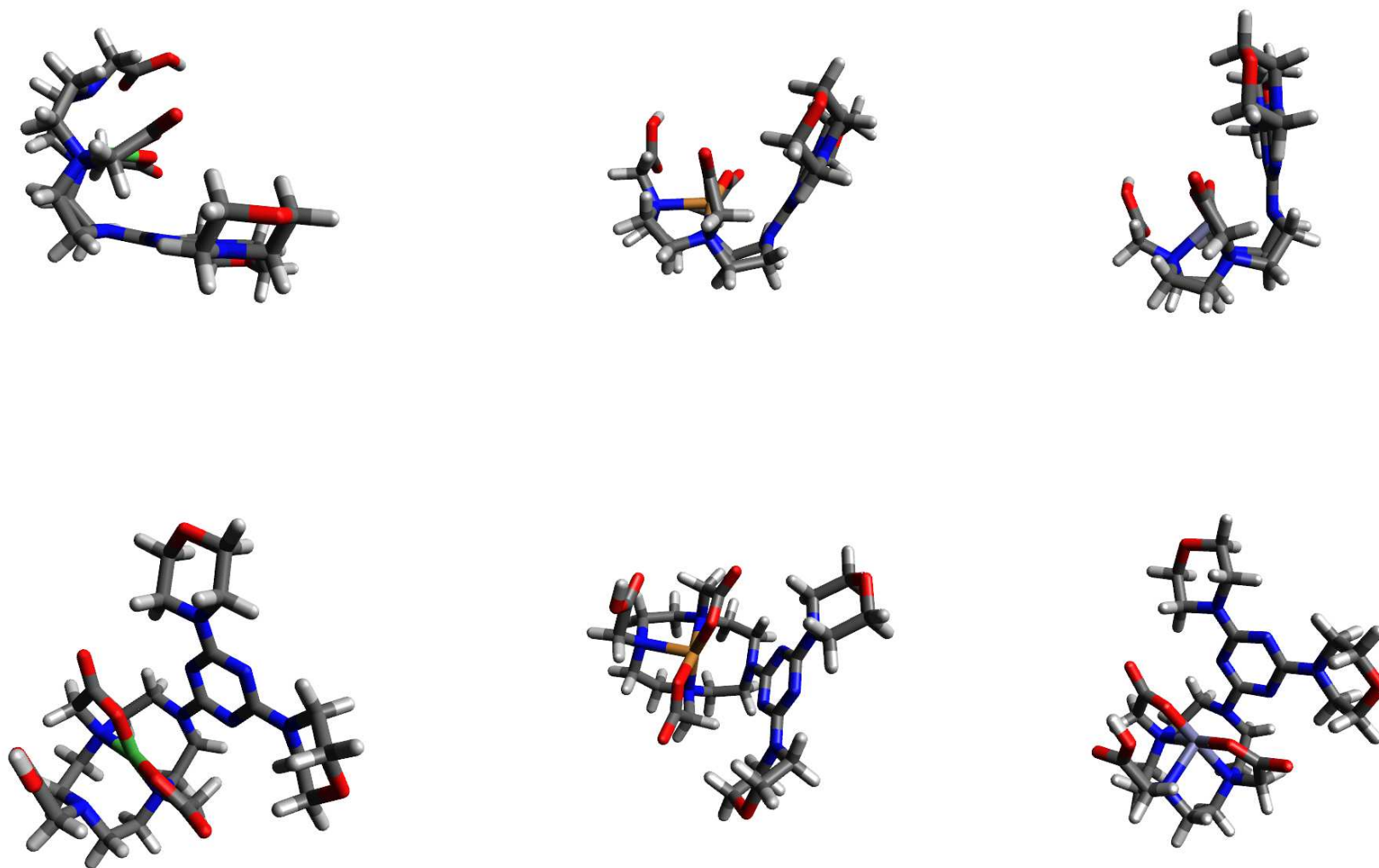


Figure 3.10: DFT calculated structures of Ni (left), Cu, and Zn (right) complexes. Above: side on view. Below: showing metal coordination pocket

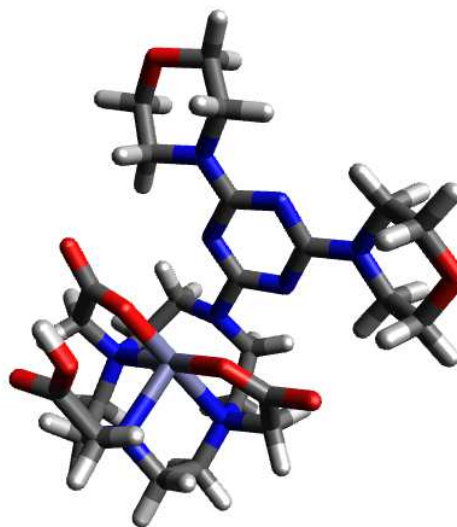


Figure 3.11: DFT structure of Zn(II) complex
Selected Bond Lengths: Zn-N(19) 2.306 Å, Zn-N(25) 2.289 Å, Zn-O(36) 1.960 Å,
Zn-O(42) 1.962 Å

The nickel(II) complex is a 4 coordinate N_2O_2 donor set species, forming a slightly distorted square planar structure, with no bonding of note between the amines attached to and furthest from the triazine (fig. 3.12).

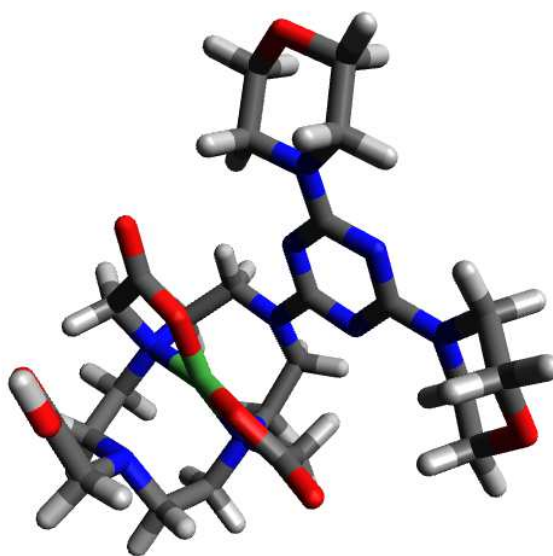


Figure 3.12: DFT structure of Ni(II) complex
Selected Bond Lengths: Ni-N(19) 2.016 Å, Ni-N(25) 1.995 Å, Ni-O(36) 1.845 Å, Ni-O(42) 1.853 Å

The copper(II) complex is a 5 coordinate N_3O_2 structure, with an elongated Cu-N bond to the furthest amine of the DO3A ring. The middle amines and acetates are arranged in a distorted square planar formation, with a much larger twist than the computed nickel complex (fig. 3.13).

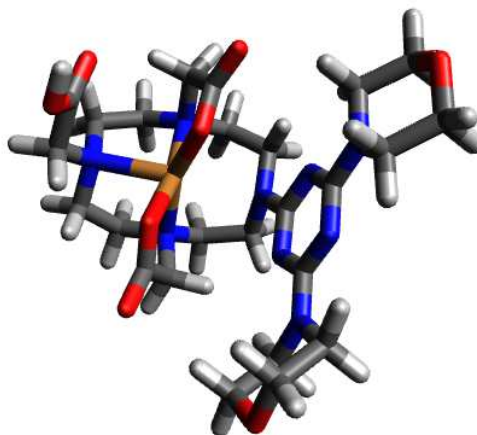


Figure 3.13: DFT structure of Cu(II) complex
Selected Bond Lengths: Cu-N(19) 2.128 Å, Cu-N(25) 2.097 Å, Cu-O(36) 1.911 Å,
Cu-O(42) 1.923 Å

3.3 Dendrimeric Triazines

Following successful addition of DO3A to substituted triazines, we decided to probe the success of addition of DO3A to unsubstituted triazines. Attempts to synthesise the mono-, bis-, and tris- DO3A-triazines were under taken, with successful addition of both one and two DO3A moieties. Addition of the third DO3A was believed to be unlikely due to the steric bulk of the DO3A moiety itself and the relatively small triazine core. It was found that addition of 3 equivalents of DO3A.HBr to a triazine slurry followed by reflux overnight afforded the bis-substituted product, and could be purified by recrystallisation away from the excess DO3A. Addition of 1 or 2 equivalents of DO3A.HBr gave the expected mono- (TzDO3ACl₂) or bis- (TzDO3A₂Cl) substituted triazines (fig. 3.14). The remaining chlorines could then be substituted with a smaller cyclic amine such as morpholine, to give an asymmetrically substituted triazine.

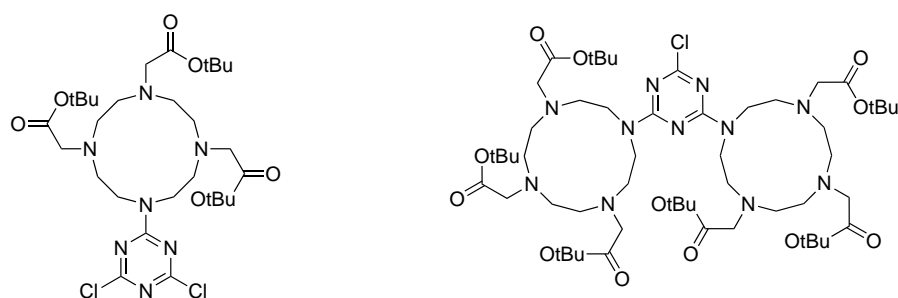
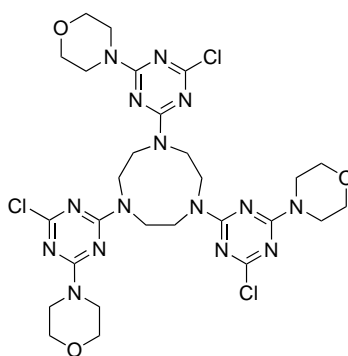


Figure 3.14: Mono- and bis- DO3A substituted s-triazine

We decided to use these DO3A-amino-chlorotriazines to make some interesting dendrimeric ‘snowflake’ compounds (fig. 3.17). Using a macrocyclic core – either TACN or cyclen – we are able to add the substituted triazines through an S_NAr reaction at the final chlorine, forming large, potentially highly symmetrical ligands, capable of coordinating multiple metal centres. The completely unsubstituted compound, TCl_6 , was accessed through addition of TACN to excess cyanuric chloride in the presence of base. Reaction of TACN with 3 equivalents of morpholino-dichlorotriazine (TzMorph₂Cl) resulted in the formation of a trisubstituted TACN ring with 3 triazines each with a morpholino and chlorine moiety (TM₃Cl₃ - fig. 3.15).

Figure 3.15: TM₃Cl₃

The 1H NMR shows a broad multiplet with little defining character, which can be attributed to the TACN and morpholine protons all being in a similar environments and at similar frequencies. The ^{13}C NMR is more complicated with a number of signals around a similar frequency, indicating the presence of rotamers, which would also contribute to the broad peak of the 1H NMR. Characterisation of the molecule was therefore difficult, and is based on the single species seen in the high resolution mass spectrum with a m/z

equal to that expected of the desired molecule (724.2245), and also a distinctive isotopic pattern, which matched that predicted for the compound. It was therefore preferable to have a totally symmetrical compound formed using the same conditions, so that the NMRs would be clear. The presence of 3 'free' chlorines on this structure allows access to further functionalisation of the molecule through substitution at these positions, and any reaction of the sort would also prove the starting material was as believed. The reaction of DO3A.HBr with the molecule resulted in the formation of a symmetrical DO3A – morpholine derivative (TD₃M₃). This was shown by distinct peaks in the ¹H NMR, and by the correct number of signals in the ¹³C NMR. Furthermore, the ¹³C NMR shows that the 3 triazinyl carbons are all in different environments, which would also be expected of this molecule. This therefore proves that the previous molecule was indeed as was expected.

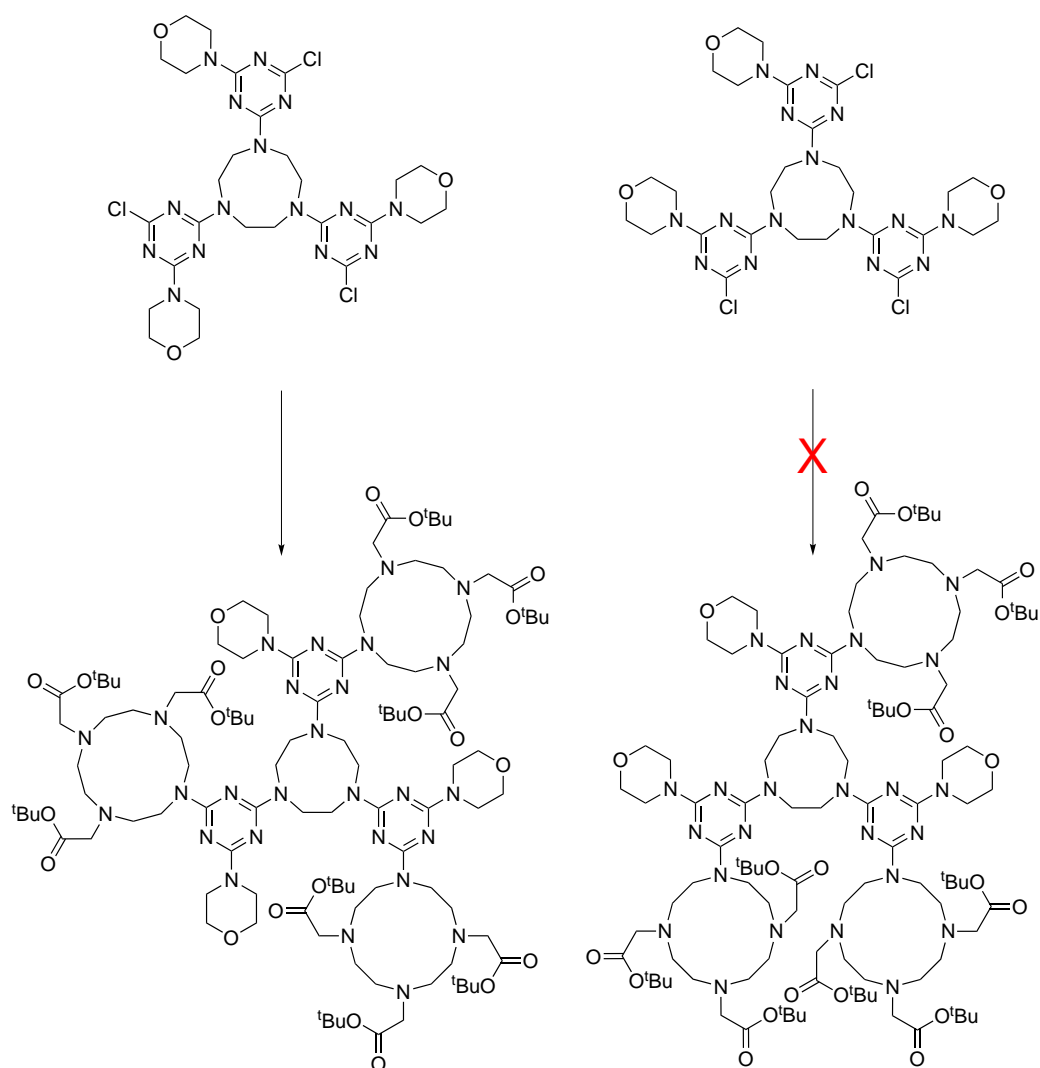


Figure 3.16: Steric explanation for lack of rotamers

The loss of rotamers explains the low yield. Formation of the molecule is sterically hindered when there are 2 DO3A moieties oriented in to the same space, meaning that these molecules will form with either the loss of a DO3A molecule, or will not form at all (fig. 3.16). It is believed that these possible reaction outcomes are removed during the work up, leaving the singular trisubstituted isomer only.

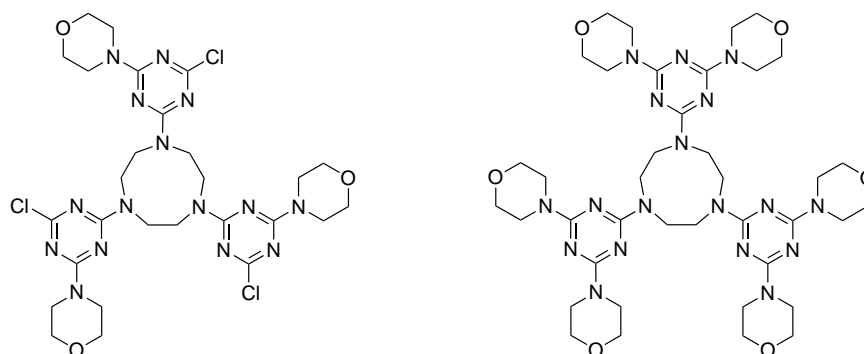
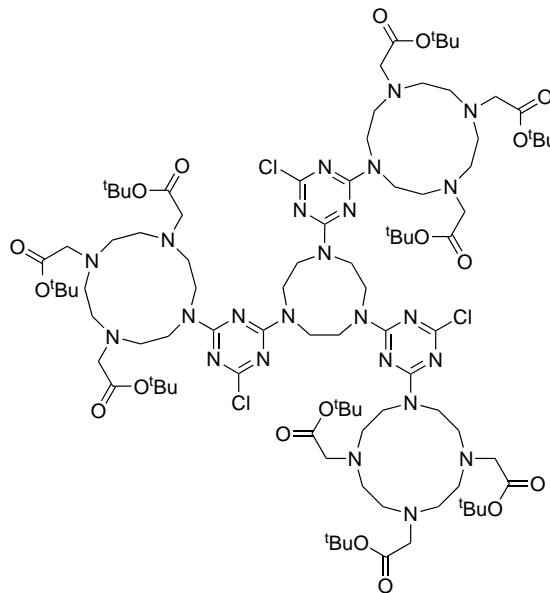


Figure 3.17: Morpholine dendrimers

Addition of bismorpholinochlorotriazine to TACN resulted in the expected trisubstituted TACN molecule, TM_6 (fig. 3.17). 1H NMR showed 2 distinct signals, one at 3.79 ppm attributed to that of the TACN ring, and a broader resonance at 3.74 – 3.61 ppm assigned to the morpholine rings. ^{13}C NMR shows the 5 signals expected of the C_3 symmetrical molecule, with 2 distinct triazinyl environments and 3 allylic carbon environments. High resolution mass spectrum shows the mass and isotope pattern expected of this molecule.

Figure 3.18: TD_3Cl_3 molecule

After success with the model compounds, synthesis of the DO3A analogues was undertaken. DO3A-dichlorotriazine ($TzDO_3ACl_2$) was reacted with TACN to form the trisubstituted TACN compound (TD_3Cl_3 - fig. 3.18). 1H NMR data showed the pres-

ence of distinct environments for the DO3A ring protons, TACN ring protons, acetate protons, and *t*-butyl protons, indicating no formation of rotamers. This was confirmed with ^{13}C NMR data which showed a number of signals that would be expected in a C_3 symmetrical molecule. The lack of rotamers is most likely due to the sterics of the compound, with large bulky DO3A moieties trying not to interact and thus forming in an ordered pattern.

3.4 Synthesis of RGD nonpeptidic mimic

In the RGD cyclic peptide the active pharmacophors are a guanidinyl and carboxylic acid group. This functionality can be added to the triazine core through the use of functionalised amines (*vide supra*). To this end, cyanuric chloride was reacted with 1 equivalent of the hydrochloride salt of ethyl glycine using the general conditions described previously, resulting in the mono-substituted triazine in moderate yields (66 %).

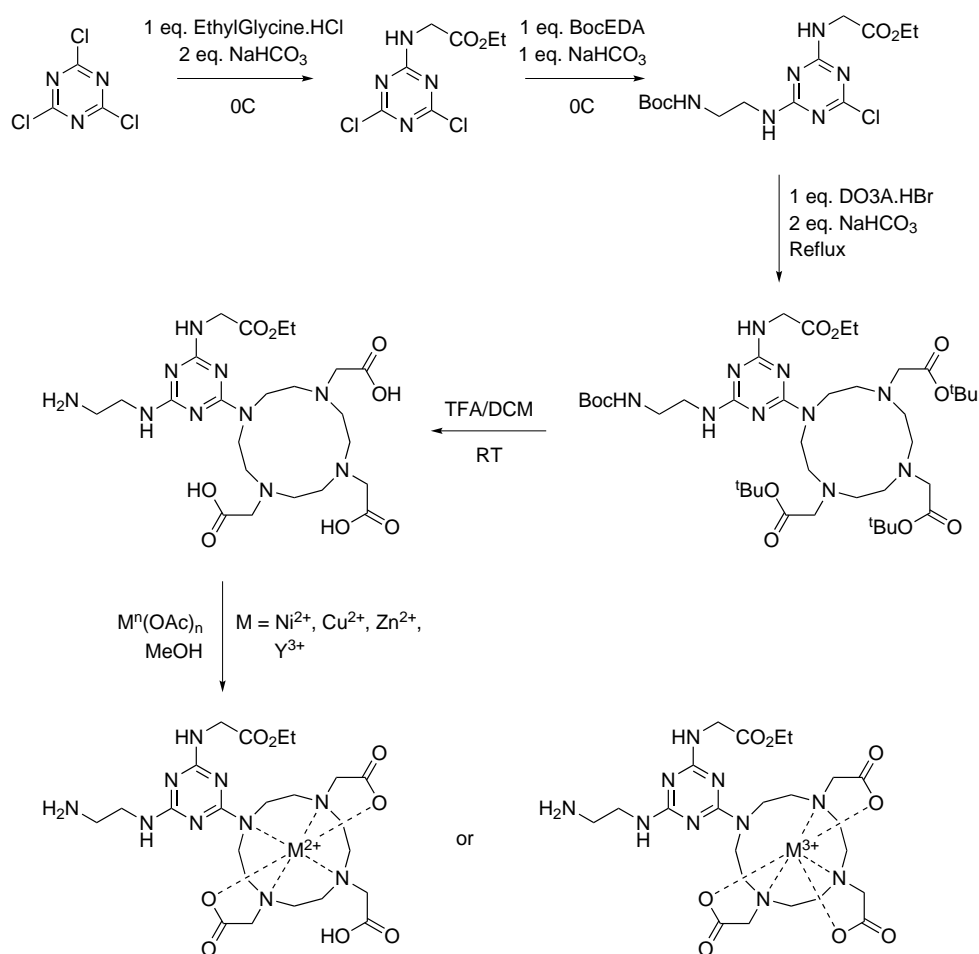


Figure 3.19: First attempt at preparation of the RGD mimic

Addition of the guanidyl moiety was initially attempted through a 2 step process; first, addition of a mono-Boc-protected diamine, and subsequent deprotection, followed by addition of a di-Boc-guanidinyll group to the terminal amine, which could then be deprotected yielding the target molecule. Both mono-Boc-ethylene diamine (Boc-EDA), and mono-Boc-propylene diamine (Boc-PDA) were synthesised by dropwise addition of Boc-anhydride into a large excess ($< \times 10$) of the required diamine under an inert atmosphere at 0°C. Removal of solvent and excess diamine *in vacuo*, and an acid/base work up, resulted in pale yellow oils of the required mono-protected diamines in reasonable yields (~ 50 %). Addition of the mono-protected diamines to the triazine core (TzEtGlyCl₂) using standard conditions yielded the required disubstituted intermediate, TzEtGlyBoc-E(P)DACl. Before deprotection of the terminal amine, substitution of the final chlorine at the triazine core was undertaken using DO3A.HBr, using the same

conditions as upon addition to the bis-morpholino compound, TzMorph₂Cl (*vide supra*). Deprotection using TFA then afforded the compound with an unprotected DO3A coordination core, as well as a free terminal amine. Addition of various d-block metals gave the desired metal complexes of the compound as shown by high resolution mass spectral analysis (fig. 3.19). Addition of the guanidinyl pharmacophore was explored through reaction of the terminal amine with a bis-Boc-mono-triflate-guanidine moiety previously reported by Feichtinger.[77] However the reaction did not proceed as expected, and ¹H NMR data suggested the isolated compounds did not include additional Boc moieties (incorrect integration of the peak at 1.5 ppm) and confusing signals in the aliphatic region, which are as of yet unidentified.

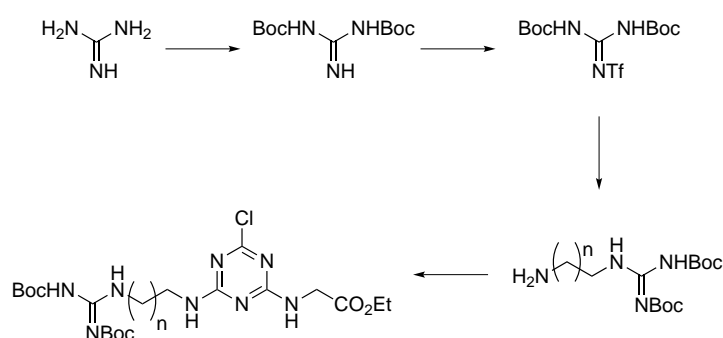


Figure 3.20: Synthesis of guanidine arm triazine

Conditions: i) Boc-anhydride, Dioxane, NaOH, 0°C ii) Triflic anhydride, Et₃N, DCM, -78°C iii) Diamine, Et₃N, DCM, r.t. iv) TzGlyCl₂, NaHCO₃, acetone/water, 0°C

It was therefore decided to synthesise the complete protected guanidinyl amine arm before addition to the triazine core. Synthesis of the protected guanidine using the method described by Feichtinger, followed by dropwise addition into a large excess of ethylene diamine in a manner similar to the mono-boc diamines, and purification by column chromatography (EtOAc/MeOH/Et₃N) yielded the desired monosubstituted diamines as previously reported by Castagnolo.[77, 78] Attempts to scale the reaction from that reported resulted in significantly lower yields, and thus was deemed unacceptable. It should also be noted that this method is not appropriate when wishing to use propylene diamine, as formation of a cyclic guanidine is favoured over the linear product.[78] However, if the compound were to be synthesised for PET purposes then the low yield would not be a hindrance as the required volumes of the target molecule are so small. Also if this reaction were to be automated the possibility of

parallel experiments would facilitate higher output of this key intermediate. Addition of the guanidinyll amine to the triazine core by the standard procedure was a success (TzEtGlyBocGuanCl), although the yield was relatively low for this step as well (23 %) (fig. 3.20). Due to the scarcity of the product and the difficulty in its synthesis, addition of the DO3A macrocycle and subsequent deprotection has not been attempted.

Click Chemistry

Although the DO3A group allows incorporation of various metal ions into the structure, we were interested in ways of easily incorporating other functionalisable moiety to the triazine core. "Click" chemistry was first described by Barry Sharpless, and is a chemical philosophy based on the way nature forms chemical bonds that allows a vast library of chemicals to be made from a few simple chemical reactions.[79] One of the most commonly used click techniques involves a [2+3] cycloaddition to an azide moiety forming the triazole, as the azides are generally stable to dimerisation and hydrolysis. Addition of an azide moiety directly to cyanuric chloride has already been used experimentally in the synthesis of more water soluble HMM based antitumour drugs, as well as in the formation of stable energetic materials.[80, 81] In the case of Simmonds, synthesis involved the addition of sodium azide to a solution of the disubstituted triazine in boiling acetic acid, followed by addition of water and recrystallisation from ethanol. Addition of an azide moiety to our disubstituted Boc-propylenediamine-ethylglycine triazine was achieved by addition of sodium azide to the monochloro-triazine in acetonitrile. Successful addition was shown by the addition of a band at 2137 cm^{-1} in the IR spectrum, consistent with that of an aryl azide, as well as high resolution mass spectrometry. Due to the availability of ^{18}F , we decided to 'click' on a glycidic alkyne chain, in order to perform a functional group conversion from an alcohol to a halide as the last step (fig. 3.21).

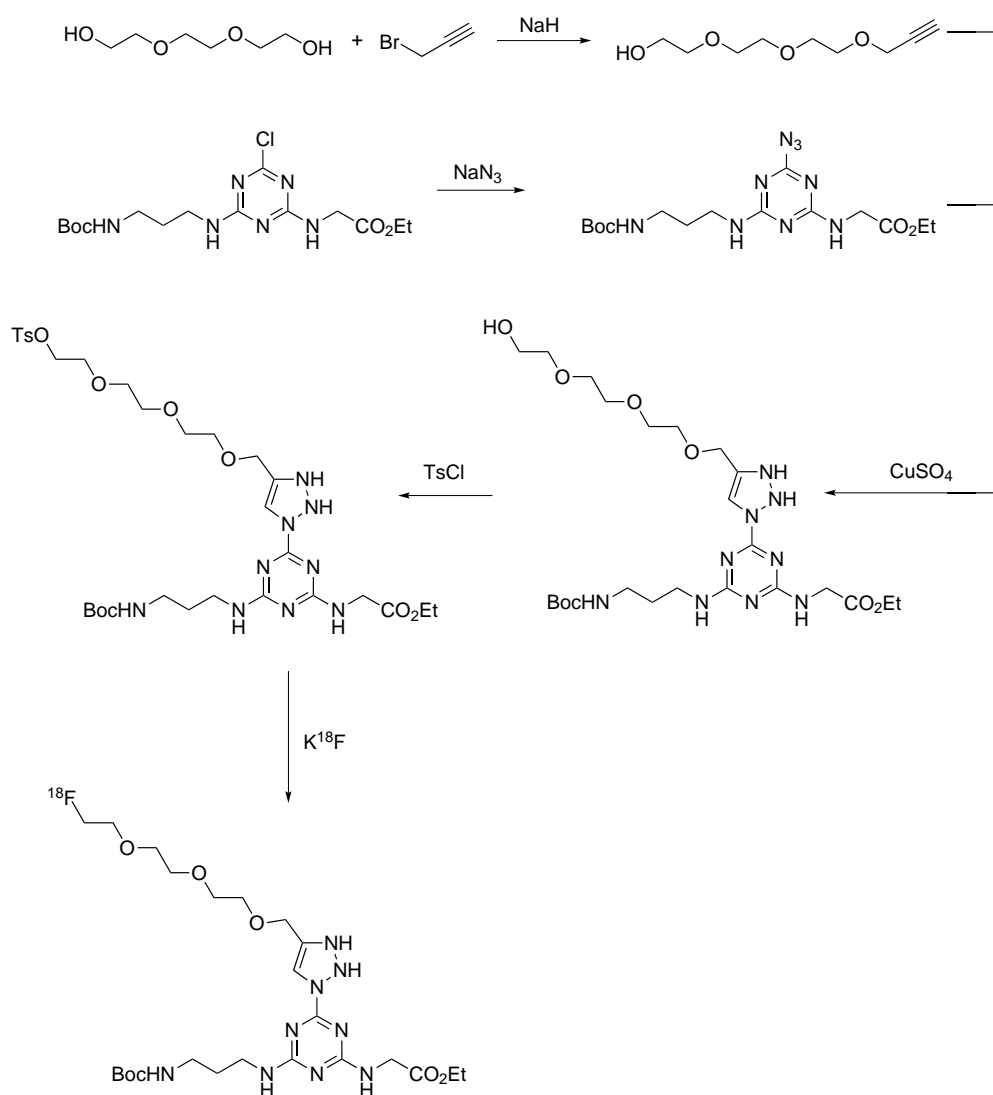


Figure 3.21: Click synthesis

Synthesis of the glycidic chain, AlkyGlycol, was achieved through addition of propargyl bromide to a large excess of triethylene glycol in the presence of a strong base (NaH). Extraction from water, followed by flash column purification yielded the target molecule as a yellow oil, shown in the ¹H NMR by the addition of an alkyne signal at 1.98 ppm. 'Clicking' of the alkyne to the azide was attempted with catalytic copper sulphate in the presence of ascorbic acid, yielding a mixture of products as shown by the ¹H NMR, including the desired product seen through the appearance of a triazole signal at c.4.2 ppm. So far attempts at purification of this molecule have failed.

Chapter 4

Acetate Functionalised TACNs as PET Agents

4.1 Introduction

Polyazamacrocycles have been found to exhibit exceptionally strong bonds to transition metals, which has made them ideal candidates for use in medical applications where the need for low dissociation constants is great.

Tetraazamacrocycles have been employed as successful chelators of PET active metals. The unsymmetrically substituted triacetic acid derivative of cyclen (DO3A) has found widespread use in molecular imaging as it was shown that the absence of one acetate arm (compared to the parent DOTA compound) had only a small effect on the metal dissociation constants.[82, 83] DO3A is best suited to large tripositive ions such as the lanthanides, whilst its use with smaller tripositive metals is possible but not ideal, due to the large cavity hole of the macrocycle. NO2A is a TACN analogue of DO3A, with one secondary amine available for derivatisation, and is much better suited for the PET metals considered in this work due to their smaller size (fig. 4.1).

NO2A as a bis-acid is most suited to chelation to a dipositive ion such as copper(II). With this in mind recent attention has turned to the synthesis of Cu-PET agents bearing a NO2A core. Synthesis of NO2A based compounds has so far centred on addition of a bridging moiety to the unsubstituted nitrogen centre to allow further functionalisation through the addition of the desired peptide chain using standard methods.[84]

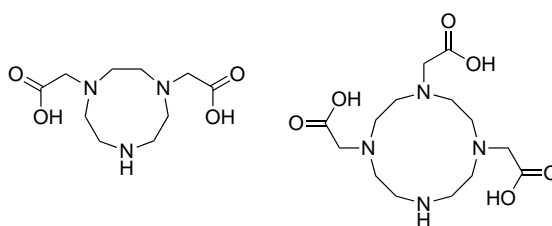


Figure 4.1: NO2A and DO3A

Copper(II) chelation has been achieved through addition of a copper salt to the desired chelating compound at neutral pH, followed by HPLC purification.

Recent work by McBride *et al.* has also shown the use of NOTA/NO2A derivatives to coordinate to an Al^{3+} atom, which can then bind strongly with an $^{18}\text{F}^-$ ion, allowing the complex to be used in PET imaging.[85] Studies have shown that this interaction between Al and F is much stronger than 60 other metals, whilst being selective for F over the other halides. McBride *et al.* used the commercially available p-SCN-Bn-NOTA starting material, to which they conjugated the desired peptide chain as previously reported.[86] The first complexes were synthesised by addition of an Al-F solution to the compounds, although later it was found that addition of the fluoride source could occur after addition of the Al salt, allowing for quicker (in terms of F decay) synthesis.

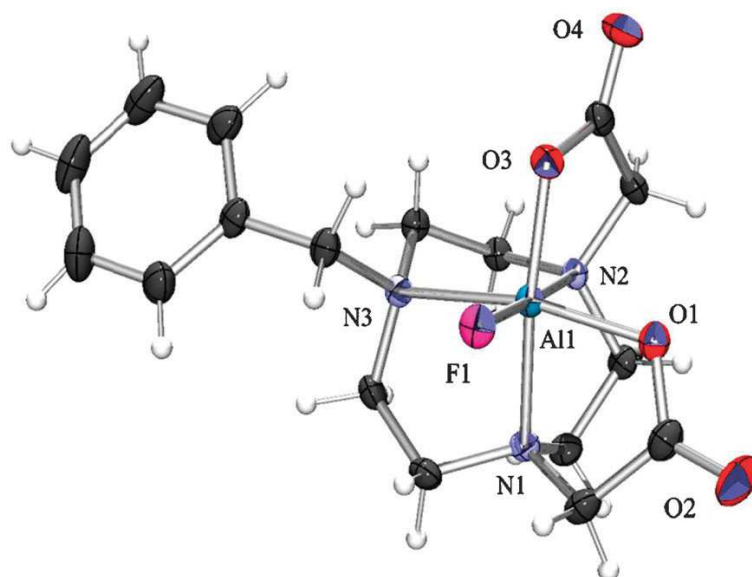


Figure 4.2: NO2A-Al-F complex

Single crystal structure data of a model NO2A-Al-F complex was obtained by Shetty *et al.* (fig.).[87] The complex was shown to form a series of 5 member chelate rings,

with the compound showing coordination to all of the TACN nitrogens on one face, and the acetic acid oxygen atoms on the other in a distorted octahedral geometry. Al-O bond lengths were comparable with the parent NOTA complex (1.8856(16) and 1.8446(16) Å vs 1.84 Å), whilst it was found the average Al-N bond lengths were slightly longer (2.083 Å) by 0.02 Å. The Al-F bond length of 1.709 (14) Å was comparable with the calculated bond length in diatomic Al-F, indicating a strong Al-F bond.

There is a strong history of TACN coordination chemistry in our group, and with the imminent arrival of ^{64}Cu and the current availability of ^{18}F at the Cardiff PET centre it was decided that we focus our efforts on the NO₂A derived complexes.

4.2 NO₂A derivatives

As discussed in previous chapters (3), it has been shown that sulphonamides act as carbonic anhydrase (CA) inhibitors. The presence of tosylate groups in the synthesis of TACN therefore lends itself to the formation of compounds that may act as CA inhibitors.

Selective detosylation of the triprotected TACN has been known for a long time, with methods of mono-, and tri-deprotections known - with diprotection best accessed through addition of one tosylgroup to monotosyl TACN (fig. 4.3).[88] Following the

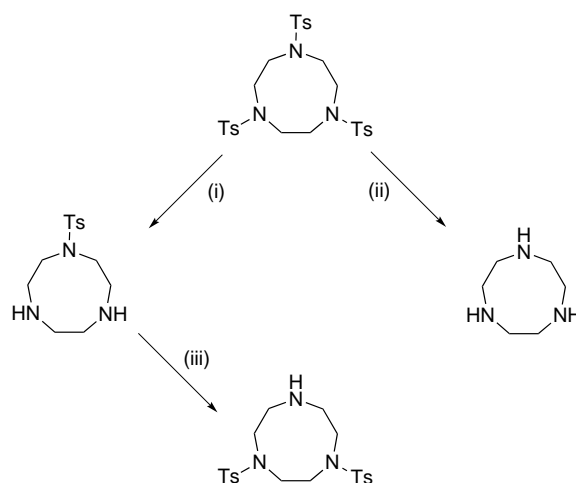


Figure 4.3: TACN deprotection routes

(i) 1. 33 % HBr/AcOH, PhOH. 2. NaOH (ii) H₂SO₄ (iii) TsCl, NaOH

established procedure by Sessler, formation of the monotosyl TACN was achieved.[89]

Addition of a slight excess of bromo *t*-butylacetate gave the desired NO₂A derivative in a high yield. Deprotection of the *t*-butyl group was accessed through addition of TFA to a DCM solution of the compound in the standard manner, and easily seen by a loss of *t*-butyl peak in the ¹H NMR spectrum. The deprotected compound was found to be slightly hygroscopic, and so was stored in a vacuum dessicator. Addition of copper acetate to a methanolic solution of the ligand resulted in a characteristic colour change from colourless to deep blue. mass spectrometry showed the presense of the desired complex and the expected isotopic pattern for the sodium salt. The UV-Vis spectrum showed a single peak at 645 nm ($\epsilon = 89 \text{ mol}^{-1} \text{ cm}^{-1}$) concordant with the ${}^2T_{2g} \leftarrow {}^2E_g$ transtion. Crystals suitable for x-ray diffraction were grown by vapour diffusion of diethyl ether in to acetonitrile. The crystal structure shows two discreet molecules, with methanol and acetonitrile in the crystal lattice (fig. 4.4). The copper atom sits in the centre of a 5 coordinate distorted square based pyramid arrangement, with the sulphonamide nitrogen filling the axial site. As expected in copper complexes, there is an elongation of the axial bond when compared to the equatorial bonds, this is due to the Jahn-Teller distortion effect (see page 5). The average Cu-O bond length over both molecules is found to be 1.927 Å which is comparable to those found by Spiccia *et al.* in their ethylene and butylene bridge NO₂A complexes (1.937 Å, and 1.940 Å respectively, see fig. 4.5).[90] The Cu-N_{base} bond lengths average at 2.007 Å, which almost identical to the Spiccia complexes (2.007 Å and 2.018 Å), whilst the average Cu-N_{axial} bond lengths of 2.4285 Å are significantly longer than those reported (2.203 Å and 2.227 Å). The longer axial bonds are believed to be caused by electron withdrawal from the nitrogen by the tosyl group, causing a weaker (longer) bond between the sulphonamide nitrogen and the metal centre. The angles at the base of the square pyramid are also slightly distorted, with O-N-N angles of 91.0° and 91.4° found in one moiety, and 91.4° and 92.4° in the other, this is caused by the rigidity imposed on the system by the TACN ring. The tosyl moiety bends away from the copper centre in both molecules due to steric reasons.

It has been previously reported by McBride that NO₂A compounds with aluminium coordinated can be used to coordinate a PET active fluoride ion.[85] We decided to test our compound with this theory and added AlCl₃ to a solution of free TsTACNA₂ in sodium acetate buffer (1 M at pH 3.5). Gentle heating and stirring followed by addi-

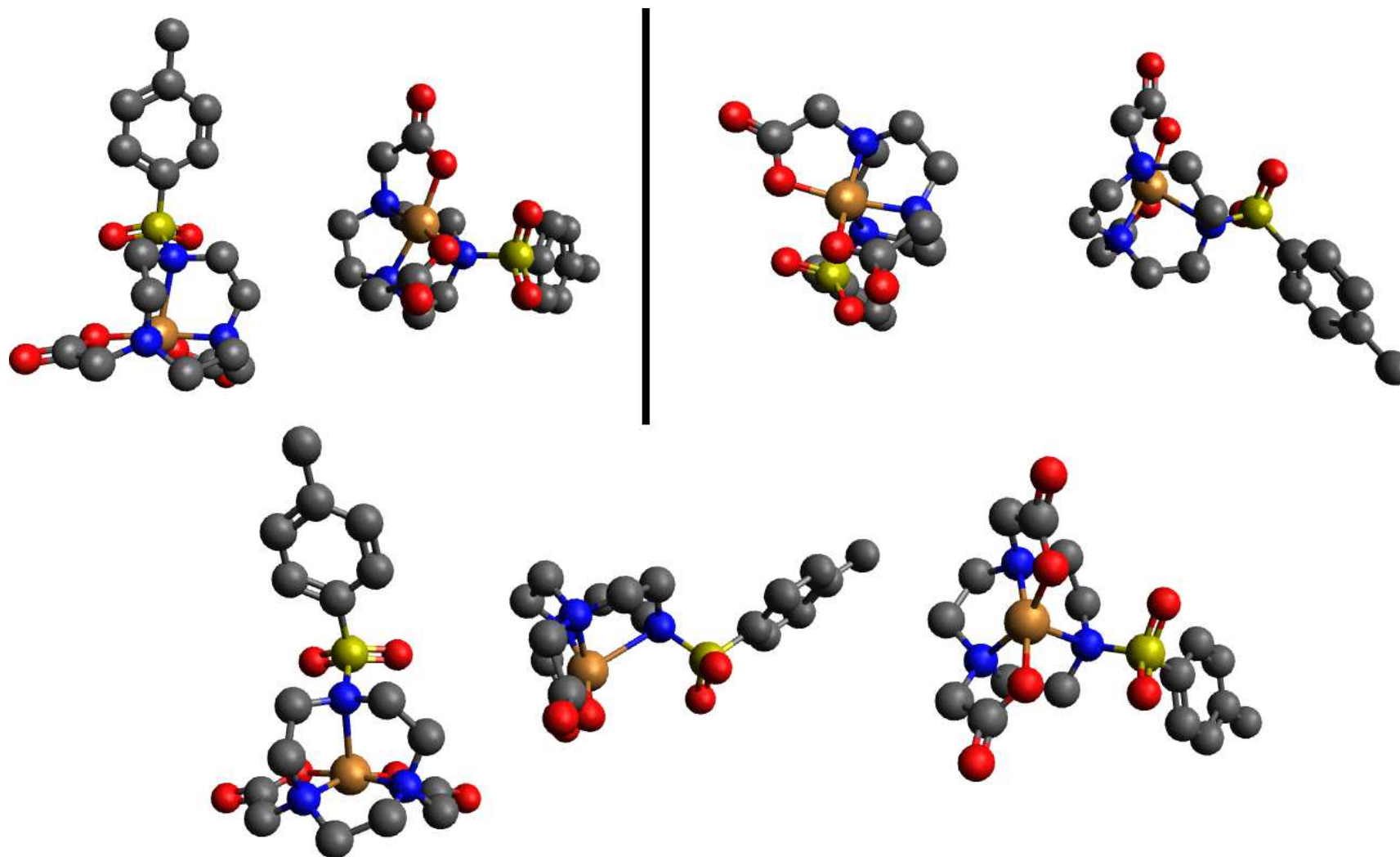


Figure 4.4: CuTsTACNA_2 (Hydrogens removed for clarity. Above: both units. Below: Single unit)
 Selected Bond Lengths: $\text{Cu}(1)\text{-N}(1)$ 2.009(3) Å, $\text{Cu}(1)\text{-N}(2)$ 2.004(3) Å, $\text{Cu}(1)\text{-N}(3)$ 2.429(3) Å, $\text{Cu}(1)\text{-O}(2)$ 1.934(2) Å, $\text{Cu}(1)\text{-O}(4)$ 1.920(2) Å,
 $\text{Cu}(2)\text{-N}(4)$ 2.017(3) Å, $\text{Cu}(2)\text{-N}(5)$ 1.998(3) Å, $\text{Cu}(2)\text{-N}(6)$ 2.428(3) Å, $\text{Cu}(2)\text{-O}(8)$ 1.930(2) Å, $\text{Cu}(2)\text{-O}(10)$ 1.924(2) Å

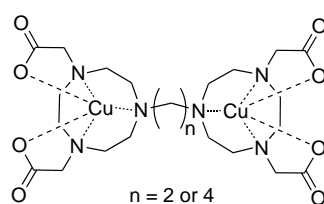
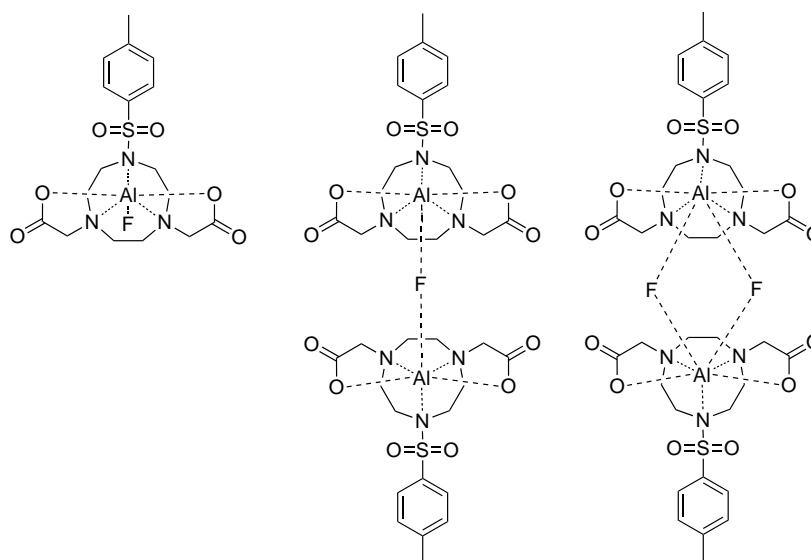


Figure 4.5: Spiccia's bridged NO2A complexes

tion of KF gave a colourless solution. Due to the scale of this test reaction, purification and isolation were not attempted. However, mass spectrum analysis show the presence of a series of related compounds, with the desired product, a bridge species, and an extended double fluoride bridge system seen in the spectrum (fig. 4.6). Further investigation and the reaction being repeated on a larger scale would allow a more thorough understanding of the bonding in these complexes and offer insights as to its potential use in PET imaging.

Figure 4.6: Bridged species seen in AlTsTACNA₂ mass spectrum

Due to successful synthesis of the acid derivative, the synthesis of the alcohol equivalent was also undertaken. Monotosyl TACN was reacted with an excess of enantiopure (R)-propylene oxide, yielding the desired product (fig. 4.7). Addition of copper(II) acetate as before gave a deep blue solution indicative of copper coordination. UV spectroscopy shows a single peak at 682 nm ($\epsilon = 57 \text{ mol}^{-1} \text{ cm}^{-1}$) associated with the ${}^2T_{2g} \leftarrow {}^2E_g$ transition. Growth of crystals suitable for x-ray diffraction was successfully achieved

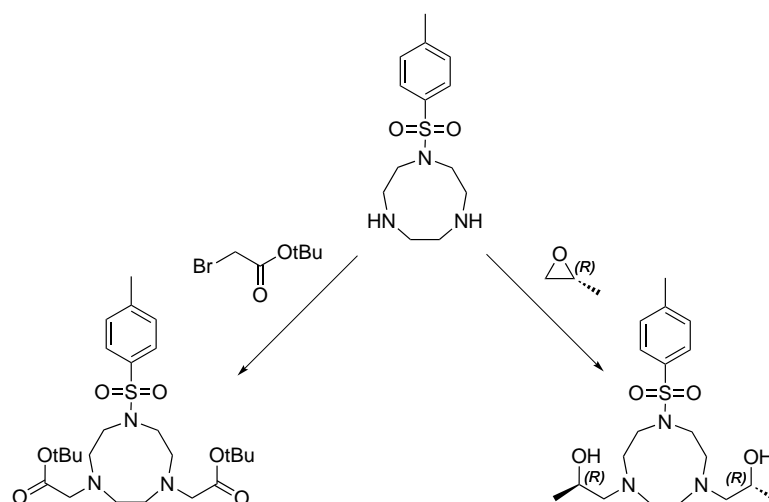
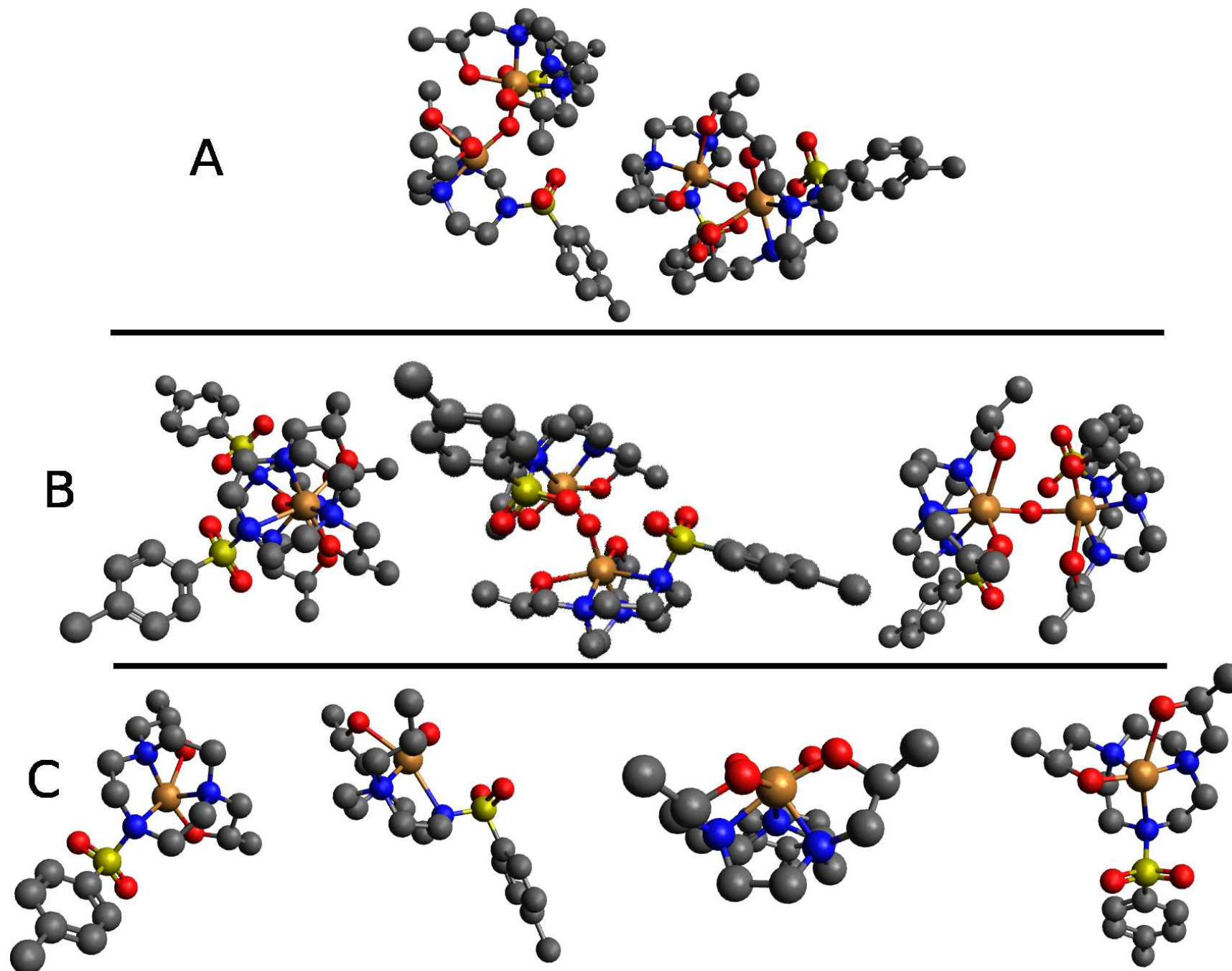


Figure 4.7: Monotosyl substituted TACNs

through slow evaporation of an ethanol/water solution. mass spectrometry showed the desired m/z and isotopic pattern for the complex. The structure shows the monoclinic P1 (1) space group, with 2 distinct complex units¹. (fig. 4.8).

The unit cell comprises of 2 different units of 2 CuTsTACNE₂ moieties bridged by a hydroxyl group. In both moieties the copper atoms sit in a distorted octahedral geometry, with an alcoholic oxygen, bridging hydroxyl, and two macrocyclic nitrogens occupying the equatorial positions, whilst the sulphonamide nitrogen and one alcoholic oxygen occupying the elongated axial sites. Although the moieties exhibit the same geometries they have distinct copper - hetero-atom bond lengths. In both cases though, the copper environments either side of the bridging water are identical. In one moiety, the Cu-alcohol bond length is found to be 1.962 Å in the equatorial position (Cu-O_e), and 2.547 Å in the axial position (Cu-O_a), showing an extreme lengthening of the axial bond, as would be expected for d⁹ Jahn-Teller distorted complexes. The bond length of the bridging oxygen to the copper centre (Cu-O_b) is found to be 1.989 Å, which is longer than its equatorial equivalent, but is explained as the electron density is split between two copper sites, and so bond strength would be expected to be weaker, thus producing a longer bond. The situation is made complicated for the Cu-N bond lengths as there are 3 separate nitrogen environments; sulphonamide nitrogen, ring nitrogen with alcohol moiety bound equatorially to the copper atom (N_{ring-e}), and ring nitrogen with

¹Data return by the Crystallography service was incomplete, with only cartesian coordinate returned. All bond lengths are found using the Avogadro program[91].



A

B

C

Figure 4.8: X-Ray structure of CuTsTACNE₂ (A: Both units. B: Single unit. C: Single copper moiety)

Selected Bond Lengths: Cu(1)-N(1) 2.077(9) Å, Cu(1)-N(2) 2.116(9) Å, Cu(1)-O(3) 1.969(8) Å, Cu(1)-O(4) 1.995(6) Å, Cu(2)-N(4) 2.023(10) Å, Cu(2)-N(5) 2.079(9) Å, Cu(2)-O(8) 1.997(8) Å, Cu(2)-O(9) 1.983(6) Å

axial alcohol moiety (N_{ring-a}). The sulphonamide nitrogen is bound in an axial position, and so has a long bond length of 2.641 Å, in keeping with the weak donor nature of a sulphonamide (although still within the combined van der Waals radii). The Cu- N_{ring} bond lengths are different by 0.012 Å, with the Cu- N_{ring-e} bond shorter at 2.080 Å, and the Cu- N_{ring-a} bond length 2.092 Å. In the second moiety this is found to be reversed, with the Cu- N_{ring-e} bonds longer than Cu- N_{ring-a} bonds by 0.004 Å at 2.056 Å and 2.052 Å respectively. It is also found that the bridging oxygen is bound more strongly than the alcohol oxygen, shown by the bond lengths 1.982 Å and 1.997 Å respectively. This also indicates that the copper is more strongly coordinated by the equatorial nitrogen atoms in the second moiety than in the first, as the bond lengths between Cu-N are relatively shorter, and the Cu-O bond lengths relatively longer than their immediate relatives. This is also seen by longer bonds to the axial atoms, with the Cu- $N_{sulphonamide}$ bond length 2.726 Å (vs 2.641 Å), and Cu- O_a bond length 2.565 Å (vs 2.547 Å).

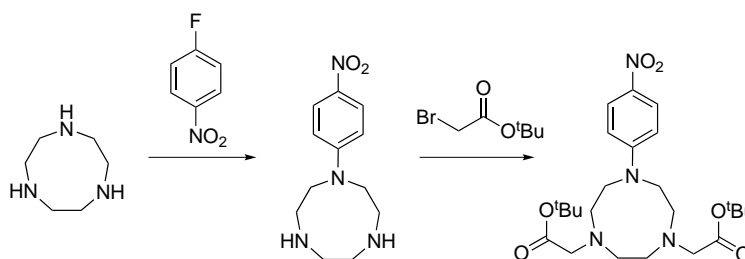


Figure 4.9: Synthesis of NPhTACNA₂

The success of the tosyl compounds lead us to try and add a potential linker group to triazine molecules as discussed in chapter 3, allowing facile access to a library of 'PETable' target specific compounds. The triazine moiety reacts well with amines, so addition of an amine group to the TACN molecule was sort. Use of our fluoronitrobenzene-TACN chemistry as described in chapter 2 would allow access to an amine through reduction of a nitro moiety. Addition of 4-fluoronitrobenzene to an acetonitrile solution of TACN without the presence of base yielded (after recrystallisation) pure the desired product. Addition of 2.2 equivalents of bromo ^tbutylacetate gave the desired NO₂A derivative in good yield (fig. 4.9). Deprotection by TFA and addition of copper acetate in methanol as before gave a deep blue solution indicative of TACN coordinated copper. mass spectrometry showed the correct m/z and isotopic pattern for the desired complex. Slow evaporation of the methanolic solution gave crystals of suitable quality

for x-ray analysis (fig. 4.10).

The complex is found to have a monoclinic, $p 21/c$ space group with each unit cell containing a single complex molecule and the ligand forming an N_3O_2 donor set. Whilst similar values are noted for the Cu-O bond distances (1.9245(15) Å and 1.9323(16) Å²), 3 different distances are seen for the Cu-N bond. The average Cu-O bond distance of 1.927 Å is identical to that of the CuTsTACNA₂ complex (*vide supra*). The shorter Cu-N bond distances of 1.9945(18) Å and 2.0195(17) Å occur for the acetate substituted nitrogen centres that use the equatorial coordination sites, whilst the longer value of 2.4464(17) Å found along the nitrophenyl substituted nitrogen bond, occurring in an axial geometry. This is a similar value to that found in the CuTsTACNA₂ complex showing the nitrophenyl moiety to have a similar electron withdrawing strength to the tosyl group as well as the Jahn-Teller distortion associated with Cu(II) complexes. UV spectroscopy showed a single peak at 603 nm ($\epsilon = 82 \text{ mol}^{-1} \text{ cm}^{-1}$) resulting from the ${}^2T_{2g} \leftarrow {}^2E_g$ transition.

4.3 PET Data

The compounds TsTACNA₂, NPhTACNA₂, and TsTACNE₂ were deemed to be successful enough for PET studies. The studies were undertaken at the University of Alberta, by Dr. James Knight, and currently only preliminary results for TsTACNA₂ and NPhTACNA₂ is available. The maximum specific activity of the complexes was assessed through addition of ${}^{64}\text{Cu}(\text{OAc})_2$ (1 MBq) to a dilution series of the ligand (2.5 → 50 ng). The radiolabelling efficiency is determined through radio-TLC (MeOH/10% NH₄OAc on C18 plates) where any uncoordinated ${}^{64}\text{Cu}(\text{OAc})_2$ remains on the baseline. The results show maximum efficiency occurs for both complexes above 20 ng, with a strong drop off for concentration under 10 ng (fig. 4.11).

An HPLC purification method³ was also obtained for each ${}^{64}\text{Cu}$ complex with retention times for the copper complexes being shorter than those of the ligand: CuTsTACNA₂ = 16 mins, TsTACNA₂ = 20 mins; CuNPhTACNA₂ = 14.5 mins, NPhTACNA₂ = 21

² Full refinement data was not supplied, so no root mean squared values were available.

³ Phenomenex C18 Luna column, linear gradient from 100:0 (H₂O : MeCN) to 0:100 (H₂O : MeCN)

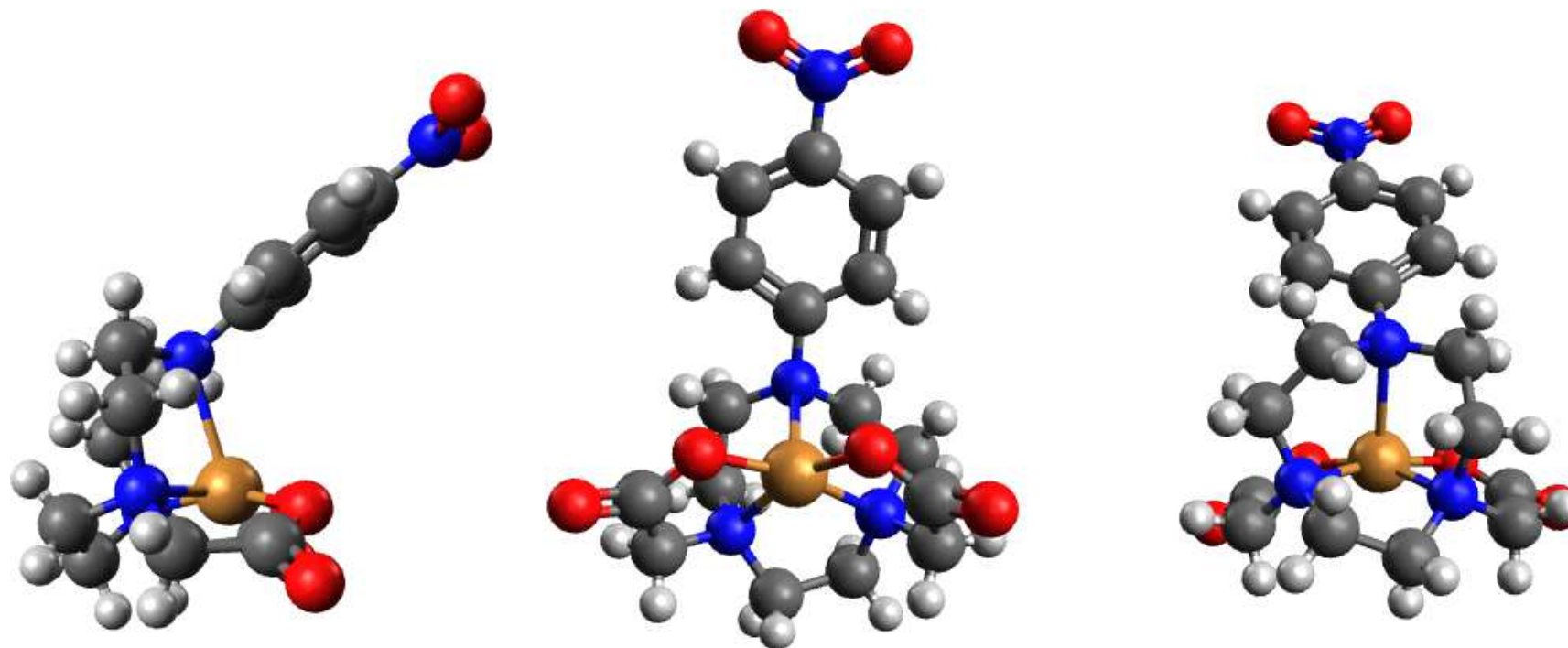


Figure 4.10: Single crystal structure of CuNPhTACNA_2
Selected Bond Lengths: Cu-N(1) 2.4464(17) Å, Cu-N(2) 2.0195(17) Å, Cu-N(3) 1.9945(18) Å, Cu-O(1) 1.9245(15) Å, Cu-O(3) 1.9323(16) Å

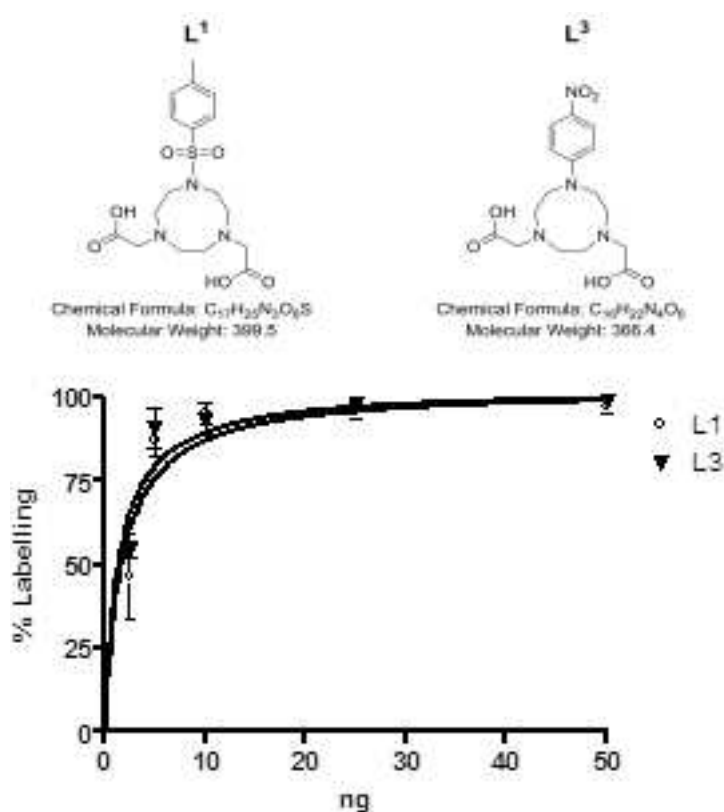
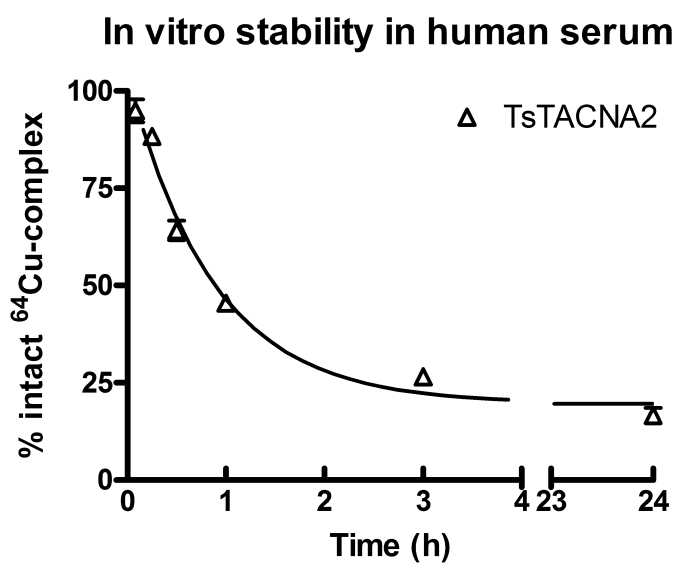
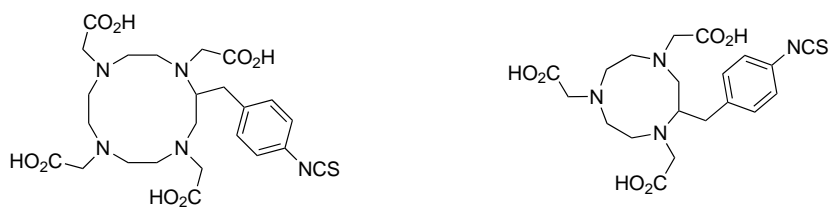


Figure 4.11: Radiolabelling efficiency of CuTsTACNA₂ and CuNPhTACNA₂

mins. \log_p values were also determined for the complexes showing the partitioning of the complexes between water and octan-1-ol. Values of -1.69 (CuTsTACNA₂) and -1.63 (CuNPhTACNA₂) show the hydrophilic nature of the complexes.

The stability of the CuTsTACNA₂ complex in human serum was also studied. Human serum was added to a solution of the ⁶⁴Cu complex, this was shaken (400 rpm) at 37 °C and the percentage of remaining ⁶⁴Cu complex was analysed by reverse phase radio-TLC (*vide supra*). Measurement were taken after 7.5, 15, 30, and 60 minutes as well as at 3 and 24 hours (fig. 4.12). The percentage of ⁶⁴Cu complex remaining after 1 hour fell quickly to around 50 %, with a similar fall to 25 % noted after 2 hours. The value of intact complex stayed steady at around 25 % for the 24 hour period. This stability compares badly with C-substituted full acetate macrocycles such as *p*-SCN-Bn-DOTA and *p*-SCN-Bn-NOTA (fig. 4.13) that commonly have stabilities of > 50 % after t = 12 hrs.[92]

Figure 4.12: Stability of CuTsTACNA_2 complex in human serumFigure 4.13: *p*-SCN-Bn-DOTA (left) and *p*-SCN-Bn-NOTA (right)

Chapter 5

Other Work

This section of the thesis is about some of the side projects that developed throughout the course of our investigation. The work contained herein is unfinished, but the early results are interesting and further work could result in the formation of further final year projects, or PhDs.

5.1 Glutamate Chemistry

5.1.1 Introduction

During the research into RGD non-peptidic mimics, we aimed to make a compound where the arginine residue was replaced by a functional chelating moiety. The theory behind the idea is that the rigidity of the chelate would increase the bond strength between the metal and the ligand, whilst at the same time forcing the position of the outer groups into one more akin to that in the RGD-Integrin crystal structure (62). Initial DFT calculations suggested that a homopiperazine ring with appropriately functionalised benzene rings would be too long for the coordination site on the protein ($\sim 18 \text{ \AA}$ as against coordination site length of $\sim 12 \text{ \AA}$, fig. 5.1).

Substitution of the functional groups directly onto the macrocycle would therefore be needed. The use of a bis-acid arm was theorised as one acid could act as the acetate arm common to good PET chelators (DO3A, NO2A), whilst the other would function as the coordinating ligand to the protein site (fig. 5.2).

Alternatively, the 'outer' acid could be converted into an aspartate mimic through amide synthesis. As well as getting the 'spacer' length correct for the molecule, we

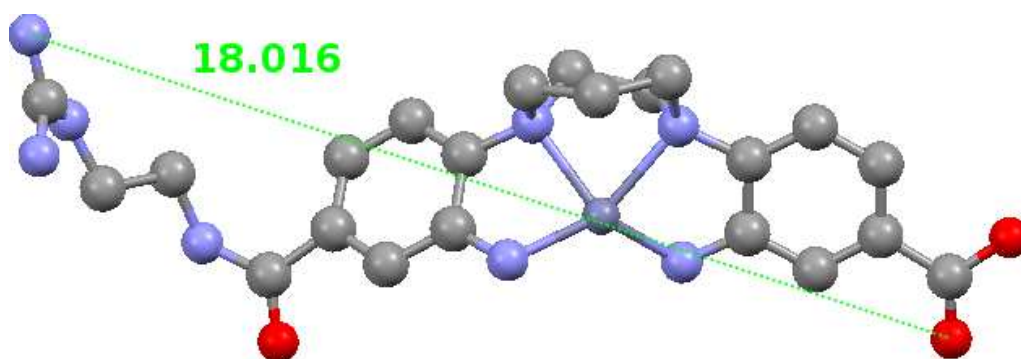


Figure 5.1: DFT calculated distance of model compound

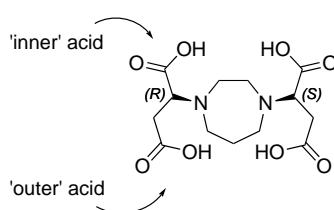


Figure 5.2: Inner/outer acid shown on direct substitution of macrocycle

believe that adding chirality to it will also increase the binding to the specific integrin. The use of amino acids allows facile access to the introduction of chirality as amino acids are inherently chiral. Whilst formation of macrocycles from amino-acids directly is known, we wanted to use a generic core, followed by addition of targeting pendant arms that could be more easily changed in a modular way, than by total synthesis from step one.[40] Functional group interconversion of the amine group of an amino-acid to a bromine would allow an S_N2 addition of the amino-acid to the nitrogen atoms of the macrocycles. Such interconversion of an amino-acid amine to a halogen can be easily accessed through diazotisation, and addition of the appropriate acid (e.g.. for Br, HBr), as shown by Koppenhoefer.[93] The exact length of the chain needed could not be usefully calculated by DFT, so we planned on forming a series of compounds with varying chain length and determining the best by in vivo studies.

5.1.2 Amino acid type bis-acid interconversion

Formation of the desired halogenated bis-acid was first attempted with aspartic acid. Before diazotisation, the acid groups were protected as simple ethyl esters, using the standard acid catalysed reaction. The aspartate ester was diazotised with sodium nitrite, and then added dropwise to HBr (fig. 5.3). Polarimetry (qualitative) of the com-

pound showed there had been a racemisation. This can be rationalised through an E_2 elimination of the diazonium in solution to give the racemic product. E_2 elimination is likely given the acidic nature of the β -proton and would result in the formation of a fumarate. Addition of bromide to the fumarate could occur from either face, and hence form a racemic mixture. If the nature of the substitution were S_N2 , as expected then there would be no loss but rather an inversion of chirality, whilst S_N1 substitution would result in racemisation through the planar transition state.

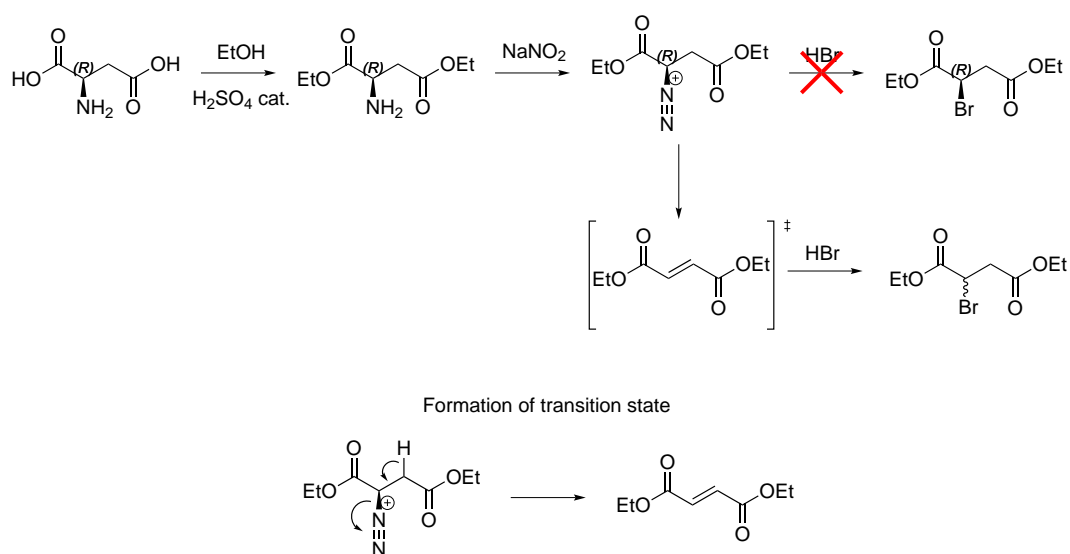


Figure 5.3: Attempted synthesis of ethyl bromosuccinate

To overcome this problem, glutamic acid was used. The extra carbon in the backbone means that the β -proton is less acidic due to resonance structures, and so E_2 elimination should be stopped. Glutamic acid was protected as the ethyl ester as before, and diazotised with sodium nitrite, followed by dropwise addition to HBr. Polarimetry (qualitative) indicated chirality in the molecule, and so the ethyl bromoglutamate could be used in the next step confident of its chirality.

5.1.3 Synthesis of Glutaric Macrocycles

Addition of the glutamate pendant arms to homopiperazine, TACN and 1,8-dimethylcyclam (DMC) was attempted. Addition of a slight excess of ethyl bromoglutamate to each macrocycle in the presence of equal moles of base resulted in the fully substituted

macrocycle (fig. 5.4).

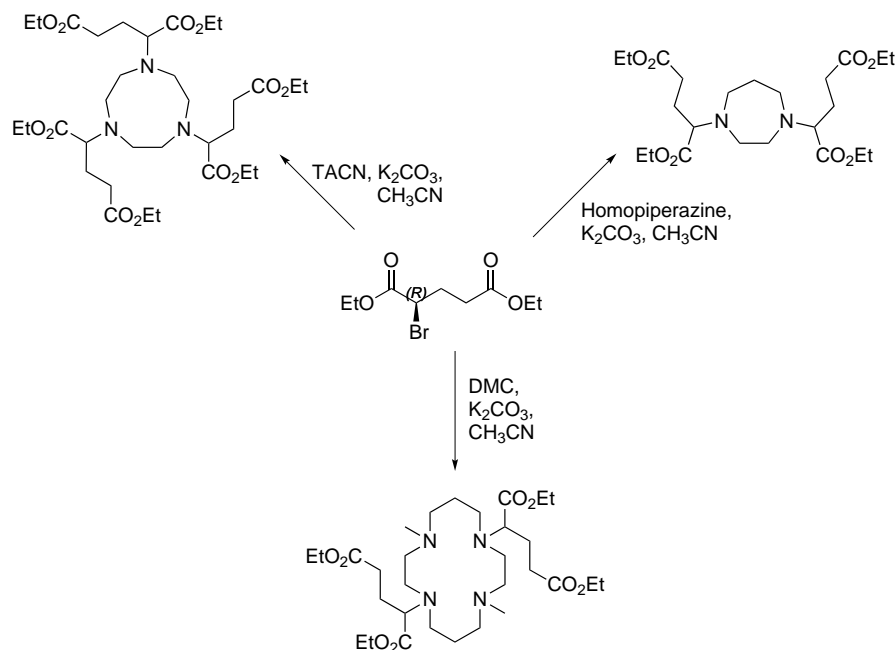


Figure 5.4: Synthesis of glutarate functionalised macrocycles

Acid hydrolysis of the ester function resulted in the formation of the salt of the free acid. Before coordination this salt must be neutralised. Attempts to synthesise partially substituted macrocycles always resulted in the presence of multiple species in the mixture, and separation of these species was not attempted. Coordination of a metal to the macrocyclic compounds was accessed through addition of NaOH until neutral (as shown by pH paper) and addition of metal acetate to an ethanolic solution of the ligand (fig. 5.5). Slow evaporation of an ethanolic solution of the CuDMC-Glut complex yielded crystals suitable for x-ray diffraction (fig. 5.6).

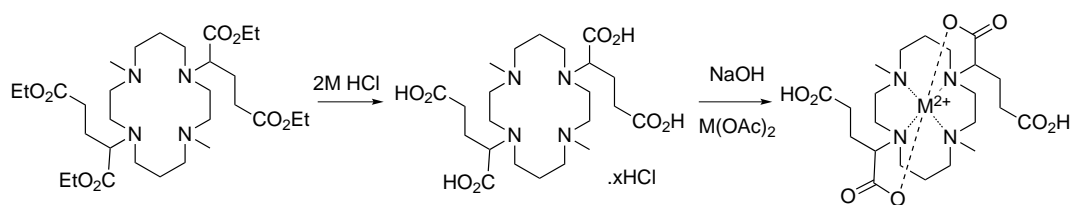


Figure 5.5: Synthesis of metal complexes

The CuDMC-Glut crystals exhibit a triclinic unit cell in the P-1 space group. It is C_2 symmetrical and the copper sits in the middle of a distorted N_4O_2 octahedron. The distance between 'outer' acid groups is found to be 11.5 Å, which is very close to the

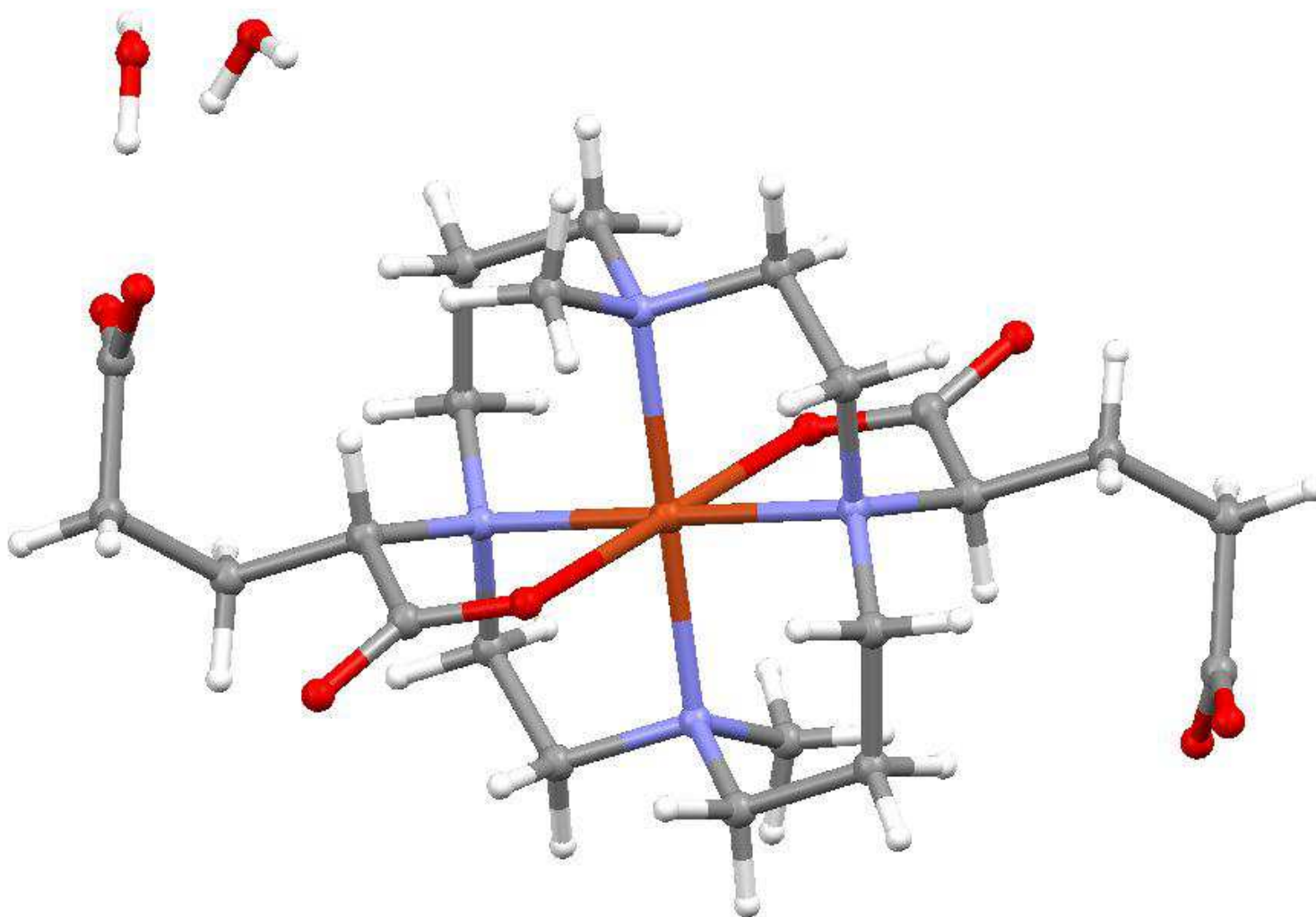


Figure 5.6: CuDMC-Glut X-ray structure
Selected Bond Lengths: Cu-N(1) 2.12(3) Å, Cu-N(2) 2.08(3) Å, Cu-O(1) 2.33(3) Å

distance found between RGD extremities. The Cu-N_{Me} distance is found to be 2.125(3) Å whilst the Cu-N_{acid} distance is found to be 2.084(3) Å. The Cu-O distance is longer at 2.329(3) Å. The N-Cu-N bond angles are found to be 93.37(13)° and 86.4(13)°, whilst the N_{Me}-Cu-O angles are 86.7(11)° and 93.3(11)°, and the N_{acid}-Cu-O angles are 78.3(11)° and 101.7(11)°. Whilst these value may appear significantly different, once the errors are taken into consideration these values can all be considered the same.

5.1.4 Potential application as an MRI contrast agent

Due to the inability to control the stepwise addition of the pendant arm, we would be unable to use these molecules in their intended purpose. However, the dimethylcyclam compound shows potential as an MRI contrast agent, due to its ability to coordinate strongly to metal centres (c.f. CuDMC-glut bond lengths) and so preliminary tests were undertaken to assess its suitability.

As with PET, it is important in MRI to have a strongly bound metal centre as the paramagnetic metals that are commonly used are highly toxic and cause cell death. Manganese and gadolinium are commonly used in MRI contrast agents due to their strong paramagnetism leading to reductions in both T₁ and T₂ relaxation times.

First, it was important to be sure of the ratio of metal to ligand binding. A useful method for determination of lanthanide concentration is a xylenol orange titration. Xylenol orange is a weak lanthanide chelator, and will therefore chelate with any free gadolinium in solution, as well as manganese ions (fig. 5.7). Xylenol orange has 2 absorption peaks in the UV/Vis spectrum, at 434 nm and 576 nm. Addition of lanthanide to the solution causes an increase in absorption at 434 nm, and a fall in absorption at 576 nm. Upon addition of xylenol orange to a solution of free ligand, one can then see by the changing absorptions, when the free ligand is coordinationally saturated, and hence work out the ratio of metal to ligand. This is an important consideration with our ligands, as the four carboxylates along with the four nitrogen donors gives the possibility of multi-metal coordination that may only be present in solution.

To a solution of the free ligand with 2 drops of xylenol orange present was titrated the metal ion (fig. 5.9 and 5.10). Addition of Gd³⁺ resulted in a steady increase in the peak at 576 nm, along with a slight decrease and blue shift in the peak at 434 nm (fig.

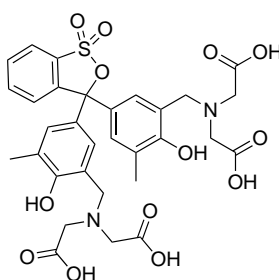
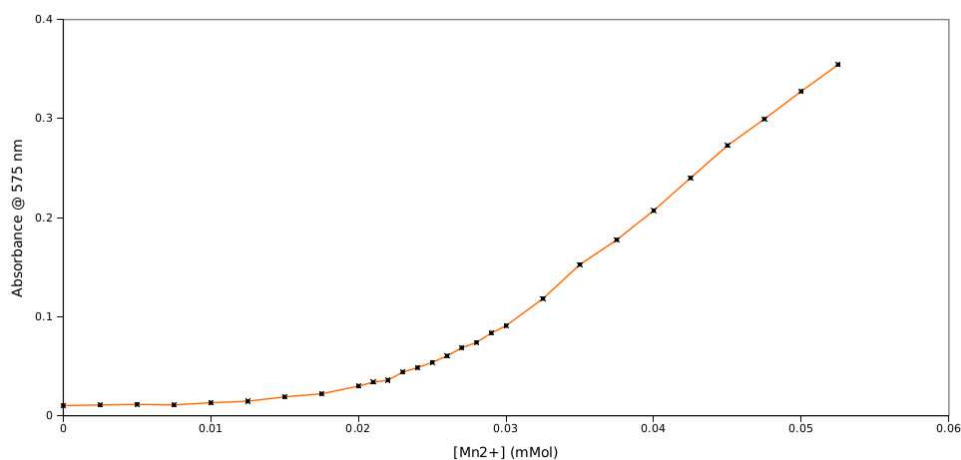


Figure 5.7: Structure of xylenol orange

5.9). The steady increase at 576 nm shows that there is always free Gd^{3+} in the solution and that the gadolinium is not coordinating to our ligand. This may be a kinetic problem due to the size of the metal ion and the cavity in which it is trying to fit. Heating between the samples would allow coordination of the metal to our ligand, but this was not tested. The Mn^{2+} titration shows a curve more consistent with coordination of metal ion. The peaks remain constant to addition of around 200 mM of metal, followed by a constant increase in peak height at 576 nm and consistent fall at 434 nm (fig. 5.8).

Figure 5.8: $[\text{Mn}^{2+}]$ vs Absorbance at 576 nm

The data indicates that the complex is forming in a 1:1 ratio of metal to ligand, consistent with the copper crystal structure. The slight variation in metal concentration to that of the ligand can be explained by the competition between the xylenol orange and our ligand. This may also hint at the relative stability of the complex, and it may be that competition *in vivo* could cause a transmetalation of the manganese ion. This competi-

tion reaction would also make an interesting study.

Following the xylenol orange titrations, we started to undertake relaxivity studies, beginning with gadolinium as that is the metal we were most familiar with. For the relaxivity study, two stock solutions were created; one of 1 mM ligand, and the other of 1 mM ligand + 4 mM Gd^{3+} . The relaxivity of each solution was then measured giving the two extremes of the relaxivity scale. The stock solution of ligand plus metal was then added in aliquots to the ligand solution, so as the molarity of metal increased by 0.0625 whilst the ligand concentration remains unaffected after each addition, and the relaxivity was measured after each addition. After 16 additions the ratio of metal to ligand is 1:1 and after 32 the ratio is 2:1. However, after 8 or so additions, it became clear that the results were the same as those expected for free Gd^{3+} (results not shown here), and so the experiment was stopped.

5.2 Functionalisation of fluorobenene substituted homopiperazines

Due to the success of our rigid arm homopiperazine complexes we decided to attempt a similar modular synthesis based upon previously unpublished work from our group. Tatchell and Fallis have shown that it is possible to add difluoro-nitrobenzenes to nitrogen macrocycles in a selective manner (see page 27).[55] If the remaining fluorine was in the ortho or para position to the nitro group (ie. 2,6- or 2,4-difluoronitrobenzene) this core could then be used to further substitute the benzene ring in the same manner as the initial addition to the macrocycle. This is because the fluorine atom would still be activated towards substitution by the strongly electron withdrawing affect of the nitro group. If using 2,6-difluoronitrobenzene then the fluorine atom would also have a convenient geometry to access the required shape for targeting the $\alpha_v\beta_3$ integrin as with our triazine core chemistry. We hypothesised a synthesis in which the core homopiperazine moiety would not change, but reaction with the targeting amines of choice would result in the desired ligand in a stepwise and modular fashion (fig. 5.11).

Formation of the homopiperazine core was easily accessed through addition of excess 2,4-, or 2-6-difluoronitrobenzene to homopiperazine in the presence of base. The

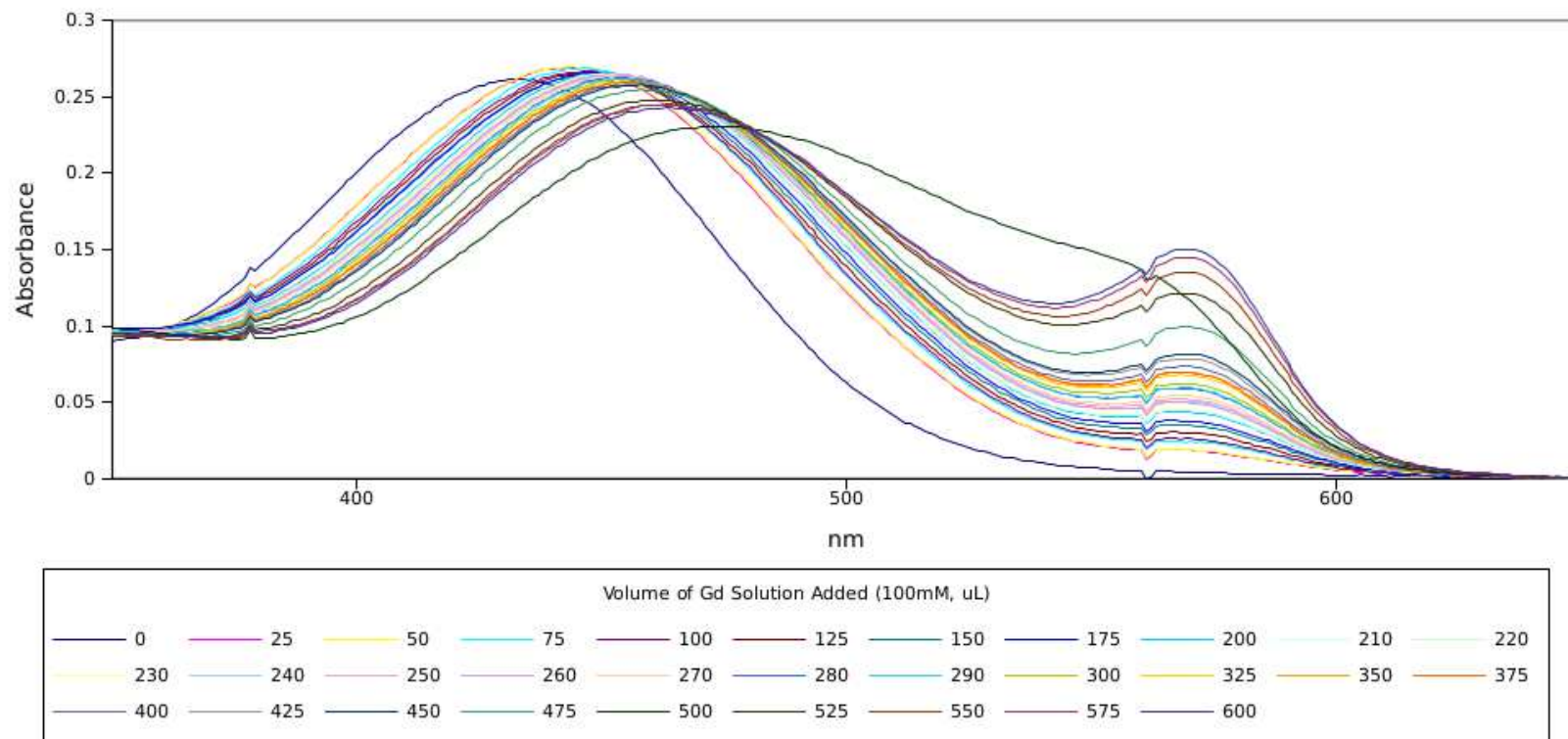


Figure 5.9: Titration of Gd^{3+} into a 1 mM solution of DMCglut ligand with 2 drops of xylene orange
Signals at ~ 380 and 560 nm are machine artifacts

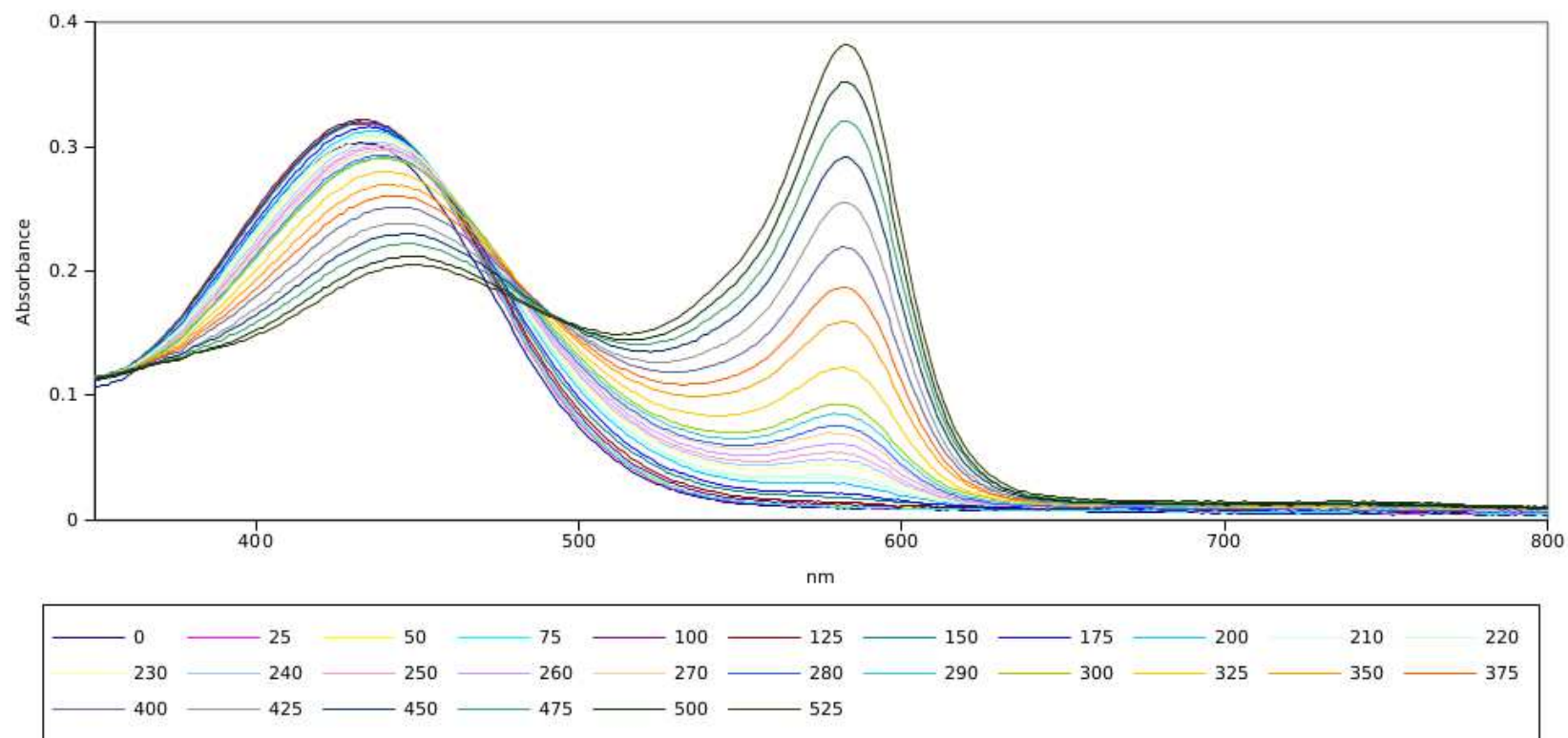


Figure 5.10: Titration of Mn^{2+} into a 1 mM solution of DMCGlut ligand with 2 drops of xylenol orange
Legend shows volume of Mn^{2+} solution added (100mM, μL)

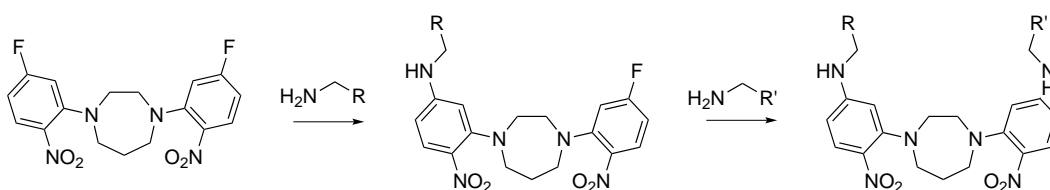


Figure 5.11: Hypothesised stepwise route to targeting ligands

mis-insertion product (in the case of 2,4-difluoronitrobenzene) was removed by recrystallisation from hot ethanol and shown by a single spot TLC. Functionalisation of the compound with a targeting moiety was attempted using the same conditions as for addition to the macrocycle (i.e. refluxing acetonitrile and potassium carbonate under an inert atmosphere), however, no reaction took place and starting material was recovered. Attempts using more forceful conditions (refluxing DMF and Cs_2CO_3) with ethyl glycine resulted in the desired product as shown by ^1H NMR (fig. 5.12).

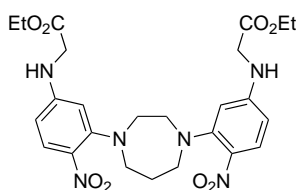


Figure 5.12: Addition of ethyl glycine

With alanine t butyl ester and 2-aminomethyl benzimidazole, synthesis was unsuccessful. It was also found that addition of just one amine to the homopiperazine core was complicated and would require column chromatography between each addition. Given this synthesis was to be simple and modular, we decided against following this route.

5.3 Synthesis of trispyrazylborate analogues for potential PET imaging

It has been previously shown by Jones *et al.*, that trispyridinepyrazylborate (Tp^{Py}) ligands with a coordinated actinide metal can abstract a fluoride from hexafluorophosphate counter ions (fig. 5.13).[94] This fluoride has been shown to be present in the mass

spectra of these complexes as well as the crystal structures and hence is implied to have an extremely strong bond to the metal centre.

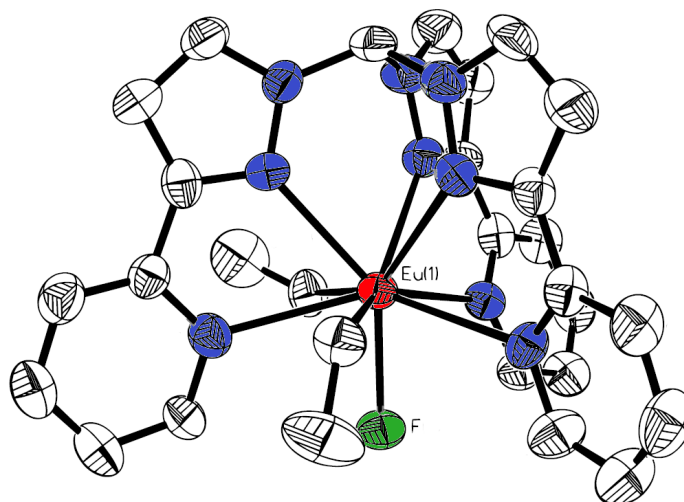


Figure 5.13: Fluoride coordinated EuTp^{Py} complex by Jones *et al.* (author?) [94]
Blue - nitrogen, Green - fluorine, Red - europium

We wanted to synthesise novel Tp^{Py} style ligands, which would show the potential to functionalise into targeting molecules, and test whether this functionalisation would have any affect on the binding of the fluoride ion. We decided to make the simplest 'functionalised' Tp^{Py} first, with the addition of a methyl group at the 4 position on the imidazole ring. Acetyl pyridine was dissolved in THF and a strong base added. Addition of ethyl acetate to this solution gave the desired acetylacetate derivative via an aldol reaction (fig. 5.14). Addition of hydrazine hydrate in the presence of an organic soluble base (*p*-tosylsulphonic acid) to this compound closes the imidazole ring, and forms the methyl substituted pyrazylpyridine ligand (MePzPy) as shown by ^1H NMR. This synthesis can be adapted to allow access to further functionalisation via the choice of ester used.

The synthesis of Tp from pyrazole and potassium borate is well established, and it was this methodology we used to synthesise the MeTpPy ligand. An excess of MePzPy was melted with potassium borate at $230\text{ }^\circ\text{C}$ until no gas was further evolved. It was believed that sterics would dictate that the molecule only substitute 3 times (as shown by Jones), however, $^{11}\text{B}\{^1\text{H}\}$ NMR showed a four fold substitution and was corroborated by mass spectra evidence – IR and ^1H NMR are inconclusive when trying to determine

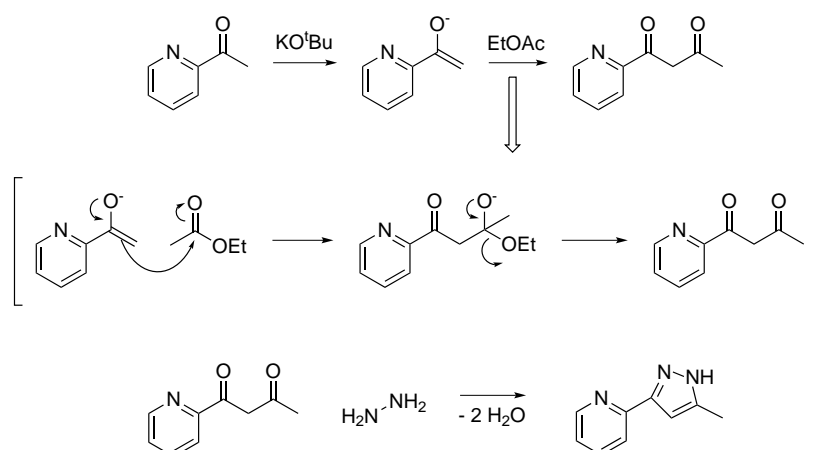


Figure 5.14: Synthesis of MePzPy

the degree of substitution. The shift of the boron peak in the $^{11}\text{B}\{^1\text{H}\}$ NMR spectra is indicative of its substitution.[95] A signal at around -7 ppm is assigned to disubstitution, -1 - 0 ppm for tri-, and > 1 ppm for tetra- substituted compounds, however it should be noted that the boron signals obtained were very broad due to interference from the boro-silicate nmr tube used. We believe that the temperature was too hot, allowing the reaction to overcome the activation barrier for the final substitution. Synthesis in the presence of a high boiling solvent was subsequently attempted, whilst simultaneously reducing the number of equivalents of MePzPy to the required 3. Addition of MePzPy to a suspension of potassium borate in dimethylacetamide (DMAC), followed by heating to 160°C enabled a reaction that evolved only 2 equivalents of hydrogen. Upon cooling a solid precipitated and was isolated by filtration. $^{11}\text{B}\{^1\text{H}\}$ NMR showed this to be the disubstituted borate (MeDpPy), as did mass spectral evidence. Reactions at various temperatures between 160°C and 230°C have so far failed to yield the desired trisubstituted compound (fig. 5.15).

In a test reaction to see how the ligands coordinate to PET active metals, copper acetate was added to a solution of MeDpPy and left to stand. Evaporation of this solution resulted in deep blue crystals suitable for x-ray diffraction and gave a surprising result (fig. 5.16).

As can be seen the crystal structure shows two MePzPy molecules coordinated to two copper atoms with coordinating acetates. The copper atoms are in a distorted square based pyramid geometry with 3 unique nitrogens coordination environments. Despite being different imidazole nitrogens, the Cu-N_{imid} bond lengths are identical

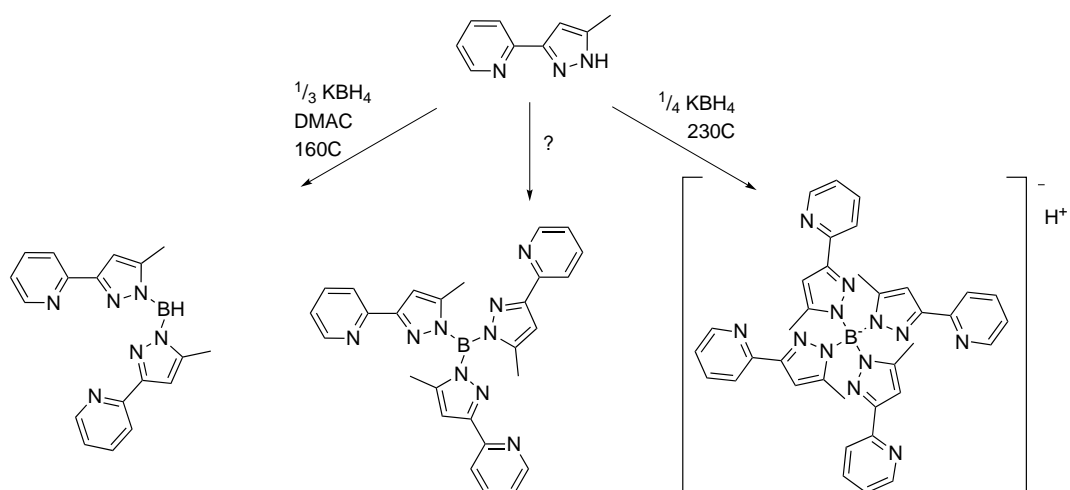


Figure 5.15: Synthesis of MeXpPy ligands

(within experimental error) at around 1.96 \AA ($1.947(9) \text{ \AA}$ and $1.960(9) \text{ \AA}$). The Cu-N_{py} bond lengths are also the same at $2.032(10) \text{ \AA}$ (Cu_1) and $2.057(9) \text{ \AA}$ (Cu_2). The acetate bonds are the same, the equatorial oxygens are shorter with $\text{Cu-O}_{eq} 1.965(7) \text{ \AA}$ (Cu_2) and $\text{Cu-O}_{eq} 1.973(8) \text{ \AA}$ (Cu_1), whilst the longer axial bonds average at $\text{Cu-O}_{ax} 2.5875 \text{ \AA}$. This is explained by the Jahn-Teller distortion associated with copper complexes. No other data has been collected yet for this sample and so no further conclusions can be drawn.

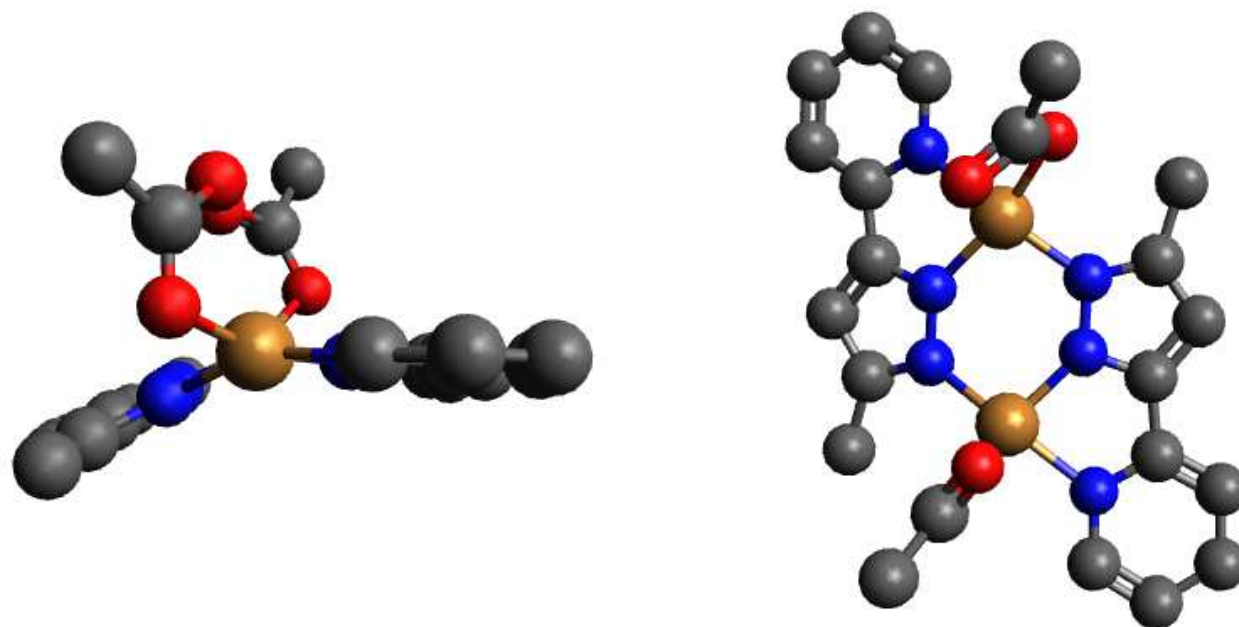


Figure 5.16: Single crystal structure of $[\text{Cu}_2(\text{MePzPy}_2)](\text{OAc})_2$
Selected Bond Lengths: Cu(1)-N(1) 2.057(9) Å, Cu(1)-N(2) 1.947(9) Å, Cu(1)-N(6) 1.960 Å, Cu(1)-O(1) 1.973(8) Å, Cu(2)-N(3) 1.961(9) Å, Cu(2)-N(4) 2.032(10) Å, Cu(2)-N(5) 1.965(10) Å, Cu(2)-O(3) 1.965(7) Å

Chapter 6

Conclusions

The synthesis of rigid arm homopiperazine complexes has shown that it is possible to add useful functionality to these chelate systems, whilst not appreciably changing their coordination properties. Little work outside of the Fallis group has previously focused on the ligand systems, and the work contained herein has greatly added to the field. DFT calculations are in good order for Ni(II), and Cu(II) complexes when compared to the data obtained from x-ray crystallography, whilst Zn(II) complexes must be studied under the assumption of coordinating solvent or anions. Further EPR studies of the Cu(II) complexes would elucidate greater information as to the structure and bonding in these systems.

Unfortunately purity data is lacking for these complexes and in order for these ligand frameworks to be useful in medical imaging studies HPLC methods should be explored. Conjugation of the homopiperazine core to an applicable protein or protein mimic is now accessible, as an appropriate methodology has been shown through the synthesis of the HP^{Amide} ligand. Competition data, either through metal - metal competition, or pH formation dependence of the complexes would give a simple insight in to how the molecules might perform *in vivo*.

The synthesis of triazine derived structures offers the largest scope for further work. The integrin $\alpha_v\beta_3$ focused compound TzEtGlyBocGuanCl is the most promising compound in the work. It would be necessary to focus effort on the current synthesis to allow for larger volumes of the BocGuan arm to be synthesised successfully. Reduction in temperature, or greater control over the speed of addition of the two composition

moieties, may allow for this to be possible. Further derivatisation to include a common metal coordinating macrocycle (e.g.. DO3A) or chelate would afford the proposed structure of a $\alpha_v\beta_3$ imaging agent. Work would then need to be undertaken on the suitability of such a structure for use as a imaging agent. This could be achieved using either the desired metal complexes in cell cultures and imaging as would be the case for a proper organism, or through the synthesis of similar structures that contain fluorophores in place of the coordination site, and studied via their fluorescence (fig. 6.1). If the compound was found to be suitable for *in vitro* and then *in vivo* studies, the methodology could be used to synthesise a large library of simple and affordable imaging agents targeted for specific anatomical functions, reducing the need for expensive cyclic amino acids, and therefore making the imaging agents themselves more economically accessible. The dipyridamole analogues tentatively explored in this work should also be evaluated for use *in vitro*. Whilst it is unlikely that these molecules themselves will have any biological function, similar derivatives more alike to the dipyridamole compound could be easily synthesised and explored using the described methodologies.

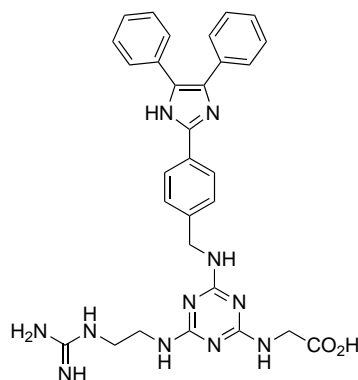


Figure 6.1: Possible structure of proposed fluorescent $\alpha_v\beta_3$ probe

Addition of moieties to the triazine core through a click synthesis would allow facile access to a vast range of complexes. Current attempts at these reactions have so far failed due to difficulties in the purification step. HPLC methodologies for the purification and analysis of the products would allow access to these compounds on scales acceptable in PET chemistry.

Whilst the dendrimer compounds and complexes are not designed with medical imaging function in mind, their highly symmetrical nature, and synthetic beauty afford these molecules a bright future. It would be interesting to produce multilayer den-

dimers, with each layer affording specific coordination sites, making them ideal for multi metal compounds, or even complexes that can accommodate varying oxidation states of a metal; i.e. Cu(I) and Cu(II) for imaging, or Fe(II) and Fe(III) for electron transfer studies (fig. 6.2).

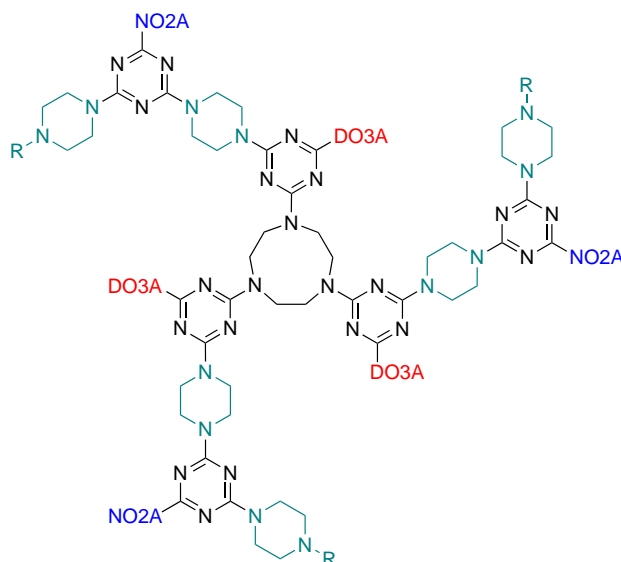


Figure 6.2: Possible multilayer dendrimer
Green denotes new layer

Synthesis of acetate functionalised TACN compounds led to initial PET studies. Whilst the results from the compounds were not ideal, they can be assessed as a solid basis from which to work. The ligands TsTACNA₂ and NPhTACNA₂ both show good initial uptake of radio-copper, allowing formation of the complexes in a short period of time. The sulfonamide containing complex showed a weak bond between the metal centre and the sulfonamide nitrogen, this is significant, as it shows that a strongly electron withdrawing group does not completely remove the donor power of the tertiary amine. Further derivatisation of the NPhTACNA₂ compounds through reduction of the nitro group to an aniline and subsequent addition to it would allow access to a peptide conjugate, or a molecule that could be attached to the triazine cores *vide supra*. Effort should be afforded in the purification of the AlF complexes. Due to the (relatively) abundant nature of ¹⁸F cyclotrons, PET agents based upon Al-F compounds will become common in the coming years. This work could also be expanded with the use on mono anionic ligand frameworks and Ca²⁺ ions to afford similar Ca-F complexes (fig. 6.3).

The glutaric acid compounds DMCGLut, TACNGLut, and HPGLut should be anal-

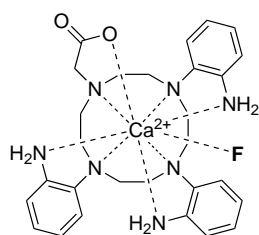


Figure 6.3: Potential Ca-F compound

ysed further for their suitability for use as MRI agents. The initial results for the Mn(II) complex, MnDMCGLut, show a good binding affinity of the metal to the macrocyclic cavity when compared to that of the Gd(III) complex. Mn(II) complexes have fallen out of fashion in the recent MRI literature, with work focusing more commonly on Gd(III) complexes and iron nanoparticle. This means that work on the Mn(II) complex would be of reasonable importance in the development of new MRI contrast agents.

It is accepted that the work in this thesis does not contain a successful PET imaging agent, and therefore meet the initial aim of the project. However, what this work has achieved is the formation of a series of solid fundamental foundations in the quest for future PET imaging agents. The triazine core work is tantalisingly close to a potential imaging agent, and, more importantly, a general methodology in the synthesis of targeted imaging agents. The homopiperazine chelates now have a focused purpose, with facile access to a series of amino acid functionalised complexes now shown through the generic amide complexes contained herein. It has also been shown that Al- ^{18}F coordination is possible based on a NO2A style framework.

Chapter 7

Experimental

7.1 Experimental conditions

Non-synthesised reagents were purchased from Sigma-Aldrich, Alfa Aesar, Apollo Scientific, and Bachem, and used as found. Solvents were pre-dried according to standard protocols. Mass spectra were obtained by atmospheric pressure chemical ionisation (APCI), electronic ionisation (EI), or electrospray ionisation (ES), in either positive (+) or negative (-) modes. IR spectra were obtained from KBr discs using a Jasco FTIR 110 series spectrometer. UV/Vis spectra were recorded on a Perkin-Elmer Lambda 20 spectromometer. NMR spectra were obtained on either a Bruker 500 Ultrashield, Bruker Avance AMX 400, Bruker Avance 250 or JEOL Eclipse 300 spectrometer and referenced to external TMS.

7.2 DFT calculations

Density functional theory (DFT) calculations were undertaken on the ARCCA SRIF-3 (Merlin) cluster, using the Gaussian '03 software package[96] and the B3LYP[97, 98, 99, 100] hybrid function with a 6-31G[101, 102, 103, 104, 105, 106, 107, 108, 109, 110] basis set unless otherwise stated.

DFT calculations are of ideal gas phase molecules with no solvent interactions. All geometry calculations have been checked to be minima with the appearance of no imaginary frequencies.

7.3 EPR Measurements

All X-band EPR spectra were recorded on a Bruker EMX spectrometer operating at 100 kHz field modulation and equipped with a high sensitivity X-band cavity (ER 4119HS). The spectra were recorded at a microwave power of 10 mW at 140 K.

7.4 X-Ray data

X-Ray crystallographic data was collected using a Nonius KappaCCD area detector, Bruker AXS machine, and the Collect software. Structural solution and refinement was achieved using SHELXS97 and SHELXL97 software, and absorption correction analysed using SADABS software.

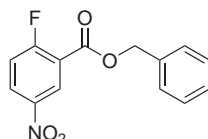
7.5 Radiolabelling

All radiolabelling studies were carried out by Dr. J. Knight at the University of Alberta. No details of the experimental machinery have been provided.

7.6 Rigid Arm Polyazamacrocycles

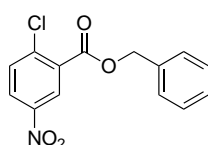
7.6.1 Pendant arms

7.6.1.1 Benzyl-2-fluoro-5-nitrobenzoate (1-NO₂)



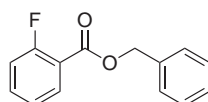
2-Fluoro-5-nitrobenzoic acid (3.27 g, 17.7 mmol), benzyl bromide (2.3 ml, 19.4 mmol), potassium carbonate (2.68 g, 19.4 mmol), tetrabutylammonium iodide (50 mg), and DMF (50 ml) were stirred for 18 hours at 50°C in a stoppered flask. Ethyl acetate (150 ml) was added, and the solution washed successively with sodium bicarbonate (100 ml), water (4 x 100 ml), and brine (1 x 50 ml). The organic phase was collected and dried over MgSO₄, filtered, and solvent removed *in vacuo*. The resulting oil was dissolved in the minimum amount of hot CHCl₃, and added drop-wise to a stirred beaker of hexane (100ml). The resulting precipitate was filtered and dried under suction for 30 minutes yielding the title product as an orange/yellow powder (4.46 g, 16.2 mmol, 92 %); ¹H NMR (400 MHz, CDCl₃, ppm) δ_H: 8.86 (dd, 1 H, Ar-H, J_{H-H,H-F} = 2.9 + 6.1 Hz), 8.43 (dt, 1 H, Ar-H, J_{H-H,H-F} = 2.9 + 6.1 Hz), 8.40 (dt, 1 H, Ar-H, J_{H-H,H-F} = 2.9 + 6.1 Hz), 7.50-7.36 (m, 4 H, Ar'-H), 7.33 (t, 1 H, Ar'-H, ²J_{H-H} = 9.2 Hz), 5.43 (s, 2 H, CH₂); ¹³C NMR (62.90 MHz, CDCl₃, ppm) δ_C: 167.3, 162.5 (d, ¹J_{C-F} = 31.2 Hz), 162.5, 135.0, 129.6, 128.8, 128.7, 128.4, 128.3, 120.0, 118.5, 67.9; IR (KBr, ν_{max}, cm⁻¹) 3091 (w), 3072 (w) 3034 (w), 2964 (w), 2942 (w), 2875 (w), 1722 (s), 1632 (s), 1587 (s), 1532 (s), 1498 (s), 1483 (s), 1421 (s), 1378 (s), 1353 (s), 1325 (s), 1274 (br, s), 1140 (s), 1122 (w), 1079 (s), 982 (s), 926 (s), 864 (s), 843 (s), 816 (w), 780 (w), 746 (s), 735 (s); MS (HR EI⁺) calc. for C₁₇H₉NO₃ (M⁺) 275.0582 found 275.0592

7.6.1.2 Benzyl-2-chloro-5-nitrobenzoate (1-NO₂) (Cl)



2-Chloro-5-nitrobenzoic acid (10.1 g, 50.1 mmol), benzyl bromide (6.55 ml, 55.2 mmol), potassium carbonate (7.61 g, 55.1 mmol), tetrabutylammonium iodide (200 mg), and DMF (50 ml) were stirred for 18 hours at 50°C in a stoppered flask. Ethyl acetate (200 ml) was added, and the solution washed successively with sodium bicarbonate (100 ml), water (2 x 100 ml), and brine (2 x 100 ml). The organic phase was collected, dried over MgSO₄, filtered, and solvent removed *in vacuo*. The resulting oil was dissolved in the hot CHCl₃, and added drop-wise to a stirred beaker of hexane (200ml). The precipitate was filtered, and dried under vacuum, affording the title compound as a pale yellow powder (9.85 g, 34 mmol, 67.5 %); ¹H NMR (400 MHz, CDCl₃, ppm) δ_H: 8.59 (d, 1 H, Ar-H, ²J_{H-H} = 2.7 Hz), 8.15 (d, 1 H, Ar-H, ²J_{H-H} = 2.7 Hz), 8.13 (d, 1 H, Ar-H, ²J_{H-H} = 2.7 Hz), 7.53 (d, 1 H, Ar-H, ²J_{H-H} = 8.8 Hz), 7.38 - 7.35 (m, 1 H, Ar'-H), 7.33 - 7.26 (m, 1 H, Ar'-H), 5.31 (s, 1H, CH₂); IR (KBr, ν_{max}, cm⁻¹) 3106 (w), 3080 (w), 2971 (w), 2922 (w), 2853 (w), 1735 (s), 1610 (s), 1573 (s), 1523 (s), 1496 (w), 1460 (s), 1398 (w), 1368 (w), 1353 (s), 1307 (s), 1252 (s), 1242 (s), 1216 (w), 1137 (w), 1126 (s), 1103 (w), 1045 (s), 943 (s), 921 (s), 890 (s), 841 (s), 832 (w), 814 (w), 780 (s), 756 (s), 741 (s); MS (HR EI⁺) calc. for C₁₄H₁₀NO₄Cl (M⁺) 291.0298 found 291.0294.

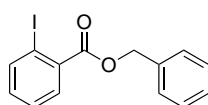
7.6.1.3 Benzyl-2-fluorobenzoate (1)



2-Fluorobenzoic acid (9.84 g, 70.3 mmol), benzyl bromide (9.2 ml, 77.5 mmol), potassium carbonate (10.0 g, 72.5 mmol), tetrabutylammonium iodide (150 mg), and DMF (150 ml) were stirred for 18 hours at 50°C in a stoppered flask. Ethyl acetate (250 ml) was added, and the solution washed successively with sodium bicarbonate (150 ml), water (4 x 200 ml), and brine (1 x 100 ml). The organic phase was collected and dried over MgSO₄, filtered, and solvents removed *in vacuo*. The resulting oil was dissolved in the minimum amount of hot CHCl₃, and added drop-wise to a stirred beaker of hexane (300ml). The resulting precipitate was filtered and dried under suction for 30 minutes yielding the title compound as an orange/yellow powder (15.04 g, 65 mmol, 98.0 %) ¹H NMR (400 MHz, CDCl₃, ppm) δ_H: 7.97 (dt, 1 H, Ar-H, J_{H-H,H-F} = 1.8 + 7.6 Hz), 7.55 - 7.49 (m, 1

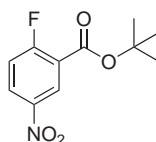
H, Ar-H), 7.47 (d, 2 H, Ar'-H, $^2J_{H-H} = 7.3$ Hz), 7.43 - 7.31 (m, 3 H, Ar'-H), 7.20 (dt, 1 H, Ar-H, $^2J_{H-H} = 1.0 + 7.6$ Hz), 7.14 (ddd, 1H, Ar-H, $J_{H-H,H-F} = 1.0 + 8.4 + 10.9$ Hz), 5.40 (s, 2H, Ar'CH₂); ¹³C NMR (100 MHz, CDCl₃, ppm) δ_C : 164.2, 160.3, 135.8, 134.7, 134.5, 132.2, 128.6, 128.3, 128.1, 124.0, 124.0, 117.2, 116.9, 67.0; MS (HR APCI⁺) calc. for C₁₄H₁₂O₂F (M + H⁺) 231.0821 found 231.0812.

7.6.1.4 Benzyl-2-iodobenzoate (1) (I)



2-Iodobenzoic acid (1.11 g, 4.48 mmol), benzyl bromide (0.58 ml, 4.88 mmol), potassium carbonate (0.68 g, 4.93 mmol), tetrabutylammonium iodide (40 mg), and DMF (20 ml), were stirred for 18 hours at 50°C in a stoppered flask. Ethyl acetate (50 ml) was added, and the solution washed successively with sodium bicarbonate (50 ml), water (2 x 50 ml), and brine (2 x 50 ml). The organic phase was collected, dried over MgSO₄, filtered, and solvent removed *in vacuo*, affording the title compound as a brown liquid (1.06 g, 3.14 mmol, 70 %) ¹H NMR (400 MHz, CDCl₃, ppm) δ_H : 7.81 (d, 1 H, Ar-H, $^2J_{H-H} = 7.9$ Hz), 7.66 (dd, 1 H, Ar-H, $^2J_{H-H} = 1.6 + 7.8$ Hz), 7.33 (d, 2 H, Ar-H, $^2J_{H-H} = 8.0$ Hz), 7.26 - 7.18 (m, 3 H, Ar-H), 6.95 (dt, 2 H, Ar-H, $^{2,3}J_{H-H} = 1.6 + 7.7 + 7.9$ Hz), 5.23 (s, 2 H, CH₂); MS (HR APCI⁺) calc. for C₁₄H₁₂O₂I (M + H⁺) 338.9882 found 338.9878 also seen (M + MeCN + H⁺): 380.0125

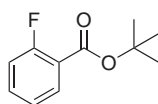
7.6.1.5 ^tButyl-2-fluoro-5-nitrobenzoate (2-NO₂)



2-Fluoro-5-nitrobenzoic acid (0.665 g, 3.59 mmol), butyl-boc-anhydride (0.86 g, mmol), butanol (10 ml), and dimethylaminopyridine (0.050 g) were heated under reflux for 72 hours. After cooling to room temperature, ethyl acetate (100 ml) was added, and

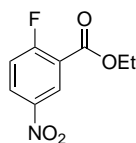
washed with saturated sodium bicarbonate solution (50 ml), water (3 x 50 ml), and brine (1 x 50 ml). The organic phase was collected and dried over MgSO_4 , filtered, and the solvents removed *in vacuo*, yielding the title compound as a yellow oil (0.340 g, 1.41 mmol, 38.9 %) ^1H NMR (400 MHz, CDCl_3 , ppm) δ_{H} : 8.68 (dd, 1 H, Ar-H, $J_{\text{H-H}, \text{H-F}} = 2.9 + 6.2$ Hz), 8.31 (m, 1 H, Ar-H), 7.22 (t, 1 H, Ar-H, $J_{\text{H-H}} = 9.2$ Hz), 1.55 (s, 9 H, CH_3); ^{13}C NMR (62.3 MHz, CDCl_3 , ppm) δ_{C} : 167.2, 162.0 ($^1\text{J}_{\text{C-F}} = 56$ Hz), 143.8, 128.9, 128.0, 121.9, 118.3, 83.6, 28.1; MS (HR EI^+) calc. for $\text{C}_{11}\text{H}_{12}\text{NO}_4\text{F}$ (M^+) 241.0750 found 241.0745

7.6.1.6 *t*-Butyl-2-fluorobenzoate (2)



2-Fluorobenzoic acid (0.93 g, 6.64 mmol), butyl-boc-anhydride (1.59 g, mmol), butanol (8 ml), and dimethylaminopyridine (0.100 g), were heated under reflux for 72 hours. Ethyl acetate was added (100 ml), and washed with saturated sodium bicarbonate solution (50 ml), water (3 x 50 ml), and brine (50 ml). The organic phase was collected and dried over MgSO_4 , filtered, and the solvents removed *in vacuo*, yielding the title compound as a pale yellow oil (0.51 g, 2.60 mmol, 39 %) ^1H NMR (400 MHz, CDCl_3 , ppm) δ_{H} : 7.76 (dt, 1 H, Ar-H, $J_{\text{H-H}, \text{H-F}} = 1.9 + 7.6$ Hz), 7.39 - 7.33 (m, 1 H, Ar-H), 7.06 (dt, 1 H, Ar-H, $J_{\text{H-H}, \text{H-F}} = 1.1 + 7.6 + 7.7$ Hz), 6.99 (ddd, 1 H, Ar-H, $J_{\text{H-H}, \text{H-F}} = 0.9 + 8.3 + 10.8$ Hz), 1.50 (s, 9 H, CH_3); MS (HR EI^+) calc. for $\text{C}_{11}\text{H}_{13}\text{O}_2\text{F}$ (M^+) 196.0900 found 196.0900

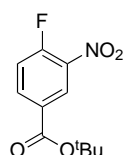
7.6.1.7 Ethyl-2-fluoro-5-nitrobenzoate (3- NO_2)



2-Fluoro-5-nitrobenzoic acid (1.0 g, 5.41 mmol), was dissolved in ethanol (20 ml), and sulphuric acid (1 ml) added. The solution was refluxed for 3 hours, before the solvent was removed *in vacuo* and water (10 ml) added. Neutralisation with NaHCO_3 solution,

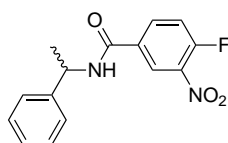
was followed by extraction with DCM (3 x 20 ml). The organic phases were combined and washed with brine (20 ml), then dried over MgSO₄, filtered, and the solvent removed *in vacuo* yielding the title product as a light orange solid (806 mg, 3.84 mmol, 71 %) ¹H NMR (250 MHz, CDCl₃, ppm) δ_H: 8.77-8.73 (m, 1 H, Ar-H), 8.35 - 8.28 (m, 1 H, Ar-H), 7.27 - 7.19 (m, 1 H, Ar-H), 4.36 - 4.34 (m, 2 H, CH₂CH₃), 1.34 (t, 3 H, CH₃CH₂); IR (KBr, ν_{max}, cm⁻¹) 3119 (w), 3101 (s), 3087 (w), 2986 (s), 2944 (w), 2909 (w), 2875 (w), 2739 (w), 2652 (w), 1944 (s), 1841 (s), 1740 (br, s), 1626 (s), 1584 (s), 1532 (s), 1482 (s), 1444 (w), 1413 (s), 1351 (s), 1324 (s), 1265 (br), 1169 (w), 1138 (w), 1120 (s), 1068 (s), 1015 (s), 974 (w), 925 (s), 867 (w), 848 (s), 808 (w), 780 (s), 748 (s)

7.6.1.8 ^tButyl 4-fluoro-3-nitrobenzoate (^tButyl)



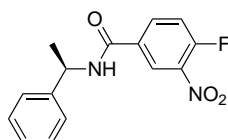
3-Nitro-4-fluorobenzoic acid (1 g, 5.41 mmol), ^tbutyl acetate (30 ml), and perchloric acid (2 drops, cat.), were stirred over night at room temperature. The organic phase was washed with water (2 x 50 ml), sodium bicarbonate (50 ml), and brine (50 ml), dried over MgSO₄, filtered, and the solvent removed *in vacuo*, yielding the title compound as an orange solid (0.95 g, 3.94 mmol, 73 %) ¹H NMR (400 MHz, CDCl₃, ppm) δ_H: 8.59 - 8.53 (m, 1 H, C(NO₂)CHC(CO₂)), 8.20 - 8.15 (m, 1 H, CHCHC(CO₂)), 7.32 - 7.23 (m, 1 H, CHCF), 1.54 (s, 9 H, CH₃); IR (KBr, ν_{max}, cm⁻¹) 3103 (s), 3079 (w), 3068 (w), 3009 (s), 2994 (s), 2941 (w), 2878 (w), 1946 (w), 1847 (w), 1718 (s), 1616 (s), 1594 (w), 1539 (br, s), 1492 (w), 1472 (w), 1460 (w), 1410 (w), 1395 (w), 1368 (s), 1353 (s), 1300 (br, s), 1267 (s), 1238 (w), 1168 (w), 1148 (s), 1125 (s), 1078 (w), 974 (w), 926 (s), 848 (s), 838 (s), 811 (w), 767 (w), 760 (s), 749 (s)

7.6.1.9 4-Fluoro-3-nitro-N-((+/-)-1-phenylethyl)-benzamide (AmideRac)



Under a nitrogen atmosphere and at 0°C, oxalyl chloride (2 ml, 23.2 mmol) and DMF (1 drop, cat.) were added to 4-fluoro-3-nitrobenzoic acid (790 mg, 4.27 mmol) in DCM (50 ml), and stirred for 1 hr at 0°C. The solvents were then removed *in vacuo* resulting in a brown solid. The solid was dissolved in fresh DCM (50 ml), and cooled again to 0°C, (+/-)phenylethylamine (0.55 ml, 4.32 mmol) was added and the solution allowed to warm to room temperature whilst stirring overnight. The solvents were removed *in vacuo*. The resulting oil was dissolved in DCM (30 ml) and washed with saturated aqueous NaHCO₃ (30 ml), water (2 x 30 ml), and brine (30 ml). The organic phase was then dried over MgSO₄, filtered and the solvents removed *in vacuo*. The yellow solid was dissolved in minimum hot CHCl₃ and added dropwise to stirred hexane (50 ml). The title compound was isolated by filtration as a yellow solid (470 mg, 1.63 mmol, 38 %). ¹H NMR (400 MHz, CDCl₃, ppm) δ_H: 8.44 (dd, 1 H, Ar_F-H, J_{H-F} = 2.3 + 6.9 Hz), 8.11 (ddd, 1 H, Ar_F-H, J_{H-F} = 2.3 + 4.1 + 8.7 Hz), 7.40 - 7.29 (m, 6 H, ⁵H Ar-H + ¹H Ar_F-H), 6.42 (d, 1 H, NH, ²J_{H-H} = 7.0 Hz), 5.32 (p, 1 H, NHCH, ²J_{H-H} = 7.0 Hz), 1.64 (d, 1 H, CH₃, ²J_{H-H} = 7.0 Hz); ¹³C (125 MHz, CDCl₃, ppm) δ_C: 162.2, 157.2, 155.1, 143.7, 134.5 (d, J_{C-F} = 10 Hz), 131.4 (d, J_{C-F} = 4 Hz), 127.8 (d, J_{C-F} = 8 Hz), 126.4, 125.7, 124.7 (d, J_{C-F} = 1 Hz), 118.0 (d, J_{C-F} = 21 Hz), 48.8, and 20.9; IR (KBr, ν_{max}, cm⁻¹) 3312 (br, s), 3090 (w), 3068 (w), 3030 (w), 2926 (w), 2855 (w), 1653 (w), 1635 (s), 1623 (s), 1560 (s), 1538 (br, s), 1494 (s), 1451 (s), 1407 (w), 1381 (w), 1350 (s), 1330 (w), 1321 (w), 1268 (s), 1234 (w), 1210 (w), 1130 (s), 1085 (w), 1076 (w), 1013 (w), 928 (s), 854 (w), 846 (s), 754 (s).

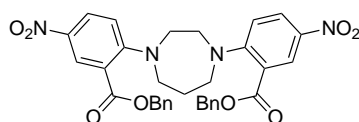
7.6.1.10 4-Fluoro-3-nitro-N-((R)-1-phenylethyl)-benzamide (AmideR)



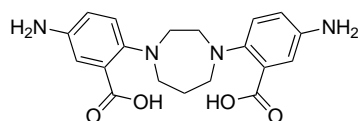
Using the same method as for 4-fluoro-3-nitro-N-((+/-)-1-phenylethyl)-benzamide with 4-fluoro-3-nitrobenzoic acid (714 mg, 3.86 mmol), oxalyl chloride (1.67 ml, 19.4 mmol), DMF (1 drop), DCM (40 ml), and (R)-phenylethylamine (0.50 ml, 3.88 mmol) the title compound was isolated as a white solid (782 mg, 2.72 mmol, 70%). ^1H NMR (400 MHz, CDCl_3 , ppm) δ_{H} : 8.44 (dd, 1 H, $\text{Ar}_F\text{-H}$, $J_{\text{H-F}} = 2.4 + 6.9$ Hz), 8.11 (ddd, 1 H, $\text{Ar}_F\text{-H}$, $J_{\text{H-F}} = 2.4 + 4.1 + 8.7$ Hz), 7.39 - 7.27 (m, 6 H, $^5\text{H Ar-H} + ^1\text{H Ar}_F\text{-H}$), 6.42 (d, 1 H, NH, $^2\text{J}_{\text{H-H}} = 7.0$ Hz), 5.34 (p, 1 H, NHCH, $^2\text{J}_{\text{H-H}} = 6.9$ Hz), 1.62 (d, 1 H, CH_3CH , $^2\text{J}_{\text{H-H}} = 6.9$ Hz); ^{13}C (125 MHz, CDCl_3 , ppm) δ_{C} : 162.2, 157.1, 155.1, 141.4, 133.6 (d, $^1\text{J}_{\text{C-F}} = 10$ Hz), 130.4, 127.9, 126.8, 125.3, 123.7, 118.0, 48.9, 48.9, and 20.5

7.6.2 Synthesis of Carboxy Ligands

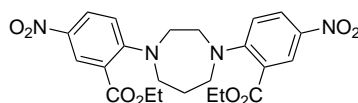
7.6.2.1 Benzyl-6,6'-(1,4-diazepane-1,4-diyl)bis(3-nitrobenzoate) ($\text{HP}^{1-\text{NO}_2}$)



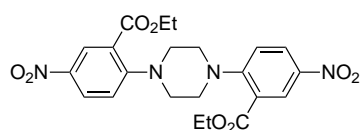
1- NO_2 (Cl) (2.63 g, 9.04 mmol), homopiperazine (0.43 g, 4.25 mmol), caesium carbonate (2.91 g, 8.93 mmol), and acetonitrile (20 ml) were heated under reflux for 18 hours. Chloroform (30ml) was added, the solution filtered, then solvent removed *in vacuo*, leading to a brown solid. This was washed with hot ethanol (50 ml), followed by cold diethyl ether (30 ml), affording the title compound as a brown-yellow solid (2.10 g, 3.44 mmol, 81 %) ^1H NMR (400 MHz, CDCl_3 , ppm) δ_{H} : 8.57 - 8.52 (m, 1 H, Ar-H), 8.15 (dd, 1 H Ar-H , $^2\text{J}_{\text{H-H}} = 2.8 + 9.3$ Hz), 7.46 (dd, 2 H, $\text{Ar}'\text{-H}$, $^2\text{J}_{\text{H-H}} = 1.5 + 8.0$ Hz), 7.42 - 7.35 (m, 3 H, $\text{Ar}'\text{-H}$), 6.81 (d, 1 H, Ar-H , $^2\text{J}_{\text{H-H}} = 9.4$ Hz), 5.36 (s, 2 H), 3.41 (s, 2 H CH_2), 3.36 (t, 2 H, CH_2), 1.58 (s, 1 H, CH_2); ^{13}C NMR (126 MHz, CDCl_3) 166.4, 154.6, 138.3, 135.4, 128.7, 128.7, 128.5, 127.4, 118.7, 116.3, 67.5, 56.6, 52.3, 27.8; IR (KBr, ν_{max} , cm^{-1}) 3454 (br), 2925 (w), 2857 (w), 1717 (s), 1602 (s), 1579 (s), 1498 (s), 1457 (w), 1328 (s), 1283 (w), 1224 (w), 1205 (w), 1176 (w), 1128 (s), 1083 (w), 959 (w), 929 (w), 748 (s); MS (HR ES^-) calc. for $\text{C}_{33}\text{H}_{30}\text{N}_4\text{O}_8\text{Cl}$ ($\text{M} + \text{Cl}^-$) 645.1752 found 645.1755

7.6.2.2 6,6'-(1,4-Diazepane-1,4-diyl)bis(3-aminobenzoate) (HP^R)

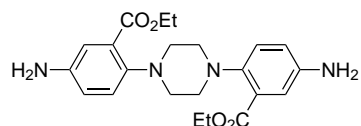
Into a schlenk under an atmosphere of H₂ were placed, HP^{1-NO₂} (0.188 g, mmol), THF (20 ml), acetic acid (0.1 ml), and palladium on carbon (10 %, 50 mg) in methanol (1 ml). The hydrogenolysis was left stirring under an atmosphere of hydrogen for 18 hours. The air sensitive liquid was removed via filter cannula, and the solvent removed *in vacuo* resulting in a very air sensitive white solid. The solid was used without further purification.

7.6.2.3 Diethyl 6,6'-(1,4-diazepane-1,4-diyl)bis(3-nitrobenzoate) (HP^{3-NO₂})

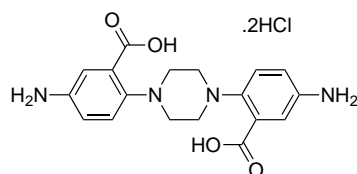
3-NO₂ (440 mg, 2.10 mmol), homopiperazine (95 mg, 0.95 mmol), potassium carbonate (290 mg, 2.10 mmol), and acetonitrile (20 ml) were heated under reflux for 18 hours. Chloroform (30ml) was added, the solution filtered, then solvent removed *in vacuo*, leading to a brown solid. The solid was dissolved in the minimum cold CHCl₃ and then added dropwise to a stirred beaker of hexane. The resulting precipitate was filtered, washed with ether and dried *in vacuo*, affording the title compound as a yellow solid (362 mg, 0.75 mmol, 79 %) IR (KBr, ν_{max} , cm⁻¹) 3446 (br), 3085 (w), 2965 (w), 2904 (w), 2865 (w), 1717 (s), 1700 (s), 1600 (s), 1568 (s), 1499 (s), 1475 (w), 1453 (w), 1429 (s), 1393 (s), 1373 (s), 1320 (br, s), 1284 (s), 1256 (s), 1224 (w), 1211 (w), 1177 (s), 1143 (w), 1127 (s), 1109 (w), 1068 (s), 1018 (s), 970 (s), 956 (w), 941 (s), 918 (s), 895 (w), 864 (s), 832 (w), 812 (s), 778 (s), 747 (s), 732 (s), 719 (s); MS (HR ES⁻) calc. for C₂₃H₂₆N₄O₈Cl (M + Cl⁻) 521.1439 found 521.1422

7.6.2.4 Diethyl 6,6'-(piperazine-1,4-diyl)bis(3-nitrobenzoate) (Pip^{3-NO₂})

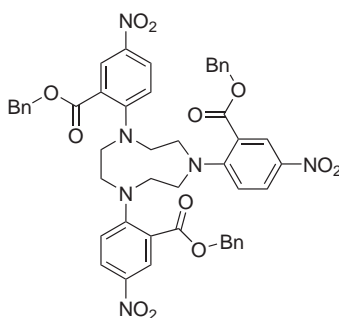
3-NO₂ (230 mg, 1.10 mmol), piperazine (43 mg, 0.50 mmol), Et₃N (100 mg, 1.00 mmol), and acetonitrile (20 ml) were heated under reflux for 18 hours. The solvents were removed *in vacuo*, leading to a yellow solid. The yellow solid was recrystallised from DCM/ethanol yielding the title compound as a yellow solid (128 mg, 0.27 mmol, 54 %). ¹H NMR (400 MHz, CDCl₃, ppm) δ_H: 8.66 – 8.53 (m, 2 H, Ar-H), 8.25 – 8.12 (m, 2 H, Ar-H), 7.01 – 6.87 (m, 2 H, Ar-H), 4.33 (q, 4 H, CH₂CH₃, ²J_{H-H} = 7 + 14 Hz), 3.44 (s, 4 H, CH₂CH₂), 3.32 – 3.26 (m, 2 H, CH₍₂₎CH₂), 3.19 – 3.08 (m, 2 H, CH₍₂₎CH₂), 1.45 – 1.27 (m, 6 H, CH₃CH₂); IR (KBr, ν_{max}, cm⁻¹) 3240 (br), 2976 (s), 2938 (s), 2806 (w), 2738 (w), 2677 (s), 2492 (s), 1699 (s), 1606 (s), 1567 (s), 1506 (s), 1476 (w), 1449 (s), 1434 (s), 1397 (s), 1382 (w), 1336 (br, s), 1265 (s), 1229 (br), 1186 (w), 1169 (w), 1129 (s), 1071 (s), 1034 (br, s), 972 (w), 944 (s), 932 (s), 867 (s), 849 (w), 830 (s), 806 (w), 784 (s), 749 (s), 712 (s), 706 (w); MS (HR ES⁻) calc. for C₂₂H₂₄N₄O₈³⁵Cl (M + Cl⁻) 507.1283 found 507.1299

7.6.2.5 Diethyl 6,6'-(piperazine-1,4-diyl)bis(3-aminobenzoate) (Pip^{3-NH₂})

Into a schlenk under an atmosphere of H₂ were placed Pip^{3-NO₂} (305 mg, 0.65 mmol), Pd-C (10%, 60 mg), and MeOH (20 ml), and stirred for 3 hours until the solution turned colourless. This solution was used as found in the synthesis of Pip^{R,2HCl}.

7.6.2.6 6,6'-(Piperazine-1,4-diyl)bis(3-aminobenzoate) (Pip^{R,2HCl})

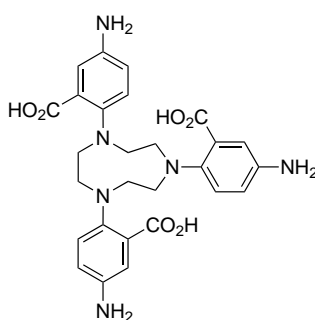
Solution of Pip^{3-NH₂} was cannulated directly into degassed HCl (2M) and stirred for 18 hours. The solvent was removed *in vacuo* yielding the title compound as a hygroscopic white solid that was stored in a vacuum desiccator (259 mg, 0.60 mmol, 95%) ¹H NMR (400 MHz, D₂O, ppm) δ_H : 7.91 (s, 1 H), 7.61 (s, 2 H, Ar-H), 3.63 (s, 4 H, CH₂); MS (HR ES⁻) calc. for C₁₈H₂₁N₄O₄ (M + H⁺) 357.1563 found 357.1565

7.6.2.7 Benzyl-6,6',6''-(1,4,7-triazonane-1,4,7-triyl)tris(3-nitrobenzoate) (TACN^{1-NO₂})

Triazacyclononane (0.430 g, 3.33 mmol), 1-NO₂ (2.84 g, 10.3 mmol), potassium carbonate (1.5 g, 10.9 mmol), and acetonitrile (50 ml) were heated under reflux for 18 hours resulting in a yellow solution. Chloroform (50ml) was added, and the solution filtered. The filtrate was collected and dried *in vacuo* resulting in a yellow solid. This was dissolved in DCM, and EtOH added. The DCM was allowed to evaporate over night. The resulting crystals were filtered and dried under reduced pressure. Crystals of sufficient quality for X-Ray crystallography were obtained by vapour diffusion of pentane into toluene plus 2 drops of methanol (2.43 g, 2.72 mmol, 81.5 %) ¹H NMR (400 MHz, CDCl₃, ppm) δ_H : 8.46 (1 H, d, Ar-H, ²J_{H-H} = 2.8 Hz), 8.03 (1 H, dd, Ar-H, ²J_{H-H} = 2.8 + 9.3 Hz), 7.41 - 7.35 (5 H, m, Ar'-H), 6.58 (1 H, d, Ar-H, ²J_{H-H} = 9.4 Hz), 5.30 (2 H, s, Ar'CH₂), 3.45 (4 H, s, NCH₂); ¹³C NMR (100 MHz, CDCl₃, ppm) δ_C : 167.1, 153.7, 139.0,

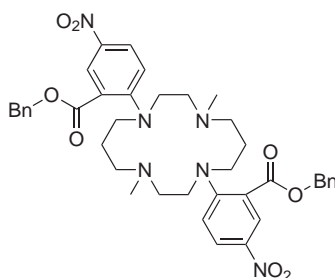
135.7, 129.4, 129.3, 129.2, 128.7, 128.1, 119.8, 116.7, 68.0, 54.0; IR (KBr, ν_{max} , cm^{-1}) 3446 (br), 3033 (w), 2973 (w), 2919 (w), 2849 (w), 1714 (s), 1602 (s), 1575 (s), 1499 (s), 1456 (w), 1429 (w), 1320 (br, s), 1260 (w), 1220 (w), 1186 (w), 1122 (s), 1059 (s), 972 (w), 943 (w), 814 (s), 781 (w), 749 (s), 720 (w); MS (HR APCI⁺) calc. for $\text{C}_{48}\text{H}_{43}\text{N}_6\text{O}_{12}$ ($\text{M} + \text{H}^+$): 895.2939, found: 895.2935

7.6.2.8 6,6',6''-(1,4,7-Triazonane-1,4,7-triyl)tris(3-aminobenzoate) (TACN^R)



Into a schlenk under an atmosphere of H_2 were placed, TACN^{1-NO₂} (115 mg, 0.13 mmol), THF:MeOH (7:1, 35 ml), and palladium on carbon (10 %, 88 mg) in methanol (3 ml). The hydrogenolysis was left stirring under an atmosphere of hydrogen for 48 hours. Completion of the reaction was judged by a colour change from yellow to colourless. The air sensitive liquid was removed via filter cannula, and the solvent removed *in vacuo* resulting in a very air sensitive white solid. The solid was used as found for coordination.

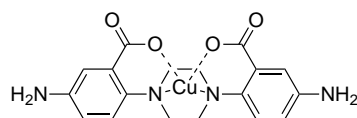
7.6.2.9 Benzyl-6,6'-(4,11-dimethyl-1,4,8,11-tetraazacyclotetradecane-1,8-diyl)bis(3-nitrobenzoate) (DMC^{1-NO₂})



1,8-Dimethylcyclam (0.450 g, 1.97 mmol), 1-NO₂ (1.19 g, 4.33 mmol), potassium carbonate (0.60 g, 4.34 mmol), and acetonitrile (30 ml) were heated under reflux for 18 hours. Chloroform (50 ml) was added, and the solution filtered. The solvent was removed *in vacuo* resulting in a yellow solid, which was dissolved in minimum amount of room temperature chloroform, and methanol added (5 ml). The title compound (0.91 g, 1.23 mmol, 78.9%) was afforded as yellow crystals that slowly formed at the methanol-chloroform interface ¹H NMR (400 MHz, CDCl₃, ppm) δ_H: 8.50 (1 H, d, Ar-H, ²J_{H-H} = 2.8 Hz), 8.13 (1 H, dd, Ar-H, ²J_{H-H} = 2.8 + 9.4 Hz), 7.47 - 7.34 (5 H, m, Ar'-H), 6.90 (1 H, d, Ar-H, ²J_{H-H} = 9.4 Hz), 5.35 (2 H, s, Ar'-CH₂), 3.54 (2 H, t, ring-CH₂, ²J_{H-H} = 8.6 Hz), 3.28 (2 H, t, ring-CH₂, ²J_{H-H} = 5.8 Hz), 2.49 (2 H, t, ring-CH₂, ²J_{H-H} = 5.9 Hz), 2.25 (2 H, t, ring-CH₂, ²J_{H-H} = 5.7 Hz), 2.07 (3 H, s, CH₃), 1.70 (2 H, m, ring-CH₂); ¹³C NMR (126 MHz, CDCl₃, ppm) δ_C: 166.6, 154.6, 137.4, 135.4, 128.7, 128.6, 128.5, 127.2, 116.5, 67.3, 55.4, 54.0, 52.1, 49.0, 43.2, 24.0; IR (KBr, ν_{max}, cm⁻¹) 3007 (w), 2979 (w), 2954 (w), 2845 (s), 2788 (s), 1704 (s), 1600 (s), 1573 (s), 1496 (s), 1480 (w), 1493 (w), 1456 (w), 1448 (s), 1425 (s), 1398 (w), 1321 (s), 1292 (s), 1260 (s), 1240 (w), 1218 (s), 1201 (s), 1165 (s), 1125 (br, s), 1084 (w), 1057 (w), 1039 (s), 959 (s), 953 (w), 940 (s), 919 (s), 883 (s), 859 (w), 820 (s), 810 (w), 786 (w), 780 (w), 763 (w), 757 (s), 749 (w), 721 (s); MS (HR ES⁺) calc. for C₄₀H₄₇N₆O₈ (M + H⁺) 739.3455 found 739.3456

7.6.3 Metal Complexes of Carboxyl Ligands

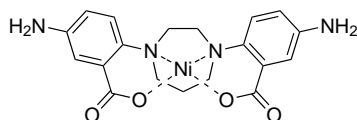
7.6.3.1 Copper(II) (6,6'-(piperazine-1,4-diyl)bis(3-aminobenzoate)) (CuPip^R)



To Pip^{R,2HCl} (48.5 mg, 0.1 mmol) in degassed methanol (10 ml) under an atmosphere of nitrogen was added Et₃N (0.14 ml, 0.1 mmol). CuCl₂·2H₂O (17 mg, 0.1 mmol) in degassed methanol (5 ml) was added resulting in a colour change from colourless to dark blue, and the solution stirred at room temperature for 18 hours. The solvents were removed *in vacuo*, leaving a dark blue solid. This was dissolved in the minimum cold CHCl₃, and added to hexane, yielding the title compound as a blue solid (19 mg, 0.046

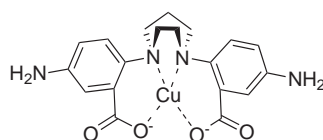
mmol, 46 %) IR (KBr, ν_{max} , cm^{-1}) 3446 (br), 3356 (br), 3221 (br), 2979 (s), 2821 (w), 1714 (s), 1597 (s), 1495 (s), 1447 (s), 1377 (w), 1230 (br, s), 1080 (br, w), 1026 (br, w), 806 (br, s)

7.6.3.2 Nickel(II) (6,6'-(1,4-diazepane-1,4-diyl)bis(3-aminobenzoate)) (NiHP^R)

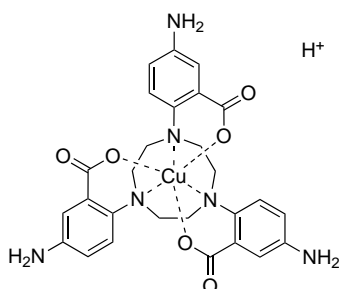


HP^R (67 mg, 0.11 mmol) was dissolved in fresh THF and kept under a nitrogen atmosphere. To this, nickel acetate (28 mg, 0.11 mmol) in ethanol (10 ml) was added via cannula. The solution changed colour from blue to grey after stirring for 5 minutes. The solvent was removed *in vacuo* and the resulting solid was air stable (21 mg, 0.049 mmol, 45 %). ; IR (KBr, ν_{max} , cm^{-1}) 3429 (br), 2925 (w), 2852 (w), 1634 (br, s), 1506 (w), 1458 (w), 1384 (w), 1340 (w), 1313 (w), 1234 (w), 797 (w); MS (LR ES⁺) 426.81 (M + H⁺), 444.81 (M + H₂O + H⁺)

7.6.3.3 Copper(II) (6,6'-(1,4-diazepane-1,4-diyl)bis(3-aminobenzoate)) (CuHP^R)

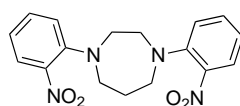


HP^R (189 mg, 0.31 mmol) was dissolved in fresh THF and kept under a nitrogen atmosphere. To this, copper acetate (60 mg, 0.30 mmol) in ethanol (10 ml) was added via cannula. The solution changed colour from blue to green after stirring for 5 minutes. The solvent was removed *in vacuo* and the resulting solid was air stable. IR (KBr, ν_{max} , cm^{-1}) 3437 (br), 3217 (br), 2977 (s), 2939 (s), 2740 (s), 2678 (s), 2603 (s), 2494 (s), 1711 (s), 1596 (br, s), 1473 (s), 1444 (s), 1398 (s), 1206 (br, w), 1037 (s); MS (HR ES⁺) calc. for C₁₉H₂₀N₄O₄Cu Na (M + Na⁺) 454.0678 found 454.0698

7.6.3.4 Copper(II) 6,6',6''-(1,4,7-triazonane-1,4,7-triyl)tris(3-aminobenzoate) (CuTACN^R)

TACN^R (150 mg, 0.28 mmol) was dissolved in THF and kept under an atmosphere of nitrogen. To this, copper nitrate (67 mg, 0.29 mmol) in ethanol (10 ml) was added via filter canula. There was an instant colour change from colourless to dark purple. Gentle heat was applied for 2 minutes, followed by stirring at room temperature for 18 hours. Filtration by filter canula, followed by removal of solvent *in vacuo* yielded the title product as a dark purple/black solid (79 mg, 0.13 mmol, 46 %) IR (KBr, ν_{max} , cm^{-1}) 3352 (br, s), 3216 (br), 2962 (w), 2922 (w), 2865 (w), 1612 (w), 1588 (s), 1560 (br, s), 1495 (s), 1435 (s), 1374 (br, s), 1261 (s), 1163 (w), 1089 (s), 802 (s); MS (LR ES⁻) 594.18 (M⁻); MS (HR ES⁻) calc. for C₂₇H₂₇N₆O₆⁶³Cu (M⁻) 594.1288 found 594.1289

7.6.4 Synthesis of Anilino Ligands

7.6.4.1 General Experimental Procedure (A) - 1,4-Bis(2-nitrophenyl)-1,4-diazepane (L^{22-NO₂})

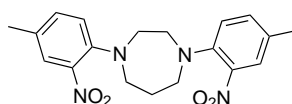
To a solution of homopiperazine (1 eq.) in acetonitrile, was added fluorobenzene (2.2 eq.) and potassium carbonate (2.2 eq.). Under a nitrogen atmosphere, the mixture was refluxed for 18 hrs and the allowed to cool. The solution was filtered, and the solvent removed in *vacuo*.

A typical procedure is that of 1,4-bis(2-nitrophenyl)-1,4-diapane as reported by Perkins:

To a solution of homopiperazine (4.08 g, 40.8 mmol) in acetonitrile (100 ml), were added fluoronitrobenzene (9.5 ml, 89.6 mmol), and potassium carbonate (12.4 g, 89.8

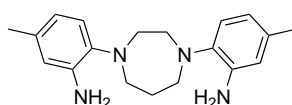
mmol). Under a nitrogen atmosphere, the mixture was refluxed for 18 hrs and then allowed to cool. The solution was filtered, and the solvents removed *in vacuo*, yielding the title as an orange solid (12.6 g, 36.8 mmol, 90 %). ^1H NMR (400 MHz, CDCl_3 , ppm) δ_{H} : 7.71 (2 H, dd, Ar-H, $^2J_{\text{H-H}} = 1.5 + 8.4$ Hz), 7.42 (2 H, ddd, Ar-H, $^2,3J_{\text{H-H}} = 1.5 + 6.6 + 8.4$ Hz), 7.13 (2 H, dd, Ar-H, $^2J_{\text{H-H}} = 1.5 + 8.4$ Hz), 6.94 (2 H, ddd, Ar-H, $^2,3J_{\text{H-H}} = 1.5 + 6.6 + 8.4$ Hz), 3.48 (4 H, s, CH_2N), 3.36 - 3.34 (4 H, m, $\text{CH}_2\text{CH}_2\text{N}$), 2.11 - 2.05 (2 H, m, $\text{CH}_2\text{CH}_2\text{CH}_2$)

7.6.4.2 1,4-Bis(2-nitro-4-tolyl)-1,4-diazepane ($\text{HP}^{\text{Tol-NO}_2}$)



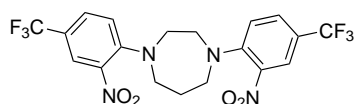
Using general procedure A; homopiperazine (70 mg, 0.70 mmol) in acetonitrile (10 ml), 4-fluoro-3-nitrotoluene (238 mg, 1.54 mmol), and potassium carbonate (212 mg, 1.54 mmol) yielded the crude title compound. The crude product was dissolved in minimum hot CHCl_3 and added dropwise to a stirred beaker of hexane (20 ml). The precipitate was filtered, and gave the title compound as an orange solid (160 mg, 0.68 mmol, 97 %). ^1H NMR (400 MHz, CDCl_3 , ppm) δ_{H} : 7.61 (2 H, d, Ar-H, $^2J_{\text{H-H}} = 8.3$ Hz), 6.84 (2 H, s, Ar-H), 6.67 (2 H, d, Ar-H, $^2J_{\text{H-H}} = 8.3$ Hz), 3.42 (4 H, s, CH_2N), 3.29 - 3.25 (4 H, m, $\text{CH}_2\text{CH}_2\text{N}$), 2.30 (6 H, s, Ar- CH_3), 2.03 - 1.97 (2 H, m, $\text{CH}_2\text{CH}_2\text{CH}_2$); ^{13}C (125 MHz, CDCl_3 , ppm) δ_{C} : 146.3, 144.4, 139.2, 126.4, 120.9, 120.9, 53.8, 53.5, 28.9, and 21.8; IR (KBr, ν_{max} , cm^{-1}) 3446 (br), 2950 (w), 2922 (w), 2855 (w), 1604 (s), 1576 (s), 1506 (s), 1454 (w), 1424 (w), 1383 (w), 1340 (s), 1329 (s), 1308 (w), 1260 (s), 1188 (w), 1172 (w), 1149 (w), 1084 (w), 958 (s), 944 (s), 861 (w), 838 (s), 829 (w), 815 (w), 753 (w), 749 (s); MS (HR ES^+) calc. for $\text{C}_{19}\text{H}_{23}\text{N}_4\text{O}_4$ ($\text{M} + \text{H}^+$) 371.1719 found 371.1731

7.6.4.3 1,4-Bis(2-amino-4-tolyl)-1,4-diazepane (HP^{Tol})



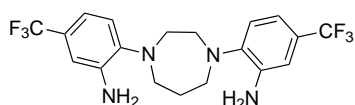
1,4-bis(2-nitro-4-tolyl)-1,4-diazepane (993 mg, 2.68 mmol), and Pd-C (10 %, 150 mg) were placed in MeOH (50 ml) and degassed. The mixture was then stirred under an atmosphere of hydrogen for 18 hrs. The solids were removed by filter cannula and the mother liquor was concentrated *in vacuo* yielding the title compound as a pale yellow air-sensitive solid (618 mg, 1.99 mmol, 74 %); IR (KBr, ν_{max} , cm^{-1}) 3392 (s), 3304 (m), 2919 (s), 2827 (s), 1617 (s), 1585 (s), 1510 (s), 1448 (s), 1380 (s), 1359 (s), 1295 (s), 1248 (s), 1205 (s), 1158 (s), 1092 (s)

7.6.4.4 1,4-Bis(2-nitro-4-trifluoromethylphenyl)-1,4-diazepane (HP^{CF₃-NO₂})



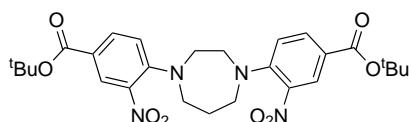
Using general procedure A; homopiperazine (76 mg, 0.76 mmol), in acetonitrile (10 ml), 4-fluoro-3-nitrobenzo-trifluoride (0.23 ml, 1.67 mmol), and potassium carbonate (230 mg, 1.67 mmol) yielded the title compound as an orange solid (170 mg, 0.36 mmol, 47 %). ¹H NMR (400 MHz, CDCl₃, ppm) δ_H : 7.95 (2 H, d, Ar-H, ²J_{H-H} = 1.6 Hz), 7.56 (2 H, dd, Ar-H, ²J_{H-H} = 1.6, ³J_{H-F} = 8.8 Hz), 7.09 (2 H, d, Ar-H, ³J_{H-F} = 8.8 Hz), 3.51 (4 H, s, CH₂N), 3.37 (4 H, m, CH₂CH₂N), 2.10 (2 H, m, CH₂CH₂CH₂); ¹³C (125 MHz, CDCl₃, ppm) δ_C : 147.4, 139.3, 129.8, 124.4, 122.2, 121.4, 119.9, 52.7, 52.5, and 28.2; IR (KBr, ν_{max} , cm^{-1}) 3411 (br), 2973 (w), 2922 (w), 2848 (w), 1630 (s), 1560 (s), 1538 (s), 1507 (w), 1462 (w), 1423 (s), 1396 (w), 1328 (s), 1289 (s), 1261 (s), 1211 (w), 1188 (w), 1172 (w), 1147 (w), 1118 (s), 1040 (w), 1019 (w), 964 (w), 945 (w), 925 (w), 901 (s), 886 (w), 863 (w), 818 (s), 782 (s), 760 (w), 740 (w), 729 (w), 714 (s); MS (HR ES⁻) calc. for C₁₉H₁₆N₄O₄F₆³⁵Cl (M + Cl⁻) 513.0764 found 513.0783

7.6.4.5 1,4-Bis(2-amino-4-trifluoromethylphenyl)-1,4-diazepane (HP^{CF₃})



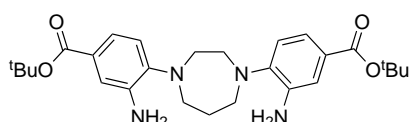
1,4-bis(2-nitro-4-trifluoromethylphenyl)-1,4-diazepane (1.03 g, 2.15 mmol), and Pd-C (10%, 200 mg) were placed in MeOH:THF (2:1, 30 ml) and degassed. The mixture was then stirred under an atmosphere of hydrogen for 3 hrs. The solids are removed by filter cannula and the mother liquor was concentrated *in vacuo* yielding the title compound as a pale yellow air-sensitive solid (714 mg, 1.71 mmol, 80 %) ^1H NMR (400 MHz, CDCl_3 , ppm) δ_{H} : 7.04 - 7.02 (m, 1 H, Ar-H), 6.92 - 6.87 (m, 2 H, Ar-H), 4.05 (br s, 4 H, NH_2), 3.20 - 3.17 (m, 8 H, CH_2N), 1.98 (m, 2 H, $\text{CH}_2\text{CH}_2\text{CH}_2$)

7.6.4.6 Di-tert-butyl 4,4'-(1,4-diazepane-1,4-diyl)bis(3-nitrobenzoate) ($\text{HP}^{\text{tButyl-NO}_2}$)



Homopiperazine (120 mg, 1.20 mmol), t Butyl 4-fluoro-3-nitrobenzoate (640 mg, 2.66 mmol), potassium carbonate (364 mg, 2.64 mmol), and acetonitrile (40 ml) were refluxed overnight under an atmosphere of nitrogen. Methanol (20 ml) was added, the solution filtered, and the solvent removed *in vacuo*, yielding the title product as a yellow solid (584 mg, 1.08 mmol, 90 %) ^1H NMR (300 MHz, CDCl_3 , ppm) 8.32 (s, 2 H, Ar-H), 7.98 (dd, 2 H, Ar-H, $J_{\text{H-H}} = 2 + 12$ Hz), 7.03 (d, 2 H, Ar-H, $J_{\text{H-H}} = 9$ Hz), 3.56 (s, 4 H, CH_2N), 3.42 (m, 4 H, CH_2N), 2.14 (m, 2 H, $\text{CH}_2\text{CH}_2\text{CH}_2$), 1.57 (s, 18 H, CH_3); IR (KBr, ν_{max} , cm^{-1}) 3446 (br), 2968 (w), 2922 (w), 2851 (w), 1700 (s), 1616 (s), 1559 (w), 1524 (s), 1456 (w), 1384 (s), 1368 (w), 1306 (br, s), 1167 (s), 1119 (s), 912 (w), 848 (w), 755 (w)

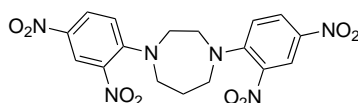
7.6.4.7 Di-tert-butyl 4,4'-(1,4-diazepane-1,4-diyl)bis(3-aminobenzoate) ($\text{HP}^{\text{tButyl}}$)



di-tert-butyl 4,4'-(1,4-diazepane-1,4-diyl)bis(3-nitrobenzoate) (816 mg, 1.51 mmol), and Pd-C (10%, 160 mg) were placed in MeOH:THF (15:2, 17 ml) and degassed. The mixture was then stirred under an atmosphere of hydrogen for 24 hrs. The solids are removed

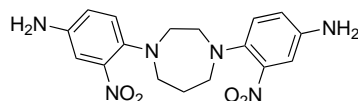
by filter cannula and the mother liquor was concentrated *in vacuo* yielding the title compound as a pale yellow air-sensitive solid (508 mg, 1.05 mmol, 68 %) ^1H NMR (400 MHz, CDCl_3 , ppm) δ_{H} : 7.40 - 7.33 (m, 1 H, Ar-H), 7.09 - 7.01 (m, 2 H, Ar-H), 4.0 (br s, 4 H, NH_2), 3.28 - 3.25 (m, 8 H, CH_2N), 2.10 - 2.02 (m, 2 H, $\text{CH}_2\text{CH}_2\text{CH}_2$), 1.56 (s, 18 H, CH_3)

7.6.4.8 1,4-Bis(2,4-dinitrophenyl)-1,4-diazepane ($\text{HP}^{\text{Sang-NO}_2}$)



Homopiperazine (105 mg, 1.05 mmol), 2,4-dinitrofluorobenzene (0.29 ml, 2.30 mmol), potassium fluoride (133 mg, 2.29 mmol), and acetonitrile (10 ml) were placed in a pressure tube and heated to 95°C for 24 hrs. After cooling to 80°C the product was filtered and the solution left to cool to room temperature. The solvent was reduced by half under reduced pressure, and then filtered yielding the product as a yellow solid (220 mg, 0.51 mmol, 49 %). ^1H NMR (400 MHz, MeOD, ppm) δ_{H} : 8.56 (2 H, d, Ar-H, $^2J_{\text{H-H}} = 2.8$ Hz), 8.21 (2 H, dd, Ar-H, $^2J_{\text{H-H}} = 2.8 + 9.5$ Hz), 7.26 (2 H, d, Ar-H, $^2J_{\text{H-H}} = 9.5$ Hz), 3.62 (4 H, s, CH_2N), 3.58 - 3.52 (4 H, m, $\text{CH}_2\text{CH}_2\text{N}$), 1.98 - 1.95 (2 H, m, $\text{CH}_2\text{CH}_2\text{CH}_2$); IR (KBr, ν_{max} , cm^{-1}) 3446 (br), 3105 (w), 3081 (w), 2919 (w), 2851 (w), 1602 (s), 1576 (s), 1526 (s), 1490 (s), 1433 (s), 1402 (w), 1381 (w), 1330 (s), 1309 (s), 1290 (w), 1248 (w), 1233 (w), 1176 (s), 1145 (w), 1135 (s), 1068 (s), 977 (w), 946 (w), 933 (s), 912 (s), 842 (w), 827 (s), 804 (w), 751 (s), 743 (s), 717 (s).

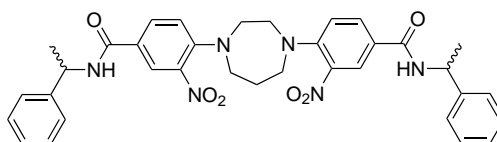
7.6.4.9 1,4-Bis(2-amino-4-nitrophenyl)-1,4-diazepane (HP^{NH_2})



Using general procedure A; homopiperazine (148 mg, 1.48 mmol) in acetonitrile (20 ml), 4-amino-2-nitroaniline (480 mg, 3.08 mmol), and potassium carbonate (448 mg, 3.25 mmol) yielded the crude product as a red-brown solid. Recrystallisation from hot EtOH:Hexane (100 ml, 9:1) gave the title compound as red-brown crystals (502 mg, 1.35

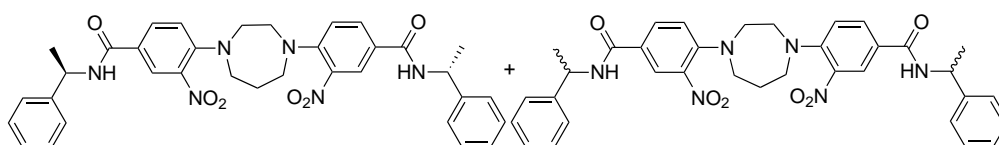
mmol, 91 %). ^1H NMR (400 MHz, CDCl_3 , ppm) δ_{H} : 7.01 (2 H, d, Ar-H, $^2J_{\text{H-H}} = 8.7$ Hz), 6.89 (2 H, d, Ar-H, $^2J_{\text{H-H}} = 2.8$ Hz), 6.73 (2 H, dd, Ar-H, $^2J_{\text{H-H}} = 2.8 + 8.7$ Hz), 3.61 (4 H, s, Ar-NH₂), 3.18 (4 H, s, CH₂N), 3.16 - 3.12 (4 H, m, CH₂CH₂N), 1.90 - 1.84 (2 H, m, CH₂CH₂CH₂); ^{13}C (125 MHz, CDCl_3 , ppm) δ_{C} : 145.2, 141.6, 139.2, 124.7, 120.0, 110.1, 56.4, 55.1, and 29.3; IR (KBr, ν_{max} , cm^{-1}) 3462 (br, s), 3374 (br, s), 2925 (w), 2851 (w), 2833 (w), 1635 (s), 1520 (s), 1362 (s), 1307 (s), 1264 (w), 1211 (w), 1153 (w), 910 (s), 851 (w), 813 (s); MS (HR ES⁺) calc. for C₁₇H₂₁N₆O₄ (M + H⁺) 373.1624 found 373.1616

7.6.4.10 1,4-Bis(2-nitro-N-((+/-)-1-phenylethyl)-4-benzamide)-1,4-diazepane (HP^{AmideRac})



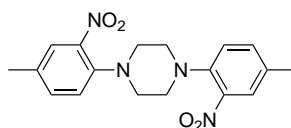
Using general procedure A; homopiperazine (34 mg, 0.34 mmol) in acetonitrile (20 ml), ((+/-)-1-phenylethyl)-4-fluoro-3-nitrobenzamide (197 mg, 0.68 mmol), and potassium carbonate (94 mg, 0.68 mmol) yielded the crude product as a yellow oil. The yellow oil was dissolved in minimum hot CHCl_3 and added dropwise to a stirred beaker of hexane. The purified product was isolated by filtration as a yellow solid (165 mg, 0.26 mmol, 76 %). ^1H NMR (400 MHz, CDCl_3 , ppm) δ_{H} : 8.05 (2 H, d, Ar-H, $^2J_{\text{H-H}} = 2.2$ Hz), 7.80 (2 H, dd, Ar-H, $^2J_{\text{H-H}} = 2.2 + 8.8$ Hz), 7.29 (10 H, m, Ar'-H), 7.01 (2 H, d, Ar-H, $^2J_{\text{H-H}} = 8.8$ Hz), 6.19 (2 H, d, NH, $^2J_{\text{H-H}} = 7.6$ Hz), 5.24 (2 H, m, CH₃CHNH), 3.47 (4 H, s, CH₂N), 3.35 (4 H, m, CH₂CH₂N), 2.07 (2 H, m, CH₂CH₂CH₂), 1.54 (6 H, d, CH₃CH, J = 6.9 Hz); IR (KBr, ν_{max} , cm^{-1}) 3441 (br, s), 2973 (w), 2923 (w), 2855 (w), 1616 (br, s), 1516 (s), 1456 (w), 1412 (w), 1336 (br), 1264 (br), 1205 (w), 1153 (w), 1013 (w), 823 (w), 760 (s); MS (HR ES⁻) calc. for C₃₅H₃₅N₆O₆ (M - H⁺) 635.2618 found 635.2611

7.6.4.11 1,4-Bis(2-nitro-N-((R)-1-phenylethyl)-4-benzamide)-1,4-diazepane "doped"

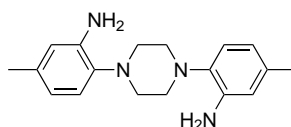


Using the same method as for 1,4-bis(2-nitro-N-((+/-)-1-phenylethyl)-4-benzamide)-1,4-diazepane with homopiperazine (35 mg, 0.35 mmol), 4-fluoro-3-nitro-N-((+/-)-1-phenylethyl)-benzamide (180 mg, 0.625 mmol), 4-fluoro-3-nitro-N-((R)-1-phenylethyl)-benzamide (21.6 mg, 0.75 mmol) and potassium carbonate (96 mg, 0.70 mmol) yielded the title compound as a yellow solid (165 mg, 0.26 mmol, 74 %). ^1H NMR (400 MHz, CDCl_3 , ppm) δ_{H} : 8.04 (2 H, d, Ar-H, $^2\text{J}_{\text{H-H}} = 2.2$ Hz), 7.79 (2 H, dd, Ar-H, $^2\text{J}_{\text{H-H}} = 2.2 + 8.8$ Hz), 7.33 - 7.21 (10 H, m, Ar'-H), 6.99 (2 H, d, Ar-H, $^2\text{J}_{\text{H-H}} = 8.8$ Hz), 6.25 (2 H, d, NH, $^2\text{J}_{\text{H-H}} = 7.0$ Hz), 5.23 (2 H, p, CH_3CHN , $^2\text{J}_{\text{H-H}} = 7.0$ Hz), 3.46 (4 H, s, CH_2N), 3.38 - 3.30 (4 H, m, $\text{CH}_2\text{CH}_2\text{N}$), 2.10 - 2.02 (2 H, m, $\text{CH}_2\text{CH}_2\text{CH}_2$), 1.54 (6 H, d, CH_3CH , $^2\text{J}_{\text{H-H}} = 7.0$ Hz); ^{13}C (125 MHz, CDCl_3 , ppm) δ_{C} : 147.3, 142.9, 139.2, 132.1, 128.8, 127.6, 127.5, 126.3, 125.4, 119.3, 52.6, 52.5, 49.5, 28.2, and 21.7

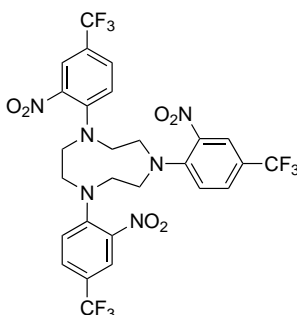
7.6.4.12 1,3-Bis(2-nitro-4-tolyl)-1,3-diazacyclohexane ($\text{Pip}^{\text{Tol-NO}_2}$)



To a solution of piperazine (146 mg, 1.70 mmol) in acetonitrile (30 ml), were added 4-fluoro-3-nitrotoluene (530 mg, 3.42 mmol), and potassium carbonate (470 mg, 3.41 mmol). Under a nitrogen atmosphere, the mixture was refluxed for 18 hrs and then allowed to cool. The solution was filtered, and the solvents removed *in vacuo*. The solid was dissolved in the minimum hot CHCl_3 and added dropwise to stirred hexane (30 ml). The purified title compound was isolated by filtration of the orange precipitate (527 mg, 1.48 mmol, 87 %) ^1H NMR (400 MHz, CDCl_3 , ppm) δ_{H} : 7.61 (2 H, s, Ar-H), 7.34 (2 H, dd, Ar-H, $^2\text{J}_{\text{H-H}} = 1.8 + 8.4$ Hz), 7.16 (2 H, d, Ar-H, $^2\text{J}_{\text{H-H}} = 8.4$ Hz), 3.18 (8 H, s, CH_2N), 2.38 (6 H, s, Ar- CH_3); IR (KBr, ν_{max} , cm^{-1}) 3430 (br), 2064 (w), 3001 (s), 2958 (s), 2926 (w), 2892 (w), 1619 (s), 1559 (s), 1521 (s), 1498 (s), 1453 (s), 1382 (w), 1377 (s), 1343 (br, s), 1288 (s), 1256 (s), 1223 (s), 1165 (s), 1135 (w), 1087 (w), 1041 (s), 969 (w), 943 (s), 909 (s), 835 (w), 824 (s), 799 (s), 764 (w), 724 (w).

7.6.4.13 1,3-Bis(2-amino-4-tolyl)-1,3-diazacyclohexane (Pip^{Tol})

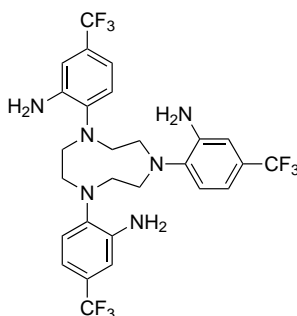
1,3-Bis(2-nitro-4-tolyl)-1,3-diazacyclohexane (53 mg, 0.15 mmol), and Pd-C (10%, 15 mg) were placed in MeOH (15 ml) and degassed. The mixture was then stirred under an atmosphere of hydrogen for 3 hr. The colourless liquid was transferred by filter cannula and the volatiles removed *in vacuo* yielding the title compound as a pale yellow air-sensitive solid. This was used immediately for coordination experiments.

7.6.4.14 1,4,7-Tris(2-nitro-4-trifluoromethylphenyl)-1,4,7-triazacyclononane (TACN^{CF₃-NO₂})

To a solution of triazacyclononane (208 mg, 1.61 mmol) in acetonitrile (30 ml), were added 4-fluoro-3-nitrobenzo-trifluoride (1.01 g, 4.83 mmol), and potassium carbonate (670 mg, 4.86 mmol). Under a nitrogen atmosphere, the mixture was refluxed for 18 hrs and then allowed to cool. The solution was filtered, and the solvent removed *in vacuo*. The solid was redissolved in the minimum hot CHCl₃ and added dropwise to stirred hexane (50 ml). The purified title compound was isolated as a yellow solid by filtration (860 mg, 1.24 mmol, 77 %) ¹H NMR (400 MHz, CDCl₃, ppm) δ_H: 7.84 (3 H, d, Ar-H, ²J_{H-H} = 1.7 Hz), 7.56 (3 H, dd, Ar-H, ²J_{H-H} = 2.0 Hz, ³J_{H-F} = 8.8 Hz), 7.10 (3 H, d, Ar-H, ³J_{H-F} = 8.8 Hz), 3.55 (12 H, s, CH₂N); IR (KBr, ν_{max}, cm⁻¹) 3402 (br), 3093 (br), 2960 (w), 2930 (br), 1871 (w), 1624 (s), 1561 (s), 1532 (s), 1466 (w), 1439 (w), 1427 (w), 1402 (s), 1328 (br, s) 1290 (s), 1275 (s), 1248 (w), 1227 (s), 1194 (w), 1163 (s), 1118 (s), 1090 (s), 1024 (w), 991 (w), 970 (w), 909 (s), 882 (w), 875 (w), 854 (w), 811 (s), 787 (s), 7557 (w), 718 (s),

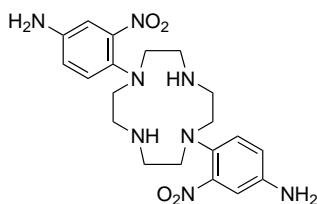
712 (s); MS (HR ES⁻) calc. for C₂₇H₂₁N₆O₆F₉Cl (M + Cl⁻) 731.1067 found 731.1074

7.6.4.15 1,4,7-Tris(2-amino-4-trifluoromethylphenyl)-1,4,7-triazacyclononane (TACN^{CF₃})



1,4,7-tris(2-nitro-4-trifluoromethylphenyl)-1,4,7-triazacyclononane (85 mg, 0.12 mmol) and Pd-C (10 %, 25 mg) were placed in MeOH (15 ml) and degassed, the mixture was then stirred for 3 hrs in an atmosphere of hydrogen. The colourless liquid was removed by filter cannula and the solvent was removed *in vacuo* yielding the title compound as a white solid that was used immediately.

7.6.4.16 1,7-Bis(2-nitro-4-aniliny)-1,4,7,10-tetraazacyclododecane (Cyclen^{NH₂})

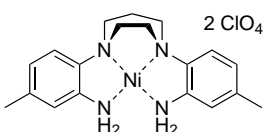


To a solution of tetraazacyclododecane (117 mg, 0.68 mmol) in acetonitrile (25 ml), were added 4-fluoro-3-nitroaniline (540 mg, 3.46 mmol), and potassium carbonate (470 mg, 3.41 mmol). Under a nitrogen atmosphere, the mixture was refluxed for 18 hrs and then allowed to cool. The solution was filtered, and the solvent removed *in vacuo*. The solid was dissolved in hot THF (20 ml) and allowed to cool. The resulting orange crystals were isolated by filtration, yielding the title compound as an orange solid (263 mg, 0.59 mmol, 87 %). ¹H NMR (400 MHz, MeOD, ppm) δ_H: 7.45 (2 H, m, Ar-H), 6.93 (2 H, d,

Ar-H, $^2J_{H-H} = 1.8$ Hz), 6.91 (2 H, d, Ar-H, $^2J_{H-H} = 2.7$ Hz), 3.33 (4 H, m, Ar-NH₂), 3.12 (8 H, s, CH₂NAr), 2.63 (8 H, s, CH₂NH); MS (LR, ES⁺) 444.84 (M⁺)

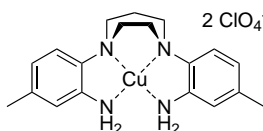
7.6.5 Metal Complexes of Anilino Ligands

7.6.5.1 Nickel(II) 1,4-bis(2-amino-4-tolyl)-1,4-diazepane (perchlorate salt) (NiHP^{Tol})



Under an inert atmosphere Ni(ClO₄)₂·6H₂O (80 mg, 0.22 mmol) was dissolved in degassed EtOH (10 ml), and added via cannula to 1,4-bis(2-amino-4-tolyl)-1,4-diazepane (62 mg, 0.20 mmol), gently heated for 2 minutes, and then stirred for 1 hr at room temperature. The solution was then reduced in volume by half under reduced pressure, and Et₂O (20 ml) added, which initiates precipitation of the product. The title product was isolated by filtration as a cream solid (74 mg, 0.13 mmol, 59 %). ¹H NMR (400 MHz, Acetone-d₆, ppm) δ_H: 7.49 (2 H, s, Ar-H), 7.29 - 7.25 (4 H, m, Ar-H), 5.02 - 4.94 (4 H, m, Mac-H), 4.78 - 4.68 (2 H, m, Mac-H), 4.22 - 4.16 (2 H, m, Mac-H), 4.12 - 4.02 (2 H, m, Mac-H), 3.77 - 3.59 (2 H, m, Mac-H), 2.97 - 2.87 (6 H, m, Mac-H), 2.70 - 2.51 (2 H, m, Mac-H), 2.37 (6H, s, Ar-CH₃); UV (acetone, nm) 435 (ε = 76 mol⁻¹cm⁻¹), 583 (ε = 18 mol⁻¹cm⁻¹), 764 (ε = 11 mol⁻¹cm⁻¹); IR (Diamond anvil, ν_{max}, cm⁻¹) 3226 (m), 3186 (m), 2970 (w), 1730 (s), 1706 (s), 1506 (s), 1411 (s), 1342 (s), 1234 (s), 1112 (s); MS (LR ES⁺) 367.13 (M²⁺ - H⁺), (HR ES⁺) calc. for C₁₉H₂₆N₄O₄Cl⁵⁸Ni (M²⁺ + ClO₄⁻) 467.0996, found 467.0979

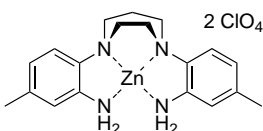
7.6.5.2 Copper(II) 1,4-bis(2-amino-4-tolyl)-1,4-diazepane (perchlorate salt) (CuHP^{Tol})



Under an inert atmosphere Cu(ClO₄)₂·6H₂O (60 mg, 0.16 mmol) was dissolved in degassed EtOH (10 ml), and added via cannula to 1,4-bis(2-amino-4-tolyl)-1,4-diazepane

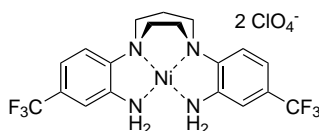
(54 mg, 0.17 mmol), gently heated for 2 minutes and then stirred for 1 hr at room temperature. The solution was then reduced in volume by half under reduced pressure, and Et₂O (20 ml) added, which initiates precipitation of the product. The title product was isolated by filtration as a purple solid (40 mg, 0.11 mmol, 67 %). UV (acetone, nm) 577 ($\epsilon = 292 \text{ mol}^{-1} \text{ cm}^{-1}$); IR (KBr, ν_{max} , cm^{-1}) 3522 (b), 3243 (b), 2963 (w), 2941 (w), 2905 (w), 2360 (m), 2342 (m), 1621 (m), 1601 (m), 1568 (m), 1503 (s), 1464 (m), 1261 (s), 1209 (s), 1088 (b); MS (LR ES⁺) 311.23 ($\text{M}^{2+} - {}^{63}\text{Cu}^{2+} + \text{H}^+$, 100 %), 372.14 ($\text{M}^{2+} - \text{H}^+$, 10 %) (HR ES⁺) calc. for C₁₉H₂₅N₄Cu ($\text{M}^{2+} - \text{H}^+$) 372.1375 found 372.1383

7.6.5.3 Zinc(II) 1,4-bis(2-amino-4-tolyl)-1,4-diazepane (perchlorate salt) (ZnHP^{Tol})



Under an inert atmosphere Zn(ClO₄)₂·6H₂O (63 mg, 0.17 mmol) was dissolved in degassed EtOH (10 ml), and added via cannula to 1,4-bis(2-amino-4-tolyl)-1,4-diazepane (48 mg, 0.15 mmol), gently heated for 2 minutes and then stirred for 1 hr at room temperature. The solution was then reduced in volume by half in vacuo, and Et₂O (20 ml) added, which initiates precipitation of the product. The title product was isolated by filtration as an off white solid (53 mg, 0.093 mmol, 62 %) MS (LR ES⁺) 373.14 ($\text{M}^{2+} - \text{H}^+$, 100 %), (HR ES⁺) calc. for C₁₉H₂₅N₄⁶⁴Zn ($\text{M}^{2+} - \text{H}^+$) 373.1371 found 373.1381

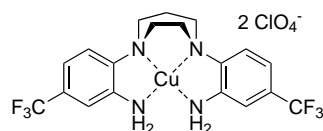
7.6.5.4 Nickel(II) 1,4-bis(2-amino-4-trifluoromethylphenyl)-1,4-diazepane (perchlorate salt) (NiHP^{CF₃})



Under an inert atmosphere Ni(ClO₄)₂·6H₂O (60 mg, 0.16 mmol) was dissolved in degassed EtOH (10 ml), and added via cannula to 1,4-bis(2-amino-4-trifluoromethylphenyl)-1,4-diazepane (68 mg, 0.16 mmol), gently heated for 2 minutes, and then stirred for 1 hr

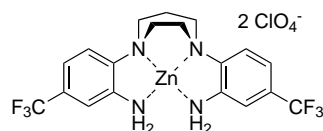
at room temperature. The solution was then filtered, and the solvent removed *in vacuo* yielding the title product as a cream solid (31 mg, 0.05 mmol, 29 %). UV (acetone, nm) 507 ($\epsilon = 20 \text{ mol}^{-1} \text{ cm}^{-1}$), 562 ($\epsilon = 12 \text{ mol}^{-1} \text{ cm}^{-1}$), 803 ($\epsilon = 11 \text{ mol}^{-1} \text{ cm}^{-1}$); IR (KBr, ν_{max} , cm^{-1}) 3419 (br, w), 3344 (br), 2967 (w), 2934 (w), 2854 (w), 1630 (s), 1554 (w), 1431 (w), 1332 (s), 1261 (w), 1119 (br, s), 802 (w); MS (LR ES⁺) 475.09 ($\text{M}^{2+} - \text{H}^+$, 100 %), (HR ES⁺) calc. for $\text{C}_{19}\text{H}_{19}\text{N}_4\text{F}_6$ ^{58}Ni ($\text{M}^{2+} - \text{H}^+$) 475.0867 found 475.0880

7.6.5.5 Copper(II) 1,4-bis(2-amino-4-trifluoromethylphenyl)-1,4-diazepane (perchlorate salt) ($\text{CuHP}^{\text{CF}_3}$)



Under an inert atmosphere $\text{Cu}(\text{ClO}_4)_2 \cdot 6\text{H}_2\text{O}$ (47 mg, 0.13 mmol) was dissolved in degassed EtOH (10 ml), and added via cannula to 1,4-bis(2-amino-4-tolyl)-1,4-diazepane (53 mg, 0.13 mmol), gently heated for 2 minutes and then stirred for 1 hr at room temperature. The solution was then filtered, and the solvent removed *in vacuo* yielding the title product as a purple solid (52 mg, 0.08 mmol, 59 %). UV (acetone, nm) 572 ($\epsilon = 143 \text{ mol}^{-1} \text{ cm}^{-1}$); IR (KBr, ν_{max} , cm^{-1}) 3519 (br, w), 3433 (br), 2965 (w), 2925 (w), 2854 (w), 1635 (s), 1532 (w), 1435 (w), 1332 (s), 1260 (w), 1121 (br), 1109 (br, s), 1087 (br, s), 808 (w); MS (LR ES⁺) 480.08 ($\text{M}^{2+} - \text{H}^+$, 100 %), (HR ES⁺) calc. for $\text{C}_{19}\text{H}_{19}\text{N}_4\text{F}_6$ ^{63}Cu ($\text{M}^{2+} - \text{H}^+$) 480.0810 found 480.0813

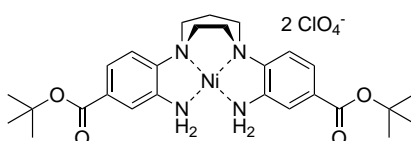
7.6.5.6 Zinc(II) 1,4-bis(2-amino-4-trifluoromethylphenyl)-1,4-diazepane (perchlorate salt) ($\text{ZnHP}^{\text{CF}_3}$)



Under an inert atmosphere $\text{Zn}(\text{ClO}_4)_2 \cdot 6\text{H}_2\text{O}$ (58 mg, 0.16 mmol) was dissolved in degassed EtOH (10 ml), and added via cannula to 1,4-bis(2-amino-4-trifluoromethylphenyl)-

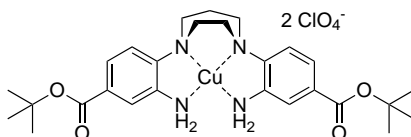
1,4-diazepane (65 mg, 0.16 mmol), gently heated for 2 minutes, and then stirred for 1 hr at room temperature. The solution was then filtered, and the solvent removed *in vacuo* yielding the title product as a cream solid (42 mg, 0.06 mmol, 38 %). IR (KBr, ν_{max} , cm^{-1}) 3287 (br), 2963 (w), 2925 (w), 2894 (w), 2856 (w), 1627 (s), 1576 (w), 1512 (s), 1429 (s), 1334 (s), 1291 (w), 1262 (w), 1122 (br, s), 897 (w), 798 (w), 746 (s)

7.6.5.7 Nickel(II) di-tert-butyl 4,4'-(1,4-diazepane-1,4-diyl)bis(3-aminobenzoate) (NiHP^{tButyl})



Under an inert atmosphere $\text{Ni}(\text{ClO}_4)_2 \cdot 6\text{H}_2\text{O}$ (52 mg, 0.14 mmol) was dissolved in degassed EtOH (10 ml), and added via cannula to di-tert-butyl 4,4'-(1,4-diazepane-1,4-diyl)bis(3-aminobenzoate) (68 mg, 0.14 mmol), gently heated for 2 minutes, and then stirred for 1 hr at room temperature. The solution was then filtered, and the solvent removed *in vacuo* yielding the title product as a cream solid (50 mg, 0.07 mmol, 48 %) UV (MeOH, nm) 487 ($\epsilon = 131 \text{ mol}^{-1} \text{ cm}^{-1}$), 623 ($\epsilon = 85 \text{ mol}^{-1} \text{ cm}^{-1}$); IR (KBr, ν_{max} , cm^{-1}) 3399 (br, s), 2968 (w), 2930 (w), 2879 (w), 1635 (s), 1540 (s), 1496 (s), 1456 (w), 1399 (w), 1331 (w), 1263 (s), 1147 (s), 1115 (s), 1088 (s), 802 (w), 764 (w); MS (LR ES⁺) 483.29 (M - Ni²⁺ + 2H⁺, 50 %), 539.22 (M²⁺ - H⁺, 100 %), (HR ES⁺) calc. for $\text{C}_{27}\text{H}_{37}\text{N}_4\text{O}_4$ ⁵⁸Ni (M²⁺ - H⁺) 539.2168 found 539.2165

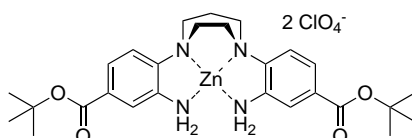
7.6.5.8 Copper(II) di-tert-butyl 4,4'-(1,4-diazepane-1,4-diyl)bis(3-aminobenzoate) (CuHP^{tButyl})



Under an inert atmosphere $\text{Cu}(\text{ClO}_4)_2 \cdot 6\text{H}_2\text{O}$ (52 mg, 0.14 mmol) was dissolved in degassed EtOH (10 ml), and added via cannula to di-tert-butyl 4,4'-(1,4-diazepane-1,4-diyl)bis(3-aminobenzoate) (68 mg, 0.14 mmol), gently heated for 2 minutes, and then

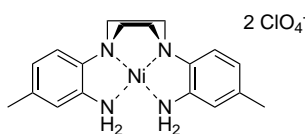
stirred for 1 hr at room temperature. The solution was then filtered, and the solvent removed *in vacuo* yielding the title product as a cream solid (50 mg, 0.07 mmol, 48 %) UV (MeOH, nm) 410 ($\epsilon = 654 \text{ mol}^{-1}\text{cm}^{-1}$), 612 ($\epsilon = 458 \text{ mol}^{-1}\text{cm}^{-1}$), 813 ($\epsilon = 371 \text{ mol}^{-1}\text{cm}^{-1}$); IR (KBr, ν_{max} , cm^{-1}) 3382 (br, w), 3245 (br, w), 2966 (w), 2931 (w), 2871 (w), 1635 (s), 1537 (s), 1495 (s), 1451 (w), 1380 (w), 1318 (w), 1262 (w), 1088 (br, s), 904 (w), 803 (w), 762 (w), 742 (w), 702 (w); MS (LR ES⁺) 483.29 (M - Cu²⁺ + 2H⁺, 80 %), 544.21 (M²⁺ - H⁺, 100 %), (HR ES⁺) calc. for C₂₇H₃₇N₄O₄ ⁶³Cu (M²⁺ - H⁺) 544.211 found 544.2096

7.6.5.9 Zinc(II) di-tert-butyl 4,4'-(1,4-diazepane-1,4-diyl)bis(3-aminobenzoate) (ZnHP^tButyl)



Under an inert atmosphere Zn(ClO₄)₂·6H₂O (40 mg, 0.11 mmol) was dissolved in degassed EtOH (10 ml), and added via cannula to di-tert-butyl 4,4'-(1,4-diazepane-1,4-diyl)bis(3-aminobenzoate) (51 mg, 0.11 mmol), gently heated for 2 minutes, and then stirred for 1 hr at room temperature. The solution was then filtered, and the solvent removed *in vacuo* yielding the title product as a cream solid (57 mg, 0.08 mmol, 69 %) IR (KBr, ν_{max} , cm^{-1}) 3466 (br, w), 3260 (br, w) 2975 (w), 2925 (w), 2855 (w), 1714 (s), 1616 (s), 1501 (w), 1456 (w), 1419 (w), 1370 (w), 1312 (s), 1260 (w), 1122 (br, s), 844 (w), 814 (w), 770 (s), 732 (w); MS (LR ES⁺) 546.22 (M²⁺ - H⁺, 100 %)

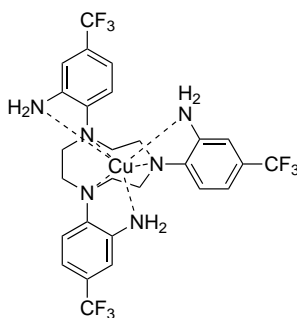
7.6.5.10 Nickel(II) 1,3-bis(2-amino-4-tolyl)-1,3-diazacyclohexane (perchlorate salt) (NiPip^{Tol})



Ni(ClO₄)₂·6H₂O (69 mg, 0.19 mmol) was dissolved in EtOH and degassed. Under a nitrogen atmosphere the nickel solution was added by cannula to 1,3-bis(2-amino-4-tolyl)-1,3-diazacyclohexane (56.5 mg, 0.19 mmol) and the mixture was gently heated for

2 minutes stirred for an hour at room temperature. A fine yellow precipitate formed, which was isolated by centrifugation, and then redissolved in MeOH. The insoluble residue was discarded. The mother liquor concentrated *in vacuo*, yielding the title compound as a yellow solid. IR (KBr, ν_{max} , cm^{-1}) 3421 (br, s), 3222 (br, w), 2927 (w), 2849 (w), 1616 (s), 1559 (w), 1506 (s), 1456 (w), 1145 (s), 1113 (br, s), 1089 (s), 797 (w); MS (LR ES⁺): 353.13 (M + H⁺)

7.6.5.11 Copper(II) 1,4,7-tris(2-amino-4-trifluoromethylphenyl)-1,4,7-triazacyclononane (perchlorate salt) (CuTACN^{CF₃})

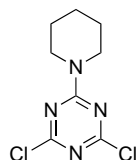


Cu(ClO₄)₂·6H₂O (52 mg, 0.14 mmol) was dissolved in EtOH (10 ml) and degassed. The copper solution was then transferred via canula onto 1,4,7-tris(2-amino-4-trifluoromethylphenyl)-1,4,7-triazacyclononane (85 mg, 0.14 mmol), then gently heated for 2 minutes and then stirred for an hour at room temperature. The solvent was then removed *in vacuo*, giving a green oil, which was then redissolved in a minimum of EtOH. Single crystals for x-ray diffraction were obtained by vapour diffusion of pentane into this solution. X-Ray data - see appendix.

7.7 Triazine Core Derived Compounds

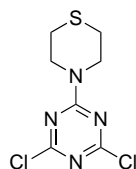
7.7.1 Dipyridamole type complexes

7.7.1.1 2,4-Dichloro-6-(piperidin-1-yl)-1,3,5-triazine (TzPipCl₂)



Cyanuric chloride (48.1 g, 261 mmol) was dissolved in a mixture of acetone (400 ml) and THF (200 ml), added to ice water (400 ml) to form a slurry, and cooled to 0°C. Piperidine (25.8 ml, 261 mmol) in acetone (100 ml), was added dropwise to the stirred slurry. Na₂CO₃ (27.7 g, 261 mmol) was added portion-wise throughout so as to keep the pH neutral. The mixture was stirred at room temperature for 48 hours, filtered, and the solid was recrystallised from hot MeOH (2.5 g/50 ml), yielding the title product as colourless crystals (40.1 g, 172 mmol, 66 %) ¹H NMR (400 MHz, MeOD, ppm) δ_H: 3.90 – 3.77 (m, 4 H, NCH₂), 1.77 – 1.71 (m, 2 H, CH₂CH₂CH₂), 1.69 – 1.58 (m, 4 H, NHCH₂CH₂); IR (KBr, ν_{max}, cm⁻¹) 2943 (s), 2927 (s), 2862 (w), 1615 (s), 1594 (s), 1552 (s), 1466 (s), 1441 (s), 1348 (s), 1329 (s), 1289 (s), 1258 (w), 1229 (s), 1170 (s), 1155 (s), 1116 (s), 1064 (s), 1022 (w), 987 (s), 951 (w), 903 (w), 843 (s), 790 (s).

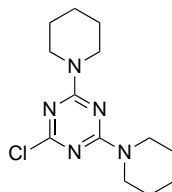
7.7.1.2 4,6-dichloro-2-thiomorphyl-1,3,5-triazine (TzMorphCl₂)



Cyanuric chloride (1.8 g, 10 mmol) was dissolved in acetone (10 mL) and added to ice-water to form a slurry. Thiomorpholine (1 ml, 11 mmol) in acetone (10 ml) was added dropwise to the stirred slurry. Na₂CO₃ (0.9 g, 10 mmol) was added portionwise throughout so as to keep the pH neutral. The mixture was stirred at room temperature for 24 hours, filtered, and the solid was recrystallised from hot EtOH, yielding the title

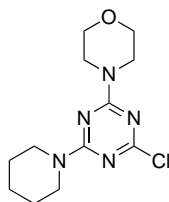
product as colourless crystals (1.46 g, 5 mmol, 61%) ^1H NMR (500MHz, CDCl_3 , ppm) δ_{H} : 4.12 - 4.03 (m, 4 H, NCH_2), 2.73 - 2.68 (m, 4 H, SCH_2). ^{13}C NMR (500MHz, CDCl_3 , ppm) δ_{C} : 170.4, 164.0, 46.9, 27.4

7.7.1.3 4,4'-(6-chloro-1,3,5-triazine-2,4-diyl)dipiperidine (TzPip₂Cl)



TzPipCl₂ (3.25 g, 13.9 mmol) was dissolved in acetone (15 ml) and added to ice water resulting in a slurry. Piperidine (1.4 ml, 14.2 mmol) was dissolved in acetone (15 ml) added dropwise to the TzPipCl₂ slurry. NaHCO₃ (1.17 g, 13.9 mmol) was added portion-wise so as the pH remained neutral, and the mixture stirred over night at room temperature. The mixture was filtered, and the solid recrystallised from hot EtOH yielding the title compound as a white solid (2.5 g, 8.9 mmol, 64 %) ^1H NMR (250 MHz, CDCl_3 , ppm) δ_{H} : 3.86 - 3.76 (m, 8 H, NCH_2), 1.74 - 1.71 (m, 4 H, $\text{CH}_2\text{CH}_2\text{CH}_2$), 1.62 - 1.53 (m, 8 H, NHCH_2CH_2); MS (HR AP⁺) calc. for C₁₃H₂₁N₅Cl (M + H⁺) 282.1485 found 282.1478

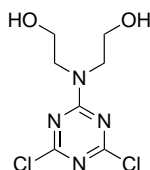
7.7.1.4 4-(4-chloro-6-(piperidin-1-yl)-1,3,5-triazin-2-yl)morpholine (TzPipMorphCl)



TzPipCl₂ (3.18 g, 13.6 mmol) was dissolved in acetone (15 ml) and added to ice water resulting in a slurry. Morpholine (1.19 ml, 13.6 mmol) was dissolved in acetone (15 ml) added dropwise to the TzPipCl₂ slurry. NaHCO₃ (1.15 g, 13.7 mmol) was added portion-wise so as the pH remained neutral, and the mixture stirred over night at room

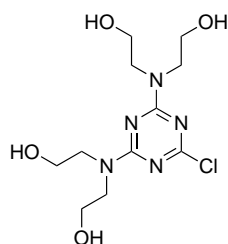
temperature. The mixture was filtered, and the solid recrystallised from hot EtOH yielding the title compound as a white solid (2.2 g, 7.8 mmol, 57 %) ^1H NMR (250 MHz, CDCl_3 , ppm) δ_{H} : 3.85 – 3.63 (m, 12 H), 1.76 – 1.47 (m, 6 H)

7.7.1.5 2,2'-((4,6-Dichloro-1,3,5-triazin-2-yl)azanediyl)diethanol (TzDEACl₂)



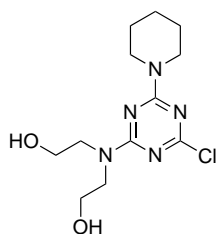
Cyanuric chloride (9.2 g, 49.9 mmol) was dissolved in acetone (50 ml) and added to ice water (100 ml) to form a slurry. Diethanolamine (5.2 g, 49.5 mmol) was dissolved in acetone (50 ml) and added dropwise to the slurry at 0°C over 1 hr. NaHCO_3 (4.2 g, 50 mmol) was added periodically so as to keep pH neutral. The solution was allowed to warm to room temperature and stirred for a further 12 hours. The resulting precipitate was filtered, washed with water (50 ml) and Et_2O (50 ml), and dried *in vacuo*, yielding the title product as a white solid (9.7 g, 38.3 mmol, 77 %) ^1H NMR (500 MHz, DMSO-d_6 , ppm) δ_{H} : 3.98 (s, CH_2OH), 3.66 (t, 4 H, $^2\text{J}_{\text{H-H}} = 5.7$ Hz, NCH_2), 3.59 (t, 4 H, $^2\text{J}_{\text{H-H}} = 5.8$ Hz, CH_2OH); ^{13}C NMR (126 MHz, DMSO-d_6 , ppm) δ_{C} : 168.7, 164.3, 57.7, 50.8; IR (KBr, ν_{max} , cm^{-1}) 3237 (br), 3156 (br), 2997 (w), 2965 (w), 2889 (w), 2847 (w), 1596 (s), 1559 (s), 1478 (s), 1424 (s), 1363 (s), 1350 (s), 1328 (s), 1292 (s), 1225 (s), 1185 (s), 1153 (s), 1060 (s), 1023 (s), 985 (w), 954 (w), 922 (s), 859 (s), 842 (s), 793 (s), 751 (br, w); MS (LR ES^-) 286.99 ($\text{M} + \text{Cl}^-$), (HR ES^-) calc. for $\text{C}_7\text{H}_{10}\text{N}_4\text{O}_2\text{Cl}_3$ ($\text{M} + \text{Cl}^-$) 286.9869 found 286.9864.

7.7.1.6 2,2',2'',2'''-((6-Chloro-1,3,5-triazine-2,4-diyl)bis(azanetriyl))tetraethanol (TzDEA₂Cl)



TzDEACl₂ (2.71 g, 10.7 mmol) was dissolved in acetone (50 ml) and added to ice water (50 ml) to form a slurry. Diethanolamine (1.12 g, 10.7 mmol) was dissolved in acetone (50 ml) and added dropwise to the slurry at 0°C over 1 hr. NaHCO₃ (0.90 g, 10.7 mmol) was added periodically so as to keep pH neutral. The solution was stirred at room temperature overnight and the solvent removed *in vacuo*. The resulting solid was dissolved in hot methanol (100 ml), filtered, and the solvent removed *in vacuo*, yielding the title product as an off white solid (3.08 g, 9.6 mmol, 90 %) ¹H NMR (500 MHz, DMSO-d₆, ppm) δ_H: 4.83 (s, 4 H, CH₂OH), 3.64 – 3.48 (m, 16 H, NCH₂ and CH₂OH); ¹³C NMR (126 MHz, DMSO-d₆, ppm) δ_C: 168.1, 164.1, 58.7, 58.5, 50.7, 50.3; IR (KBr, ν_{max}, cm⁻¹) 3407 (br), 2951 (w), 2911 (w), 2886 (w), 1585 (s), 1511 (s), 1482 (s), 1463 (s), 1440 (s), 1412 (w), 1369 (s), 1333 (w), 1308 (s), 1235 (s), 1185 (w), 1163 (s), 1129 (s), 1080 (s), 1065 (s), 1054 (s), 1041 (s), 1009 (w), 979 (s), 925 (s), 870 (s), 807 (w), 794 (s), 732 (w); MS (LR ES⁺) 322.13 (7 %, M + H⁺), 344.11 (100 %, M + Na⁺), 385.14 (20 %, M + MeCN + Na⁺) (HR ES⁺) calc. for C₁₁H₂₁N₅O₄Cl (M + H⁺) 322.1282 found 322.1283.

7.7.1.7 2,2'-((4-Chloro-6-(piperidin-1-yl)-1,3,5-triazin-2-yl)azanediyl)diethanol (TzPipDEACl)

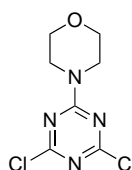


TzPipCl₂ (2.33 g, 10 mmol) was dissolved in acetone (50 ml) and added to ice water (50 ml) to form a slurry, and cooled to 0°C. To this slurry was added dropwise diethanolamine (1.05 g, 10 mmol) with NaHCO₃ (0.84 g, 10 mmol) added portion-wise so as to keep the pH neutral. The mixture was stirred at room temperature for 18 hours, filtered, and chloroform (100 ml) added. KBr was added to the solution until the aqueous phase was saturated, and the organic phase separated, washed with brine (50 ml), dried over MgSO₄, filtered, and solvent removed *in vacuo* resulting in a colourless oil. This was dissolved in EtOAc (20 ml) and placed in the freezer for 24 hours. The solution was filtered and the solvent removed *in vacuo* leaving an off white solid (1.86 g, 6.2 mmol, 62 %). ¹H NMR (500 MHz, CDCl₃, ppm) δ_H: 3.85 – 3.77 (m, 8 H), 3.76 – 3.70 (m,

2 H), 3.70 – 3.59 (m, 4 H), 1.62 – 1.57 (m, 2 H), 1.53 – 1.46 (m, 2 H); ^{13}C NMR (126 MHz, CDCl_3 , ppm) δ_{C} : 169.0, 165.8, 163.5, 61.9, 61.5, 52.3, 52.0, 44.7, 25.7, 25.6, 24.5; MS (LR ES^+) 302.14 (100 %, $\text{M} + \text{H}^+$), 324.12 (90 %, $\text{M} + \text{Na}^+$), (HR ES^+) calc for $\text{C}_{12}\text{H}_{21}\text{N}_5\text{O}_2\text{Cl}$ ($\text{M} + \text{H}^+$) 302.1384 found 302.1377.

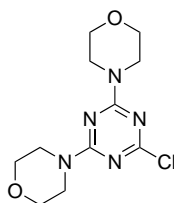
7.7.2 DO3A Ligands

7.7.2.1 4-(4,6-dichloro-1,3,5-triazin-2-yl)morpholine (TzMorphCl₂)



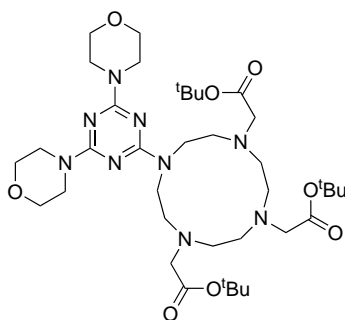
Cyanuric chloride (11.0 g, 59.6 mmol) was dissolved in acetone (100 ml) and added to ice water (100 ml) to form a slurry, and cooled to 0°C. Morpholine (5.19 g, 59.6 mmol) was dissolved in acetone (100 ml), and added dropwise to the stirred solution. NaHCO_3 (5.00 g, 59.5 mmol) was added portion-wise so as to keep the pH neutral. The solution was warmed to room temperature and stirred for 18 hours. The white solid was collected by filtration and recrystallised from hot EtOH yielding the title product as a colourless solid (8.53 g, 36.3 mmol, 61 %) ^1H NMR (500 MHz, CDCl_3 , ppm) δ_{H} : 3.85 – 3.82 (m, 4 H), 3.72 – 3.69 (m, 4 H); ^{13}C NMR (126 MHz, CDCl_3 , ppm) δ_{C} : 170.4, 164.1, 66.4, 44.5; IR (KBr, ν_{max} , cm^{-1}) 2970 (s), 2924 (s), 2862 (s), 1587 (s), 1558 (s), 1478 (s), 1457 (w), 1442 (s), 1361 (s), 1343 (s), 1322 (w), 1300 (s), 1279 (s), 1261 (w), 1231 (s), 1194 (s), 1161 (s), 1126 (w), 1113 (s), 1075 (s), 1069 (w), 1019 (s), 993 (s), 922 (w), 847 (s), 837 (s), 804 (w), 790 (s).

7.7.2.2 4,4'-(6-chloro-1,3,5-triazine-2,4-diyl)dimorpholine (TzMorph₂Cl)



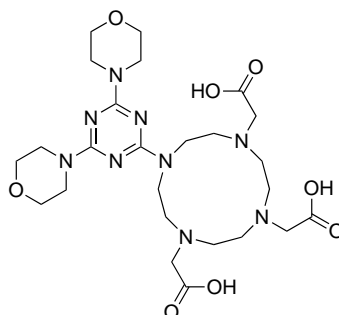
TzMorphCl₂ (8.23 g, 35.0 mmol) was dissolved in acetone (50 ml) and added to ice water (100 ml) to form a slurry. Morpholine (3.05 g, 35.1 mmol) was dissolved in acetone (50 ml) and added dropwise to the solution. NaHCO₃ (2.94 g, 35.0 mmol) was added portion-wise so as to keep the pH neutral. The solution was stirred for 18 hours, the solid collected by filtration and recrystallised from hot EtOH, yielding the title product as colourless crystals (6.47 g, 22.7 mmol, 65 %) ¹H NMR (500 MHz, CDCl₃, ppm) δ_H: 3.81 – 3.69 (m, 4 H), 3.68 – 3.64 (m, 4 H); ¹³C NMR (126 MHz, CDCl₃, ppm) δ_C: 169.7, 164.5, 66.6, 43.9; IR (KBr, ν_{max}, cm⁻¹) 2966 (s), 2920 (s), 2852 (s), 1575 (s), 1489 (s), 1451 (s), 1362 (s), 1299 (s), 1269 (s), 1245 (s), 1233 (s), 1183 (s), 1116 (s), 1063 (s), 1008 (s), 981 (s), 956 (s), 860 (s), 817 (s), 798 (s), 730 (s).

7.7.2.3 Tri-tert-butyl 2,2',2''-(10-(4,6-dimorpholino-1,3,5-triazin-2-yl)-1,4,7,10-tetraazacyclododecane-1,4,7-triyl)triacetate (TzMorph₂DO3A)



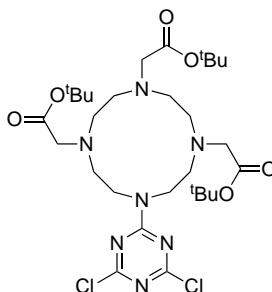
TzMorph₂Cl (87 mg, 0.30 mmol), DO3A.HBr (182 mg, 0.31 mmol), and NaHCO₃ (51 mg, 0.61 mmol) were refluxed in CH₃CN (30 ml) under an atmosphere of nitrogen for 5 days. The solvents were removed *in vacuo*, and the solid dissolved in CHCl₃, washed with water then brine, and dried over MgSO₄. The solvents were removed *in vacuo* yielding the title compound as a white hygroscopic solid (213 mg, 0.28 mmol, 84 %) ¹H NMR (500 MHz, CDCl₃, ppm) δ_H: 3.79 – 3.58 (m, 16 H, CH₂O + CH₂N), 3.39 – 3.21 (m, 6 H, CH₂CO₂), 3.11 – 2.99 (m, 8 H, Mac-H), 2.94 – 2.68 (m, 8 H, Mac-H), 1.44 (s, 9 H, CH₃), 1.43 (s, 9 H, CH₃), 1.41 (s, 9 H, CH₃); ¹³C NMR (126 MHz, CDCl₃, ppm) δ_C: 170.67, 169.83, 165.46, 81.87, 81.75, 80.97, 80.81, 67.05, 58.35, 57.38, 55.07, 52.87, 52.65, 52.05, 51.53, 49.42, 47.64, 47.02, 43.80, 28.36, 28.34, 28.31, 18.53; MS (HR EI⁺) calc. for C₃₇H₆₅N₉O₈ (M⁺) 763.4956 found 763.4940

7.7.2.4 2,2',2''-(10-(4,6-dimorpholino-1,3,5-triazin-2-yl)-1,4,7,10-tetraazacyclododecane-1,4,7-triyl)triacetic acid (TzMorph₂DO3a)



TzMorph₂DO3A (213 mg, 0.28 mmol), was dissolved in DCM (3 ml), and TFA (3 ml) added. The solution was stirred at room temperature for 48 hours. The solvents were removed *in vacuo* and MeOH (5 ml) added, this was repeated 3 times yielding an off white oil, which was triturated with Et₂O yielding the title product as an off white solid (157 mg, 0.26 mmol, 93 %) ¹H NMR (500 MHz, MeOD, ppm) δ_H: 3.84 – 3.59 (m, 16 H, CH₂O + CH₂N), 3.40 – 3.23 (m, 6 H, CH₂CO₂), 3.00 – 2.62 (br m, 16 H, Mac-H); IR (KBr, ν_{max}, cm⁻¹) 3436 (br), 2925 (s), 2852 (s), 1739 (w), 1679 (w), 1558 (w), 1528 (w), 1483 (w), 1447 (w), 1376 (w), 1369 (w), 1313 (w), 1263 (w), 1198 (s), 1139 (s), 811 (w), 721 (w), 704 (w); MS (LR ES⁺) 596.32 (100 %, M + H⁺), 618.34 (20 %, M + Na⁺), (HR ES⁺) calc. for C₂₅H₄₂N₉O₈ (M + H⁺) 596.3156 found 596.3151

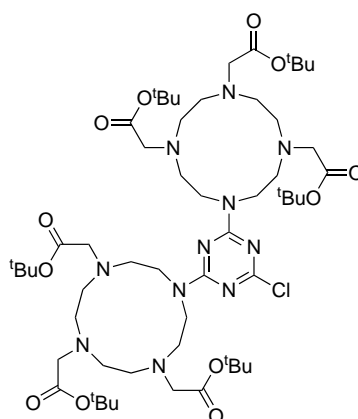
7.7.2.5 Tri-tert-butyl 2,2',2''-(10-(4,6-dichloro-1,3,5-triazin-2-yl)-1,4,7,10-tetraazacyclododecane-1,4,7-triyl)triacetate (TzDO3ACl₂)



Cyanuric chloride (205 mg, 1.11 mmol) was dissolved in acetone (50 ml) and added to stirred ice water (50 ml) resulting in a slurry. DO3A.HBr (660 mg, 1.11 mmol) was

dissolved in acetone (50 ml) and added dropwise to the slurry at 0°C. NaHCO₃ (187 mg, 2.23 mmol) was added at such a rate as to keep the pH neutral. The mixture was stirred for 18 hours at room temperature, the resulting solid was collected by filtration, and recrystallised from hot EtOH, yielding the title product as a white solid (466 mg, 0.70 mmol, 63 %) ¹H NMR (250 MHz, CDCl₃, ppm) δ_H: ¹³C NMR (126 MHz, CDCl₃, ppm) δ_C: ; IR (KBr, ν_{max}, cm⁻¹) 3438 (br), 2976 (s), 2932 (s), 2846 (w), 1733 (s), 1571(s), 1510 (w), 1450 (w), 1433 (w), 1367 (s), 1307 (w), 1260 (w), 1159 (s), 848 (w), 805 (w), 752 (w) ; MS (LR EI⁺) 661.31 (10 %, M⁺), 560.25 (50 %, M - TzCl₂) (HR EI⁺) calc. for C₂₉H₄₉N₇O₆⁶⁵Cl₂ (M⁺) 661.3121 found 661.3124

7.7.2.6 Tri-tert-butyl 2,2',2''-(10-(2-chloro-1,3,5-triazin-4,6-yl)-di-1,4,7,10-tetraazacyclododecane-1,4,7-triyl)triacetate (TzDO3A₂Cl)

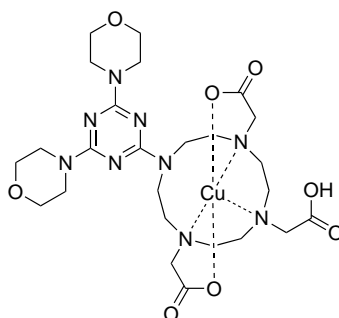


Cyanuric chloride (115 mg, 0.62 mmol) was dissolved in acetone (30 ml) and added to stirred ice water (30 ml) resulting in a slurry. DO3A.HBr (742 mg, 1.24 mmol) was dissolved in acetone (30 ml) and added dropwise to the slurry at 0°C. NaHCO₃ was added portion-wise at a rate so as the pH was neutral. The mixture was stirred at room temperature for 18 hours, the solid filtered and recrystallised from hot EtOH, yielding the title product as a white solid (620 mg, 0.54 mmol, 88 %) ¹H NMR (500 MHz, MeOD, ppm) δ_H: 3.51 – 3.33 (br, m, 16 H), 3.25 – 3.10 (br, m, 8 H), 3.10 – 2.88 (br, m, 8 H), 2.84 – 2.55 (br, m, 12 H), 1.52 – 1.44 (m, 54 H); IR (KBr, ν_{max}, cm⁻¹) 3441 (br), 2977 (s), 2930 (s), 2849 (w), 1733 (s), 1664 (w), 1569 (s), 1505 (w), 1459 (w), 1428 (w), 1368 (s), 1305 (w), 1259 (w), 1226 (w), 1156 (s), 849 (w), 801 (w), 755 (w); MS (LR ES⁺) 1140.71 (65 %, M +

H^+) 1162.69 (65 %, $M + Na^+$) (HR ES^+) calc. for $C_{55}H_{99}N_{11}O_{12}Cl$ ($M + H^+$) 1140.7163
found 1140.7133

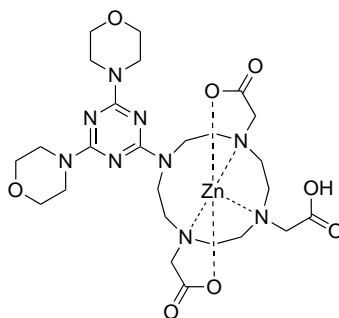
7.7.3 DO3A Complexes

7.7.3.1 Copper(II) 2,2',2''-(10-(4,6-dimorpholino-1,3,5-triazin-2-yl)-1,4,7,10-tetraazacyclododecane-1,4,7-triyl)triacetate (CuTzM₂D)



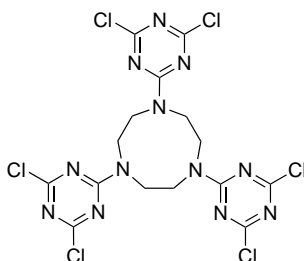
TzMorph₂DO3a (24 mg, 0.04 mmol) and $Cu(OAc)_2 \cdot 6H_2O$ (12 mg, 0.04 mmol) were heated in MeOH (10 ml) for 10 minutes. MS (HR ES^+) calc. for $C_{25}H_{40}N_9O_8^{63}Cu$ ($M + H^+$) 657.2296 found 657.2296

7.7.3.2 Zinc(II) 2,2',2''-(10-(4,6-dimorpholino-1,3,5-triazin-2-yl)-1,4,7,10-tetraazacyclododecane-1,4,7-triyl)triacetate (ZnTzM₂D)

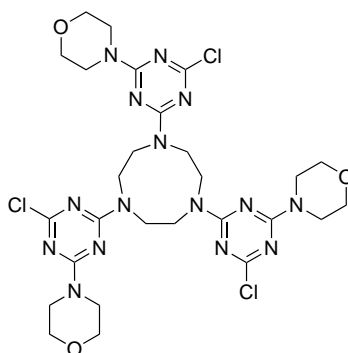


TzMorph₂DO3a (21 mg, 0.04 mmol) and $ZnCl_2 \cdot 2H_2O$ (8 mg, 0.04 mmol) were heated in MeOH (5 ml) for 10 minutes. MS (HR ES^+) calc. for $C_{25}H_{40}N_9O_8^{64}Zn$ ($M + H^+$) 658.2291 found 658.2310

7.7.4 Dendrimers

7.7.4.1 1,4,7-tris(4,6-dichloro-1,3,5-triazin-2-yl)-1,4,7-triazonane (TCl₆)

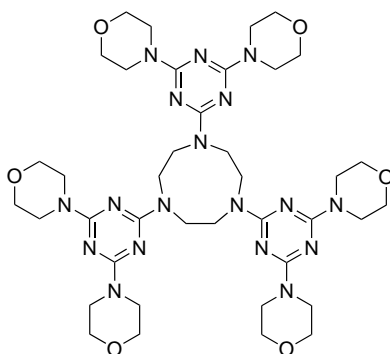
To stirred cyanuric chloride (2.58 g, 14.0 mmol) in acetone (50 ml) was added dropwise TACN (200 mg, 1.55 mmol) in THF (20 ml). NaHCO₃ (403 mg, 4.8 mmol) was added portion-wise to keep the pH neutral. The mixture was stirred at room temperature for 18 hours then water (50 ml) was added, the solid collected by vacuum filtration, and recrystallised from hot MeOH, yielding the title product as a white solid (883 mg, 1.54 mmol, 99 %) ¹H NMR (400 MHz, DMSO-d₆, ppm) δ_H: 3.87 (s, 12 H, TACN-H). ¹³C NMR (126 MHz, CDCl₃, ppm) δ_C: 169.0, 165.3, 48.7; IR (KBr, ν_{max}, cm⁻¹) 3211 (br, s), 3085 (br), 2922 (w), 2832 (w), 2780 (w), 2123 (w), 1717 (br, s), 1562 (s), 1483 (s), 1400 (s), 1365 (w), 1350 (w), 1330 (s), 1307 (s), 1234 (s), 1167 (s), 1071 (s), 1045 (s), 1022 (w), 977 (w), 965 (s), 907 (w), 849 (s), 75 (s), 762 (w), 742 (w)

7.7.4.2 1,4,7-tris(4-chloro-6-morpholino-1,3,5-triazin-2-yl)-1,4,7-triazonane (TM₃Cl₃)

TACN (125 mg, 0.97 mmol), TzMorphCl₂ (700 mg, 2.98 mmol), and K₂CO₃ (411 mg, 2.98 mmol) in MeCN (50 ml) were stirred in an inert atmosphere under reflux for 18 hours.

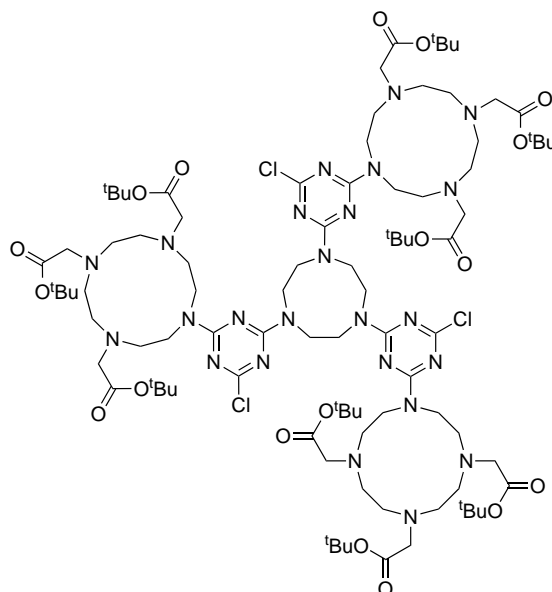
After cooling, the solvent was removed *in vacuo*. The solid was suspended in water (50 ml), extracted in CHCl₃ (3 x 50 ml), the organic phases dried over MgSO₄, filtered and solvent removed *in vacuo*, yielding the title product as an off white solid (423 mg, 0.58 mmol, 60 %) ¹H NMR (500 MHz, CDCl₃, ppm) δ_H: 3.97 – 3.54 (m, 36 H), ¹³C NMR (125 MHz, CDCl₃, ppm) δ_C: 171.5, 170.4, 169.4, 169.3, 169.2, 168.7, 165.7, 165.7, 165.6, 165.5, 164.3, 164.3, 66.6, 66.4, 66.4, 49.9, 49.7, 49.5, 49.4, 48.4, 48.2, 47.7, 44.5, 44.5, 44.4, 43.8; IR (KBr, ν_{max}, cm⁻¹) 2964 (w), 2921 (w), 2855 (s), 1564 (s), 1495 (s), 1418 (s), 1362 (s), 1303 (w), 1254 (w), 1234 (s), 1176 (s), 1114 (s), 1069 (w), 1028 (w), 984 (s), 971 (s), 931 (w), 852 (w), 799 (s), 752 (w); MS (LR ES⁺) 724.22 (M + H⁺), 787.37 (M + MeCN + Na⁺), (HR ES⁺) calc. for C₂₇H₃₇N₁₅O₃Cl₃ (M + H⁺) 724.2269 found 724.2245

7.7.4.3 1,4,7-tris(4,6-dimorpholino-1,3,5-triazin-2-yl)-1,4,7-triazonane (TM₆)



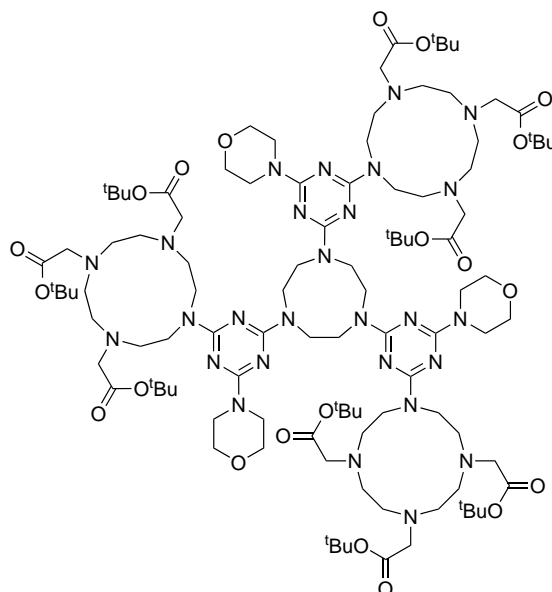
TACN (66 mg, 0.51 mmol), TzMorph₂Cl (510 mg, 1.78 mmol), and K₂CO₃ (246 mg, 1.78 mmol) in MeCN (40 ml) were stirred under reflux for 18 hours. Acetone (30 ml) was added, the solid was collected by filtration, washed with water, and dried under vacuum yielding the title product as a white solid (427 mg, 0.49 mmol, 96 %) ¹H NMR (250 MHz, CDCl₃, ppm) δ_H: 3.79 (s, 12 H, CH₂N), 3.74 – 3.61 (m, 48 H, Morph-H), ¹³C NMR (125 MHz, CDCl₃, ppm) δ_C: 166.06, 165.30, 67.06, 48.89, 43.72. ; IR (KBr, ν_{max}, cm⁻¹) 2969 (w), 2923 (w), 2855 (s), 1541 (s), 1477 (s), 1447 (s), 1411 (w), 1362 (s), 1327 (w), 1302 (w), 1254 (s), 1215 (w), 1191 (w), 1113 (s), 1028 (w), 1008 (s), 957 (w), 860 (s), 808 (s); MS (LR ES⁺) 628.38 (M -), 877.50 (70 %, M + H⁺), (HR ES⁺) calc. for C₃₉H₆₁N₁₈O₆ (M + H⁺) 877.5021 found 877.5016

7.7.4.4 1,4,7-tris(4-chloro-6-(tri-tert-butyl 2,2',2''-1,4,7,10-tetraazacyclododecane-1,4,7-triyl)triacetate)-1,3,5-triazin-2-yl)-1,4,7-triazonane (TD₃Cl₃)



TACN (15 mg, 0.12 mmol), TzDO₃ACl₂ (241 mg, 0.36 mmol), and K₂CO₃ (50 mg, 0.36 mmol) in MeCN (10 ml) were stirred in a pressure tube at 70°C for 48 hours. After cooling, the solution was filtered, and the solvent removed *in vacuo* yielding the title product as an off-white solid (100 mg, 0.05 mmol, 41 %) ¹H NMR (500 MHz, CDCl₃, ppm) δ_H: 3.78 – 3.65 (br, m, 24 H, cyclen-*H* and TACN-*H*), 3.34 – 3.12 (br, m, 24 H, cyclen-*H*), 3.01 – 2.87 (br, m, 12 H, cyclen-*H*), 2.83 – 2.57 (br, m, 18 H, CH₂CO₂), 1.38 (s, 81 H, CCH₃). ¹³C NMR (125 MHz, CDCl₃, ppm) δ_C: 170.96, 164.41, 122.92, 122.15, 110.09, 80.78, 65.86, 57.97, 55.19, 53.32, 52.08, 47.52, 46.94, 28.30, 28.27, 22.66, 15.31; IR (KBr, ν_{max}, cm⁻¹) 3448 (br), 2978 (s), 2930 (s), 2849 (w), 1733 (s), 1675 (w), 1569 (s), 1543 (s), 1490 (s), 1418 (w), 1368 (s), 1297 (w), 1257 (w), 1221 (w), 1155 (s), 848 (w), 810 (w)

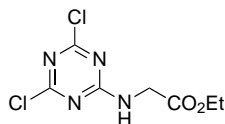
7.7.4.5 1,4,7-tris(4-morpholino-6-(tri-tert-butyl 2,2',2''-1,4,7,10-tetraazacyclododecane-1,4,7-triyl)triacetate)-1,3,5-triazin-2-yl)-1,4,7-triazonane (TD₃M₃)



TM₃Cl₃ (200 mg, 0.28 mmol), DO3A.HBr (542 mg, 0.91 mmol), and K₂CO₃ (252 mg, 1.83 mmol) in MeCN (30 ml) were stirred in an inert atmosphere under reflux for 72 hours after cooling the solvent was removed *in vacuo*. The resulting solid was taken up in DCM (50 ml), washed with water (50 ml), and brine (50 ml), dried over MgSO₄, filtered, and the solvent was removed *in vacuo* yielding the title compound as a yellow solid (212 mg, 0.10 mmol, 36 %) ¹H NMR (500 MHz, CDCl₃, ppm) δ_H: 3.71 – 3.46 (br, m, 36 H), 3.33 – 3.16 (br, m, 24 H), 3.05 – 2.87 (br, m, 12 H), 2.80 – 2.61 (br, m, 30 H, CH₂CO₂ and NCH₂), 1.39-1.35 (m, 81 H, CCH₃). ¹³C NMR (126 MHz, CDCl₃, ppm) δ_C: 171.3, 165.3, 164.5, 80.9, 80.7, 67.2, 57.7, 54.9, 52.9, 52.1, 47.0, 43.9, 28.4; IR (KBr, ν_{max}, cm⁻¹) 3450 (br), 2976 (s), 2927 (s), 2852 (s), 1733 (s), 1683 (w), 1539 (s), 1489 (s), 1425 (w), 1392 (w), 1367 (s), 1301 (w), 1258 (s), 1216 (w), 1154 (s), 1118 (w), 1026 (w), 993 (w), 849 (s), 809 (s), 741 (w); MS (LR ES⁺) 2160.24 (20 %, M⁺), 1080.71 (100 %, M²⁺)

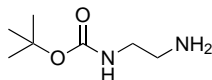
7.7.5 RGD type ligands

7.7.5.1 Ethyl 2-((4,6-dichloro-1,3,5-triazin-2-yl)amino)acetate (Tz(EtGly)Cl₂)



1,3,5-triazine (9.11 g, 49.4 mmol) was dissolved in acetone and added to water (100 ml) and the resulting slurry cooled to 0°C. Ethylglycine hydrochloride (6.80 g, 48.7 mmol) in water (100 ml) was added dropwise to the stirred slurry over 1 hour with the addition of NaHCO₃ (8.30 g, 98.8 mmol) periodically to keep the pH neutral. After complete addition of the amino acid, the solution was allowed to stir at room temperature for 1 hour, then filtered, and the precipitate washed with water (2 x 25 ml). The solid was dried under vacuum before being recrystallised from hot ethanol, yielding the title product as a white solid (8.08 g, 32.2 mmol, 66 %) ¹H NMR (500 MHz, CDCl₃, ppm) δ_H: 4.23 – 4.14 (m, 4 H, NCH₂ and CH₂CH₃), 1.23 (t, 3 H, ²J_{H-H} = 7.1 Hz, CH₂CH₃); ¹³C NMR (126 MHz, CDCl₃, ppm) δ_C: 171.0, 169.9, 168.7, 166.0, 62.0, 43.0, 14.1; IR (KBr, ν_{max}, cm⁻¹) 3478 (s), 3272 (br, s), 3178 (w), 3123 (w), 2998 (s), 2937 (w), 1749 (s), 1614 (s), 1548 (s), 1425 (w), 1397 (w), 1375 (w), 1327 (w), 1255 (s), 1213 (s), 1135 (s), 1034 (s), 1021 (s), 979 (s), 936 (s), 918 (s), 897 (w), 852 (s), 799 (s), 714 (br, s); MS (LR EI⁻) (100 %, M - H⁺) 248.99, (HR EI⁻) (M - H⁺) calc: 248.9946, found: 248.9939

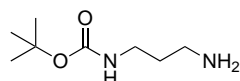
7.7.5.2 ^tButyl (2-aminoethyl)carbamate (BocEDA)



Under an atmosphere of Argon: Into a solution of ethylene diamine (32 ml, 470 mmol) and triethylamine (2.8 ml, mmol) in ethanol (30 ml) was added dropwise di-^tbutyl dicarbonate (4.45 g, 20.4 mmol) in ethanol (20 ml) at 0°C. After complete addition the solution was stirred at room temperature for a further hour, before being evaporated to dryness. The resulting solid was dissolved in DCM (50 ml), extracted in acetic acid (1 M, 3 x 50 ml), then neutralised with NaOH (2 M) and extracted with DCM (3 x 50 ml).

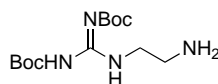
The organic layer was dried over MgSO_4 , filtered, and the solvent removed *in vacuo* resulting in the title compound as a pale yellow oil (1.76 g, 11.0 mmol, 55 %) ^1H NMR (400 MHz, CDCl_3 , ppm) δ_{H} : 4.81 (s, 1 H, NH_2CH_2), 3.16 - 3.06 (m, 2 H, NHCH_2), 2.77 - 2.70 (m, 2 H, NH_2CH_2), 1.38 (s, 9 H, CCH_3)

7.7.5.3 *t*-Butyl (3-aminopropyl)carbamate (BocPDA)



Under an atmosphere of Argon: Into a solution of diaminopropane (30 ml, 361 mmol) and triethylamine (2.8 ml, mmol) in ethanol (30 ml) was added dropwise di-*t*-butyl dicarbonate (4.45 g, 20.4 mmol) in ethanol (20 ml) at 0°C . After complete addition the solution was stirred at room temperature for a further hour, before being evaporated to dryness. The resulting solid was dissolved in DCM (50 ml), extracted in acetic acid (1 M, 3 x 50 ml), then neutralised with NaOH (2 M) and extracted with DCM (3 x 50 ml). The organic layer was dried over MgSO_4 , filtered, and the solvent removed *in vacuo* resulting in the title compound as a pale yellow oil (1.74 g, 10.0 mmol, 49 %) ^1H NMR (400 MHz, CDCl_3 , ppm) δ_{H} : 4.89 (s, 2 H, NH_2), 3.21 (q, 2 H, $^2\text{J}_{\text{H-H}} = 6.3$ Hz, CH_2NHCO_2), 2.76 (t, 2 H, $^2\text{J}_{\text{H-H}} = 6.6$ Hz, CH_2NH_2), 1.61 (p, 2 H, $^2\text{J}_{\text{H-H}} = 6.6$ Hz, $\text{CH}_2\text{CH}_2\text{CH}_2$), 1.44 (s, 9 H, CCH_3)

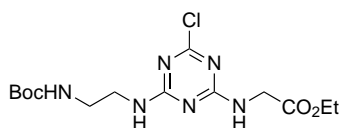
7.7.5.4 1-(2-Aminoethyl)-2,3-di-Boc-guanidine (BocGuanEDA)



Under an inert atmosphere ethylene diamine (0.03 ml, 0.45 mmol) and triethylamine (0.017 ml, 0.12 mmol) were dissolved in dry DCM (5 ml). To this was added dropwise a solution of Boc₂GuanTf (47 mg, 0.12 mmol) in dry DCM (5 ml). The mixture was stirred at room temperature for 12 hours. The solvents were removed *in vacuo*, and the resulting solid purified by flash column chromatography (EtOAc, MeOH, Et₃N, 5 : 3 :

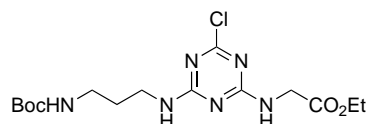
2) yielding the title product as a tan oil (19 mg, 0.06 mmol, 50 %) ^1H NMR (250 Mhz, CDCl_3 , ppm) δ_{H} : 3.56 (m, 2 H, CH_2NH), 2.96 (m, 2 H, CH_2NH_2), 1.43 (s, 18 H, CH_3); MS (HR ES^+) calc. for $\text{C}_{13}\text{H}_{27}\text{N}_4\text{O}_4$ ($\text{M} + \text{H}^+$) 303.2032 found 303.2039

7.7.5.5 Ethyl 2-((4-((2-((tert-butoxycarbonyl)amino)ethyl)amino)-6-chloro-1,3,5-triazin-2-yl)amino)acetate (Tz(EtGly)(BocEDA)Cl)



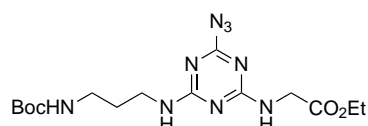
TzEtGlyCl₂ (762 mg, 3.04 mmol) was dissolved in acetone (50 ml) and added to water (50 ml), the resulting slurry was cooled to 0°C. BocEDA (2) (485 mg, 3.03 mmol) in acetone (20 ml) was added to the stirred slurry dropwise over 1 hour with addition of NaHCO_3 (255 mg, 3.03 mmol) at a rate so as to keep a neutral pH. After complete addition the mixture was allowed to warm to room temperature, and stirred for 3 hours. The precipitate was then filtered, washed with water, and recrystallised from hot ethanol, yielding the title product as a white solid (667 mg, 1.78 mmol, 59 %) ^1H NMR (500 MHz, CDCl_3 , ppm) δ_{H} : 4.26 – 4.07 (m, 4 H, CH_2CO_2 and CH_2CH_3), 3.46 - 3.41 (m, 2 H, NHCH_2), 3.28 – 3.21 (m, 2 H, NH_2CH_2), 1.35 (s, 9 H, CCH_3), 1.21 (t, 3 H, CH_2CH_3); ^{13}C NMR (126 MHz, CDCl_3 , ppm) δ_{C} : 169.8, 168.2, 165.9, 165.7, 156.3, 61.6, 43.1, 41.3, 40.2, 28.5, 14.3; IR (KBr, ν_{max} , cm^{-1}) 3354 (s), 3256 (s), 3105 (s), 2978 (s), 1749 (s), 1720 (w), 1689 (s), 1642 (s), 1558 (br, s), 1415 (w), 1274 (w), 1248 (w), 1202 (s), 1175 (w), 1122 (s), 1029 (w), 990 (s), 873 (s), 800 (s), 726 (w); MS (LR EI^+) 257.05 (100 %, $\text{M} - \text{HNHCO}_2^t\text{Bu}$), 301.08 (90 %, $\text{M}^+ - ^t\text{BuO}$), 374.15 (10 %, M^+); (HR EI^+) calc. for $\text{C}_{14}\text{H}_{23}\text{N}_6\text{O}_4\text{Cl}$ (M^+) 374.1469 found 374.1458

7.7.5.6 Ethyl 2-((4-((3-((tert-butoxycarbonyl)amino)propyl)amino)-6-chloro-1,3,5-triazin-2-yl)amino)acetate (Tz(EtGly)(BocPDA)Cl)



TzEtGlyCl₂ (575 mg, 2.29 mmol) was dissolved in acetone (50 ml) and added to water (50 ml), the resulting slurry was cooled to 0°C. BocPDA (3) (394 mg, 2.29 mmol) in acetone (20 ml) was added to the stirred slurry dropwise over 1 hour with addition of NaHCO₃ (193 mg, 2.29 mmol) at a rate so as to keep a neutral pH. After complete addition the mixture was allowed to warm to room temperature, and stirred for 3 hours. The precipitate was then filtered, washed with water, and recrystallised from hot ethanol, yielding the title product as a white solid (513 mg, 1.32 mmol, 58 %) ¹H NMR (400 MHz, CDCl₃, ppm) δ_H: 4.30 – 4.14 (m, 4 H, CH₂CH₃ and CH₂CO₂), 3.47 - 3.43 (m, 2 H, NHBocCH₂), 3.19 - 3.15 (m, 2 H, CH₂NH), 1.70 (q, 2 H, ²J_{H-H} = 6.2 Hz, CH₂CH₂CH₂), 1.43 (s, 9 H, CCH₃), 1.28 (t, 3 H, ²J_{H-H} = 7.1 Hz, CH₂CH₃); ¹³C NMR (126 MHz, CDCl₃, ppm) δ_C: 169.8, 165.9, 165.8, 156.4, 79.6, 61.7, 43.2, 42.9, 38.1, 37.6, 30.4, 28.5, 14.3; IR (KBr, ν_{max}, cm⁻¹) 3359 (s), 3257 (s), 3110 (s), 2978(s), 2871(w), 1748 (s), 1717 (w), 1688 (s), 1641 (s), 1558 (s), 1415 (w), 1365 (w), 1278 (w), 1247 (s), 1203 (w), 1175 (w), 1118 (s), 1029 (w), 995 (w), 887 (w), 865 (w), 800 (s), 740 (br); MS (LR EI⁺) 258.08 (M⁺ - ^tBuCO₂ - Et), 270.08 (M⁺ - ^tBuO - EtO), 331.10 (M⁺ - ^tBu), 388.16 (M⁺), (HR EI⁺) calc. for C₁₅H₂₅N₆O₄Cl (M⁺) 388.1626 found 388.1637

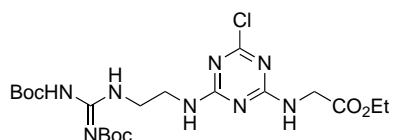
7.7.5.7 Ethyl 2-((4-azido-6-((3-((tert-butoxycarbonyl)amino)propyl)amino)-1,3,5-triazin-2-yl)amino)acetate (TzEtGlyBocPDAN₃)



TzEtGlyBocPDACl (94 mg, 0.24 mmol) was dissolved in CH₃CN (2 ml), and NaN₃ (32 mg, 0.49 mmol) added. The solution was heated to 60°C with stirring for 3 hours, after which a solid precipitate appeared. The solvents were removed *in vacuo* and water (10

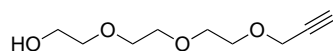
ml) added. The product was extracted with CHCl_3 (2 x 10 ml), washed with brine (10 ml), and dried over MgSO_4 . The solution was filtered and the solvents removed in vacuo yielding the title compound as a white solid (84 mg, 0.23 mmol, 94 %) IR (KBr, ν_{max} , cm^{-1}) 3356 (s), 3259 (s), 3111 (s), 2978 (s), 2937 (w), 2871 (w), 2137 (s), 1747 (s), 1690 (s), 1641 (s), 1558 (br, s), 1414 (w), 1365 (w), 1275 (s), 1201 (s), 1172 (s), 1118 (w), 1027 (s), 996 (s), 866 (s), 800 (s), 757 (w); MS (HR ES^+) calc. for $\text{C}_{15}\text{H}_{26}\text{N}_9\text{O}_4$ ($\text{M} + \text{H}^+$) 396.2108 found 396.2098

7.7.5.8 Ethyl 2-((4-((2-(2,3-bis(tert-butoxycarbonyl)guanidino)ethyl)amino)-6-chloro-1,3,5-triazin-2-yl)amino)acetate (TzEtGlyBocGuanCl)



TzEtGlyCl₂ (32 mg, 0.13 mmol) was dissolved in acetone (5 ml) and added to water (10 ml), the resulting slurry was cooled to 0°C. BocGuanEDA (40 mg, 0.13 mmol) in acetone (5 ml) was added to the stirred slurry dropwise over 30 minutes with addition of NaHCO_3 (12 mg, 0.13 mmol) at a rate so as to keep a neutral pH. After complete addition the mixture was allowed to warm to room temperature, and stirred for 3 hours. The solvents were removed *in vacuo* and the solid washed with water (5 ml). The title product was isolated as a white solid (15 mg, 0.03 mmol, 23 %) MS (HR ES^+) calc. for $\text{C}_{20}\text{H}_{34}\text{N}_8\text{O}_6\text{Cl}$ ($\text{M} + \text{H}^+$) 517.2290 found 517.2286

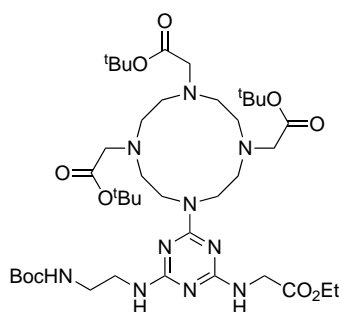
7.7.5.9 2-(2-(2-(prop-2-yn-1-yloxy)ethoxy)ethoxy)ethanol (AlkyGly)



NaH (60 %, 1.03 g, 25.75 mmol) was dissolved in degassed THF (40 ml) under an inert atmosphere, cooled to 0°C, and triethylene glycol (6.9 ml, 51.5 mmol) added dropwise. Propargyl bromide (80 % w/toluene, 2.87 ml, 32.2 mmol) was added slowly so as the temperature didnt increase. After 2 hours at the reduced temperature the solution was

allowed to warm to room temperature and stirred for 20 hours. The solution was poured onto water (100 ml) and the product extracted with DCM (3 x 50 ml). The organic phase was dried over MgSO_4 , filtered, and the solvents removed in vacuo resulting in a dark yellow oil. The product was purified by flash chromatography (EtOAc, Hexane, 3 : 2), yielding the title product as a yellow oil (4.3 g, 22.9 mmol, 89 %) ^1H NMR (400 MHz, CDCl_3 , ppm) δ_{H} : 4.15 (s, 2 H, OCH_2C), 3.68 - 3.54 (m, 13 H, CH_2 and CH); MS (HR ES⁺) calc. for $\text{C}_9\text{H}_{16}\text{O}_4^{23}\text{Na}$ ($\text{M} + \text{Na}^+$) 211.0946 found 211.0945

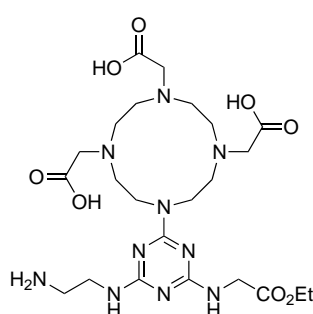
7.7.5.10 Tri-tert-butyl 2,2',2''-(10-(4-((tert-butoxycarbonyl)amino)ethyl)amino)-6-((2-ethoxy-2-oxoethyl)amino)-1,3,5-triazin-2-yl)-1,4,7,10-tetraazacyclododecane-1,4,7-triyl)triacetate (Tz(EtGly)(BocEDA)(DO3A))



To a solution of Tz(EtGly)(BocEDA)Cl (55 mg, 0.15 mmol) in MeCN (50 ml) was added NaHCO_3 (50 mg, 60 mmol) and DO3A.HBr (112 mg, 0.19 mmol). The solution was refluxed for 72 hours, and the solvent removed *in vacuo*. The resulting solid was dissolved in DCM (50 ml) and washed with water (50 ml), brine (50 ml), dried over MgSO_4 , and the solvent removed *in vacuo*, yielding the title product as a white solid (104 mg, 0.12 mmol, 82 %) ^1H NMR (500 MHz, CDCl_3 , ppm) δ_{H} : 4.19 – 4.06 (m, 2 H, CH_2CH_3), 4.02 (br, m, 2 H, $\text{NHCH}_2\text{CO}_2\text{Et}$), 3.73 – 3.57 (br, m, 2 H, NCH_2CO_2), 3.46 – 3.34 (br, m, 2 H, NCH_2CO_2), 3.33 – 3.30 (br, m, 2 H, NHCH_2CH_2), 3.27 – 3.22 (br, m, 4 H, NHCH_2CH_2 and NCH_2CO_2), 3.06 – 2.90 (br, m, 4 H, Ring-H), 2.89 – 2.62 (br, m, 12 H, Ring-H), 1.41 – 1.32 (m, 36 H, CCH_3), 1.20 (t, 3 H, $^2\text{J}_{\text{H-H}} = 7.1$ Hz, CH_2CH_3); ^{13}C NMR (126 MHz, CDCl_3 , ppm) δ_{C} : 171.2, 171.1, 171.0, 170.6, 169.8, 165.6, 165.0, 156.3, 81.7, 80.7, 61.4, 61.0, 58.2, 57.7, 55.1, 55.0, 53.3, 52.8, 52.0, 51.4, 49.4, 49.1, 47.5, 46.9, 42.9, 40.7, 28.4, 28.4, 28.2, 28.2, 14.2; IR (KBr, ν_{max} , cm^{-1}) 3404 (br), 2978 (s), 2932 (s), 2870 (s), 2732 (w), 1732 (s),

1558 (s), 1511 (s), 1456 (w), 1426 (w), 1393 (w), 1368 (s), 1259 (s), 1028 (w), 937 (w), 917 (w), 849 (s), 812 (s), 728 (s) ; MS (LR ES⁺) 515.37 (100 %, M - Tz(EtGly)(BocEDA) + H⁺), 537.37 (40 %, M - Tz(EtGly)(BocEDA) + Na⁺), 853.55 (35 %, M + H⁺), (HR ES⁺) calc. for C₄₀H₇₂N₁₀O₁₀ (M + H⁺) 853.5511 found 853.5530

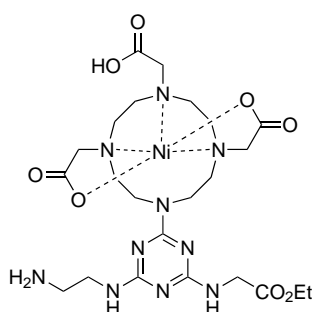
7.7.5.11 2,2',2''-(10-(4-((2-Aminoethyl)amino)-6-((2-ethoxy-2-oxoethyl)amino)-1,3,5-triazin-2-yl)-1,4,7,10-tetraazacyclododecane-1,4,7-triyl)triacetic acid (Tz(EtGly)(EDA)(DO3a))



To a solution of Tz(EtGly)(BocEDA)(DO3A) (80 mg, 0.09 mmol) in DCM (3 ml) was added TFA (3 ml), and stirred for 48 hours at room temperature. The solvents were removed *in vacuo* and the resulting oil redissolved in methanol. The solvent was removed *in vacuo* and the sequence repeated twice more. This yielded the title product as a white solid (54 mg, 0.09 mmol, 98 %) ¹H NMR (400 MHz, MeOD, ppm) δ_H: 4.26 – 3.84 (br, m), 3.80 – 3.28 (br, m), 3.14 - 2.84 (br, m), 2.83 – 2.62 (br, m) [total integration = 34 H], 1.19 (br, apparent t, 3 H, ²J_{H-H} = 6.2 Hz, CH₂CH₃); ¹³C NMR (126 MHz, MeOD, ppm) δ_C: 175.1, 169.6, 163.4, 163.1, 162.9, 162.6, 122.1, 119.4, 116.9, 62.9, 56.5, 54.3, 53.9, 53.1, 50.7, 43.6, 39.6, 14.5; IR (KBr, ν_{max}, cm⁻¹) 3406 (br), 3105 (br), 2965 (br), 1738 (w), 1676 (s), 1530 (w), 1430 (br), 1202 (s), 1132 (s), 1025 (w), 834 (s), 799 (s), 722 (s) ; MS (LR ES⁺) 347.19 (100 %, M - Tz(EtGly)(EDA) + H⁺), 369.18 (25 %, M - Tz(EtGly)(EDA) + Na⁺), 585.31 (30 %, M + H⁺), 607.29 (15 %, M + Na⁺), (HR ES⁺) calc. for C₂₃H₄₀N₁₀O₈ (M + H⁺) 585.3109 found 585.3108

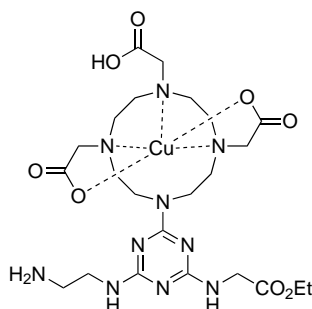
7.7.6 RGD type complexes

7.7.6.1 Nickel(II) 2,2',2''-(10-(4-((2-aminoethyl)amino)-6-((2-ethoxy-2-oxoethyl)amino)-1,3,5-triazin-2-yl)-1,4,7,10-tetraazacyclododecane-1,4,7-triyl)triacetate (NiTzEtGlyEDADO3a)



TzEtGlyEDADO3a (20 mg, 0.03 mmol) and Ni(OAc)₂·6H₂O (10 mg, 0.03 mmol) were heated in MeOH (10 ml) for 10 minutes. MS (HR ES⁺) calc. for C₂₃H₃₉N₁₀O₈⁵⁸Ni (M + H⁺) 641.2306 found 641.2294

7.7.6.2 Copper(II) 2,2',2''-(10-(4-((2-aminoethyl)amino)-6-((2-ethoxy-2-oxoethyl)amino)-1,3,5-triazin-2-yl)-1,4,7,10-tetraazacyclododecane-1,4,7-triyl)triacetate (CuTzEtGlyEDADO3a)

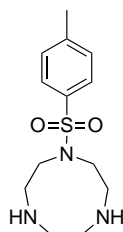


TzEtGlyEDADO3a (26 mg, 0.04 mmol) and Cu(OAc)₂·6H₂O (12 mg, 0.03 mmol) were heated in MeOH (5 ml) for 10 minutes. MS (HR ES⁺) calc. for C₂₃H₃₉N₁₀O₈⁶³Cu (M + H⁺) 646.2248 found 646.2266

7.8 Acetate and Alcohol Functionalised TACNs and Homopiperazines

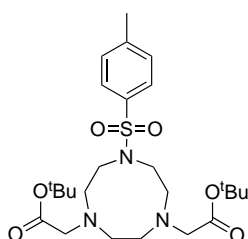
7.8.1 Functionalised TACNs

7.8.1.1 1-tosyl-1,4,7-triazonane (TsTACN)



Using the method of Sessler [89] Ts₃TACN (4.87g, mmol), phenol (5.6 g, mmol), and HBr.AcOH (45% w/w) (60 ml) were heated under an inert atmosphere to reflux for 18 hours, with the gas evolved bubbled through a NaOH bubbler. The solution was filtered, and washed with Et₂O, leaving a colourless solid. The solid was dissolved in NaOH (1 M), and the product extracted in CHCl₃ (3 x 70 ml). The organic fractions were combined and washed with brine, dried over MgSO₄, and the solvents removed *in vacuo*, yielding the title product as a white solid. ¹H data correlated with that of Sessler

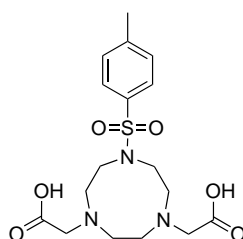
7.8.1.2 Di-tert-butyl 2,2'-(7-tosyl-1,4,7-triazonane-1,4-diyl)diacetate (TsTACNtBu₂)



TsTACN (1.37 g, 4.84 mmol), ^tbutyl bromoacetate (1.43 ml, 9.68 mmol), and potassium carbonate (1.34 g, 9.71 mmol) were dissolved in acetonitrile (50 ml) and stirred in a stoppered flask for 18 hours. Filtration, followed by removal of solvents *in vacuo* gave an off white oil. Tritration of the oil with diethyl ether followed by filtration yielded the title product as a white solid (2.31 g, 4.52 mmol, 93 %) ¹H NMR (250 MHz, CDCl₃, ppm)

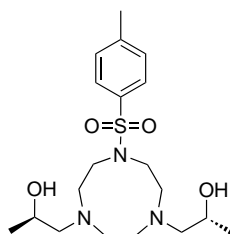
δ_H : 7.66 (d, 2 H, Ar-H, $^2J_{H-H} = 8$ Hz), 7.29 (d, 2 H, Ar-H, $^2J_{H-H} = 8$ Hz), 3.39 – 3.18 (m, 8 H; 4 H, CH_2CO_2 , 4 H, Mac-H), 3.11 (s, 4 H, Mac-H), 2.80 (s, 4 H, Mac-H), 2.41 (s, 3 H, Ar- CH_3), 1.44 (s, 18 H, CH_3); MS (LR ES⁺) 512.28 (M + H⁺, 100 %), 534.26 (M + Na⁺, 50 %), (HR ES⁺) calc. for C₂₅H₄₂N₃O₆S (M + H⁺) 512.2794 found 512.2808

7.8.1.3 2,2'-(7-tosyl-1,4,7-triazonane-1,4-diyl)diacetic acid (TsTACNA₂)



TsTACNtBu₂ (725 mg, 1.42 mmol) was dissolved in DCM (20 ml). To this TFA (5 ml) was added, and the mixture stirred for 48 hours in a stoppered flask. The solvents were removed *in vacuo*, and then MeOH (10 ml) added and stirred for 5 minutes. The solvents were removed *in vacuo* and the MeOH step repeated 5 times yielding the title product as a colourless solid (558 mg, 1.40 mmol, 99 %) ¹H NMR (400 MHz, MeOD, ppm) δ_H : 7.77 (d, 2 H, Ar-H, $^2J_{H-H} = 8.3$ Hz), 7.44 (d, 2 H, Ar-H, $^2J_{H-H} = 8.0$ Hz), 3.95 (s, 4 H, CH_2CO_2), 3.45 – 3.28 (m, 12 H, obscured by MeOH signal), 2.45 (s, 3 H, CH_3); MS (LR ES⁺) 400.1532 (M + H⁺, 100 %), (HR ES⁺) calc. for C₁₇H₂₆N₃O₆S (M + H⁺) 400.1542 found 400.1532

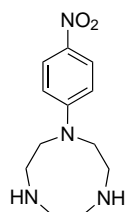
7.8.1.4 (2R,2'R)-1,1'-(7-tosyl-1,4,7-triazonane-1,4-diyl)bis(propan-2-ol) (TsTACNE₂)



TsTACN (1.16 g, 4.10 mmol) and (R)-propylene oxide (0.6 ml, 8.59 mmol) in EtOH (25 ml) were stirred in a stoppered flask for 48 hours. The solvents were removed *in vacuo*,

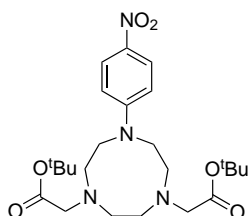
yielding the title product as a colourless oil that solidified overnight (1.57 g, 3.93 mmol, 96 %) ^1H NMR (500 MHz, CDCl_3 , ppm) δ_{H} : 7.66 – 7.55 (m, 2 H, Ar-H), 7.27 - 7.25 (m, 2 H, Ar-H, obscured by CHCl_3), 3.83 – 3.69 (m, 2 H, CHOH), 3.30 – 3.08 (m, 4 H, Mac-H), 2.99 – 2.80 (m, 6 H, Mac-H), 2.72 – 2.63 (m, 2 H, Mac-H), 2.55 (m, 2 H, CH_2CH), 2.37 (s, 3 H, CH_3), 2.29 – 2.18 (m, 2 H, CH_2CH), 1.03 (d, 6 H, CH_3CH , $^2\text{J}_{\text{H-H}} = 6.2$ Hz).; ^{13}C NMR (126 MHz, CDCl_3 , ppm) 143.5, 135.6, 129.6, 127.2, 67.0, 64.2, 57.8, 55.7, 54.6, 21.5, 20.0; MS (LR ES^+) 400.23 ($\text{M} + \text{H}^+$, 100 %), (HR ES^+) calc. for $\text{C}_{19}\text{H}_{34}\text{N}_3\text{O}_4\text{S}$ ($\text{M} + \text{H}^+$) 400.2270 found 400.2280

7.8.1.5 1-(4-nitrophenyl)-1,4,7-triazonane (NPhTACN)



TACN (482 mg, 3.74 mmol) and 4-fluoronitrobenzene (0.39 ml, 3.67 mmol) in acetonitrile (150 ml) were stirred at room temperature. The solvent was reduced to half its volume, and the solid precipitate collected by vacuum filtration. Recrystallisation from hot EtOH yielded the title product as an orange solid (874 mg, 3.50 mmol, 95 %)

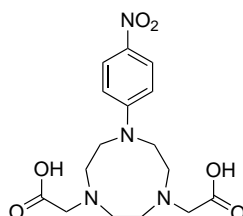
7.8.1.6 Di-tert-butyl 2,2'-(7-(4-nitrophenyl)-1,4,7-triazonane-1,4-diyl)diacetate (NPhTACNtBu₂)



NPhTACN (360 mg, 1.44 mmol), *t*butyl bromoacetate (0.45 ml, 3.05 mmol), and potassium carbonate (420 mg, 3.04 mmol) were dissolved in acetonitrile/THF (2:1, 100 ml), and heated with stirring to reflux under an inert atmosphere for 18 hours. Filtration,

followed by washing of the solid with methanol, gave an orange solution. Removal of the solvents *in vacuo* followed by recrystallisation from hot MeOH yielded the title product as a bright yellow solid (609 mg, 1.27 mmol, 88 %) ^1H NMR (250 MHz, CDCl_3 , ppm) δ_{H} : 8.02 (d, 2 H, Ar-H, $J_{\text{H-H}} = 9.5$ Hz), 6.57 (d, 2 H, Ar-H, $J_{\text{H-H}} = 9.5$ Hz), 3.73 – 3.48 (m, 4 H, Mac-H), 3.32 – 3.25 (m, 4 H, Mac-H), 3.18 – 2.95 (m, 4 H, Mac-H), 2.55 (s, 4 H, CH_2CO_2), 1.39 (s, 18 H, CH_3); MS (LR ES^+) 479.29 ($\text{M} + \text{H}^+$, 100 %), (HR ES^+) calc. for $\text{C}_{24}\text{H}_{39}\text{N}_4\text{O}_6$ ($\text{M} + \text{H}^+$) 479.2870 found 479.2879

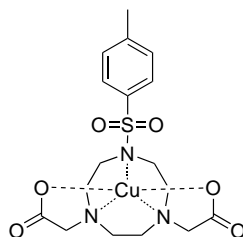
7.8.1.7 2,2'-(7-(4-nitrophenyl)-1,4,7-triazonane-1,4-diyl)diacetic acid (NPhTACNA₂)



NPhTACNtBu₂ (150 mg, 0.314 mmol) was dissolved in DCM (10 ml). TFA (1 ml) was added, and the solution stirred for 48 hours. The solvents were removed *in vacuo*, and MeOH (10 ml) added and the solution stirred for 5 minutes. The MeOH was removed *in vacuo* and the process repeated 5 times, yielding the title product as a yellow solid (113 mg, 310 μmol , 99 %) ^1H NMR (400 MHz, MeOD, ppm) δ_{H} : 8.05 (d, 2 H, Ar-H, $J = 9.3$ Hz), 6.76 (d, 2 H, Ar-H, $J = 9.4$ Hz), 3.89 (br s, 6 H, Mac-H), 3.53 (br s, 2 H, Mac-H), 3.44 – 3.28 (br m, 4 H, CH_2CO_2), 3.04 (br m, 4 H, Mac-H); MS (LR ES^+) 367.16 ($\text{M} + \text{H}^+$, 100 %), (HR ES^+) calc. for $\text{C}_{16}\text{H}_{23}\text{N}_4\text{O}_6$ 367.1618 found 367.1616

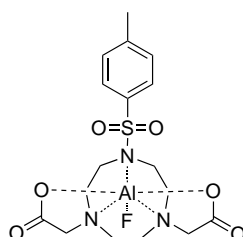
7.8.2 TACN Complexes

7.8.2.1 Copper(II) 2,2'-(7-tosyl-1,4,7-triazonane-1,4-diyl)diacetic acid (CuTsTACNA₂)

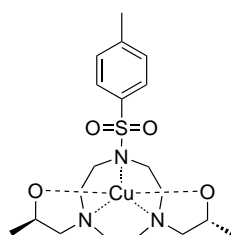


TsTACNA₂ (52 mg, 0.13 mmol) was dissolved in MeOH (10 ml) and Cu(OAc)₂·H₂O (26 mg, 0.13 mmol) added. Gentle heat was applied for 5 minutes, and the solvents removed *in vacuo*, yielding the title product as a deep blue solid (46 mg, 0.10 mmol, 78 %) Crystals suitable for x-ray diffraction were grown from slow vapour diffusion of diethyl ether into acetonitrile. UV (MeOH, nm) 645 ($\epsilon = 89 \text{ mol}^{-1}\text{cm}^{-1}$); MS (HR ES⁺) calc. for C₁₇H₂₃N₃O₆²³Na S ⁶⁴Cu (M+Na⁺) 483.0501 found 483.0500

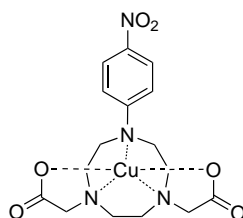
7.8.2.2 Aluminium(III) 2,2'-(7-tosyl-1,4,7-triazonane-1,4-diyl)diacetic acid fluoride (AlTsTACNA₂F)



TsTACNA₂ (15 mg, 0.038 mmol) was dissolved in sodium acetate buffer (1 M, pH 3.5) and AlCl₃·6H₂O (10 mg, 0.041 mmol) added. After gentle heating for 10 minutes, KF (4 mg, 0.069 mmol) was added. The products were not isolated, but the solution was used for mass spectrometry. MS (HR ES⁺) calc. for C₁₇H₂₄N₃O₆S ²⁷Al F (M + H⁺) 444.1185 found 444.1186

7.8.2.3 CuTsTACNE₂

TsTACNE₂ (220 mg, 0.55 mmol) and Cu(OAc)₂.H₂O (110 mg, 0.55 mmol) were dissolved in EtOH (10 ml). Gentle heat for 5 minutes, followed by removal of the solvents *in vacuo* yielded the title product as a deep blue solid (240 mg, 0.52 mmol, 95 %) Crystal suitable for x-ray diffraction were grown by slow evaporation of an ethanol/water solution. UV (MeOH, nm) 682 ($\epsilon = 57$); MS (LR ES⁺) 461.14 (M + H⁺, 100 %), 400.23 (M - ⁶³Cu + 3H⁺, 50 %), (HR ES⁺) calc. for C₁₉H₃₂N₃O₄S ⁶³Cu (M + H⁺) 461.1410 found 461.1410

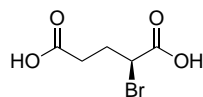
7.8.2.4 CuNPhTACNA₂

NPhTACNA₂ (50 mg, 0.14 mmol) was dissolved in methanol (10 ml) and Cu(OAc)₂.H₂O (28 mg, 0.14 mmol) added. Gentle heat was applied for 5 minutes, and the solvents removed *in vacuo*, yielding the title product as a deep blue solid (56 mg, 0.13 mmol, 93 %) Crystals suitable for x-ray diffraction were grown from slow vapour diffusion of diethyl ether into acetonitrile. UV (MeOH, nm) 603 ($\epsilon = 82$); MS (HR ES⁺) calc. for C₁₆H₂₁N₄O₆ ⁶³Cu (M + H⁺) 428.0757 found 428.0763

7.9 Other Work

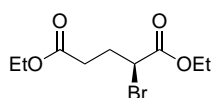
7.9.1 Glutamate Chemistry

7.9.1.1 (S)-Bromoglutamic acid



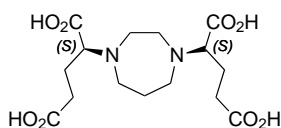
Monosodium glutamate (MSG) (18.9 g, 11.2 mmol) was dissolved in HBr (9 M, 100 ml) and cooled to 0°C. NaNO₂ (14.0 g, 20.3 mmol) was dissolved in the minimum amount of cold water, and added dropwise to the solution over a period of 3 hours. Upon complete addition, the solution was stirred for a further 15 minutes, before H₂SO₄ (6 ml) was added. The solution was stirred for 15 minutes and then allowed to warm slowly to room temperature. The product was extracted in diethyl ether (3 x 100 ml), washed with brine (100 ml) and sodium sulfite (100 ml), dried over MgSO₄, filtered and the solvents removed *in vacuo*, yielding the title product as a yellow oil (21.6 g, 10.3 mmol, 92 %) ¹H NMR (400 Mhz, CDCl₃, ppm) δ_H: 4.35 - 4.33 (t, 1 H, CH, ²J_{H-H} = 7 Hz), 2.66 - 2.48 (m, 2 H, CH₂CO₂), 2.43 - 2.26 (m, 2 H, CH₂CH)

7.9.1.2 Ethyl (S)-bromoglutarate



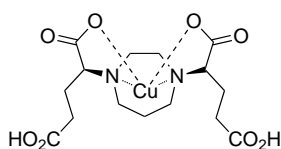
(S)-Bromoglutamic acid (7.4 g, 3.51 mmol) and ethanol (50 ml) were refluxed in the presence of H₂SO₄ (3 drops) for 3 hours. Diethyl ether (100 ml) was added, and the solution was neutralised with NaHCO₃ (aq). The organic layer was separated and washed with brine (100 ml) before being dried over MgSO₄. Filtration followed by removal of the solvents *in vacuo* yielded the title product as a colourless oil (8.33 g, 3.12 mmol, 89 %) ¹H NMR (400 Mhz, CDCl₃) δ_H: 4.29 (dd, 1 H, CH, ²J_{H-H} = 5.8 + 8.5 Hz), 4.23 - 4.12 (m, 2 H, CH₂CH₃), 4.13 - 4.03 (m, 2 H, CH₂CH₃), 2.51 - 2.38 (m, 2 H, CH₂CH₂), 2.37 - 2.14 (m, 2 H, CH₂CH₂), 1.29 - 1.20 (m, 6 H, CH₃CH₂)

7.9.1.3 (2S,2'S)-2,2'-(1,4-diazepane-1,4-diyl)dipentanedioic acid (HPGluT)



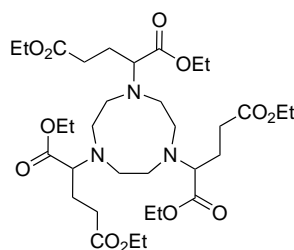
Homopiperazine (96 mg, 0.96 mmol), potassium carbonate (300 mg, 2.17 mmol), and ethyl (S)-bromoglutamate (590 mg, 2.21 mmol) were refluxed in acetonitrile (100 ml) for 18 hours. MeOH (20 ml) was added, and the solution filtered. The solvents were removed *in vacuo* resulting in a yellow oil. To this oil was added HCl (2 M, 20 ml), and the solution refluxed for 6 hours. The solvents were removed *in vacuo* yielding the dihydrochloride salt of the title compound as a white solid (274 mg, 0.76 mmol, 79 %) MS (LR ES⁺ - intermediate step) 474.14 (M + H⁺); ¹H NMR (400 Mhz, D₂O, ppm) δ_H: 4.23 (br s, 2 H, CH), 3.60 (br m, 8 H, CH₂N), 2.59 (br m, 4 H, CH₂CO₂), 2.18 (br m, 4 H, CH₂CH), 1.25 (br s, 2 H, CH₂CH₂CH₂); IR (KBr, ν_{max}, cm⁻¹) 2963 (s), 2923 (s), 2853 (s), 1733 (s), 1628 (s), 1455 (w), 1416 (w), 1262 (s), 803 (w); MS (LR ES⁻) 359.19 (M - H⁺, 100 %)

7.9.1.4 Copper (2S,2'S)-2,2'-(1,4-diazepane-1,4-diyl)dipentanedioic acid (CuHPGluT)



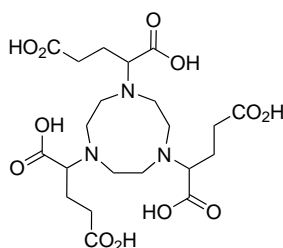
HPGluT (237 mg, 0.55 mmol), was dissolved in water, and NaOH (44 mg, 1.1 mmol) added. To this was added BaCl₂ (134 mg, 0.55 mmol) and gently heated for 5 minutes. Cu(SO₄)₂·5H₂O (171 mg, 0.55 mmol) was added to the solution and gently heated for 10 minutes. The solution was filtered, the residue washed with MeOH (5 ml), and the solvent removed *in vacuo*. The blue solid was dissolved in the minimum volume of hot MeOH, filtered, and the solvents removed *in vacuo* yielding the title product as a blue solid (93 mg, 0.22 mmol, 40 %); UV (H₂O, nm) 680 (ε = 4) IR (KBr, ν_{max}, cm⁻¹) 3429 (br, s), 2960 (s), 2925 (s), 2853 (s), 1627 (s), 1581 (s), 1463 (s), 1408 (s), 1261 (s), 1106 (w), 1032 (s), 803 (s); MS (HR ES⁻) calc. for C₁₅H₂₁N₂O₈⁶³Cu (M - H⁺) 420.0594 found 420.0600

7.9.1.5 Hexaethyl 2,2',2''-(1,4,7-triazonane-1,4,7-triyl)tripentanedioate (TACNEtGlut)



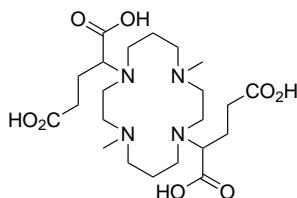
TACN (129 mg, 1.00 mmol) and potassium carbonate (455 mg, 3.30 mmol) were dissolved in acetonitrile (50 ml). To this was added ethyl bromoglutamate (881 mg, 3.3 mmol). The solution was refluxed for 4 hours, and then MeOH (10 ml) added. The solution was filtered, and the solvent removed *in vacuo* resulting in a yellow oil. The oil was dissolved in the minimum hot MeOH and diethyl ether added until precipitation occurred. The precipitate was placed in a fridge for 3 hours, and isolated by filtration, yielding the title compound as a white solid (519 mg, 0.755 mmol, 76 %) ^1H NMR (400 MHz, CDCl_3) δ_{H} : 4.26 – 4.01 (m, 12 H, CH_2CH_3), 3.30 – 3.15 (m, 3 H, CH), 2.99 – 2.53 (m, 12 H, Mac-H), 2.53 – 2.37 (m, 6 H, CH_2CO_2), 2.10 – 1.95 (m, 3 H, CH_2CH), 1.93 – 1.79 (m, 3 H, CH_2CH), 1.24 (t, 18 H, CH_3 , $J_{\text{H-H}} = 5.0$ Hz); ^{13}C NMR (126 MHz, CDCl_3) δ_{C} : 173.1, 66.3, 60.4, 54.5, 31.2, 25.4, 14.6; MS (LR ES^+) 716.70 ($\text{M} + \text{H}^+$, 100 %)

7.9.1.6 2,2',2''-(1,4,7-triazonane-1,4,7-triyl)tripentanedioic acid (TACNGlut)



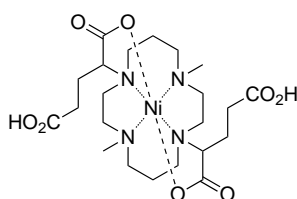
TACNEtGlut (234 mg, 0.34 mmol) was dissolved in HCl (2M, 20 ml) and refluxed for 4 hours. The solvents were removed *in vacuo*, and the resulting solid washed with MeOH (5 ml), yielding the title product as a white solid (129 mg, 0.24 mmol, 72 %) ^1H NMR (400 MHz, D_2O , ppm) δ_{H} : 3.65 (d, 3 H, CH, $^2J_{\text{H-H}} = 12$ Hz), 3.28 - 3.27 (m, 6 H, Mac-H), 2.61 – 2.58 (m, 6 H, Mac-H), 2.48 – 2.40 (m, 6 H, CH_2CO_2), 2.15 – 1.90 (m, 6 H, CH_2CH)

7.9.1.7 2,2'-(4,11-dimethyl-1,4,8,11-tetraazacyclotetradecane-1,8-diyl)dipentanedioic acid (DMCGLut)



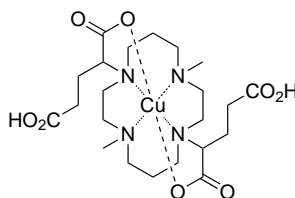
To a solution of dimethylcyclam (657 mg, 2.88 mmol) in acetonitrile (50 ml), was added ethyl bromoglutamate (1.69 g, 6.33 mmol) and potassium carbonate (875 mg, 6.34 mmol) and refluxed under an inert atmosphere for 18 hours. The solution was filtered and the solvent removed *in vacuo* yielding the ethyl ester. HCl (6 M, 50 ml) was added, and refluxed for 18 hours, the solvents were removed *in vacuo*. The solid was dissolved in methanol and diethyl ether added until a precipitate formed and was then put in a fridge for 5 hours. The solid was filtered and dried under vacuum yielding the title product as a white solid (967 mg, 1.53 mmol, 53 %) ^1H NMR (250 MHz, D_2O , ppm) δ_{H} : 3.68 – 3.16 (m, 18 H), 3.05 – 2.76 (m, 10 H), 2.74 – 2.58 (m, 2 H), 2.59 – 2.37 (m, 2 H), 2.21 – 1.98 (m, 4 H, CH_2CH), 1.98 – 1.75 (m, 4 H, $\text{CH}_2\text{CH}_2\text{CH}_2$)

7.9.1.8 Nickel 2,2'-(4,11-dimethyl-1,4,8,11-tetraazacyclotetradecane-1,8-diyl)dipentanedioic acid (NiDMCGLut)



DMCGLut (50 mg, 0.08 mmol) was dissolved in water, and NaOH (2M) added until neutral. $\text{Ni}(\text{OAc})_2 \cdot 4\text{H}_2\text{O}$ (20 mg, 0.08 mmol) was added and the solution gently heated for 5 minutes. The solvents were removed *in vacuo* yielding the title product as a grey solid (31 mg, 0.057 mmol, 71 %) MS (LR ES^-) 449.16 (M - pendant arm $^+$ + 2 H_2O , 60 %), 485.14 (M - CH_2CO_2^- - H^+ , 80 %), 487.13 (M - 2 CO_2H + MeOH - H^+)

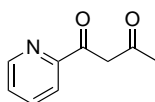
7.9.1.9 Copper 2,2'-(4,11-dimethyl-1,4,8,11-tetraazacyclotetradecane-1,8-diyl)dipentanedioic acid (CuDMCGLut)



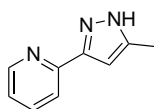
DMCGLut (60 mg, 0.09 mmol) was dissolved in water, and NaOH (2 M) added until neutral. $\text{Cu}(\text{OAc})_2 \cdot \text{H}_2\text{O}$ (20 mg, 0.10 mmol) was added, and the solution gently heated for 5 minutes. The solution turned a deep blue colour. Slow evaporation of this solution resulted in crystals of x-ray quality (31 mg, 0.056 mmol, 63 %); MS (HR ES^-) calc. for $\text{C}_{22}\text{H}_{37}\text{N}_4\text{O}_8^{63}\text{Cu}$ ($\text{M} - \text{H}^+$) 548.1907 found 548.1921

7.9.2 Trispyrazylborate analogues

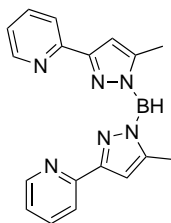
7.9.2.1 1-(pyridin-2-yl)butane-1,3-dione (PyAcac)



2-Acetyl pyridine (0.35 ml, mmol) was dissolved in degassed THF under an inert atmosphere. Potassium ^tbutoxide (1.04 g, 9.29 mmol) was added slowly, and the mixture stirred for 20 minutes. Dry EtOAc (3 ml) was added and the mixture stirred for 18 hours. Water (10 ml) was added slowly, followed by diethyl ether (10 ml). The aqueous layer was separated and acetic acid added until pH 7. The product was extracted in diethyl ether (5 × 100 ml), the fractions combined, and dried over MgSO_4 . The solvents were removed *in vacuo* yielding the title product as a brown oil (437 mg, mmol, %) ¹H NMR (250 MHz, CDCl_3 , ppm) δ_{H} : 8.70 (d, 1 H, Ar-H, ²J_{H-H} = 4 Hz), 8.13 - 8.10 (m, 1 H, Ar-H), 7.91-7.90 (m, 1 H, Ar-H), 7.47 - 7.45 (m, 1 H, Ar-H), 6.87 (s, 1 H, COCH_2CO), 2.30 (s, 3 H, CH_3)

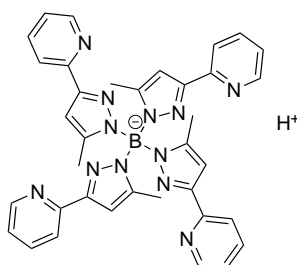
7.9.2.2 2-(5-methyl-1H-pyrazol-3-yl)pyridine (MePzPy)

PyAcac (437 mg, mmol), hydrazine hydrate (0.45 ml), *p*-TSA (10 mg) and ethanol (25 ml) were refluxed for 18 hours under an inert atmosphere. The solvents were removed *in vacuo*, and the resulting solid dissolved in water (20 ml). The product was extracted in DCM (4 x 50 ml), the fractions combined, dried over MgSO₄, filtered, and the solvent removed *in vacuo* yielding the title product as a yellow oil (493 mg, mmol, %) ¹H NMR (250 MHz, CDCl₃, ppm) δ_H: 8.54 - 8.52 (m, 1 H, Ar-*H*), 7.66 - 7.61 (m, 2 H, Ar-*H*), 7.15 - 7.11 (m, 1 H, Ar-*H*), 6.50 (s, 1 H, Pz-*H*), 2.30 (s, 3 H, CH₃); MS (HR APCI⁺) calc. for C₉H₁₀N₃ (M + H⁺) 160.0875 found 160.0877

7.9.2.3 Bis(5-methyl-3-(pyridin-2-yl)-1H-pyrazol-1-yl)borane (MeDpPy)

MePzPy (300 mg, 1.89 mmol) and KBH₄ (34 mg, 0.63 mmol) were dissolved in DMAC (10 ml), and heated to 160°C under a inert atmosphere for 18 hours. After cooling, the solid precipitate was isolated by filtration, yielding the title product as a white solid (183 mg, 0.56 mmol, 89 %); ¹¹B NMR (96 MHz, DMSO-*d*₆, ppm) δ_B: -12.7 (br s); IR (KBr, ν_{max}, cm⁻¹) 3413 (br, w), 3301 (br, w), 3179 (br, w), 3053 (br, w), 2846 (br, w), 2361 (s), 2342 (w), 1669 (br, s), 1612 (br, s), 1498 (s), 1368 (s), 1137 (br, w), 1085 (s), 812 (w), 741 (w); MS (HR ES⁻) calc for C₁₈H₁₈¹¹B N₆ (M + H⁻) 329.1686 found 329.1688

7.9.2.4 Hydrogen tetra(5-methyl-3-(pyridin-2-yl)-1H-pyrazol-1-yl)borate (MeQpPy)



MePzPy (2.03 g, 12.8 mmol) and KBH_4 (200 mg, 3.70 mmol) were melted together at 230°C until no further gas was evolved (2 hours), yielding the title product as a white solid (1.94 g, 3.02 mmol, 82 %) ^{11}B NMR (96 MHz, DMSO-d_6) δ_{B} : 2.0 - 0.8 (br s); IR (KBr, ν_{max} , cm^{-1}) 3219 (br, w), 3137 (br, w), 3056 (br, w), 2927 (s), 2860 (s), 2362 (w) 2341 (w), 1594 (s), 1500 (s), 1449 (s), 1342 (s), 1182 (br, s), 1096 (w), 968 (s), 840 (s), 814 (s), 783 (s), 743 (w); MS (HR ES^-) calc. for $\text{C}_{36}\text{H}_{32}^{11}\text{B N}_{12}$ (M^-) 643.2966 found 643.2987

7.10 PET experiments

These experiments were performed by Dr. J. Knight, University of Alberta

7.10.1 ^{64}Cu radiolabelling

For both TsTACNA_2 and NPhTACNA_2 , a dilution series was prepared in 0.1 M NH_4OAc buffer (pH 5.5) to give final chelating agent masses in the range 2.5 to 50 ng. To each of these eppendorf tubes was added $^{64}\text{Cu}(\text{OAc})_2$ (1 MBq) and the volume was adjusted to 100 μL with 0.1 M NH_4OAc buffer (pH 5.5). Each eppendorf tube was vortexed briefly and then placed in a thermoshaker (750 rpm) at 37°C for 1 h. The radiolabeling efficiency of each reaction was then monitored by radio-TLC (C18) using $\text{MeOH} / 10\% \text{NH}_4\text{OAc}$ (1/1) as the solvent system. All reactions were performed in triplicate.

7.10.2 Determination of \log_p values

$^{64}\text{CuTsTACNA}_2$ or $^{64}\text{CuNPhTACNA}_2$ (5 μL) was added to a biphasic mixture consisting of deionised water (1 mL) and octan-1-ol (1 mL). Each mixture was vortexed thoroughly for 5 minutes followed by centrifugation at 1,000 rpm for a further 5 minutes. A single portion of 100 μL was taken from each layer using a micropipette and transferred to separate eppendorf tubes. The radioactivity in each eppendorf tube was measured using a gamma scintillation counter. This experiment was performed in triplicate.

7.10.3 Stability in human serum

To a solution of TsTACNA_2 (35 ng, 0.088 nmol) in 0.1 M NH_4OAc (95 μL , pH 5.5) in an eppendorf tube was added $^{64}\text{Cu}(\text{OAc})_2$ (5 μL , 2.2 MBq). The eppendorf tube was vortexed briefly and then placed in a thermoshaker (750 rpm) at 37 °C for 30 minutes. The progress of the reaction was monitored by reverse phase (C18) radio-TLC using $\text{MeOH} / 10\% \text{NH}_4\text{OAc}$ (1/1). Upon completion of the complexation reaction (> 96 %), human serum (900 μL) was added to the reaction mixture. The eppendorf tube was vortexed briefly and then placed in a thermoshaker (400 rpm) at 37 °C and the percentage of intact ^{64}Cu -complex was determined by reverse phase radio-TLC (*vide supra*) at 0.08, 0.25, 0.5, 1, 3, and 24 h.

Bibliography

- [1] Greenwood, N., Earnshaw, A. *Chemistry of the Elements*, (Butterworth-Heinemann Ltd1997)
- [2] Schwarzenbach, G. *Helv. Chim. Acta*, 1952. **35(7)**, 2344–2359
- [3] Jahn, H.a., Teller, E. *Proc. R. Soc. Lond. A*, 1937. **161(905)**, 220–235
- [4] Gambhir, S.S., Czernin, J., Schwimmer, J., Silverman, D.H., Coleman, R.E., Phelps, M.E. *J. Nuc. Med.*, 2001. **42(5 Suppl)**, 1S–93S
- [5] Bailey, D.L., Townsend, D.W., Valk, P.E., Maisey, M.M. *Positron Emission Tomography: Basic Sciences*, (Springer2005), 1 edition
- [6] Rowshanfarzad, P., Sabet, M., Jalilian, A.R., Kamalidehghan, M. *Appl. Radiat. Isot.*, 2006. **64(12)**, 1563–73
- [7] Ā, V.S.L., Howse, J., Zaw, M., Pellegrini, P., Katsifis, a., Greguric, I., Weiner, R., Le, V.S. *Appl. Radiat. Isot.*, 2009. **67(7-8)**, 1324–31
- [8] Zhernosekov, K.P., Filosofov, D.V., Baum, R.P., Aschoff, P., Bihl, H., Razbash, A.a., Jahn, M., Jennewein, M., Rösch, F. *J. Nuc. Med.*, 2007. **48(10)**, 1741–8
- [9] Yoo, J., Tang, L., Perkins, T.A., Rowland, D.J., Laforest, R., T, J.S.L., Welch, M.J., Lewis, J.S. *Nucl. Med. Biol.*, 2005. **32(8)**, 891–7
- [10] Hohn, A., Zimmermann, K., Schaub, E., Hirzel, W., Schubiger, P.a., Schibli, R. *Q J Nucl. Med. Mol. Imaging*, 2008. **52(2)**, 145–50
- [11] Bu, X.H., Zhang, Z.H., An, D.L., Chen, Y.T., Shionoya, M., Kimura, E. *Inorg. Chim. Acta*, 1996. **249(1)**, 125–130

- [12] Polyakova, I., Poznyak, A., Sergienko, V. *Crystallography Reports*, 2000. **45(1)**, 4
- [13] Ma, D., Lu, F., Overstreet, T., Milenic, D.E., Brechbiel, M.W. *Nucl. Med. Biol.*, 2002. **29(1)**, 91–105
- [14] Jarjayes, O., Mortini, F., du Moulinet dHardemare, A., Philouze, C., Serratrice, G. *Eur. J. Inorg. Chem.*, 2005. **2005(21)**, 4417–4424
- [15] Motekaitis, R.J., Martell, A.E., Koch, S.A., Quarless, D.A., Welch, M.J. *Inorg. Chem.*, 1998. **37(22)**, 5902–5911
- [16] Ma, R., Motekaitis, R.J., Martell, A.E. *Inorg. Chim. Acta*, 1994. **224(1-2)**, 151–155
- [17] Wadas, T.J., Wong, E.H., Weisman, G.R., Anderson, C.J. *Chem. Rev.*, 2010. **110(5)**, 2858–902
- [18] Kreher, U., Hearn, M.T., Moubaraki, B., Murray, K.S., Spiccia, L. *Polyhedron*, 2007. **26(13)**, 3205–3216
- [19] Wieghardt, K., Bossek, U., Chaudhuri, P., Herrmann, W., Menke, B.C., Weiss, J. *Inorg. Chem*, 1982. **21(12)**, 4308–4314
- [20] Broan, C.J., Cox, J.P.L., Craig, A.S., Katakya, R., Parker, D., Harrison, A., Randall, A.M., Ferguson, G. *J. Chem. Soc., Perkin Trans. 2*, 1991. **(1)**, 87
- [21] Moore, D.A., Fanwick, P.E., Welch, M.J. *Inorg. Chem.*, 1990. **29(4)**, 672–676
- [22] Riesen, A., Zehnder, M., Kaden, T.A. *Helv. Chim. Acta*, 1986. **69(8)**, 2067–2073
- [23] Kumar, K., Tweedle, M.F., Malley, M.F., Gougoutas, J.Z. *Inorg. Chem.*, 1995. **34(26)**, 6472–6480
- [24] Viola, N.A., Rarig, R.S., Ouellette, W., Doyle, R.P. *Polyhedron*, 2006. **25(18)**, 3457–3462
- [25] Boswell, C.A., Sun, X., Niu, W., Weisman, G.R., Wong, E.H., Rheingold, A.L., Anderson, C.J. *J. Med. Chem.*, 2004. **47(6)**, 1465–74
- [26] Heppeler, A., Froidevaux, S., Mäcke, H.R., Jermann, E., Béhé, M., Powell, P., Hennig, M. *Chemistry*, 1999. **5(7)**, 1974–1981
- [27] Fani, M., André, J.a.P., Maecke, H.R. *Contrast Media Mol. Imaging*. **3(2)**, 67–77

- [28] Clarke, E.T., Martell, A.E. *Inorg. Chim. Acta*, 1991. **190(1)**, 37–46
- [29] Aneetha, H., Lai, Y.H., Lin, S.C., Panneerselvam, K., Lu, T.H., Chung, C.S. *Dalton Trans.*, 1999. **(16)**, 2885–2892
- [30] Silversides, J.D., Allan, C.C., Archibald, S.J. *Dalton Trans.*, 2007. **(9)**, 971–8
- [31] Moi, M.K., Yanuck, M., Deshpande, S.V., Hope, H., DeNardo, S.J., Meares, C.F. *Inorg. Chem.*, 1987. **26(21)**, 3458–3463
- [32] Sprague, J.E., Peng, Y., Fiamengo, A.L., Woodin, K.S., Southwick, E.A., Weisman, G.R., Wong, E.H., Golen, J.A., Rheingold, A.L., Anderson, C.J. *J. Med. Chem.*, 2007. **50(10)**, 2527–35
- [33] Woodin, K.S., Heroux, K.J., Boswell, C.A., Wong, E.H., Weisman, G.R., Niu, W., Tomellini, S.A., Anderson, C.J., Zakharov, L.N., Rheingold, A.L. *Eur. J. Inorg. Chem.*, 2005. **2005(23)**, 4829–4833
- [34] Lewis, E.A., Boyle, R.W., Archibald, S.J. *Chem. Commun.*, 2004. **(19)**, 2212–3
- [35] Terova, O. *Characterisation and Inertness Studies of Gallium (III) and Indium (III) Complexes of Dicarboxymethyl Pendant-armed Cross-Bridged Cyclam*. Ph.D. thesis, University of New Hampshire, Durham, NH, 2008
- [36] Di Bartolo, N.M., Sargeson, A.M., Donlevy, T.M., Smith, S.V. *Dalton Trans.*, 2001. **(15)**, 2303–2309
- [37] Bernhardt, P.V., Bramley, R., Engelhardt, L.M., Harrowfield, J.M., Hockless, D.C.R., Korybut-Daszkiewicz, B.R., Krausz, E.R., Morgan, T., Sargeson, A.M. *Inorg. Chem.*, 1995. **34(14)**, 3589–3599
- [38] Cai, W., Guzman, R., Hsu, A.R., Wang, H., Chen, K., Sun, G., Gera, A., Choi, R., Bliss, T., He, L., Li, Z.B., Maag, A.L.D., Hori, N., Zhao, H., Moseley, M., Steinberg, G.K., Chen, X. *Stroke*, 2009. **40(1)**, 270–7
- [39] Ma, M.T., Karas, J.A., White, J.M., Scanlon, D., Donnelly, P.S. *Chem. Commun.*, 2009. **(22)**, 3237–9
- [40] Cox, J.P.L., Craig, A.S., Helps, I.M., Jankowski, K.J., Parker, D., Eaton, M.A.W., Millican, A.T., Millar, K., Beeley, N.R.A., Boyce, B.A. *J. Chem. Soc., Perkin Trans. 1*, 1990. **(9)**, 2567

- [41] Moi, M.K., Meares, C.F., Denardo, S.J. *J. Am. Chem. Soc.*, 1988. **110(18)**, 6266–7
- [42] Morphy, J.R., Parker, D., Katakya, R., Eaton, M.A.W., Millican, A.T., Alexander, R., Harrison, A., Walker, C. *J. Chem. Soc., Perkin Trans. 2*, 1990. **(4)**, 573
- [43] Moore, D.A., Fanwick, P.E., Welch, M.J. *Inorg. Chem.*, 1989. **28(8)**, 1504–1506
- [44] Beissel, T., Buerger, K.S., Voigt, G., Wiegardt, K., Butzlaff, C., Trautwein, A.X. *Inorg. Chem.*, 1993. **32(2)**, 124–126
- [45] Prata, M., Santos, A., Geraldés, C., Lima, J. *Nucl. Med. Biol.*, 1999. **26(6)**, 707–710
- [46] Baykal, U., Akkaya, M.S., Akkaya, E.U. *J. Mol. Catal. A*, 1999. **145(1-2)**, 309–312
- [47] McMurry, T.J., Brechbiel, M.W., Wu, C., Gansow, O.A. *Bioconj. Chem*, 1993. **4(3)**, 236–245
- [48] Fallis, I.A., Farrugia, L.J., Macdonald, N.M., Peacock, R.D. *Dalton Trans.*, 1993. **(18)**, 2759
- [49] Tei, L., Baum, G., Blake, A.J., Fenske, D., Schröder, M. *Dalton Trans.*, 2000. **(16)**, 2793–2799
- [50] Mabeza, G.F., Loyevsky, M., Gordeuk, V.R., Weiss, G. *Pharmacology & Therapeutics*, 1999. **81(1)**, 53–75
- [51] Haselhorst, G., Stoetzel, S., Strassburger, A., Walz, W., Wiegardt, K., Nuber, B. *Dalton Trans.*, 1993. **(1)**, 83
- [52] Farrugia, L.J., Lopinski, S., Lovatt, P.A., Peacock, R.D. *Inorg. Chem.*, 2001. **40(3)**, 558–559
- [53] Ellis, D., Farrugia, L.J., Peacock, R.D. *Polyhedron*, 1999. **18(8-9)**, 1229–1234
- [54] Fallis, I.A., Farley, R.D., Malik, K.M.A., Murphy, D.M., Smith, H.J. *Dalton Trans.*, 2000. **(20)**, 3632–3639
- [55] Tatchell, T. *The Coordination Chemistry of Pendant Aniline Aza-Macrocycles*. Ph.D. thesis, Cardiff University, 2005
- [56] Fallis, I.A., Perkins, W.T.S., Malik, K.M.A. 2001

- [57] Hancock, R.D., Ngwenya, M.P., Evers, A., Wade, P.W., Boeyens, J.C.A., Dobson, S.M. *Inorg. Chem.*, 1990. **29(2)**, 264–270
- [58] Ray, R., Kauffman, G.B. *Inorg. Chim. Acta*, 1990. **173(2)**, 207–214
- [59] Kavana, M., Powell, D.R., Burstyn, J.N. *Inorg. Chim. Acta*, 2000. **297(1-2)**, 351–361
- [60] Arya, K., Dandia, A. *Bioorg. Med. Chem. Lett.*, 2007. **17(12)**, 3298–304
- [61] Garaj, V., Puccetti, L., Fasolis, G., Winum, J.Y., Montero, J.L., Scozzafava, A., Vullo, D., Innocenti, A., Supuran, C.T. *Bioorg. Med. Chem. Lett.*, 2005. **15(12)**, 3102–8
- [62] Matsuno, T., Kato, M., Tsuchida, Y., Takahashi, M., Yaguchi, S., Terada, S. *Chemical & pharmaceutical bulletin*, 1997. **45(2)**, 291–6
- [63] Supuran, C.T., Scozzafava, A., Casini, A. *Medicinal research reviews*, 2003. **23(2)**, 146–89
- [64] Chegwiddden, W.R., Spencer, I.M. *Inflammopharmacology*, 1995. **3(3)**, 231–239
- [65] Garaj, V., Puccetti, L., Fasolis, G., Winum, J.Y., Montero, J.L., Scozzafava, A., Vullo, D., Innocenti, A., Supuran, C.T. *Bioorg. Med. Chem. Lett.*, 2004. **14(21)**, 5427–33
- [66] Haubner, R., Finsinger, D., Kessler, H. *Angew. Chem. Int. Ed.*, 1997. **36(1314)**, 1374–1389
- [67] Gladson, C.L., Cheresch, D.A. *J. Clin. Inv.*, 1991. **88(6)**, 1924–32
- [68] Albelda, S.M., Mette, S.A., Elder, D.E., Stewart, R., Damjanovich, L., Herlyn, M., Buck, C.A. *Cancer Res.*, 1990. **50(20)**, 6757–6764
- [69] Marshall, J.F., Nesbitt, S.A., Helfrich, M.H., Horton, M.A., Polakova, K., Hart, I.R. *Cancer*, 1991. **49(6)**, 924–931
- [70] Felding-Habermann, B., Mueller, B.M., Romerdahl, C.A., Cheresch, D.A. *J. Clin. Inv.*, 1992. **89(6)**, 2018–22
- [71] Folkman, J., Shing, Y. *J. Biol. Chem.*, 1992. **267(16)**, 10,931–10,934
- [72] Xiong, J.p., Stehle, T., Zhang, R., Joachimiak, A., Frech, M., Goodman, S.L., Arnaout, M.A. *Science*, 2002. **296(5)**, 151–155

- [73] Cox, D., Aoki, T., Seki, J., Motoyama, Y., Yoshida, K. *Medicinal Research Reviews*, 1994. **14(2)**, 195–228
- [74] Veber, D.F. In *21 st Pept. Proc. Eur. Pept. Symp.* (1990), 784–786
- [75] Greenspoon, N., Hershkovich, R., Alon, R., Varon, D., Shenkman, B., Marx, G., Federman, S., Kapustina, G., Lider, O. *Biochemistry*, 1993. **32(4)**, 1001–8
- [76] Thurston, J.T., Dudley, J.R., Kaiser, D.W., Hechenbleikner, I., Schaefer, F.C., Holm-Hansen, D. *J. Am. Chem. Soc.*, 1951. **2988(6)**, 2981–2983
- [77] Feichtinger, K., Zapf, C., Sings, H.L., Goodman, M. *The Journal of Organic Chemistry*, 1998. **63(12)**, 3804–3805
- [78] Castagnolo, D., Raffi, F., Giorgi, G., Botta, M. *European Journal of Organic Chemistry*, 2009. **2009(3)**, 334–337
- [79] Kolb, H.C., Finn, M.G., Sharpless, K.B. *Angew. Chem. Int. Ed.*, 2001. **40(11)**, 2004–2021
- [80] Simmonds, R.J., Stevens, M.F.G. *J. Chem. Soc., Perkin Trans. 1*, 1982, 1821
- [81] Garg, S., Shreeve, J.M. *J. Mat. Chem.*, 2011. **21(13)**, 4787
- [82] Cacheris, W.P., Nickle, S.K., Sherry, A.D. *Inorg. Chem.*, 1987. **26(6)**, 958–960
- [83] Kumar, K., Chang, C.A., Tweedle, M.F. *Inorg. Chem.*, 1993. **32(5)**, 587–593
- [84] Lattuada, L., Barge, A., Cravotto, G., Giovenzana, G.B., Tei, L. *Chem. Soc. Rev.*, 2011. **40(5)**, 3019–49
- [85] McBride, W.J., Sharkey, R.M., Karacay, H., D'Souza, C.A., Rossi, E.A., Laverman, P., Chang, C.H., Boerman, O.C., Goldenberg, D.M. *J. Nuc. Med.*, 2009. **50(6)**, 991–8
- [86] McBride, W.J., Goldenberg, D.M. *WO Patent 2,008,088,648*, 2008, 41
- [87] Shetty, D., Choi, S.Y., Jeong, J.M., Lee, J.Y., Hoigebazar, L., Lee, Y.S., Lee, D.S., Chung, J.K., Lee, M.C., Chung, Y.K. *Chem. Commun.*, 2011. **47(34)**, 9732–4
- [88] Cao, R., Müller, P., Lippard, S.J. *J. Am. Chem. Soc.*, 2010. **132(49)**, 17,366–9
- [89] Sessler, J.L., Sibert, J.W., Lynch, V. *Inorg. Chem.*, 1990. **29(20)**, 4143–4146

- [90] Fry, F.H., Graham, B., Spiccia, L., Hockless, C.R., Tiekink, E.R.T. 1997. (**Dalton Trans.**), 827–831
- [91] Hanwell, M.D., Curtis, D.E., Lonie, D.C., Vandermeersch, T., Zurek, E., Hutchison, G.R. *Journal of cheminformatics*, 2012. **4(1)**, 17
- [92] Cooper, M.S., Ma, M.T., Sunassee, K., Shaw, K.P., Williams, J.D., Paul, R.L., Donnelly, P.S., Blower, P.J. *Bioconjugate chemistry*, 2012
- [93] Koppenhoefer, B., Schurig, V. *Org. Synth.*, 1988. **66**, 151–159
- [94] Jones, P.L., Amoroso, A.J., Jeffery, J.C., McCleverty, J.A., Psillakis, E., Rees, L.H., Ward, M.D. *Inorg. Chem.*, 1997. **1669(96)**, 10–18
- [95] Alkorta, I., Elguero, J., Claramunt, R.M., López, C., Sanz, D. *Heterocycl. Commun.*, 2010. **16(4-6)**, 261–268
- [96] Frisch, M.J., Trucks, G.W., Schlegel, H.B., Scuseria, G.E., Robb, M.A., Cheeseman, J.R., Montgomery, Jr., J.A., Vreven, T., Kudin, K.N., Burant, J.C., Millam, J.M., Iyengar, S.S., Tomasi, J., Barone, V., Mennucci, B., Cossi, M., Scalmani, G., Rega, N., Petersson, G.A., Nakatsuji, H., Hada, M., Ehara, M., Toyota, K., Fukuda, R., Hasegawa, J., Ishida, M., Nakajima, T., Honda, Y., Kitao, O., Nakai, H., Klene, M., Li, X., Knox, J.E., Hratchian, H.P., Cross, J.B., Bakken, V., Adamo, C., Jaramillo, J., Gomperts, R., Stratmann, R.E., Yazyev, O., Austin, A.J., Cammi, R., Pomelli, C., Ochterski, J.W., Ayala, P.Y., Morokuma, K., Voth, G.A., Salvador, P., Dannenberg, J.J., Zakrzewski, V.G., Dapprich, S., Daniels, A.D., Strain, M.C., Farkas, O., Malick, D.K., Rabuck, A.D., Raghavachari, K., Foresman, J.B., Ortiz, J.V., Cui, Q., Baboul, A.G., Clifford, S., Cioslowski, J., Stefanov, B.B., Liu, G., Liashenko, A., Piskorz, P., Komaromi, I., Martin, R.L., Fox, D.J., Keith, T., Al-Laham, M.A., Peng, C.Y., Nanayakkara, A., Challacombe, M., Gill, P.M.W., Johnson, B., Chen, W., Wong, M.W., Gonzalez, C., Pople, J.A. Gaussian 03, Revision C.02. Gaussian, Inc., Wallingford, CT, 2004
- [97] Becke, A.D. *J. Chem. Phys.*, 1993. **98(7)**, 5648
- [98] Lee, C., Yang, W., Parr, R.G. *Phys. Rev. B*, 1988. **37(2)**, 785–789
- [99] Vosko, S.H., Wilk, L., Nusair, M. *Can. J. Phys.*, 1980. **58(8)**, 1200–1211

- [100] Stephens, P.J., Devlin, F.J., Chabalowski, C.F., Frisch, M.J. *J. Phys. Chem.*, 1994. **98(45)**, 11,623–11,627
- [101] Ditchfield, R. *J. Chem. Phys.*, 1971. **54(2)**, 724
- [102] Hehre, W.J. *J. Chem. Phys.*, 1972. **56(5)**, 2257
- [103] Hariharan, P.C., Pople, J.A. *Theor. Chim. Acta*, 1973. **28(3)**, 213–222
- [104] Hariharan, P., Pople, J. *Mol. Phys.*, 1974. **27(1)**, 209–214
- [105] Gordon, M.S. *Chem. Phys. Lett.*, 1980. **76(1)**, 163–168
- [106] Francl, M.M. *J. Chem. Phys.*, 1982. **77(7)**, 3654
- [107] Binning, R.C., Curtiss, L.A. *Journal of Computational Chemistry*, 1990. **11(10)**, 1206–1216
- [108] Blaudeau, J.P., McGrath, M.P., Curtiss, L.A., Radom, L. *J. Chem. Phys.*, 1997. **107(13)**, 5016
- [109] Mitin, A.V., Baker, J., Pulay, P. *J. Chem. Phys.*, 2003. **118(17)**, 7775
- [110] Rassolov, V.A., Ratner, M.A., Pople, J.A., Redfern, P.C., Curtiss, L.A. *J. Comp. Chem.*, 2001. **22(9)**, 976–984

Appendix A

Crystal structures of ligands and ligand precursors

A.1 Crystal structure of $\text{HP}^{1-\text{NO}_2}$

Crystallisation method:

Hydrogen atoms removed for clarity

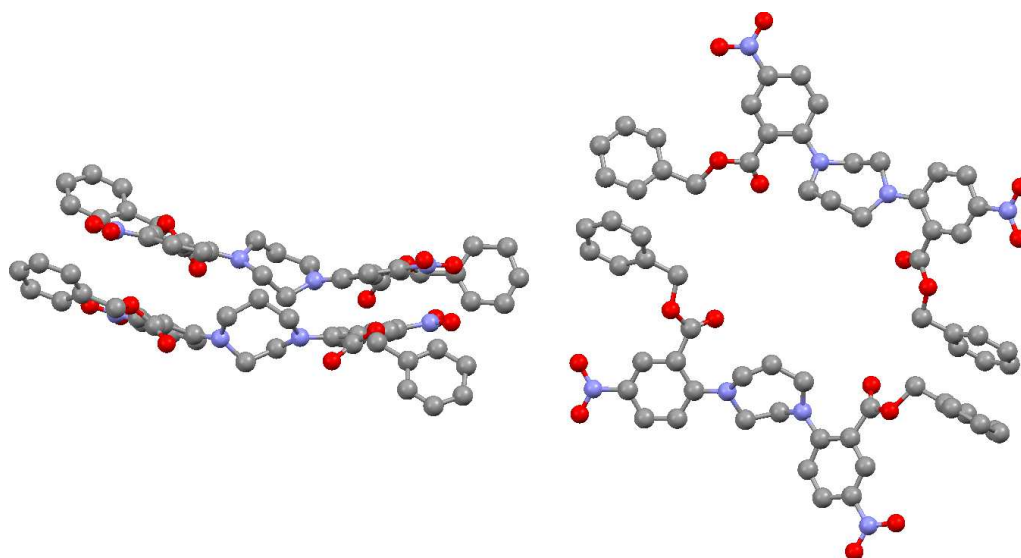


Figure A.1: Benzyl-6,6'-(1,4-diazepane-1,4-diyl)bis(3-nitrobenzoate) ($\text{HP}^{1-\text{NO}_2}$)

A.2 Crystal structure of TACN^{1-NO₂}

Crystallisation method: Slow evaporation of DCM/Ethanol solution

hydrogen atoms removed for clarity

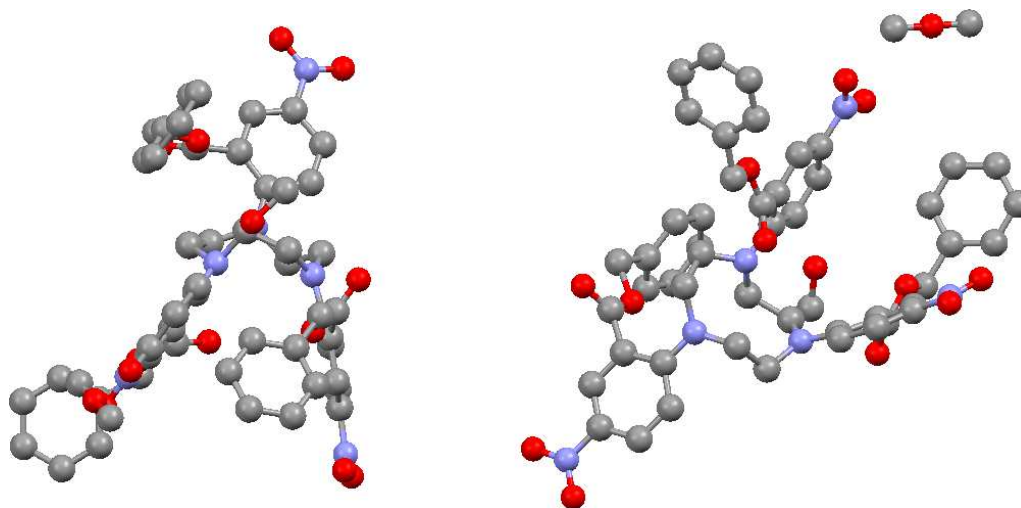


Figure A.2: Benzyl-6,6',6''-(1,4,7-triazonane-1,4,7-triyl)tris(3-nitrobenzoate) (TACN^{1-NO₂})

A.3 Crystal structure of DMC^{1-NO₂}

Crystallisation method: Vapour diffusion of pentane into a toluene/methanol solution

Hydrogen atoms removed for clarity

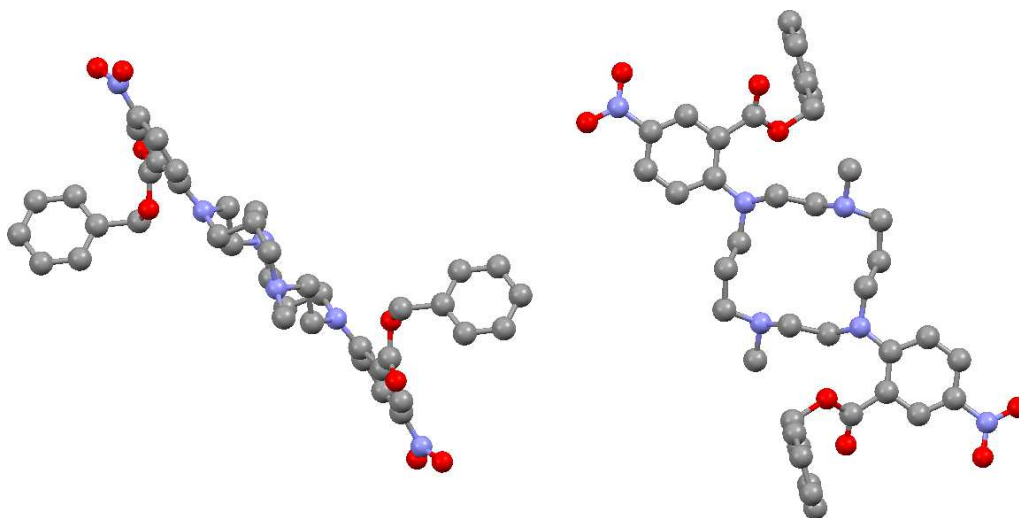


Figure A.3: Benzyl-6,6'-(4,11-dimethyl-1,4,8,11-tetraazacyclotetradecane-1,8-diyl)bis(3-nitrobenzoate) ($\text{DMC}^{1-\text{NO}_2}$)

A.4 Crystal structure of $\text{HP}^{3-\text{NO}_2}$

Crystallisation method:

Hydrogen atoms removed for clarity

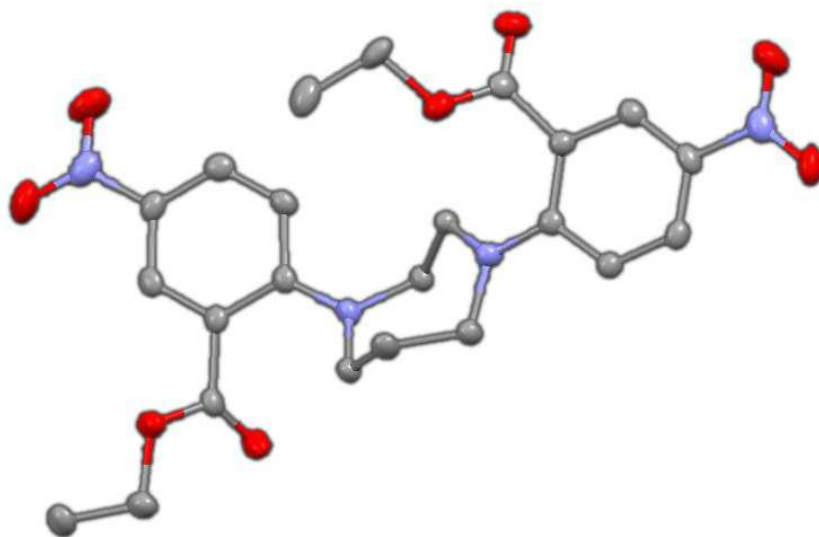


Figure A.4: Diethyl 6,6'-(1,4-diazepane-1,4-diyl)bis(3-nitrobenzoate) ($\text{HP}^3\text{-NO}_2$)

A.5 Crystal structure of $\text{HP}^{\text{Sang-NO}_2}$

Crystallisation method:

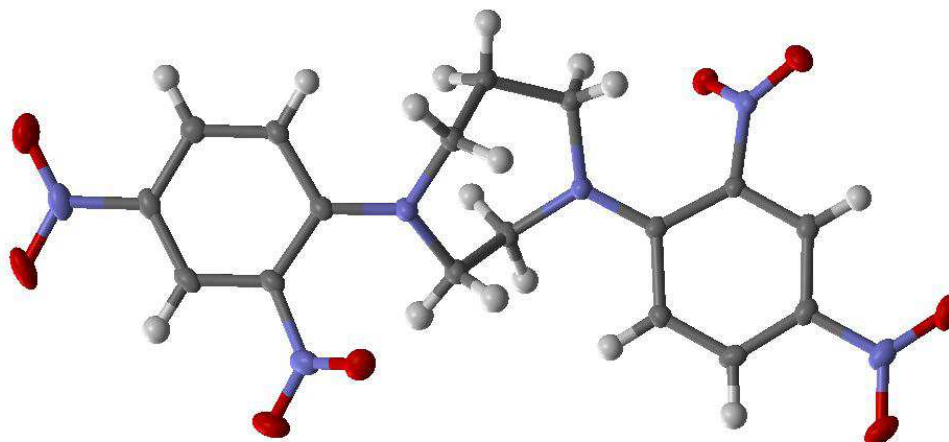


Figure A.5: 1,4-bis(2,4-dinitrophenyl)-1,4-diazepane (HP^{Sang}-NO₂)

A.6 Crystal structure of HP^{CF₃}

Crystallisation method: Isolated from attempts to crystallise metal complex - Diffusion of ether into acetonitrile.

Hydrogen atoms removed for clarity

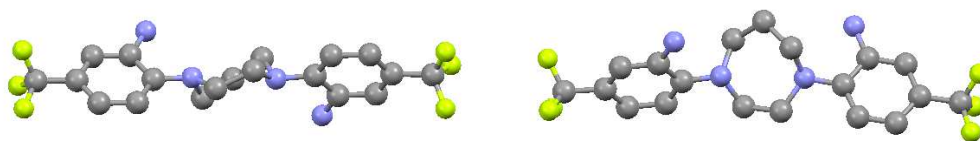


Figure A.6: 1,4-bis(2-amino-4-trifluoromethylphenyl)-1,4-diazepane (HP^{CF₃})

A.7 Crystal structure of Pip^{3-NH₂}

Crystallisation method:

Hydrogen atoms removed for clarity

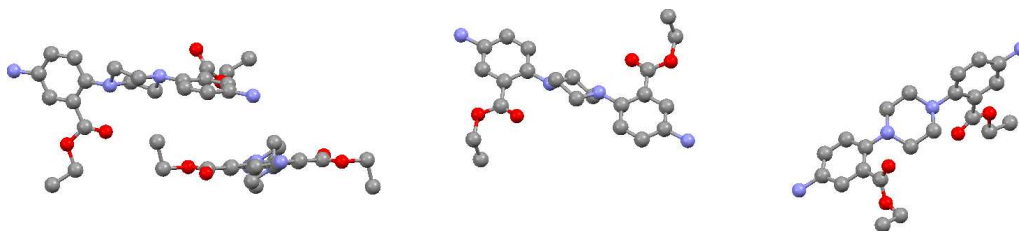


Figure A.7: Diethyl 6,6'-(piperazine-1,4-diyl)bis(3-aminobenzoate) (Pip^{3-NH₂})

A.8 Crystal structure of Pip^{Tol}

Crystallisation method: Isolated from attempts to crystallise metal complex - Diffusion of ether into acetonitrile.

Hydrogen atoms removed for clarity

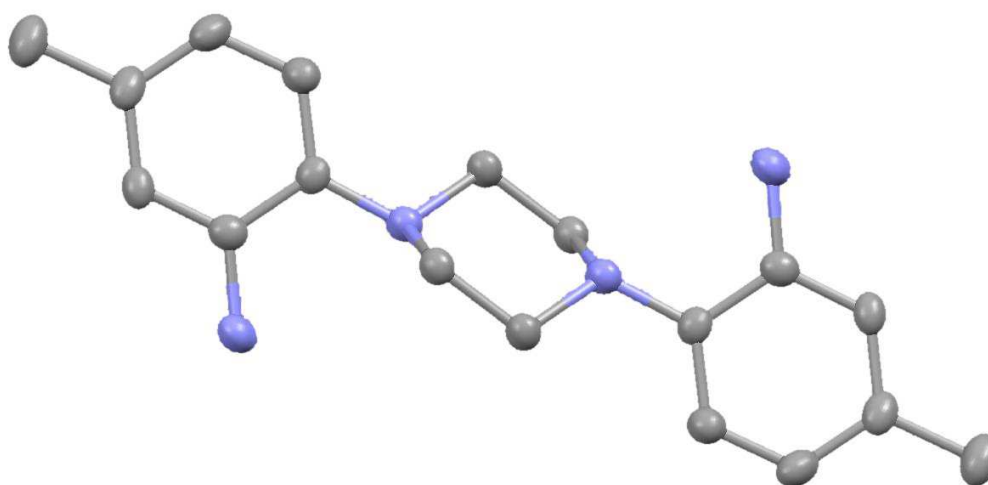
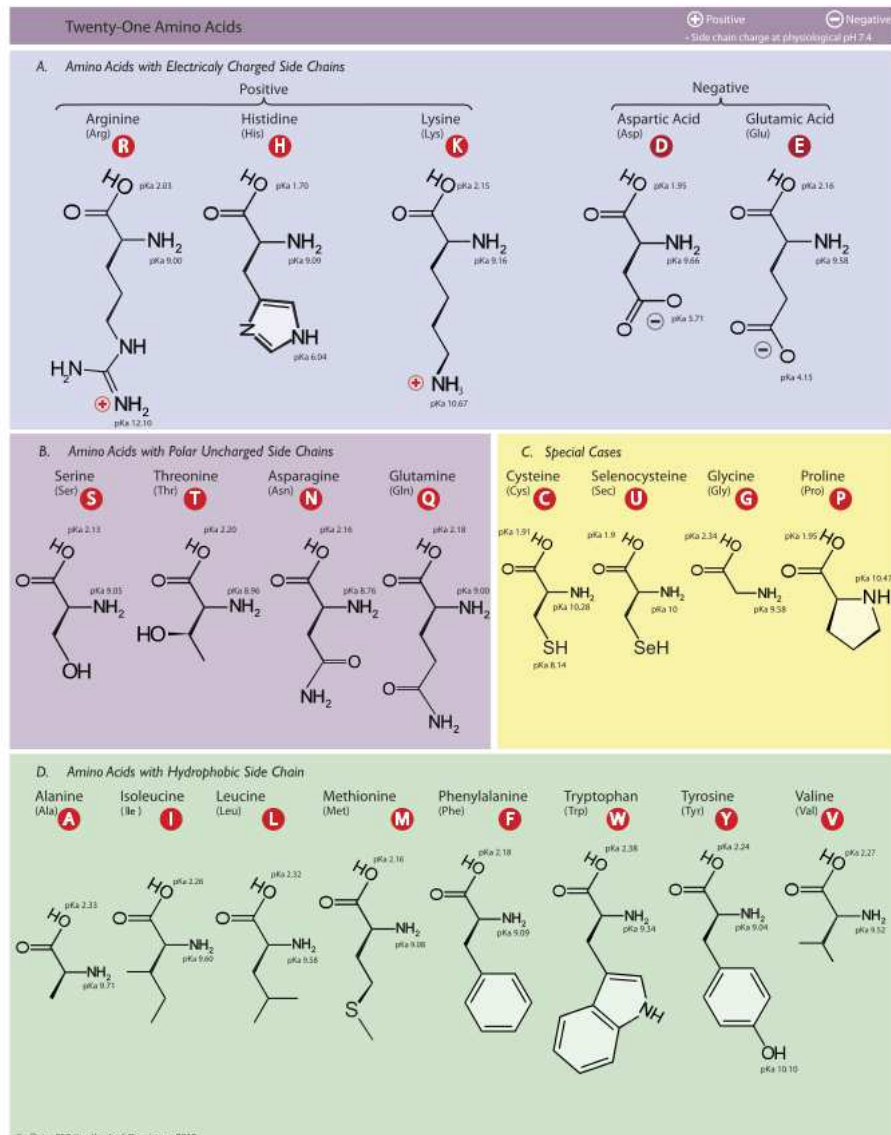


Figure A.8: 1,3-bis(2-amino-4-tolyl)-1,3-diazacyclohexane (Pip^{Tol})

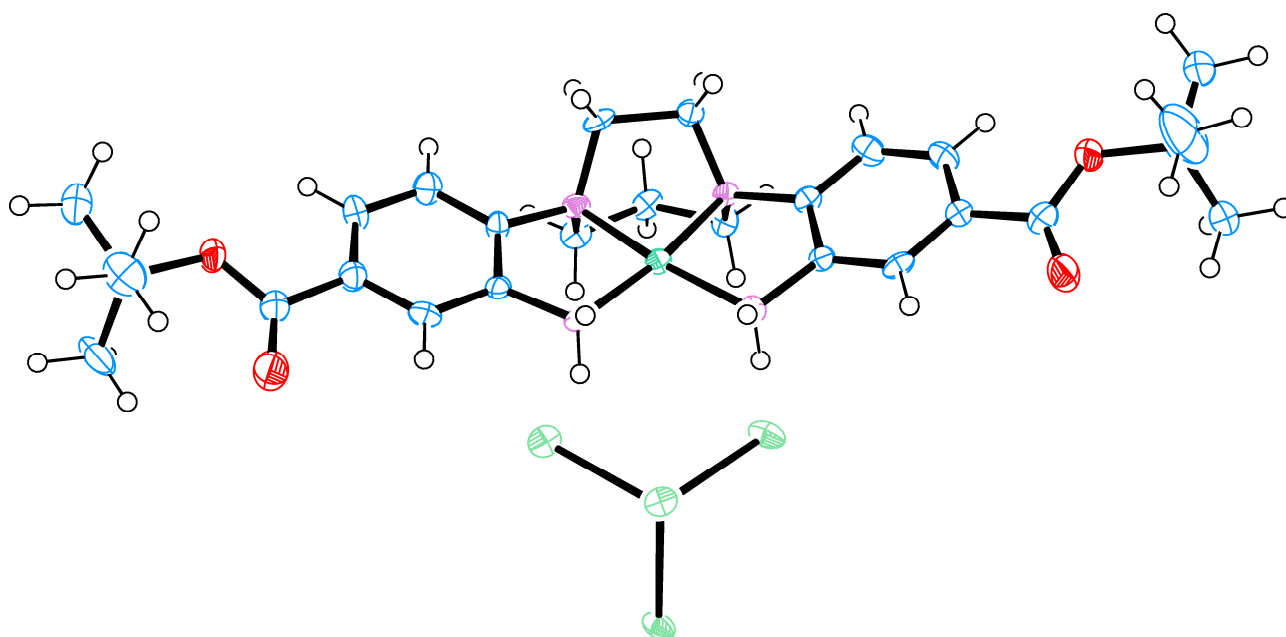
Appendix B

Amino Acids



Appendix C

X-Ray crystal structure data



Ortep plot of NiHPtButyl - Ellipsoids at 50% probability

Identification code	NiHP ^t Bu	
Empirical formula	C ₂₇ H ₃₈ Cl ₄ N ₄ Ni ₂ O ₄	
Formula weight	741.83	
Temperature	100(2) K	
Wavelength	0.71073 Å	
Crystal system	Orthorhombic	
Space group	<i>Pbca</i>	
Unit cell dimensions	<i>a</i> = 16.445(2) Å	$\alpha = 90^\circ$
	<i>b</i> = 11.9620(17) Å	$\beta = 90^\circ$
	<i>c</i> = 34.343(6) Å	$\gamma = 90^\circ$
Volume	6756.0(17) Å ³	
Z	8	
Density (calculated)	1.459 Mg / m ³	
Absorption coefficient	1.468 mm ⁻¹	
<i>F</i> (000)	3072	
Crystal	Needle; Colourless	
Crystal size	0.04 × 0.03 × 0.01 mm ³	
θ range for data collection	3.01 – 27.48°	
Index ranges	–21 ≤ <i>h</i> ≤ 12, –15 ≤ <i>k</i> ≤ 15, –44 ≤ <i>l</i> ≤ 31	
Reflections collected	23751	
Independent reflections	7733 [<i>R</i> _{int} = 0.1206]	
Completeness to $\theta = 27.48^\circ$	99.7 %	
Absorption correction	Semi-empirical from equivalents	
Max. and min. transmission	0.9855 and 0.9436	
Refinement method	Full-matrix least-squares on <i>F</i> ²	
Data / restraints / parameters	7733 / 0 / 376	
Goodness-of-fit on <i>F</i> ²	1.065	
Final <i>R</i> indices [<i>F</i> ² > 2σ(<i>F</i> ²)]	<i>R</i> 1 = 0.0846, <i>wR</i> 2 = 0.1087	
<i>R</i> indices (all data)	<i>R</i> 1 = 0.1619, <i>wR</i> 2 = 0.1339	
Largest diff. peak and hole	0.833 and –0.674 e Å ⁻³	

Bond Lengths (Å)

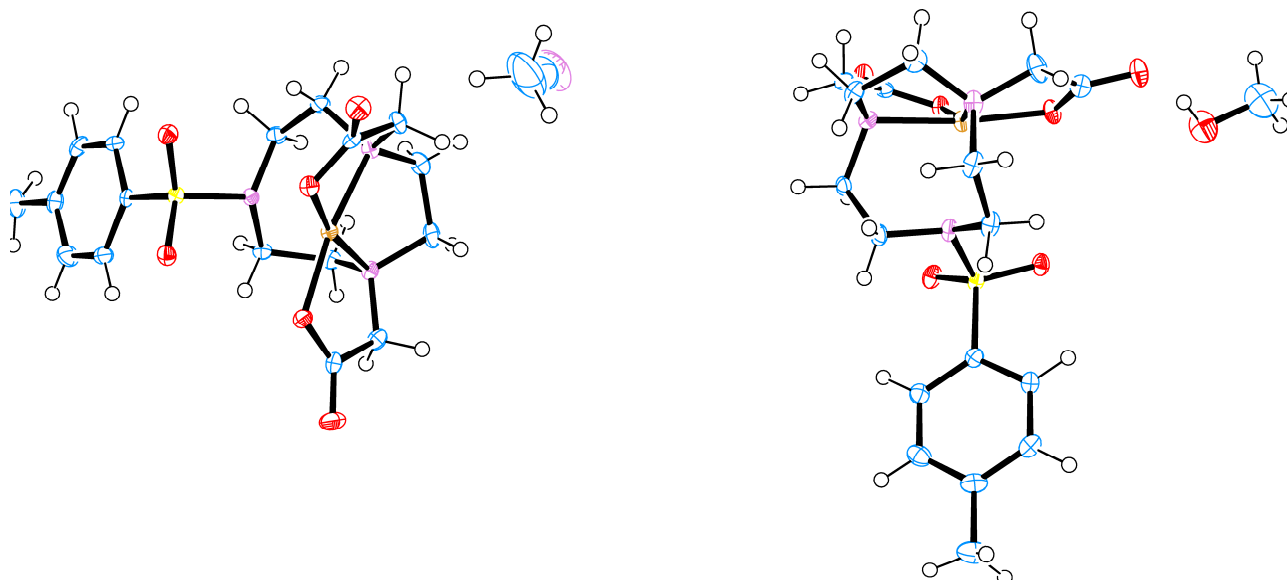
C1–N2	1.508(7)	C16–H16B	0.9800
C1–C2	1.542(8)	C16–H16C	0.9800
C1–H1A	0.9900	C17–C22	1.369(8)
C1–H1B	0.9900	C17–C18	1.383(8)
C2–N3	1.505(7)	C17–N3	1.481(7)
C2–H2A	0.9900	C18–C19	1.388(8)
C2–H2B	0.9900	C18–H18	0.9500
C3–N3	1.516(6)	C19–C20	1.388(8)
C3–C4	1.517(8)	C19–H19	0.9500
C3–H3A	0.9900	C20–C21	1.390(8)
C3–H3B	0.9900	C20–C23	1.496(8)
C4–C5	1.521(7)	C21–C22	1.397(8)
C4–H4A	0.9900	C21–H21	0.9500
C4–H4B	0.9900	C22–N4	1.458(6)
C5–N2	1.508(6)	C23–O3	1.204(7)
C5–H5A	0.9900	C23–O4	1.336(7)
C5–H5B	0.9900	C24–O4	1.504(7)
C6–C7	1.389(8)	C24–C27	1.509(8)
C6–C11	1.389(8)	C24–C25	1.531(9)
C6–N2	1.472(7)	C24–C26	1.532(8)
C7–C8	1.379(8)	C25–H25A	0.9800
C7–H7	0.9500	C25–H25B	0.9800
C8–C9	1.393(8)	C25–H25C	0.9800
C8–H8	0.9500	C26–H26A	0.9800
C9–C10	1.381(8)	C26–H26B	0.9800
C9–C12	1.502(8)	C26–H26C	0.9800
C10–C11	1.383(7)	C27–H27A	0.9800
C10–H10	0.9500	C27–H27B	0.9800
C11–N1	1.451(7)	C27–H27C	0.9800
C12–O1	1.210(7)	N1–Ni1	1.916(4)
C12–O2	1.337(8)	N1–H1C	0.9200
C13–O2	1.491(7)	N1–H1D	0.9200
C13–C14	1.507(9)	N2–Ni1	1.905(5)
C13–C15	1.513(9)	N3–Ni1	1.905(5)
C13–C16	1.515(10)	N4–Ni1	1.905(4)
C14–H14A	0.9800	N4–H4C	0.9200
C14–H14B	0.9800	N4–H4D	0.9200
C14–H14C	0.9800	C11–Ni2	2.2591(15)
C15–H15A	0.9800	C12–Ni2	2.2492(17)
C15–H15B	0.9800	C13–Ni2	2.3013(18)
C15–H15C	0.9800	C14–Ni2	2.3026(17)
C16–H16A	0.9800		

Bond Angles (°)

N2–C1–C2	108.9(5)	C17–C18–H18	121.0
N2–C1–H1A	109.9	C19–C18–H18	121.0

C2-C1-H1A	109.9	C20-C19-C18	121.5(6)
N2-C1-H1B	109.9	C20-C19-H19	119.3
C2-C1-H1B	109.9	C18-C19-H19	119.3
H1A-C1-H1B	108.3	C19-C20-C21	119.5(6)
N3-C2-C1	109.3(5)	C19-C20-C23	123.8(6)
N3-C2-H2A	109.8	C21-C20-C23	116.7(6)
C1-C2-H2A	109.8	C20-C21-C22	119.2(6)
N3-C2-H2B	109.8	C20-C21-H21	120.4
C1-C2-H2B	109.8	C22-C21-H21	120.4
H2A-C2-H2B	108.3	C17-C22-C21	120.1(6)
N3-C3-C4	111.3(5)	C17-C22-N4	117.2(5)
N3-C3-H3A	109.4	C21-C22-N4	122.7(5)
C4-C3-H3A	109.4	O3-C23-O4	125.8(7)
N3-C3-H3B	109.4	O3-C23-C20	122.6(7)
C4-C3-H3B	109.4	O4-C23-C20	111.6(6)
H3A-C3-H3B	108.0	O4-C24-C27	111.5(5)
C3-C4-C5	115.0(5)	O4-C24-C25	102.0(5)
C3-C4-H4A	108.5	C27-C24-C25	111.0(6)
C5-C4-H4A	108.5	O4-C24-C26	109.0(5)
C3-C4-H4B	108.5	C27-C24-C26	112.5(6)
C5-C4-H4B	108.5	C25-C24-C26	110.3(6)
H4A-C4-H4B	107.5	C24-C25-H25A	109.5
N2-C5-C4	110.9(4)	C24-C25-H25B	109.5
N2-C5-H5A	109.5	H25A-C25-H25B	109.5
C4-C5-H5A	109.5	C24-C25-H25C	109.5
N2-C5-H5B	109.5	H25A-C25-H25C	109.5
C4-C5-H5B	109.5	H25B-C25-H25C	109.5
H5A-C5-H5B	108.0	C24-C26-H26A	109.5
C7-C6-C11	121.2(6)	C24-C26-H26B	109.5
C7-C6-N2	122.4(5)	H26A-C26-H26B	109.5
C11-C6-N2	116.4(5)	C24-C26-H26C	109.5
C8-C7-C6	118.5(6)	H26A-C26-H26C	109.5
C8-C7-H7	120.8	H26B-C26-H26C	109.5
C6-C7-H7	120.8	C24-C27-H27A	109.5
C7-C8-C9	120.7(6)	C24-C27-H27B	109.5
C7-C8-H8	119.7	H27A-C27-H27B	109.5
C9-C8-H8	119.7	C24-C27-H27C	109.5
C10-C9-C8	120.3(6)	H27A-C27-H27C	109.5
C10-C9-C12	119.1(6)	H27B-C27-H27C	109.5
C8-C9-C12	120.6(6)	C11-N1-Ni1	108.3(4)
C9-C10-C11	119.7(6)	C11-N1-H1C	110.0
C9-C10-H10	120.2	Ni1-N1-H1C	110.0
C11-C10-H10	120.2	C11-N1-H1D	110.0
C10-C11-C6	119.6(6)	Ni1-N1-H1D	110.0
C10-C11-N1	124.5(5)	H1C-N1-H1D	108.4
C6-C11-N1	116.0(5)	C6-N2-C5	110.2(4)
O1-C12-O2	125.9(6)	C6-N2-C1	113.0(4)
O1-C12-C9	123.1(7)	C5-N2-C1	110.8(4)
O2-C12-C9	111.0(6)	C6-N2-Ni1	107.7(4)

O2-C13-C14	101.1(5)	C5-N2-Ni1	110.2(4)
O2-C13-C15	108.2(6)	C1-N2-Ni1	104.7(3)
C14-C13-C15	111.2(7)	C17-N3-C2	113.5(4)
O2-C13-C16	108.7(6)	C17-N3-C3	108.7(4)
C14-C13-C16	110.8(7)	C2-N3-C3	113.2(5)
C15-C13-C16	115.8(7)	C17-N3-Ni1	108.6(4)
C13-C14-H14A	109.5	C2-N3-Ni1	103.1(4)
C13-C14-H14B	109.5	C3-N3-Ni1	109.3(4)
H14A-C14-H14B	109.5	C22-N4-Ni1	108.8(4)
C13-C14-H14C	109.5	C22-N4-H4C	109.9
H14A-C14-H14C	109.5	Ni1-N4-H4C	109.9
H14B-C14-H14C	109.5	C22-N4-H4D	109.9
C13-C15-H15A	109.5	Ni1-N4-H4D	109.9
C13-C15-H15B	109.5	H4C-N4-H4D	108.3
H15A-C15-H15B	109.5	C12-O2-C13	122.5(5)
C13-C15-H15C	109.5	C23-O4-C24	120.0(5)
H15A-C15-H15C	109.5	N3-Ni1-N2	83.2(2)
H15B-C15-H15C	109.5	N3-Ni1-N4	89.1(2)
C13-C16-H16A	109.5	N2-Ni1-N4	172.1(2)
C13-C16-H16B	109.5	N3-Ni1-N1	172.3(2)
H16A-C16-H16B	109.5	N2-Ni1-N1	89.1(2)
C13-C16-H16C	109.5	N4-Ni1-N1	98.6(2)
H16A-C16-H16C	109.5	Cl2-Ni2-Cl1	118.19(7)
H16B-C16-H16C	109.5	Cl2-Ni2-Cl3	109.20(6)
C22-C17-C18	121.7(6)	Cl1-Ni2-Cl3	108.09(6)
C22-C17-N3	115.4(5)	Cl2-Ni2-Cl4	108.00(6)
C18-C17-N3	123.0(6)	Cl1-Ni2-Cl4	103.06(6)
C17-C18-C19	118.0(6)	Cl3-Ni2-Cl4	110.01(7)



Orteplot of CuTsTACNA2 - ellipsoids at 50% probability

Identification code	CuTsTACNA₂
Empirical formula	C ₃₇ H ₅₃ Cu ₂ N ₇ O ₁₃ S ₂
Formula weight	995.06
Temperature	100(2) K
Wavelength	0.71075 Å
Crystal system	Monoclinic
Space group	<i>P</i> 2 ₁ / <i>c</i>
Unit cell dimensions	<i>a</i> = 10.4488(3) Å $\alpha = 90^\circ$ <i>b</i> = 15.0109(4) Å $\beta = 92.900(7)^\circ$ <i>c</i> = 26.8299(18) Å $\gamma = 90^\circ$
Volume	4202.8(3) Å ³
<i>Z</i>	4
Density (calculated)	1.573 Mg / m ³
Absorption coefficient	1.184 mm ⁻¹
<i>F</i> (000)	2072
Crystal	Prism; dark blue
Crystal size	0.08 × 0.06 × 0.03 mm ³
θ range for data collection	3.04 – 27.48°
Index ranges	-13 ≤ <i>h</i> ≤ 13, -18 ≤ <i>k</i> ≤ 17, -16 ≤ <i>l</i> ≤ 34
Reflections collected	18879
Independent reflections	9506 [<i>R</i> _{int} = 0.0430]
Completeness to $\theta = 27.48^\circ$	98.6 %
Absorption correction	Semi-empirical from equivalents
Max. and min. transmission	0.9653 and 0.9112
Refinement method	Full-matrix least-squares on <i>F</i> ²
Data / restraints / parameters	9506 / 0 / 555
Goodness-of-fit on <i>F</i> ²	1.090
Final <i>R</i> indices [<i>F</i> ² > 2σ(<i>F</i> ²)]	<i>R</i> 1 = 0.0485, <i>wR</i> 2 = 0.1103
<i>R</i> indices (all data)	<i>R</i> 1 = 0.0702, <i>wR</i> 2 = 0.1184
Largest diff. peak and hole	0.669 and -0.678 e Å ⁻³

Bond Lengths (Å)

C1–N1	1.498(4)	C21–H21B	0.9900
C1–C2	1.531(5)	C22–N6	1.488(4)
C1–H1A	0.9900	C22–C23	1.522(5)
C1–H1B	0.9900	C22–H22A	0.9900
C2–N2	1.497(4)	C22–H22B	0.9900
C2–H2A	0.9900	C23–N4	1.497(4)
C2–H2B	0.9900	C23–H23A	0.9900
C3–N2	1.486(4)	C23–H23B	0.9900
C3–C4	1.521(4)	C24–N5	1.488(4)
C3–H3A	0.9900	C24–C25	1.528(4)
C3–H3B	0.9900	C24–H24A	0.9900
C4–N3	1.494(4)	C24–H24B	0.9900
C4–H4A	0.9900	C25–O7	1.229(4)
C4–H4B	0.9900	C25–O8	1.295(4)
C5–N3	1.489(4)	C26–N4	1.491(4)
C5–C6	1.513(4)	C26–C27	1.529(5)
C5–H5A	0.9900	C26–H26A	0.9900
C5–H5B	0.9900	C26–H26B	0.9900
C6–N1	1.496(4)	C27–O9	1.234(4)
C6–H6A	0.9900	C27–O10	1.288(4)
C6–H6B	0.9900	C28–C29	1.394(4)
C7–N2	1.496(4)	C28–C33	1.399(4)
C7–C8	1.531(4)	C28–S2	1.756(3)
C7–H7A	0.9900	C29–C30	1.380(5)
C7–H7B	0.9900	C29–H29	0.9500
C8–O1	1.227(4)	C30–C31	1.392(5)
C8–O2	1.292(4)	C30–H30	0.9500
C9–N1	1.487(4)	C31–C32	1.396(5)
C9–C10	1.531(5)	C31–C34	1.504(5)
C9–H9A	0.9900	C32–C33	1.386(5)
C9–H9B	0.9900	C32–H32	0.9500
C10–O3	1.227(4)	C33–H33	0.9500
C10–O4	1.288(4)	C34–H34A	0.9800
C11–C12	1.388(4)	C34–H34B	0.9800
C11–C16	1.393(4)	C34–H34C	0.9800
C11–S1	1.760(3)	C35–C36	1.510(9)
C12–C13	1.391(5)	C35–H35A	0.9800
C12–H12	0.9500	C35–H35B	0.9800
C13–C14	1.394(5)	C35–H35C	0.9800
C13–H13	0.9500	C36–N7	1.205(8)
C14–C15	1.383(5)	Cu1–O4	1.920(2)
C14–C17	1.503(5)	Cu1–O2	1.934(2)
C15–C16	1.379(5)	Cu1–N2	2.004(3)
C15–H15	0.9500	Cu1–N1	2.009(3)
C16–H16	0.9500	Cu1–N3	2.429(3)
C17–H17A	0.9800	Cu2–O10	1.924(2)
C17–H17B	0.9800	Cu2–O8	1.930(2)

C17–H17C	0.9800	Cu2–N5	1.998(3)
C18–N4	1.506(4)	Cu2–N4	2.017(3)
C18–C19	1.526(5)	Cu2–N6	2.428(3)
C18–H18A	0.9900	N3–S1	1.665(3)
C18–H18B	0.9900	N6–S2	1.674(3)
C19–N5	1.503(4)	O5–S1	1.436(2)
C19–H19A	0.9900	O6–S1	1.433(2)
C19–H19B	0.9900	O11–S2	1.432(2)
C20–N5	1.491(4)	O12–S2	1.433(2)
C20–C21	1.524(4)	O13–C37	1.384(5)
C20–H20A	0.9900	O13–H13A	0.8400
C20–H20B	0.9900	C37–H37A	0.9800
C21–N6	1.492(4)	C37–H37B	0.9800
C21–H21A	0.9900	C37–H37C	0.9800

Bond Angles (°)

N1–C1–C2	110.1(3)	O7–C25–C24	119.2(3)
N1–C1–H1A	109.6	O8–C25–C24	115.9(3)
C2–C1–H1A	109.6	N4–C26–C27	111.8(3)
N1–C1–H1B	109.6	N4–C26–H26A	109.3
C2–C1–H1B	109.6	C27–C26–H26A	109.3
H1A–C1–H1B	108.2	N4–C26–H26B	109.3
N2–C2–C1	110.5(3)	C27–C26–H26B	109.3
N2–C2–H2A	109.5	H26A–C26–H26B	107.9
C1–C2–H2A	109.5	O9–C27–O10	124.5(3)
N2–C2–H2B	109.5	O9–C27–C26	118.9(3)
C1–C2–H2B	109.5	O10–C27–C26	116.5(3)
H2A–C2–H2B	108.1	C29–C28–C33	120.4(3)
N2–C3–C4	113.7(3)	C29–C28–S2	120.6(3)
N2–C3–H3A	108.8	C33–C28–S2	118.9(2)
C4–C3–H3A	108.8	C30–C29–C28	119.1(3)
N2–C3–H3B	108.8	C30–C29–H29	120.5
C4–C3–H3B	108.8	C28–C29–H29	120.5
H3A–C3–H3B	107.7	C29–C30–C31	121.6(3)
N3–C4–C3	111.3(3)	C29–C30–H30	119.2
N3–C4–H4A	109.4	C31–C30–H30	119.2
C3–C4–H4A	109.4	C30–C31–C32	118.6(3)
N3–C4–H4B	109.4	C30–C31–C34	121.1(3)
C3–C4–H4B	109.4	C32–C31–C34	120.3(3)
H4A–C4–H4B	108.0	C33–C32–C31	120.9(3)
N3–C5–C6	111.7(3)	C33–C32–H32	119.5
N3–C5–H5A	109.3	C31–C32–H32	119.5
C6–C5–H5A	109.3	C32–C33–C28	119.3(3)
N3–C5–H5B	109.3	C32–C33–H33	120.3
C6–C5–H5B	109.3	C28–C33–H33	120.3
H5A–C5–H5B	107.9	C31–C34–H34A	109.5
N1–C6–C5	112.2(3)	C31–C34–H34B	109.5
N1–C6–H6A	109.2	H34A–C34–H34B	109.5
C5–C6–H6A	109.2	C31–C34–H34C	109.5

N1-C6-H6B	109.2	H34A-C34-H34C	109.5
C5-C6-H6B	109.2	H34B-C34-H34C	109.5
H6A-C6-H6B	107.9	C36-C35-H35A	109.5
N2-C7-C8	110.6(3)	C36-C35-H35B	109.5
N2-C7-H7A	109.5	H35A-C35-H35B	109.5
C8-C7-H7A	109.5	C36-C35-H35C	109.5
N2-C7-H7B	109.5	H35A-C35-H35C	109.5
C8-C7-H7B	109.5	H35B-C35-H35C	109.5
H7A-C7-H7B	108.1	N7-C36-C35	177.9(6)
O1-C8-O2	124.5(3)	O4-Cu1-O2	99.41(9)
O1-C8-C7	119.3(3)	O4-Cu1-N2	170.89(10)
O2-C8-C7	116.3(3)	O2-Cu1-N2	85.24(10)
N1-C9-C10	112.5(3)	O4-Cu1-N1	87.10(10)
N1-C9-H9A	109.1	O2-Cu1-N1	166.60(10)
C10-C9-H9A	109.1	N2-Cu1-N1	86.81(11)
N1-C9-H9B	109.1	O4-Cu1-N3	104.64(9)
C10-C9-H9B	109.1	O2-Cu1-N3	106.85(9)
H9A-C9-H9B	107.8	N2-Cu1-N3	81.25(10)
O3-C10-O4	124.6(3)	N1-Cu1-N3	82.51(10)
O3-C10-C9	117.9(3)	O10-Cu2-O8	98.43(9)
O4-C10-C9	117.4(3)	O10-Cu2-N5	171.61(10)
C12-C11-C16	120.3(3)	O8-Cu2-N5	85.79(10)
C12-C11-S1	119.6(2)	O10-Cu2-N4	86.35(10)
C16-C11-S1	120.0(2)	O8-Cu2-N4	159.16(11)
C11-C12-C13	119.2(3)	N5-Cu2-N4	87.20(11)
C11-C12-H12	120.4	O10-Cu2-N6	102.87(10)
C13-C12-H12	120.4	O8-Cu2-N6	116.00(10)
C12-C13-C14	121.1(3)	N5-Cu2-N6	81.54(10)
C12-C13-H13	119.4	N4-Cu2-N6	82.22(11)
C14-C13-H13	119.4	C9-N1-C6	111.5(3)
C15-C14-C13	118.2(3)	C9-N1-C1	114.1(3)
C15-C14-C17	121.3(3)	C6-N1-C1	111.7(2)
C13-C14-C17	120.5(3)	C9-N1-Cu1	105.22(19)
C16-C15-C14	121.8(3)	C6-N1-Cu1	112.37(19)
C16-C15-H15	119.1	C1-N1-Cu1	101.39(19)
C14-C15-H15	119.1	C3-N2-C7	109.3(3)
C15-C16-C11	119.3(3)	C3-N2-C2	113.0(3)
C15-C16-H16	120.4	C7-N2-C2	114.2(3)
C11-C16-H16	120.4	C3-N2-Cu1	109.25(19)
C14-C17-H17A	109.5	C7-N2-Cu1	101.66(18)
C14-C17-H17B	109.5	C2-N2-Cu1	108.7(2)
H17A-C17-H17B	109.5	C5-N3-C4	115.3(2)
C14-C17-H17C	109.5	C5-N3-S1	113.3(2)
H17A-C17-H17C	109.5	C4-N3-S1	115.9(2)
H17B-C17-H17C	109.5	C5-N3-Cu1	95.06(17)
N4-C18-C19	109.8(3)	C4-N3-Cu1	103.04(17)
N4-C18-H18A	109.7	S1-N3-Cu1	111.54(13)
C19-C18-H18A	109.7	C26-N4-C23	112.2(3)
N4-C18-H18B	109.7	C26-N4-C18	113.5(3)

C19-C18-H18B	109.7	C23-N4-C18	111.9(3)
H18A-C18-H18B	108.2	C26-N4-Cu2	104.3(2)
N5-C19-C18	110.6(3)	C23-N4-Cu2	113.0(2)
N5-C19-H19A	109.5	C18-N4-Cu2	101.26(19)
C18-C19-H19A	109.5	C24-N5-C20	109.1(2)
N5-C19-H19B	109.5	C24-N5-C19	113.6(2)
C18-C19-H19B	109.5	C20-N5-C19	112.4(2)
H19A-C19-H19B	108.1	C24-N5-Cu2	104.21(19)
N5-C20-C21	112.7(3)	C20-N5-Cu2	108.59(19)
N5-C20-H20A	109.1	C19-N5-Cu2	108.6(2)
C21-C20-H20A	109.1	C22-N6-C21	115.3(3)
N5-C20-H20B	109.1	C22-N6-S2	115.2(2)
C21-C20-H20B	109.1	C21-N6-S2	113.9(2)
H20A-C20-H20B	107.8	C22-N6-Cu2	96.26(19)
N6-C21-C20	111.3(2)	C21-N6-Cu2	102.43(18)
N6-C21-H21A	109.4	S2-N6-Cu2	111.42(13)
C20-C21-H21A	109.4	C8-O2-Cu1	111.5(2)
N6-C21-H21B	109.4	C10-O4-Cu1	113.4(2)
C20-C21-H21B	109.4	C25-O8-Cu2	113.8(2)
H21A-C21-H21B	108.0	C27-O10-Cu2	114.3(2)
N6-C22-C23	112.2(3)	C37-O13-H13A	109.5
N6-C22-H22A	109.2	O6-S1-O5	119.57(14)
C23-C22-H22A	109.2	O6-S1-N3	106.83(13)
N6-C22-H22B	109.2	O5-S1-N3	106.44(13)
C23-C22-H22B	109.2	O6-S1-C11	108.21(14)
H22A-C22-H22B	107.9	O5-S1-C11	109.28(14)
N4-C23-C22	112.9(3)	N3-S1-C11	105.65(14)
N4-C23-H23A	109.0	O11-S2-O12	119.96(14)
C22-C23-H23A	109.0	O11-S2-N6	105.51(14)
N4-C23-H23B	109.0	O12-S2-N6	106.36(14)
C22-C23-H23B	109.0	O11-S2-C28	109.16(15)
H23A-C23-H23B	107.8	O12-S2-C28	107.83(14)
N5-C24-C25	110.4(3)	N6-S2-C28	107.38(15)
N5-C24-H24A	109.6	O13-C37-H37A	109.5
C25-C24-H24A	109.6	O13-C37-H37B	109.5
N5-C24-H24B	109.6	H37A-C37-H37B	109.5
C25-C24-H24B	109.6	O13-C37-H37C	109.5
H24A-C24-H24B	108.1	H37A-C37-H37C	109.5
O7-C25-O8	124.9(3)	H37B-C37-H37C	109.5

Identification code	CuTACNCF ₃	
Empirical formula	C ₂₂ H ₂₉ Cl ₂ CuF ₆ N ₅ O ₉	
Formula weight	755.94	
Temperature	120(2) K	
Wavelength	0.71073 Å	
Crystal system	Triclinic	
Space group	<i>P</i> -1	
Unit cell dimensions	<i>a</i> = 10.7028(2) Å	<i>α</i> = 83.081(2)°
	<i>b</i> = 10.9956(4) Å	<i>β</i> = 82.641(2)°
	<i>c</i> = 12.5512(4) Å	<i>γ</i> = 81.629(2)°
Volume	1441.47(7) Å ³	
<i>Z</i>	2	
Density (calculated)	1.742 Mg / m ³	
Absorption coefficient	1.042 mm ⁻¹	
<i>F</i> (000)	770	
Crystal	Fragment; blue	
Crystal size	0.20 × 0.14 × 0.10 mm ³	
<i>θ</i> range for data collection	3.22 – 27.48°	
Index ranges	-13 ≤ <i>h</i> ≤ 13, -14 ≤ <i>k</i> ≤ 14, -16 ≤ <i>l</i> ≤ 16	
Reflections collected	30364	
Independent reflections	6592 [<i>R</i> _{int} = 0.0689]	
Completeness to <i>θ</i> = 27.48°	99.7 %	
Absorption correction	Semi-empirical from equivalents	
Max. and min. transmission	0.9030 and 0.8188	
Refinement method	Full-matrix least-squares on <i>F</i> ²	
Data / restraints / parameters	6592 / 3 / 436	
Goodness-of-fit on <i>F</i> ²	1.045	
Final <i>R</i> indices [<i>F</i> ² > 2σ(<i>F</i> ²)]	<i>R</i> 1 = 0.0531, <i>wR</i> 2 = 0.1083	
<i>R</i> indices (all data)	<i>R</i> 1 = 0.0788, <i>wR</i> 2 = 0.1197	
Largest diff. peak and hole	0.854 and -0.548 e Å ⁻³	

Bond Lengths (Å)

Cu1–N22	1.995(3)	C5–H5A	0.9900
Cu1–N12	2.008(3)	C5–H5B	0.9900
Cu1–N11	2.039(3)	C6–H6A	0.9900
Cu1–N21	2.060(3)	C6–H6B	0.9900
Cu1–N31	2.188(3)	C11–C12	1.386(4)
F11–C17	1.337(4)	C11–C16	1.386(4)
F12–C17	1.346(4)	C12–C13	1.382(4)
F13–C17	1.335(4)	C13–C14	1.391(5)
F21A–C27	1.281(6)	C13–H13	0.9500
F22A–C27	1.254(6)	C14–C15	1.381(5)
F23A–C27	1.403(7)	C14–C17	1.497(5)
F21B–C27	1.488(12)	C15–C16	1.382(4)
F22B–C27	1.251(12)	C15–H15	0.9500
F23B–C27	1.220(19)	C16–H16	0.9500
N11–C11	1.461(4)	C21–C22	1.383(4)
N11–C1	1.497(4)	C21–C26	1.388(5)

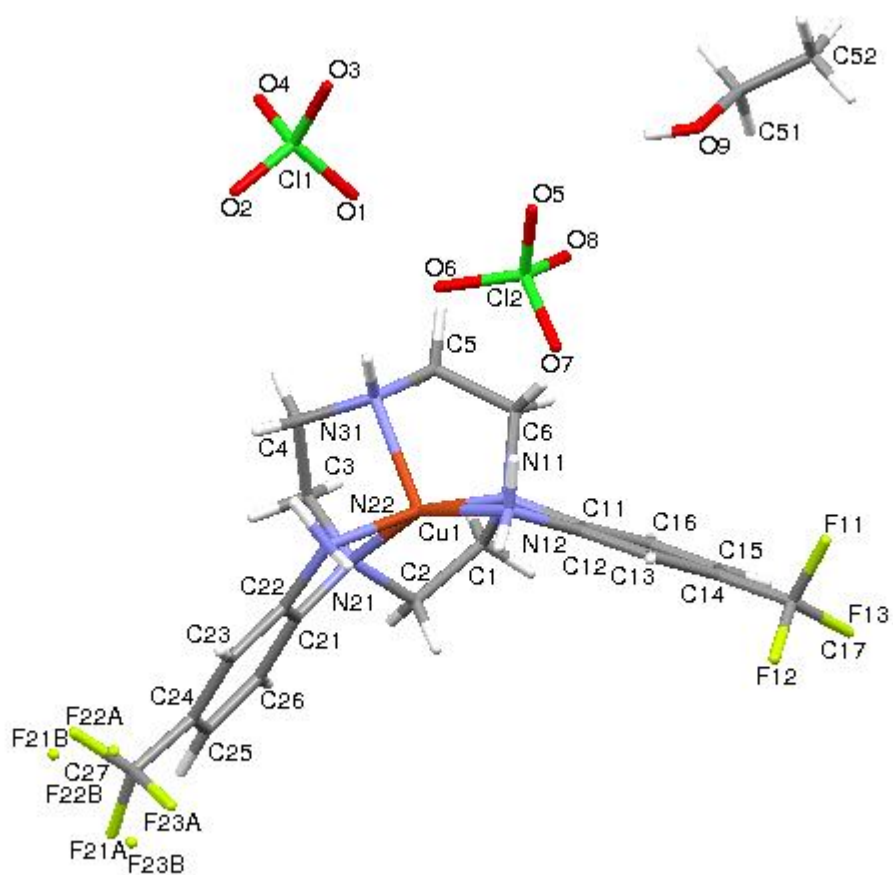
N11–C6	1.506(4)	C22–C23	1.381(4)
N12–C12	1.455(4)	C23–C24	1.385(5)
N12–H12A	0.9200	C23–H23	0.9500
N12–H12B	0.9200	C24–C25	1.383(5)
N21–C21	1.455(4)	C24–C27	1.493(5)
N21–C2	1.499(4)	C25–C26	1.388(5)
N21–C3	1.499(4)	C25–H25	0.9500
N22–C22	1.450(4)	C26–H26	0.9500
N22–H22A	0.9200	C11–O1	1.396(3)
N22–H22B	0.9200	C11–O2	1.410(3)
N31–C4	1.476(4)	C11–O4	1.423(3)
N31–C5	1.485(4)	C11–O3	1.442(3)
N31–H31	0.9300	C12–O5	1.426(3)
C1–C2	1.521(5)	C12–O7	1.430(3)
C1–H1A	0.9900	C12–O8	1.430(3)
C1–H1B	0.9900	C12–O6	1.448(3)
C2–H2A	0.9900	O9–C51	1.412(5)
C2–H2B	0.9900	O9–H9	0.8400
C3–C4	1.514(5)	C52–C51	1.442(7)
C3–H3A	0.9900	C52–H52A	0.9800
C3–H3B	0.9900	C52–H52B	0.9800
C4–H4A	0.9900	C52–H52C	0.9800
C4–H4B	0.9900	C51–H51A	0.9900
C5–C6	1.520(4)	C51–H51B	0.9900

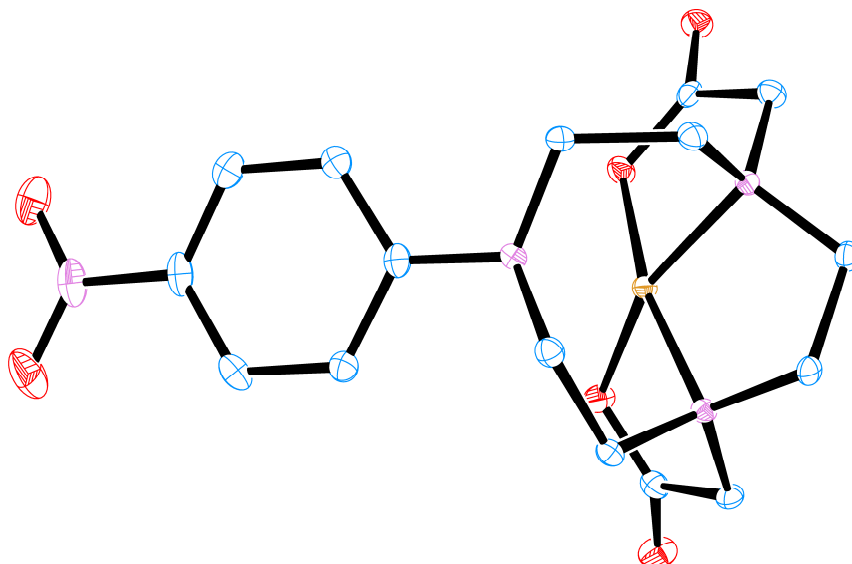
Bond Angles (°)

N22–Cu1–N12	100.23(11)	C12–C13–C14	119.6(3)
N22–Cu1–N11	167.66(10)	C12–C13–H13	120.2
N12–Cu1–N11	84.61(10)	C14–C13–H13	120.2
N22–Cu1–N21	84.48(10)	C15–C14–C13	120.4(3)
N12–Cu1–N21	153.52(11)	C15–C14–C17	121.4(3)
N11–Cu1–N21	86.24(10)	C13–C14–C17	118.2(3)
N22–Cu1–N31	102.87(10)	C14–C15–C16	120.0(3)
N12–Cu1–N31	119.91(11)	C14–C15–H15	120.0
N11–Cu1–N31	84.14(10)	C16–C15–H15	120.0
N21–Cu1–N31	83.67(10)	C15–C16–C11	119.6(3)
C11–N11–C1	114.9(2)	C15–C16–H16	120.2
C11–N11–C6	108.1(2)	C11–C16–H16	120.2
C1–N11–C6	112.3(2)	F13–C17–F11	107.1(3)
C11–N11–Cu1	107.14(18)	F13–C17–F12	106.6(3)
C1–N11–Cu1	108.29(19)	F11–C17–F12	106.5(3)
C6–N11–Cu1	105.46(19)	F13–C17–C14	112.7(3)
C12–N12–Cu1	107.57(18)	F11–C17–C14	112.0(3)
C12–N12–H12A	110.2	F12–C17–C14	111.5(3)
Cu1–N12–H12A	110.2	C22–C21–C26	120.9(3)
C12–N12–H12B	110.2	C22–C21–N21	116.8(3)
Cu1–N12–H12B	110.2	C26–C21–N21	122.3(3)
H12A–N12–H12B	108.5	C23–C22–C21	119.7(3)

C21-N21-C2	113.2(2)	C23-C22-N22	122.1(3)
C21-N21-C3	111.5(2)	C21-C22-N22	118.3(3)
C2-N21-C3	113.4(2)	C22-C23-C24	119.7(3)
C21-N21-Cu1	106.43(18)	C22-C23-H23	120.2
C2-N21-Cu1	101.55(18)	C24-C23-H23	120.2
C3-N21-Cu1	110.13(19)	C25-C24-C23	120.8(3)
C22-N22-Cu1	108.22(19)	C25-C24-C27	120.2(3)
C22-N22-H22A	110.1	C23-C24-C27	119.0(3)
Cu1-N22-H22A	110.1	C24-C25-C26	119.6(3)
C22-N22-H22B	110.1	C24-C25-H25	120.2
Cu1-N22-H22B	110.1	C26-C25-H25	120.2
H22A-N22-H22B	108.4	C25-C26-C21	119.3(3)
C4-N31-C5	113.1(3)	C25-C26-H26	120.4
C4-N31-Cu1	102.35(19)	C21-C26-H26	120.4
C5-N31-Cu1	107.79(18)	F23B-C27-F22B	116.2(14)
C4-N31-H31	111.1	F23B-C27-F22A	123.9(11)
C5-N31-H31	111.1	F22B-C27-F22A	46.4(10)
Cu1-N31-H31	111.1	F23B-C27-F21A	25.2(18)
N11-C1-C2	111.3(2)	F22B-C27-F21A	128.5(8)
N11-C1-H1A	109.4	F22A-C27-F21A	113.4(7)
C2-C1-H1A	109.4	F23B-C27-F23A	76.5(16)
N11-C1-H1B	109.4	F22B-C27-F23A	59.0(12)
C2-C1-H1B	109.4	F22A-C27-F23A	104.3(6)
H1A-C1-H1B	108.0	F21A-C27-F23A	101.3(5)
N21-C2-C1	109.9(3)	F23B-C27-F21B	94.6(15)
N21-C2-H2A	109.7	F22B-C27-F21B	96.6(12)
C1-C2-H2A	109.7	F22A-C27-F21B	51.9(7)
N21-C2-H2B	109.7	F21A-C27-F21B	72.0(10)
C1-C2-H2B	109.7	F23A-C27-F21B	143.9(6)
H2A-C2-H2B	108.2	F23B-C27-C24	119.0(11)
N21-C3-C4	111.8(3)	F22B-C27-C24	117.3(7)
N21-C3-H3A	109.3	F22A-C27-C24	113.6(4)
C4-C3-H3A	109.3	F21A-C27-C24	114.1(5)
N21-C3-H3B	109.3	F23A-C27-C24	108.7(4)
C4-C3-H3B	109.3	F21B-C27-C24	106.2(6)
H3A-C3-H3B	107.9	O1-C11-O2	108.7(3)
N31-C4-C3	110.7(3)	O1-C11-O4	109.1(2)
N31-C4-H4A	109.5	O2-C11-O4	111.9(3)
C3-C4-H4A	109.5	O1-C11-O3	111.2(2)
N31-C4-H4B	109.5	O2-C11-O3	108.76(19)
C3-C4-H4B	109.5	O4-C11-O3	107.19(17)
H4A-C4-H4B	108.1	O5-C12-O7	109.85(18)
N31-C5-C6	111.1(2)	O5-C12-O8	110.26(19)
N31-C5-H5A	109.4	O7-C12-O8	110.13(19)
C6-C5-H5A	109.4	O5-C12-O6	108.46(17)
N31-C5-H5B	109.4	O7-C12-O6	107.87(19)
C6-C5-H5B	109.4	O8-C12-O6	110.2(2)
H5A-C5-H5B	108.0	C51-O9-H9	109.5
N11-C6-C5	112.4(3)	C51-C52-H52A	109.5

N11–C6–H6A	109.1	C51–C52–H52B	109.5
C5–C6–H6A	109.1	H52A–C52–H52B	109.5
N11–C6–H6B	109.1	C51–C52–H52C	109.5
C5–C6–H6B	109.1	H52A–C52–H52C	109.5
H6A–C6–H6B	107.9	H52B–C52–H52C	109.5
C12–C11–C16	120.4(3)	O9–C51–C52	110.6(4)
C12–C11–N11	116.3(3)	O9–C51–H51A	109.5
C16–C11–N11	123.2(3)	C52–C51–H51A	109.5
C13–C12–C11	119.9(3)	O9–C51–H51B	109.5
C13–C12–N12	121.8(3)	C52–C51–H51B	109.5
C11–C12–N12	118.3(3)	H51A–C51–H51B	108.1





Ortep plot of CuNPhTACNA2 – Ellipsoids at 50% probability

Identification code	CuNPhTACNA ₂	
Empirical formula	C ₁₆ H ₂₀ CuN ₄ O ₆	
Formula weight	427.90	
Temperature	100(2) K	
Wavelength	0.71075 Å	
Crystal system	Monoclinic	
Space group	P21/c	
Unit cell dimensions	$a = 16.054(4)$ Å	$\alpha = 90^\circ$
	$b = 13.373(3)$ Å	$\beta = 99.402(3)^\circ$
	$c = 7.8011(17)$ Å	$\gamma = 90^\circ$
Volume	$1652.3(7)$ Å ³	
Z	4	
Density (calculated)	1.720 Mg / m ³	
Absorption coefficient	1.368 mm ⁻¹	
$F(000)$	884	
Crystal	Lath; blue	
Crystal size	$0.18 \times 0.03 \times 0.01$ mm ³	
θ range for data collection	2.99 – 27.49°	
Index ranges	$-20 \leq h \leq 20, -15 \leq k \leq 17, -10 \leq l \leq 10$	
Reflections collected	28242	
Independent reflections	3784 [$R_{int} = 0.0401$]	
Completeness to $\theta = 27.49^\circ$	99.9 %	
Absorption correction	Semi-empirical from equivalents	
Max. and min. transmission	0.9865 and 0.7909	
Refinement method	Full-matrix least-squares on F^2	
Data / restraints / parameters	3784 / 0 / 244	
Goodness-of-fit on F^2	1.145	
Final R indices [$F^2 > 2\sigma(F^2)$]	$R1 = 0.0350, wR2 = 0.0709$	
R indices (all data)	$R1 = 0.0386, wR2 = 0.0721$	
Largest diff. peak and hole	0.414 and -0.452 e Å ⁻³	

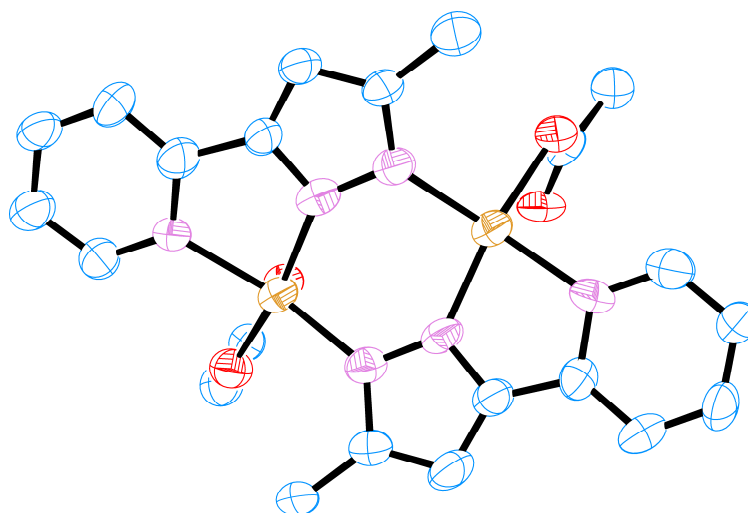
Bond Lengths (Å)

C1–N1	1.489(3)	C8–O1	1.289(3)
C1–C2	1.514(3)	C9–N3	1.485(2)
C1–H1A	0.9900	C9–C10	1.532(3)
C1–H1B	0.9900	C9–H9A	0.9900
C2–N2	1.498(2)	C9–H9B	0.9900
C2–H2A	0.9900	C10–O4	1.228(3)
C2–H2B	0.9900	C10–O3	1.291(3)
C3–N2	1.488(3)	C11–C16	1.407(3)
C3–C4	1.524(3)	C11–C12	1.408(3)
C3–H3A	0.9900	C11–N1	1.417(3)
C3–H3B	0.9900	C12–C13	1.387(3)
C4–N3	1.498(3)	C12–H12	0.9500
C4–H4A	0.9900	C13–C14	1.385(3)
C4–H4B	0.9900	C13–H13	0.9500
C5–N3	1.488(2)	C14–C15	1.388(3)
C5–C6	1.528(3)	C14–N4	1.460(3)
C5–H5A	0.9900	C15–C16	1.380(3)
C5–H5B	0.9900	C15–H15	0.9500
C6–N1	1.489(3)	C16–H16	0.9500
C6–H6A	0.9900	N1–Cu1	2.4464(17)
C6–H6B	0.9900	N2–Cu1	2.0195(17)
C7–N2	1.485(3)	N3–Cu1	1.9945(18)
C7–C8	1.525(3)	N4–O6	1.230(3)
C7–H7A	0.9900	N4–O5	1.232(3)
C7–H7B	0.9900	O1–Cu1	1.9245(15)
C8–O2	1.232(3)	O3–Cu1	1.9323(16)

Bond Angles (°)

N1–C1–C2	113.51(17)	O3–C10–C9	116.50(18)
N1–C1–H1A	108.9	C16–C11–C12	118.2(2)
C2–C1–H1A	108.9	C16–C11–N1	119.50(19)
N1–C1–H1B	108.9	C12–C11–N1	122.28(19)
C2–C1–H1B	108.9	C13–C12–C11	120.8(2)
H1A–C1–H1B	107.7	C13–C12–H12	119.6
N2–C2–C1	112.10(17)	C11–C12–H12	119.6
N2–C2–H2A	109.2	C14–C13–C12	119.4(2)
C1–C2–H2A	109.2	C14–C13–H13	120.3
N2–C2–H2B	109.2	C12–C13–H13	120.3
C1–C2–H2B	109.2	C13–C14–C15	121.2(2)
H2A–C2–H2B	107.9	C13–C14–N4	120.1(2)
N2–C3–C4	109.97(16)	C15–C14–N4	118.6(2)
N2–C3–H3A	109.7	C16–C15–C14	119.4(2)
C4–C3–H3A	109.7	C16–C15–H15	120.3
N2–C3–H3B	109.7	C14–C15–H15	120.3
C4–C3–H3B	109.7	C15–C16–C11	121.0(2)
H3A–C3–H3B	108.2	C15–C16–H16	119.5

N3-C4-C3	110.25(16)	C11-C16-H16	119.5
N3-C4-H4A	109.6	C11-N1-C6	115.06(16)
C3-C4-H4A	109.6	C11-N1-C1	115.65(17)
N3-C4-H4B	109.6	C6-N1-C1	115.35(16)
C3-C4-H4B	109.6	C11-N1-Cu1	114.69(12)
H4A-C4-H4B	108.1	C6-N1-Cu1	100.44(11)
N3-C5-C6	112.65(16)	C1-N1-Cu1	92.36(11)
N3-C5-H5A	109.1	C7-N2-C3	113.42(16)
C6-C5-H5A	109.1	C7-N2-C2	112.43(16)
N3-C5-H5B	109.1	C3-N2-C2	111.81(16)
C6-C5-H5B	109.1	C7-N2-Cu1	105.66(12)
H5A-C5-H5B	107.8	C3-N2-Cu1	102.12(12)
N1-C6-C5	113.22(16)	C2-N2-Cu1	110.72(12)
N1-C6-H6A	108.9	C9-N3-C5	110.56(16)
C5-C6-H6A	108.9	C9-N3-C4	112.91(16)
N1-C6-H6B	108.9	C5-N3-C4	112.23(15)
C5-C6-H6B	108.9	C9-N3-Cu1	102.87(12)
H6A-C6-H6B	107.7	C5-N3-Cu1	108.44(13)
N2-C7-C8	112.40(17)	C4-N3-Cu1	109.33(12)
N2-C7-H7A	109.1	O6-N4-O5	123.5(2)
C8-C7-H7A	109.1	O6-N4-C14	117.8(2)
N2-C7-H7B	109.1	O5-N4-C14	118.7(2)
C8-C7-H7B	109.1	C8-O1-Cu1	113.93(13)
H7A-C7-H7B	107.9	C10-O3-Cu1	111.56(13)
O2-C8-O1	125.0(2)	O1-Cu1-O3	97.69(6)
O2-C8-C7	117.54(19)	O1-Cu1-N3	168.46(7)
O1-C8-C7	117.43(18)	O3-Cu1-N3	86.19(7)
N3-C9-C10	111.71(17)	O1-Cu1-N2	86.37(7)
N3-C9-H9A	109.3	O3-Cu1-N2	160.42(7)
C10-C9-H9A	109.3	N3-Cu1-N2	86.46(7)
N3-C9-H9B	109.3	O1-Cu1-N1	105.66(6)
C10-C9-H9B	109.3	O3-Cu1-N1	113.08(6)
H9A-C9-H9B	107.9	N3-Cu1-N1	82.53(6)
O4-C10-O3	125.0(2)	N2-Cu1-N1	83.88(6)
O4-C10-C9	118.3(2)		



Ortep plot of CuMePyPz – Ellipsoids at 50% probability

Identification code	CuMePyPz	
Empirical formula	C ₄₄ H ₄₄ Cu ₄ N ₁₂ O ₈	
Formula weight	1123.07	
Temperature	100(2) K	
Wavelength	0.71075 Å	
Crystal system	Monoclinic	
Space group	P2 ₁ /n	
Unit cell dimensions	a = 12.12(3) Å	α = 90°.
	b = 13.34(3) Å	β = 107.72(3)°.
	c = 14.74(3) Å	γ = 90°.
Volume	2270(9) Å ³	
Z	2	
Density (calculated)	1.643 Mg/m ³	
Absorption coefficient	1.916 mm ⁻¹	
F(000)	1144	
Crystal size	0.05 x 0.05 x 0.02 mm ³	
Theta range for data collection	2.90 to 25.00°.	
Index ranges	-14 ≤ h ≤ 12, -15 ≤ k ≤ 15, -16 ≤ l ≤ 17	
Reflections collected	20500	
Independent reflections	3943 [R(int) = 0.1135]	
Completeness to theta = 25.00°	98.5 %	
Absorption correction	Semi-empirical from equivalents	
Max. and min. transmission	0.9627 and 0.9103	

Refinement method	Full-matrix least-squares on F^2
Data / restraints / parameters	3943 / 7 / 311
Goodness-of-fit on F^2	1.221
Final R indices [$I > 2\sigma(I)$]	R1 = 0.1454, wR2 = 0.3448
R indices (all data)	R1 = 0.1753, wR2 = 0.3786
Largest diff. peak and hole	5.089 and -1.182 e.Å ⁻³

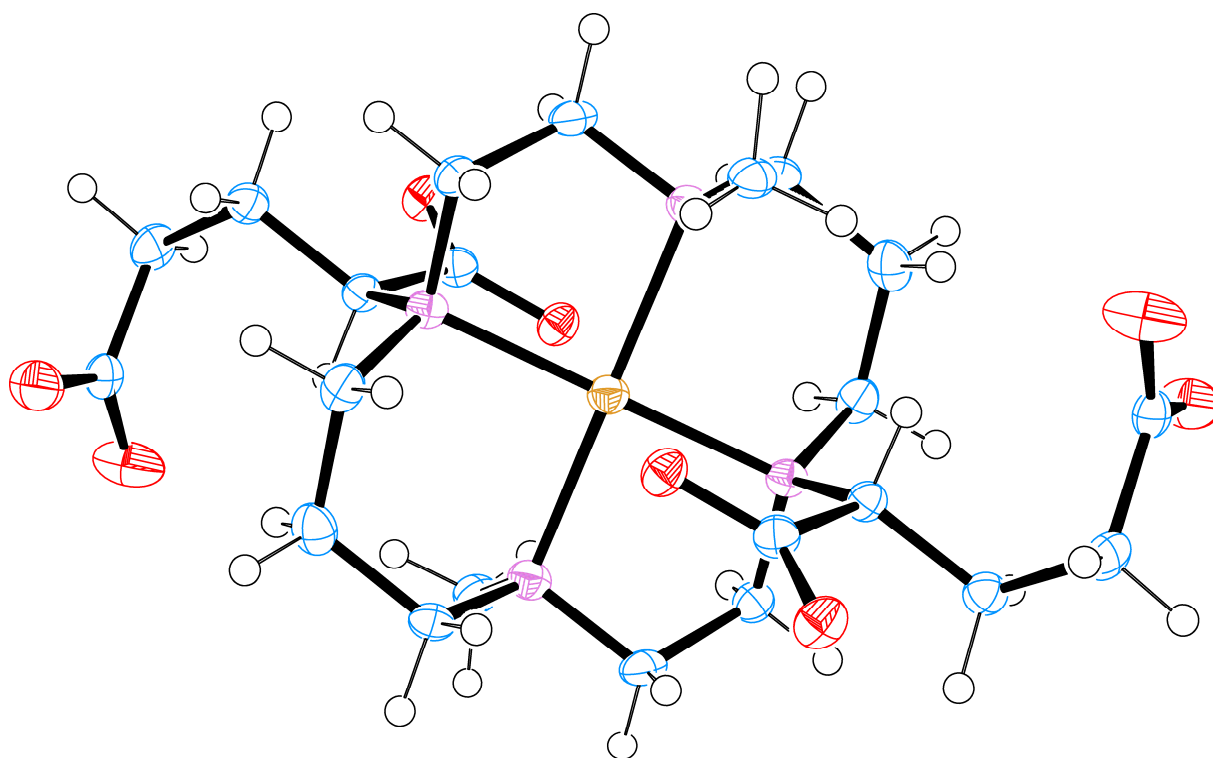
Bond lengths [Å]

C(18)-C(17)	1.514(14)	C(10)-N(4)	1.360(15)
C(18)-H(18A)	0.9800	C(10)-C(11)	1.403(15)
C(18)-H(18B)	0.9800	C(10)-H(10)	0.9500
C(18)-H(18C)	0.9800	C(11)-C(12)	1.372(16)
C(19)-O(1)	1.234(13)	C(11)-H(11)	0.9500
C(19)-O(2)	1.260(12)	C(12)-C(13)	1.349(15)
C(19)-C(20)	1.486(15)	C(12)-H(12)	0.9500
C(20)-H(20A)	0.9800	C(13)-C(14)	1.383(14)
C(20)-H(20B)	0.9800	C(13)-H(13)	0.9500
C(20)-H(20C)	0.9800	C(14)-N(4)	1.377(14)
O(1)-Cu(1)	1.973(8)	C(14)-C(15)	1.448(14)
C(1)-N(1)	1.355(13)	C(15)-N(5)	1.347(12)
C(1)-C(2)	1.386(15)	C(15)-C(16)	1.382(15)
C(1)-H(1)	0.9500	C(16)-C(17)	1.409(15)
C(2)-C(3)	1.410(16)	C(16)-H(16)	0.9500
C(2)-H(2)	0.9500	C(17)-N(6)	1.375(13)
C(3)-C(4)	1.399(16)	C(21)-O(4)	1.255(12)
C(3)-H(3)	0.9500	C(21)-O(3)	1.289(13)
C(4)-C(5)	1.378(15)	C(21)-C(22)	1.528(15)
C(4)-H(4)	0.9500	C(22)-H(22A)	0.9800
C(5)-N(1)	1.367(14)	C(22)-H(22B)	0.9800
C(5)-C(6)	1.493(15)	C(22)-H(22C)	0.9800
C(6)-N(2)	1.364(13)	Cu(1)-N(2)	1.947(9)
C(6)-C(7)	1.389(15)	Cu(1)-N(6)	1.960(9)
C(7)-C(8)	1.392(13)	Cu(1)-N(1)	2.057(9)
C(7)-H(7)	0.9500	Cu(2)-N(3)	1.961(9)
C(8)-N(3)	1.373(12)	Cu(2)-O(3)	1.965(7)
C(8)-C(9)	1.535(14)	Cu(2)-N(5)	1.965(10)
C(9)-H(9A)	0.9800	Cu(2)-N(4)	2.032(10)
C(9)-H(9B)	0.9800	N(2)-N(3)	1.393(12)
C(9)-H(9C)	0.9800	N(5)-N(6)	1.377(12)

Bond Angles [°]

C(17)-C(18)-H(18A)	109.5	C(8)-C(7)-H(7)	128.0
C(17)-C(18)-H(18B)	109.5	N(3)-C(8)-C(7)	110.6(9)
H(18A)-C(18)-H(18B)	109.5	N(3)-C(8)-C(9)	121.8(8)
C(17)-C(18)-H(18C)	109.5	C(7)-C(8)-C(9)	127.6(9)
H(18A)-C(18)-H(18C)	109.5	C(8)-C(9)-H(9A)	109.5
H(18B)-C(18)-H(18C)	109.5	C(8)-C(9)-H(9B)	109.5
O(1)-C(19)-O(2)	122.5(10)	H(9A)-C(9)-H(9B)	109.5
O(1)-C(19)-C(20)	118.0(10)	C(8)-C(9)-H(9C)	109.5
O(2)-C(19)-C(20)	119.4(11)	H(9A)-C(9)-H(9C)	109.5
C(19)-C(20)-H(20A)	109.5	H(9B)-C(9)-H(9C)	109.5
C(19)-C(20)-H(20B)	109.5	N(4)-C(10)-C(11)	122.1(10)
H(20A)-C(20)-H(20B)	109.5	N(4)-C(10)-H(10)	118.9
C(19)-C(20)-H(20C)	109.5	C(11)-C(10)-H(10)	118.9
H(20A)-C(20)-H(20C)	109.5	C(12)-C(11)-C(10)	118.1(10)
H(20B)-C(20)-H(20C)	109.5	C(12)-C(11)-H(11)	121.0
C(19)-O(1)-Cu(1)	106.0(7)	C(10)-C(11)-H(11)	121.0
N(1)-C(1)-C(2)	122.5(11)	C(13)-C(12)-C(11)	120.6(10)
N(1)-C(1)-H(1)	118.7	C(13)-C(12)-H(12)	119.7
C(2)-C(1)-H(1)	118.7	C(11)-C(12)-H(12)	119.7
C(1)-C(2)-C(3)	118.1(10)	C(12)-C(13)-C(14)	120.5(11)
C(1)-C(2)-H(2)	121.0	C(12)-C(13)-H(13)	119.7
C(3)-C(2)-H(2)	121.0	C(14)-C(13)-H(13)	119.7
C(4)-C(3)-C(2)	120.2(10)	N(4)-C(14)-C(13)	120.7(9)
C(4)-C(3)-H(3)	119.9	N(4)-C(14)-C(15)	111.7(9)
C(2)-C(3)-H(3)	119.9	C(13)-C(14)-C(15)	127.5(10)
C(5)-C(4)-C(3)	117.4(11)	N(5)-C(15)-C(16)	109.3(9)
C(5)-C(4)-H(4)	121.3	N(5)-C(15)-C(14)	118.2(9)
C(3)-C(4)-H(4)	121.3	C(16)-C(15)-C(14)	132.6(9)
N(1)-C(5)-C(4)	123.5(10)	C(15)-C(16)-C(17)	105.5(9)
N(1)-C(5)-C(6)	113.4(9)	C(15)-C(16)-H(16)	127.3
C(4)-C(5)-C(6)	123.0(11)	C(17)-C(16)-H(16)	127.3
N(2)-C(6)-C(7)	111.6(9)	N(6)-C(17)-C(16)	109.1(9)
N(2)-C(6)-C(5)	114.6(10)	N(6)-C(17)-C(18)	121.4(9)
C(7)-C(6)-C(5)	133.8(9)	C(16)-C(17)-C(18)	129.5(9)
C(6)-C(7)-C(8)	103.9(9)	O(4)-C(21)-O(3)	124.3(10)
C(6)-C(7)-H(7)	128.0	O(4)-C(21)-C(22)	118.9(11)

O(3)-C(21)-C(22)	116.8(10)	C(1)-N(1)-C(5)	118.1(9)
C(21)-C(22)-H(22A)	109.5	C(1)-N(1)-Cu(1)	128.0(8)
C(21)-C(22)-H(22B)	109.5	C(5)-N(1)-Cu(1)	113.9(6)
H(22A)-C(22)-H(22B)	109.5	C(6)-N(2)-N(3)	106.6(8)
C(21)-C(22)-H(22C)	109.5	C(6)-N(2)-Cu(1)	117.0(7)
H(22A)-C(22)-H(22C)	109.5	N(3)-N(2)-Cu(1)	136.4(7)
H(22B)-C(22)-H(22C)	109.5	C(8)-N(3)-N(2)	107.3(8)
N(2)-Cu(1)-N(6)	96.6(4)	C(8)-N(3)-Cu(2)	131.7(7)
N(2)-Cu(1)-O(1)	164.0(3)	N(2)-N(3)-Cu(2)	120.8(6)
N(6)-Cu(1)-O(1)	95.8(4)	C(10)-N(4)-C(14)	117.9(9)
N(2)-Cu(1)-N(1)	81.1(4)	C(10)-N(4)-Cu(2)	127.4(8)
N(6)-Cu(1)-N(1)	156.3(4)	C(14)-N(4)-Cu(2)	114.6(7)
O(1)-Cu(1)-N(1)	91.6(3)	C(15)-N(5)-N(6)	109.7(8)
N(3)-Cu(2)-O(3)	96.0(4)	C(15)-N(5)-Cu(2)	114.5(7)
N(3)-Cu(2)-N(5)	96.5(4)	N(6)-N(5)-Cu(2)	135.8(6)
O(3)-Cu(2)-N(5)	163.5(3)	C(17)-N(6)-N(5)	106.4(8)
N(3)-Cu(2)-N(4)	153.0(4)	C(17)-N(6)-Cu(1)	132.0(7)
O(3)-Cu(2)-N(4)	92.6(3)	N(5)-N(6)-Cu(1)	121.6(6)
N(5)-Cu(2)-N(4)	81.0(4)	C(21)-O(3)-Cu(2)	102.7(6)



Ortep plot of CuDMCglut - Ellipsoids at 50% probability

Identification code	CuDMCglut	
Empirical formula	$C_{22}H_{44}CuN_4O_{12}$	
Formula Weight	620.15	
Temperature	150(2) K	
Wavelength		
Crystal system	Triclinic	
Space group	P-1	
Unit cell dimensions	$a = 8.2527(3) \text{ \AA}$	$\alpha = 70.802(2)^\circ$
	$b = 9.4377(4) \text{ \AA}$	$\beta = 77.401(2)^\circ$
	$c = 9.4139(3) \text{ \AA}$	$\gamma = 89.393(2)^\circ$
Volume	$674.28(4) \text{ \AA}^3$	
Z	1	
Density (calculated)	0.879	
Absorption coefficient	0.879	
$F(000)$	329	
Crystal	Deep blue	
Crystal size	0.20 x 0.20 x 0.06 mm ³	
θ range for data collection	3.04 – 28.29°	
Index ranges	-9 ≤ h ≤ 10, -12 ≤ k ≤ 12, -12 ≤ l ≤ 12	
Reflections collected	3289	
Independent reflections	2773 [R _{int} = 0.0473]	
Completeness to $\theta = 28.29^\circ$	0.978	
Absorption correction	Semi-empirical from equivalents	
Max. and min. transmission		
Refinement method	Full-matrix least-squares on F^2	
Data / restraints / parameters	3289 / 196 / 4	
Goodness-of-fit on F^2	1.111	
Final R indices [$F^2 > 2\sigma(F^2)$]	R1 = 0.0686, wR2 = 0.0541	
R indices (all data)	R1 = 0.1456, wR2 = 0.1302	
Largest diff. Peak and hole		

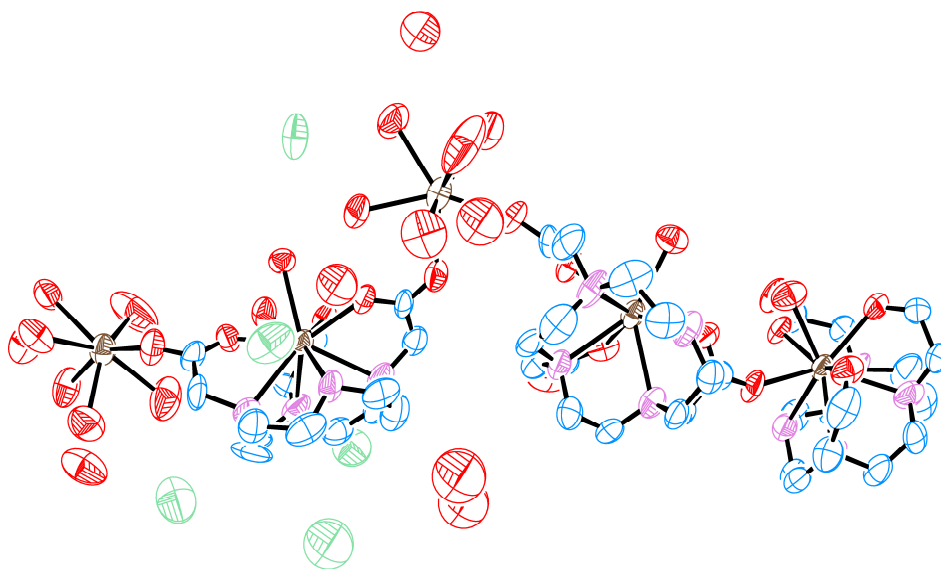
Bond Lengths (Å)

C1-N1	1.50(5)	C7-H7C	0.9800
C1-C2	1.53(6)	C8-N2	1.50(5)
C1-H1A	0.9900	C8-C9	1.53(6)
C1-H1B	0.9900	C8-C6	1.55(5)
C2-C3	1.52(6)	C8-H8	1.0000
C2-H2A	0.9900	C9-C10	1.54(6)
C2-H2B	0.9900	C9-H9A	0.9900
C3-N2	1.50(5)	C9-H9B	0.9900
C3-C2	1.52(6)	C10-C11	1.51(6)
C3-H3A	0.9900	C10-H10A	0.9900
C3-H3B	0.9900	C10-H10B	0.9900
C4-N2	1.49(5)	C11-O3	1.20(5)
C4-C5	1.51(6)	C11-O4	1.31(5)
C4-H4A	0.9900	N1-Cu1	2.12(3)
C4-H4B	0.9900	N2-Cu1	2.08(3)
C5-N1	1.49(5)	O1-Cu1	2.33(3)
C5-H5A	0.9900	O5-H6O	0.87(14)
C5-H5B	0.9900	O5-H5O	0.87(15)
C6-O2	1.24(5)	O6-H8O	0.86(15)
C6-O1	1.26(5)	O6-H7O	0.9(8)
C6-C8	1.55(5)	Cu1-N2	2.08(3)
C7-N1	1.48(5)	Cu1-N1	2.12(3)
C7-H7A	0.9800	Cu1-O1	2.33(3)
C7-H7B	0.9800		

Bond Angles (°)

N1-C1-C2	114(3)	C8-C9-C10	111(3)
N1-C1-H1A	108.7	C8-C9-H9A	109.3
C2-C1-H1A	108.7	C10-C9-H9A	109.3
N1-C1-H1B	108.7	C8-C9-H9B	109.3
C2-C1-H1B	108.7	C10-C9-H9B	109.3
H1A-C1-H1B	107.6	H9A-C9-H9B	108.0
C3-C2-C1	116(4)	C11-C10-C9	111(3)
C3-C2-H2A	108.3	C11-C10-H10A	109.5
C1-C2-H2A	108.3	C9-C10-H10A	109.5
C3-C2-H2B	108.3	C11-C10-H10B	109.5
C1-C2-H2B	108.3	C9-C10-H10B	109.5
H2A-C2-H2B	107.4	H10A-C10-H10B	108.0
N2-C3-C2	116(3)	O3-C11-O4	123(4)
N2-C3-H3A	108.4	O3-C11-C10	123(4)
C2-C3-H3A	108.4	O4-C11-C10	113(4)
N2-C3-H3B	108.4	C7-N1-C5	107(3)
C2-C3-H3B	108.4	C7-N1-C1	110(3)
H3A-C3-H3B	107.4	C5-N1-C1	109(3)
N2-C4-C5	110(3)	C7-N1-Cu1	116(2)
N2-C4-H4A	109.6	C5-N1-Cu1	104(2)
C5-C4-H4A	109.6	C1-N1-Cu1	111(2)
N2-C4-H4B	109.6	C4-N2-C3	109(3)

C5-C4-H4B	109.6	C4-N2-C8	111(3)
H4A-C4-H4B	108.2	C3-N2-C8	111(3)
N1-C5-C4	109(3)	C4-N2-Cu1	104(2)
N1-C5-H5A	109.8	C3-N2-Cu1	111(2)
C4-C5-H5A	109.8	C8-N2-Cu1	111(2)
N1-C5-H5B	109.8	C6-O1-Cu1	112(2)
C4-C5-H5B	109.8	H6O-O5-H5O	119(10)
H5A-C5-H5B	108.2	H8O-O6-H7O	110(10)
O2-C6-O1	126(4)	N2-Cu1-N2	180(3)
O2-C6-C8	118(4)	N2-Cu1-N1	86.4(13)
O1-C6-C8	116(3)	N2-Cu1-N1	93.6(13)
N1-C7-H7A	109.5	N2-Cu1-N1	93.6(13)
N1-C7-H7B	109.5	N2-Cu1-N1	86.4(13)
H7A-C7-H7B	109.5	N1-Cu1-N1	180(2)
N1-C7-H7C	109.5	N2-Cu1-O1	78.3(11)
H7A-C7-H7C	109.5	N2-Cu1-O1	101.7(11)
H7B-C7-H7C	109.5	N1-Cu1-O1	86.7(11)
N2-C8-C9	115(3)	N1-Cu1-O1	93.3(11)
N2-C8-C6	112(3)	N2-Cu1-O1	101.7(11)
C9-C8-C6	114(3)	N2-Cu1-O1	78.3(11)
N2-C8-H8	105.0	N1-Cu1-O1	93.3(11)
C9-C8-H8	105.0	N1-Cu1-O1	86.7(11)
C6-C8-H8	105.0	O1-Cu1-O1	180.0(13)



Ortep plot of EuDO3A - Ellipsoids at 50% probability

Identification code	EuDO3A	
Empirical formula	C ₄₂ H ₆₂ Cl ₄ Eu ₅ N ₁₂ O ₃₇	
Formula weight	2228.64	
Temperature	100(2) K	
Wavelength	0.71075 Å	
Crystal system	Monoclinic	
Space group	C2/c	
Unit cell dimensions	a = 36.519(16) Å	α = 90°.
	b = 15.158(7) Å	β = 91.843(9)°.
	c = 28.531(12) Å	γ = 90°.
Volume	15785(12) Å ³	
Z	8	
Density (calculated)	1.876 Mg/m ³	
Absorption coefficient	4.139 mm ⁻¹	
F(000)	8616	
Crystal size	0.04 x 0.04 x 0.01 mm ³	

Theta range for data collection	2.91 to 25.03°.
Index ranges	-42<=h<=43, -18<=k<=18, -32<=l<=33
Reflections collected	84375
Independent reflections	13898 [$R_{(int)} = 0.1669$]
Completeness to theta = 25.03°	99.7 %
Absorption correction	Semi-empirical from equivalents
Max. and min. transmission	0.9598 and 0.8519
Refinement method	Full-matrix least-squares on F^2
Data / restraints / parameters	13898 / 0 / 878
Goodness-of-fit on F^2	1.199
Final R indices [$I > 2\sigma(I)$]	$R1 = 0.1136$, $wR2 = 0.2953$
R indices (all data)	$R1 = 0.1448$, $wR2 = 0.3182$
Largest diff. peak and hole	2.499 and -1.799 e.Å ⁻³

Bond lengths [Å]

C(1)-N(12)	1.46(3)	C(10)-H(10B)	0.9900
C(1)-C(2)	1.48(3)	C(11)-N(12)	1.48(3)
C(1)-H(1A)	0.9900	C(11)-C(12)	1.51(4)
C(1)-H(1B)	0.9900	C(12)-O(28)#2	1.25(3)
C(2)-N(10)	1.48(2)	C(12)-O(5)	1.28(3)
C(2)-H(2A)	0.9900	C(12)-Eu(3)	3.24(2)
C(2)-H(2B)	0.9900	C(13)-O(1)	1.18(2)
C(3)-N(10)	1.47(3)	C(13)-O(2)	1.28(2)
C(3)-C(4)	1.52(3)	C(13)-C(14)	1.55(3)
C(3)-H(3A)	0.9900	C(14)-N(9)	1.45(2)
C(3)-H(3B)	0.9900	C(14)-H(14A)	0.9900
C(4)-O(29)#1	1.26(3)	C(14)-H(14B)	0.9900
C(4)-O(6)	1.30(2)	C(15)-O(7)	1.23(2)
C(4)-Eu(5)#1	2.87(2)	C(15)-O(4)	1.24(2)
C(5)-N(10)	1.40(3)	C(15)-C(16)	1.55(3)
C(5)-C(6)	1.50(3)	C(15)-Eu(2)	3.27(2)
C(5)-H(5A)	0.9900	C(16)-N(7)	1.44(3)
C(5)-H(5B)	0.9900	C(16)-H(16A)	0.9900
C(6)-N(9)	1.52(3)	C(16)-H(16B)	0.9900
C(6)-H(6A)	0.9900	C(17)-C(18)	1.49(3)
C(6)-H(6B)	0.9900	C(17)-N(7)	1.50(2)
C(7)-C(8)	1.42(4)	C(17)-H(17A)	0.9900
C(7)-N(9)	1.47(3)	C(17)-H(17B)	0.9900
C(7)-H(7A)	0.9900	C(18)-N(6)	1.49(3)
C(7)-H(7B)	0.9900	C(18)-H(18A)	0.9900
C(8)-N(11)	1.59(3)	C(18)-H(18B)	0.9900
C(8)-H(8A)	0.9900	C(19)-N(6)	1.49(3)
C(8)-H(8B)	0.9900	C(19)-C(20)	1.50(3)
C(9)-C(10)	1.41(3)	C(19)-H(19A)	0.9900
C(9)-N(11)	1.45(3)	C(19)-H(19B)	0.9900
C(9)-H(9A)	0.9900	C(20)-N(8)	1.52(3)
C(9)-H(9B)	0.9900	C(20)-H(20A)	0.9900
C(10)-N(12)	1.46(3)	C(20)-H(20B)	0.9900
C(10)-H(10A)	0.9900	C(21)-N(8)	1.44(3)

C(21)-C(22)	1.51(4)	C(31)-H(31A)	0.9900
C(21)-H(21A)	0.9900	C(31)-H(31B)	0.9900
C(21)-H(21B)	0.9900	C(32)-N(4)	1.43(3)
C(22)-N(5)	1.45(3)	C(32)-H(32A)	0.9900
C(22)-H(22A)	0.9900	C(32)-H(32B)	0.9900
C(22)-H(22B)	0.9900	C(33)-N(4)	1.49(3)
C(23)-N(5)	1.45(3)	C(33)-C(34)	1.52(3)
C(23)-C(24)	1.49(3)	C(33)-H(33A)	0.9900
C(23)-H(23A)	0.9900	C(33)-H(33B)	0.9900
C(23)-H(23B)	0.9900	C(34)-N(3)	1.48(3)
C(24)-N(7)	1.49(3)	C(34)-H(34A)	0.9900
C(24)-H(24A)	0.9900	C(34)-H(34B)	0.9900
C(24)-H(24B)	0.9900	C(35)-N(3)	1.44(3)
C(25)-N(5)	1.45(3)	C(35)-C(36)	1.54(3)
C(25)-C(26)	1.51(4)	C(35)-H(35A)	0.9900
C(25)-H(25A)	0.9900	C(35)-H(35B)	0.9900
C(25)-H(25B)	0.9900	C(36)-N(2)	1.44(3)
C(26)-O(10)	1.23(3)	C(36)-H(36A)	0.9900
C(26)-O(11)	1.27(3)	C(36)-H(36B)	0.9900
C(26)-Eu(2)	3.17(3)	C(37)-N(2)	1.47(3)
C(27)-O(12)	1.26(2)	C(37)-C(38)	1.49(3)
C(27)-O(9)	1.28(2)	C(37)-H(37A)	0.9900
C(27)-C(28)	1.46(3)	C(37)-H(37B)	0.9900
C(27)-Eu(2)	3.243(19)	C(38)-N(1)	1.54(2)
C(28)-N(8)	1.51(3)	C(38)-H(38A)	0.9900
C(28)-H(28A)	0.9900	C(38)-H(38B)	0.9900
C(28)-H(28B)	0.9900	C(39)-N(4)	1.48(3)
C(29)-O(19)	1.24(2)	C(39)-C(40)	1.53(3)
C(29)-O(18)	1.28(2)	C(40)-O(8)#1	1.25(2)
C(29)-C(30)	1.44(3)	C(40)-O(20)	1.28(2)
C(29)-Eu(1)	3.226(18)	C(40)-Eu(2)#1	2.93(2)
C(30)-N(1)	1.52(3)	C(41)-C(42)	1.49(3)
C(30)-H(30A)	0.9900	C(41)-N(3)	1.56(3)
C(30)-H(30B)	0.9900	C(41)-H(41A)	0.9900
C(31)-C(32)	1.43(3)	C(41)-H(41B)	0.9900
C(31)-N(1)	1.52(3)	C(42)-O(23)	1.26(2)

C(42)-O(24)	1.28(2)	Eu(3)-N(9)	2.619(16)
C(42)-Eu(1)	3.258(19)	Eu(3)-N(12)	2.652(17)
Eu(1)-O(19)	2.355(13)	Eu(3)-N(10)	2.676(19)
Eu(1)-O(23)	2.398(12)	Eu(4)-O(12)	2.290(13)
Eu(1)-O(22)	2.406(13)	Eu(4)-O(11)#1	2.303(16)
Eu(1)-O(21)	2.472(12)	Eu(4)-O(16)	2.414(19)
Eu(1)-O(20)	2.481(9)	Eu(4)-O(17)	2.432(15)
Eu(1)-N(1)	2.597(17)	Eu(4)-O(15)	2.471(17)
Eu(1)-N(2)	2.598(14)	Eu(4)-O(14)	2.48(2)
Eu(1)-N(4)	2.637(19)	Eu(4)-O(18)	2.484(14)
Eu(1)-N(3)	2.656(16)	Eu(4)-O(13)	2.52(2)
Eu(2)-O(10)	2.327(13)	Eu(5)-O(24)	2.324(16)
Eu(2)-O(9)	2.344(12)	Eu(5)-O(28)	2.359(19)
Eu(2)-O(7)	2.387(14)	Eu(5)-O(27)	2.418(17)
Eu(2)-O(8)	2.438(14)	Eu(5)-O(29)	2.438(16)
Eu(2)-N(7)	2.592(16)	Eu(5)-O(26)	2.44(2)
Eu(2)-N(6)	2.600(16)	Eu(5)-O(25)	2.53(2)
Eu(2)-N(8)	2.611(15)	Eu(5)-O(6)#1	2.561(14)
Eu(2)-N(5)	2.613(16)	Eu(5)-O(30)	2.748(16)
Eu(2)-O(20)#1	2.660(10)	Eu(5)-C(4)#1	2.87(2)
Eu(2)-C(40)#1	2.93(2)	O(6)-Eu(5)#1	2.561(14)
Eu(3)-O(4)	2.364(12)	O(8)-C(40)#1	1.25(2)
Eu(3)-O(2)	2.367(12)	O(11)-Eu(4)#1	2.303(16)
Eu(3)-O(5)	2.376(14)	O(20)-Eu(2)#1	2.660(10)
Eu(3)-O(6)	2.407(14)	O(28)-C(12)#3	1.25(3)
Eu(3)-O(3)	2.530(15)	O(29)-C(4)#1	1.26(3)
Eu(3)-N(11)	2.554(16)	Cl(4)-Cl(4)#4	1.87(4)

Bond angles [°]

N(12)-C(1)-C(2)	114(2)	C(1)-C(2)-N(10)	112.3(17)
N(12)-C(1)-H(1A)	108.8	C(1)-C(2)-H(2A)	109.1
C(2)-C(1)-H(1A)	108.9	N(10)-C(2)-H(2A)	109.1
N(12)-C(1)-H(1B)	108.9	C(1)-C(2)-H(2B)	109.1
C(2)-C(1)-H(1B)	108.9	N(10)-C(2)-H(2B)	109.1
H(1A)-C(1)-H(1B)	107.7	H(2A)-C(2)-H(2B)	107.9

N(10)-C(3)-C(4)	113.0(18)	C(10)-C(9)-N(11)	110(2)
N(10)-C(3)-H(3A)	109.0	C(10)-C(9)-H(9A)	109.7
C(4)-C(3)-H(3A)	109.0	N(11)-C(9)-H(9A)	109.7
N(10)-C(3)-H(3B)	109.0	C(10)-C(9)-H(9B)	109.7
C(4)-C(3)-H(3B)	109.0	N(11)-C(9)-H(9B)	109.7
H(3A)-C(3)-H(3B)	107.8	H(9A)-C(9)-H(9B)	108.2
O(29)#1-C(4)-O(6)	120.1(19)	C(9)-C(10)-N(12)	116(2)
O(29)#1-C(4)-C(3)	119(2)	C(9)-C(10)-H(10A)	108.3
O(6)-C(4)-C(3)	120.5(19)	N(12)-C(10)-H(10A)	108.3
O(29)#1-C(4)-Eu(5)#1	57.5(11)	C(9)-C(10)-H(10B)	108.3
O(6)-C(4)-Eu(5)#1	63.0(11)	N(12)-C(10)-H(10B)	108.3
C(3)-C(4)-Eu(5)#1	172(2)	H(10A)-C(10)-H(10B)	107.4
N(10)-C(5)-C(6)	119(2)	N(12)-C(11)-C(12)	110(2)
N(10)-C(5)-H(5A)	107.7	O(28)#2-C(12)-O(5)	122(3)
C(6)-C(5)-H(5A)	107.7	O(28)#2-C(12)-C(11)	114(2)
N(10)-C(5)-H(5B)	107.7	O(5)-C(12)-C(11)	123.5(19)
C(6)-C(5)-H(5B)	107.7	O(28)#2-C(12)-Eu(3)	160(2)
H(5A)-C(5)-H(5B)	107.1	O(5)-C(12)-Eu(3)	38.7(10)
C(5)-C(6)-N(9)	110(2)	C(11)-C(12)-Eu(3)	85.0(12)
C(5)-C(6)-H(6A)	109.8	O(1)-C(13)-O(2)	126.2(19)
N(9)-C(6)-H(6A)	109.8	O(1)-C(13)-C(14)	120.6(17)
C(5)-C(6)-H(6B)	109.8	O(2)-C(13)-C(14)	112.4(16)
N(9)-C(6)-H(6B)	109.8	N(9)-C(14)-C(13)	113.5(16)
H(6A)-C(6)-H(6B)	108.2	N(9)-C(14)-H(14A)	108.9
C(8)-C(7)-N(9)	113.9(19)	C(13)-C(14)-H(14A)	108.9
C(8)-C(7)-H(7A)	108.8	N(9)-C(14)-H(14B)	108.9
N(9)-C(7)-H(7A)	108.8	C(13)-C(14)-H(14B)	108.9
C(8)-C(7)-H(7B)	108.8	H(14A)-C(14)-H(14B)	107.7
N(9)-C(7)-H(7B)	108.8	O(7)-C(15)-O(4)	126.8(18)
H(7A)-C(7)-H(7B)	107.7	O(7)-C(15)-C(16)	115.0(18)
C(7)-C(8)-N(11)	107.7(16)	O(4)-C(15)-C(16)	118(2)
C(7)-C(8)-H(8A)	110.2	O(7)-C(15)-Eu(2)	36.3(10)
N(11)-C(8)-H(8A)	110.2	O(4)-C(15)-Eu(2)	162.3(14)
C(7)-C(8)-H(8B)	110.2	C(16)-C(15)-Eu(2)	78.7(11)
N(11)-C(8)-H(8B)	110.2	N(7)-C(16)-C(15)	113.4(17)
H(8A)-C(8)-H(8B)	108.5	N(7)-C(16)-H(16A)	108.9

C(15)-C(16)-H(16A)	108.9	C(21)-C(22)-H(22A)	108.9
N(7)-C(16)-H(16B)	108.9	N(5)-C(22)-H(22B)	108.9
C(15)-C(16)-H(16B)	108.9	C(21)-C(22)-H(22B)	108.9
H(16A)-C(16)-H(16B)	107.7	H(22A)-C(22)-H(22B)	107.7
C(18)-C(17)-N(7)	115.2(16)	N(5)-C(23)-C(24)	111.4(18)
C(18)-C(17)-H(17A)	108.5	N(5)-C(23)-H(23A)	109.3
N(7)-C(17)-H(17A)	108.5	C(24)-C(23)-H(23A)	109.3
C(18)-C(17)-H(17B)	108.5	N(5)-C(23)-H(23B)	109.3
N(7)-C(17)-H(17B)	108.5	C(24)-C(23)-H(23B)	109.3
H(17A)-C(17)-H(17B)	107.5	H(23A)-C(23)-H(23B)	108.0
N(6)-C(18)-C(17)	111.9(17)	N(7)-C(24)-C(23)	112.5(18)
N(6)-C(18)-H(18A)	109.2	N(7)-C(24)-H(24A)	109.1
C(17)-C(18)-H(18A)	109.2	C(23)-C(24)-H(24A)	109.1
N(6)-C(18)-H(18B)	109.2	N(7)-C(24)-H(24B)	109.1
C(17)-C(18)-H(18B)	109.2	C(23)-C(24)-H(24B)	109.1
H(18A)-C(18)-H(18B)	107.9	H(24A)-C(24)-H(24B)	107.8
N(6)-C(19)-C(20)	109.7(17)	N(5)-C(25)-C(26)	117(2)
N(6)-C(19)-H(19A)	109.7	N(5)-C(25)-H(25A)	108.2
C(20)-C(19)-H(19A)	109.7	C(26)-C(25)-H(25A)	108.2
N(6)-C(19)-H(19B)	109.7	N(5)-C(25)-H(25B)	108.2
C(20)-C(19)-H(19B)	109.7	C(26)-C(25)-H(25B)	108.2
H(19A)-C(19)-H(19B)	108.2	H(25A)-C(25)-H(25B)	107.3
C(19)-C(20)-N(8)	111.5(19)	O(10)-C(26)-O(11)	125(3)
C(19)-C(20)-H(20A)	109.3	O(10)-C(26)-C(25)	118(2)
N(8)-C(20)-H(20A)	109.3	O(11)-C(26)-C(25)	117(2)
C(19)-C(20)-H(20B)	109.3	O(10)-C(26)-Eu(2)	37.7(11)
N(8)-C(20)-H(20B)	109.3	O(11)-C(26)-Eu(2)	162.6(19)
H(20A)-C(20)-H(20B)	108.0	C(25)-C(26)-Eu(2)	80.2(15)
N(8)-C(21)-C(22)	110.4(16)	O(12)-C(27)-O(9)	121.2(17)
N(8)-C(21)-H(21A)	109.6	O(12)-C(27)-C(28)	120.6(19)
C(22)-C(21)-H(21A)	109.6	O(9)-C(27)-C(28)	118.1(16)
N(8)-C(21)-H(21B)	109.6	O(12)-C(27)-Eu(2)	157.9(14)
C(22)-C(21)-H(21B)	109.6	O(9)-C(27)-Eu(2)	36.8(8)
H(21A)-C(21)-H(21B)	108.1	C(28)-C(27)-Eu(2)	81.4(11)
N(5)-C(22)-C(21)	113.2(19)	C(27)-C(28)-N(8)	112(2)
N(5)-C(22)-H(22A)	108.9	C(27)-C(28)-H(28A)	109.1

N(8)-C(28)-H(28A)	109.1	C(33)-C(34)-H(34A)	109.3
C(27)-C(28)-H(28B)	109.1	N(3)-C(34)-H(34B)	109.3
N(8)-C(28)-H(28B)	109.1	C(33)-C(34)-H(34B)	109.3
H(28A)-C(28)-H(28B)	107.8	H(34A)-C(34)-H(34B)	108.0
O(19)-C(29)-O(18)	124(2)	N(3)-C(35)-C(36)	110.6(19)
O(19)-C(29)-C(30)	119.8(18)	N(3)-C(35)-H(35A)	109.5
O(18)-C(29)-C(30)	116.6(16)	C(36)-C(35)-H(35A)	109.5
O(19)-C(29)-Eu(1)	37.0(9)	N(3)-C(35)-H(35B)	109.5
O(18)-C(29)-Eu(1)	159.1(14)	C(36)-C(35)-H(35B)	109.5
C(30)-C(29)-Eu(1)	83.1(12)	H(35A)-C(35)-H(35B)	108.1
C(29)-C(30)-N(1)	113.0(16)	N(2)-C(36)-C(35)	112.7(19)
C(29)-C(30)-H(30A)	109.0	N(2)-C(36)-H(36A)	109.0
N(1)-C(30)-H(30A)	109.0	C(35)-C(36)-H(36A)	109.0
C(29)-C(30)-H(30B)	109.0	N(2)-C(36)-H(36B)	109.0
N(1)-C(30)-H(30B)	109.0	C(35)-C(36)-H(36B)	109.0
H(30A)-C(30)-H(30B)	107.8	H(36A)-C(36)-H(36B)	107.8
C(32)-C(31)-N(1)	110.8(18)	N(2)-C(37)-C(38)	113(2)
C(32)-C(31)-H(31A)	109.5	N(2)-C(37)-H(37A)	108.9
N(1)-C(31)-H(31A)	109.5	C(38)-C(37)-H(37A)	108.9
C(32)-C(31)-H(31B)	109.5	N(2)-C(37)-H(37B)	108.9
N(1)-C(31)-H(31B)	109.5	C(38)-C(37)-H(37B)	108.9
H(31A)-C(31)-H(31B)	108.1	H(37A)-C(37)-H(37B)	107.7
C(31)-C(32)-N(4)	119(2)	C(37)-C(38)-N(1)	110.8(19)
C(31)-C(32)-H(32A)	107.5	C(37)-C(38)-H(38A)	109.5
N(4)-C(32)-H(32A)	107.5	N(1)-C(38)-H(38A)	109.5
C(31)-C(32)-H(32B)	107.5	C(37)-C(38)-H(38B)	109.5
N(4)-C(32)-H(32B)	107.5	N(1)-C(38)-H(38B)	109.5
H(32A)-C(32)-H(32B)	107.0	H(38A)-C(38)-H(38B)	108.1
N(4)-C(33)-C(34)	112.7(19)	N(4)-C(39)-C(40)	112.3(17)
N(4)-C(33)-H(33A)	109.0	O(8)#1-C(40)-O(20)	120.2(18)
C(34)-C(33)-H(33A)	109.0	O(8)#1-C(40)-C(39)	117.8(17)
N(4)-C(33)-H(33B)	109.0	O(20)-C(40)-C(39)	121.8(16)
C(34)-C(33)-H(33B)	109.0	O(8)#1-C(40)-Eu(2)#1	55.0(10)
H(33A)-C(33)-H(33B)	107.8	O(20)-C(40)-Eu(2)#1	65.2(9)
N(3)-C(34)-C(33)	111.4(18)	C(39)-C(40)-Eu(2)#1	172.4(13)
N(3)-C(34)-H(34A)	109.3	C(42)-C(41)-N(3)	114.4(16)

C(42)-C(41)-H(41A)	108.7	O(20)-Eu(1)-N(4)	67.0(5)
N(3)-C(41)-H(41A)	108.7	N(1)-Eu(1)-N(4)	69.1(6)
C(42)-C(41)-H(41B)	108.7	N(2)-Eu(1)-N(4)	103.2(6)
N(3)-C(41)-H(41B)	108.7	O(19)-Eu(1)-N(3)	139.1(5)
H(41A)-C(41)-H(41B)	107.6	O(23)-Eu(1)-N(3)	67.0(4)
O(23)-C(42)-O(24)	125.8(16)	O(22)-Eu(1)-N(3)	75.3(5)
O(23)-C(42)-C(41)	120.3(16)	O(21)-Eu(1)-N(3)	127.6(5)
O(24)-C(42)-C(41)	113.9(18)	O(20)-Eu(1)-N(3)	130.8(5)
O(23)-C(42)-Eu(1)	38.1(8)	N(1)-Eu(1)-N(3)	106.5(5)
O(24)-C(42)-Eu(1)	160.8(14)	N(2)-Eu(1)-N(3)	66.0(5)
C(41)-C(42)-Eu(1)	83.6(11)	N(4)-Eu(1)-N(3)	67.8(6)
O(19)-Eu(1)-O(23)	144.6(4)	O(19)-Eu(1)-C(29)	18.5(5)
O(19)-Eu(1)-O(22)	82.8(4)	O(23)-Eu(1)-C(29)	151.9(4)
O(23)-Eu(1)-O(22)	84.1(4)	O(22)-Eu(1)-C(29)	100.6(5)
O(19)-Eu(1)-O(21)	73.5(4)	O(21)-Eu(1)-C(29)	84.3(4)
O(23)-Eu(1)-O(21)	71.1(4)	O(20)-Eu(1)-C(29)	76.8(4)
O(22)-Eu(1)-O(21)	70.3(4)	N(1)-Eu(1)-C(29)	48.6(6)
O(19)-Eu(1)-O(20)	87.4(4)	N(2)-Eu(1)-C(29)	76.3(5)
O(23)-Eu(1)-O(20)	82.0(4)	N(4)-Eu(1)-C(29)	114.2(6)
O(22)-Eu(1)-O(20)	140.2(4)	N(3)-Eu(1)-C(29)	141.1(5)
O(21)-Eu(1)-O(20)	69.9(4)	O(19)-Eu(1)-C(42)	150.2(5)
O(19)-Eu(1)-N(1)	65.8(5)	O(23)-Eu(1)-C(42)	18.9(4)
O(23)-Eu(1)-N(1)	140.6(5)	O(22)-Eu(1)-C(42)	72.9(5)
O(22)-Eu(1)-N(1)	133.6(5)	O(21)-Eu(1)-C(42)	82.1(5)
O(21)-Eu(1)-N(1)	125.9(5)	O(20)-Eu(1)-C(42)	100.2(4)
O(20)-Eu(1)-N(1)	74.0(4)	N(1)-Eu(1)-C(42)	144.0(6)
O(19)-Eu(1)-N(2)	74.1(5)	N(2)-Eu(1)-C(42)	111.4(5)
O(23)-Eu(1)-N(2)	130.2(5)	N(4)-Eu(1)-C(42)	76.0(5)
O(22)-Eu(1)-N(2)	69.1(5)	N(3)-Eu(1)-C(42)	50.1(5)
O(21)-Eu(1)-N(2)	130.3(5)	C(29)-Eu(1)-C(42)	166.2(5)
O(20)-Eu(1)-N(2)	143.7(4)	O(10)-Eu(2)-O(9)	80.5(5)
N(1)-Eu(1)-N(2)	69.9(5)	O(10)-Eu(2)-O(7)	84.9(5)
O(19)-Eu(1)-N(4)	132.7(5)	O(9)-Eu(2)-O(7)	143.4(5)
O(23)-Eu(1)-N(4)	72.9(5)	O(10)-Eu(2)-O(8)	131.2(5)
O(22)-Eu(1)-N(4)	141.7(5)	O(9)-Eu(2)-O(8)	82.3(5)
O(21)-Eu(1)-N(4)	126.5(4)	O(7)-Eu(2)-O(8)	82.5(5)

O(10)-Eu(2)-N(7)	75.9(5)	N(8)-Eu(2)-C(40)#1	100.7(6)
O(9)-Eu(2)-N(7)	139.8(5)	N(5)-Eu(2)-C(40)#1	149.6(5)
O(7)-Eu(2)-N(7)	66.0(5)	O(20)#1-Eu(2)-C(40)#1	26.0(4)
O(8)-Eu(2)-N(7)	137.3(5)	O(10)-Eu(2)-C(26)	18.8(6)
O(10)-Eu(2)-N(6)	144.1(5)	O(9)-Eu(2)-C(26)	71.1(5)
O(9)-Eu(2)-N(6)	132.4(5)	O(7)-Eu(2)-C(26)	102.0(6)
O(7)-Eu(2)-N(6)	74.5(6)	O(8)-Eu(2)-C(26)	140.9(5)
O(8)-Eu(2)-N(6)	75.4(6)	N(7)-Eu(2)-C(26)	76.4(5)
N(7)-Eu(2)-N(6)	69.0(6)	N(6)-Eu(2)-C(26)	143.5(6)
O(10)-Eu(2)-N(8)	130.7(6)	N(8)-Eu(2)-C(26)	112.1(7)
O(9)-Eu(2)-N(8)	66.9(4)	N(5)-Eu(2)-C(26)	50.4(6)
O(7)-Eu(2)-N(8)	142.1(5)	O(20)#1-Eu(2)-C(26)	93.4(5)
O(8)-Eu(2)-N(8)	81.2(6)	C(40)#1-Eu(2)-C(26)	118.0(5)
N(7)-Eu(2)-N(8)	106.0(5)	O(10)-Eu(2)-C(27)	98.1(5)
N(6)-Eu(2)-N(8)	68.5(5)	O(9)-Eu(2)-C(27)	19.1(4)
O(10)-Eu(2)-N(5)	68.2(5)	O(7)-Eu(2)-C(27)	153.9(4)
O(9)-Eu(2)-N(5)	73.4(5)	O(8)-Eu(2)-C(27)	76.1(5)
O(7)-Eu(2)-N(5)	130.8(5)	N(7)-Eu(2)-C(27)	139.9(5)
O(8)-Eu(2)-N(5)	145.9(5)	N(6)-Eu(2)-C(27)	113.4(5)
N(7)-Eu(2)-N(5)	67.9(5)	N(8)-Eu(2)-C(27)	48.5(4)
N(6)-Eu(2)-N(5)	103.9(6)	N(5)-Eu(2)-C(27)	73.2(5)
N(8)-Eu(2)-N(5)	67.6(6)	O(20)#1-Eu(2)-C(27)	83.5(4)
O(10)-Eu(2)-O(20)#1	80.5(4)	C(40)#1-Eu(2)-C(27)	78.3(5)
O(9)-Eu(2)-O(20)#1	73.1(4)	C(26)-Eu(2)-C(27)	86.0(6)
O(7)-Eu(2)-O(20)#1	71.4(4)	O(4)-Eu(3)-O(2)	86.7(4)
O(8)-Eu(2)-O(20)#1	50.8(4)	O(4)-Eu(3)-O(5)	80.1(5)
N(7)-Eu(2)-O(20)#1	132.6(4)	O(2)-Eu(3)-O(5)	146.7(5)
N(6)-Eu(2)-O(20)#1	118.4(5)	O(4)-Eu(3)-O(6)	139.9(5)
N(8)-Eu(2)-O(20)#1	120.5(5)	O(2)-Eu(3)-O(6)	88.8(4)
N(5)-Eu(2)-O(20)#1	137.1(4)	O(5)-Eu(3)-O(6)	82.2(5)
O(10)-Eu(2)-C(40)#1	106.4(4)	O(4)-Eu(3)-O(3)	71.2(5)
O(9)-Eu(2)-C(40)#1	76.3(5)	O(2)-Eu(3)-O(3)	70.6(4)
O(7)-Eu(2)-C(40)#1	76.0(5)	O(5)-Eu(3)-O(3)	76.3(5)
O(8)-Eu(2)-C(40)#1	24.8(4)	O(6)-Eu(3)-O(3)	69.7(5)
N(7)-Eu(2)-C(40)#1	141.7(5)	O(4)-Eu(3)-N(11)	72.8(5)
N(6)-Eu(2)-C(40)#1	96.7(6)	O(2)-Eu(3)-N(11)	72.6(5)

O(5)-Eu(3)-N(11)	130.3(5)	O(12)-Eu(4)-O(17)	149.0(6)
O(6)-Eu(3)-N(11)	142.4(5)	O(11)#1-Eu(4)-O(17)	86.1(7)
O(3)-Eu(3)-N(11)	129.1(5)	O(16)-Eu(4)-O(17)	72.4(7)
O(4)-Eu(3)-N(9)	137.9(6)	O(12)-Eu(4)-O(15)	139.4(6)
O(2)-Eu(3)-N(9)	66.1(5)	O(11)#1-Eu(4)-O(15)	83.9(7)
O(5)-Eu(3)-N(9)	139.4(6)	O(16)-Eu(4)-O(15)	108.6(8)
O(6)-Eu(3)-N(9)	74.0(6)	O(17)-Eu(4)-O(15)	69.5(6)
O(3)-Eu(3)-N(9)	122.9(5)	O(12)-Eu(4)-O(14)	77.1(6)
N(11)-Eu(3)-N(9)	68.7(6)	O(11)#1-Eu(4)-O(14)	143.2(9)
O(4)-Eu(3)-N(12)	74.0(5)	O(16)-Eu(4)-O(14)	67.9(10)
O(2)-Eu(3)-N(12)	138.0(5)	O(17)-Eu(4)-O(14)	111.0(8)
O(5)-Eu(3)-N(12)	66.6(5)	O(15)-Eu(4)-O(14)	73.1(8)
O(6)-Eu(3)-N(12)	129.6(5)	O(12)-Eu(4)-O(18)	78.5(5)
O(3)-Eu(3)-N(12)	132.5(5)	O(11)#1-Eu(4)-O(18)	72.8(5)
N(11)-Eu(3)-N(12)	66.2(5)	O(16)-Eu(4)-O(18)	80.1(7)
N(9)-Eu(3)-N(12)	104.6(6)	O(17)-Eu(4)-O(18)	77.6(5)
O(4)-Eu(3)-N(10)	139.0(5)	O(15)-Eu(4)-O(18)	140.7(6)
O(2)-Eu(3)-N(10)	132.0(5)	O(14)-Eu(4)-O(18)	141.1(8)
O(5)-Eu(3)-N(10)	72.4(6)	O(12)-Eu(4)-O(13)	74.1(6)
O(6)-Eu(3)-N(10)	65.8(5)	O(11)#1-Eu(4)-O(13)	70.9(7)
O(3)-Eu(3)-N(10)	128.0(6)	O(16)-Eu(4)-O(13)	140.1(8)
N(11)-Eu(3)-N(10)	102.7(6)	O(17)-Eu(4)-O(13)	136.6(6)
N(9)-Eu(3)-N(10)	67.9(6)	O(15)-Eu(4)-O(13)	71.9(6)
N(12)-Eu(3)-N(10)	67.4(5)	O(14)-Eu(4)-O(13)	74.8(10)
O(4)-Eu(3)-C(12)	70.9(6)	O(18)-Eu(4)-O(13)	125.9(6)
O(2)-Eu(3)-C(12)	154.4(5)	O(24)-Eu(5)-O(28)	84.4(7)
O(5)-Eu(3)-C(12)	19.6(7)	O(24)-Eu(5)-O(27)	152.5(6)
O(6)-Eu(3)-C(12)	100.2(7)	O(28)-Eu(5)-O(27)	73.4(7)
O(3)-Eu(3)-C(12)	90.0(6)	O(24)-Eu(5)-O(29)	129.2(6)
N(11)-Eu(3)-C(12)	110.7(7)	O(28)-Eu(5)-O(29)	125.4(6)
N(9)-Eu(3)-C(12)	139.4(6)	O(27)-Eu(5)-O(29)	77.9(6)
N(12)-Eu(3)-C(12)	48.0(7)	O(24)-Eu(5)-O(26)	111.1(8)
N(10)-Eu(3)-C(12)	73.1(6)	O(28)-Eu(5)-O(26)	140.4(8)
O(12)-Eu(4)-O(11)#1	105.2(7)	O(27)-Eu(5)-O(26)	78.6(8)
O(12)-Eu(4)-O(16)	84.3(7)	O(29)-Eu(5)-O(26)	73.5(9)
O(11)#1-Eu(4)-O(16)	148.4(7)	O(24)-Eu(5)-O(25)	78.4(6)

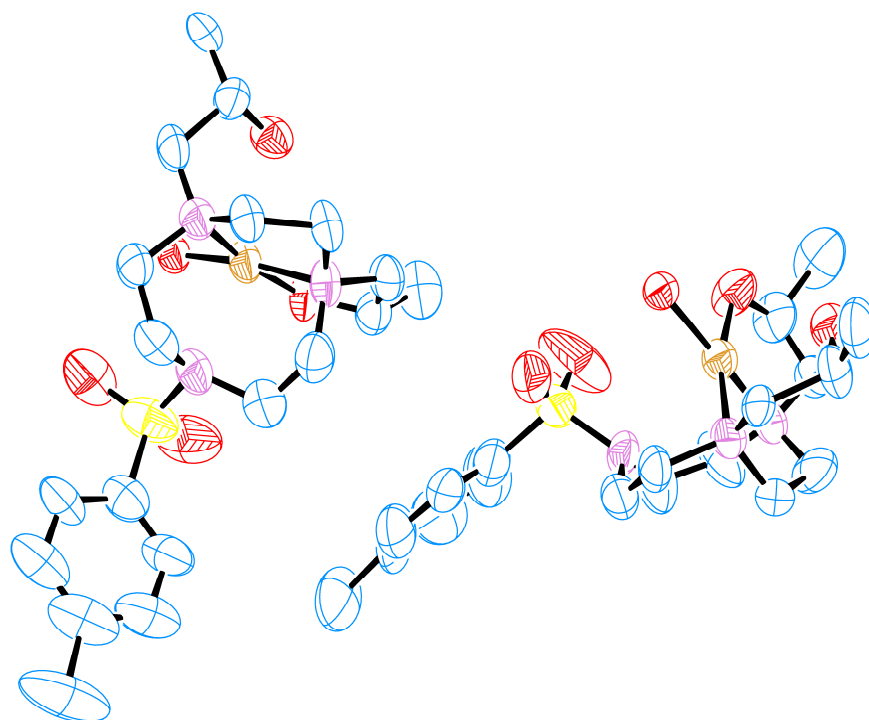
O(28)-Eu(5)-O(25)	74.0(8)	C(34)-N(3)-C(41)	107(2)
O(27)-Eu(5)-O(25)	79.9(6)	C(35)-N(3)-Eu(1)	113.3(14)
O(29)-Eu(5)-O(25)	143.5(7)	C(34)-N(3)-Eu(1)	112.7(14)
O(26)-Eu(5)-O(25)	74.0(10)	C(41)-N(3)-Eu(1)	106.1(11)
O(24)-Eu(5)-O(6)#1	80.5(5)	C(32)-N(4)-C(39)	109.5(18)
O(28)-Eu(5)-O(6)#1	149.4(6)	C(32)-N(4)-C(33)	113.0(17)
O(27)-Eu(5)-O(6)#1	126.6(5)	C(39)-N(4)-C(33)	106.2(17)
O(29)-Eu(5)-O(6)#1	52.6(5)	C(32)-N(4)-Eu(1)	108.3(14)
O(26)-Eu(5)-O(6)#1	70.2(7)	C(39)-N(4)-Eu(1)	108.0(11)
O(25)-Eu(5)-O(6)#1	127.8(6)	C(33)-N(4)-Eu(1)	111.7(13)
O(24)-Eu(5)-O(30)	84.0(5)	C(22)-N(5)-C(23)	110.4(16)
O(28)-Eu(5)-O(30)	76.1(6)	C(22)-N(5)-C(25)	109.7(18)
O(27)-Eu(5)-O(30)	105.6(5)	C(23)-N(5)-C(25)	108.6(17)
O(29)-Eu(5)-O(30)	68.3(5)	C(22)-N(5)-Eu(2)	110.6(13)
O(26)-Eu(5)-O(30)	139.4(8)	C(23)-N(5)-Eu(2)	113.6(12)
O(25)-Eu(5)-O(30)	146.5(7)	C(25)-N(5)-Eu(2)	103.7(13)
O(6)#1-Eu(5)-O(30)	76.0(4)	C(18)-N(6)-C(19)	110.1(17)
O(24)-Eu(5)-C(4)#1	106.2(6)	C(18)-N(6)-Eu(2)	112.8(13)
O(28)-Eu(5)-C(4)#1	144.7(7)	C(19)-N(6)-Eu(2)	114.2(13)
O(27)-Eu(5)-C(4)#1	101.3(7)	C(16)-N(7)-C(24)	107.7(16)
O(29)-Eu(5)-C(4)#1	25.9(5)	C(16)-N(7)-C(17)	107.5(15)
O(26)-Eu(5)-C(4)#1	67.8(9)	C(24)-N(7)-C(17)	111.3(15)
O(25)-Eu(5)-C(4)#1	140.6(8)	C(16)-N(7)-Eu(2)	108.0(11)
O(6)#1-Eu(5)-C(4)#1	26.8(5)	C(24)-N(7)-Eu(2)	110.1(11)
O(30)-Eu(5)-C(4)#1	71.9(6)	C(17)-N(7)-Eu(2)	112.0(12)
C(30)-N(1)-C(31)	113.9(17)	C(21)-N(8)-C(28)	111.3(19)
C(30)-N(1)-C(38)	106.7(17)	C(21)-N(8)-C(20)	112.1(17)
C(31)-N(1)-C(38)	108.7(19)	C(28)-N(8)-C(20)	107(2)
C(30)-N(1)-Eu(1)	107.2(12)	C(21)-N(8)-Eu(2)	112.7(15)
C(31)-N(1)-Eu(1)	109.9(12)	C(28)-N(8)-Eu(2)	105.8(11)
C(38)-N(1)-Eu(1)	110.4(12)	C(20)-N(8)-Eu(2)	107.9(13)
C(36)-N(2)-C(37)	112.7(18)	C(14)-N(9)-C(7)	113.1(17)
C(36)-N(2)-Eu(1)	116.0(14)	C(14)-N(9)-C(6)	108.0(18)
C(37)-N(2)-Eu(1)	109.0(11)	C(7)-N(9)-C(6)	109.6(19)
C(35)-N(3)-C(34)	107.6(18)	C(14)-N(9)-Eu(3)	104.4(11)
C(35)-N(3)-C(41)	109.7(19)	C(7)-N(9)-Eu(3)	110.0(14)

C(6)-N(9)-Eu(3)	111.6(14)	C(4)-O(6)-Eu(3)	121.3(12)
C(5)-N(10)-C(3)	107(2)	C(4)-O(6)-Eu(5)#1	90.1(12)
C(5)-N(10)-C(2)	111.4(19)	Eu(3)-O(6)-Eu(5)#1	140.0(6)
C(3)-N(10)-C(2)	108.4(18)	C(15)-O(7)-Eu(2)	125.9(13)
C(5)-N(10)-Eu(3)	110.6(14)	C(40)#1-O(8)-Eu(2)	100.2(12)
C(3)-N(10)-Eu(3)	108.6(14)	C(27)-O(9)-Eu(2)	124.1(10)
C(2)-N(10)-Eu(3)	110.4(13)	C(26)-O(10)-Eu(2)	123.4(15)
C(9)-N(11)-C(8)	112.4(18)	C(26)-O(11)-Eu(4)#1	150.4(16)
C(9)-N(11)-Eu(3)	116.7(14)	C(27)-O(12)-Eu(4)	162.8(14)
C(8)-N(11)-Eu(3)	109.8(12)	C(29)-O(18)-Eu(4)	133.9(12)
C(10)-N(12)-C(1)	110.9(18)	C(29)-O(19)-Eu(1)	124.5(13)
C(10)-N(12)-C(11)	110.8(19)	C(40)-O(20)-Eu(1)	118.9(11)
C(1)-N(12)-C(11)	106.7(17)	C(40)-O(20)-Eu(2)#1	88.8(10)
C(10)-N(12)-Eu(3)	107.5(12)	Eu(1)-O(20)-Eu(2)#1	151.3(5)
C(1)-N(12)-Eu(3)	111.2(13)	C(42)-O(23)-Eu(1)	123.0(11)
C(11)-N(12)-Eu(3)	109.8(14)	C(42)-O(24)-Eu(5)	144.5(15)
C(13)-O(2)-Eu(3)	126.0(12)	C(12)#3-O(28)-Eu(5)	157(2)
C(15)-O(4)-Eu(3)	150.7(15)	C(4)#1-O(29)-Eu(5)	96.6(13)
C(12)-O(5)-Eu(3)	121.7(15)		

Symmetry transformations used to generate equivalent atoms:

#1 $-x+1, -y+2, -z+1$ #2 $x-1/2, -y+3/2, z-1/2$ #3 $x+1/2, -y+3/2, z+1/2$

#4 $-x+1, y, -z+3/2$



Ortep plot of CuTsTACNE2 - Ellipsoids at 50 % probability

Identification code	CuTsTACNE ₂	
Empirical formula	C ₇₆ H ₁₂₄ Cu ₄ N ₁₂ O ₄₃ S ₄	
Formula weight	2276.27	
Temperature	100(2) K	
Wavelength	0.71075 Å	
Crystal system	Monoclinic	
Space group	C2	
Unit cell dimensions	a = 22.21(5) Å	α = 90°.
	b = 27.09(10) Å	β = 133.011(5)°.
	c = 15.19(4) Å	γ = 90°.
Volume	6683(34) Å ³	
Z	2	
Density (calculated)	1.131 Mg/m ³	
Absorption coefficient	0.761 mm ⁻¹	
F(000)	2376	
Crystal size	0.10 x 0.04 x 0.01 mm ³	

Theta range for data collection	2.92 to 24.64°.
Index ranges	-25<=h<=25, -31<=k<=31, -14<=l<=17
Reflections collected	29154
Independent reflections	11006 [R _(int) = 0.0837]
Completeness to theta = 24.64°	97.7 %
Absorption correction	Semi-empirical from equivalents
Max. and min. transmission	0.9924 and 0.9278
Refinement method	Full-matrix least-squares on F ²
Data / restraints / parameters	11006 / 190 / 611
Goodness-of-fit on F ²	0.963
Final R indices [I>2sigma(I)]	R1 = 0.0964, wR2 = 0.2471
R indices (all data)	R1 = 0.1213, wR2 = 0.2772
Absolute structure parameter	0.03(3)
Extinction coefficient	0.0008(4)
Largest diff. peak and hole	0.899 and -0.771 e.Å ⁻³

Bond lengths [Å]

C(1)-N(1)	1.520(14)	C(10)-H(10B)	0.9900
C(1)-C(2)	1.620(14)	C(11)-O(3)	1.505(13)
C(1)-H(1A)	0.9900	C(11)-C(12)	1.543(18)
C(1)-H(1B)	0.9900	C(11)-H(11)	1.0000
C(2)-N(2)	1.462(13)	C(12)-H(12A)	0.9800
C(2)-H(2A)	0.9900	C(12)-H(12B)	0.9800
C(2)-H(2B)	0.9900	C(12)-H(12C)	0.9800
C(3)-C(4)	1.538(15)	C(13)-C(14)	1.3900
C(3)-N(2)	1.556(14)	C(13)-C(18)	1.3900
C(3)-H(3A)	0.9900	C(13)-S(1)	1.821(7)
C(3)-H(3B)	0.9900	C(14)-C(15)	1.3900
C(4)-N(3)	1.468(16)	C(14)-H(14)	0.9500
C(4)-H(4A)	0.9900	C(15)-C(16)	1.3900
C(4)-H(4B)	0.9900	C(15)-H(15)	0.9500
C(5)-C(6)	1.463(18)	C(16)-C(17)	1.3900
C(5)-N(3)	1.530(16)	C(16)-C(19)	1.683(15)
C(5)-H(5A)	0.9900	C(17)-C(18)	1.3900
C(5)-H(5B)	0.9900	C(17)-H(17)	0.9500
C(6)-N(1)	1.597(15)	C(18)-H(18)	0.9500
C(6)-H(6A)	0.9900	C(19)-H(19A)	0.9800
C(6)-H(6B)	0.9900	C(19)-H(19B)	0.9800
C(7)-N(2)	1.506(13)	C(19)-H(19C)	0.9800
C(7)-C(8)	1.575(15)	C(20)-N(4)	1.561(15)
C(7)-H(7A)	0.9900	C(20)-C(21)	1.584(17)
C(7)-H(7B)	0.9900	C(20)-H(20A)	0.9900
C(8)-O(5)	1.516(12)	C(20)-H(20B)	0.9900
C(8)-C(9)	1.522(15)	C(21)-N(5)	1.547(13)
C(8)-H(8)	1.0000	C(21)-H(21A)	0.9900
C(9)-H(9A)	0.9800	C(21)-H(21B)	0.9900
C(9)-H(9B)	0.9800	C(22)-C(23)	1.513(17)
C(9)-H(9C)	0.9800	C(22)-N(5)	1.562(13)
C(10)-C(11)	1.533(16)	C(22)-H(22A)	0.9900
C(10)-N(1)	1.535(12)	C(22)-H(22B)	0.9900
C(10)-H(10A)	0.9900	C(23)-N(6)	1.452(14)

C(23)-H(23A)	0.9900	C(32)-S(2)	1.855(8)
C(23)-H(23B)	0.9900	C(33)-C(34)	1.3900
C(24)-C(25)	1.419(19)	C(33)-H(33)	0.9500
C(24)-N(6)	1.538(16)	C(34)-C(35)	1.3900
C(24)-H(24A)	0.9900	C(34)-H(34)	0.9500
C(24)-H(24B)	0.9900	C(35)-C(36)	1.3900
C(25)-N(4)	1.583(16)	C(35)-C(38)	1.699(18)
C(25)-H(25A)	0.9900	C(36)-C(37)	1.3900
C(25)-H(25B)	0.9900	C(36)-H(36)	0.9500
C(26)-N(5)	1.586(14)	C(37)-H(37)	0.9500
C(26)-C(27)	1.595(14)	C(38)-H(38A)	0.9800
C(26)-H(26A)	0.9900	C(38)-H(38B)	0.9800
C(26)-H(26B)	0.9900	C(38)-H(38C)	0.9800
C(27)-C(28)	1.426(18)	N(1)-Cu(01)	2.077(9)
C(27)-O(10)	1.550(14)	N(2)-Cu(01)	2.116(9)
C(27)-H(27)	1.0000	N(3)-S(1)	1.710(11)
C(28)-H(28A)	0.9800	N(4)-Cu(02)	2.023(10)
C(28)-H(28B)	0.9800	N(5)-Cu(02)	2.079(9)
C(28)-H(28C)	0.9800	N(6)-S(2)	1.682(8)
C(29)-C(30)	1.528(16)	O(1)-S(1)	1.505(11)
C(29)-N(4)	1.539(13)	O(2)-S(1)	1.444(12)
C(29)-H(29A)	0.9900	O(3)-Cu(01)	1.969(8)
C(29)-H(29B)	0.9900	O(4)-Cu(01)#1	1.995(6)
C(30)-O(8)	1.513(13)	O(4)-Cu(01)	1.995(6)
C(30)-C(31)	1.59(2)	O(6)-S(2)	1.488(12)
C(30)-H(30)	1.0000	O(7)-S(2)	1.442(12)
C(31)-H(31A)	0.9800	O(8)-Cu(02)	1.997(8)
C(31)-H(31B)	0.9800	O(9)-Cu(02)#2	1.983(6)
C(31)-H(31C)	0.9800	O(9)-Cu(02)	1.983(6)
C(32)-C(33)	1.3900		
C(32)-C(37)	1.3900		

Bond angles [°]

N(1)-C(1)-C(2)	105.4(8)	C(2)-C(1)-H(1A)	110.7
N(1)-C(1)-H(1A)	110.7	N(1)-C(1)-H(1B)	110.7

C(2)-C(1)-H(1B)	110.7	C(8)-C(7)-H(7B)	108.8
H(1A)-C(1)-H(1B)	108.8	H(7A)-C(7)-H(7B)	107.7
N(2)-C(2)-C(1)	114.3(8)	O(5)-C(8)-C(9)	111.1(9)
N(2)-C(2)-H(2A)	108.7	O(5)-C(8)-C(7)	107.0(8)
C(1)-C(2)-H(2A)	108.7	C(9)-C(8)-C(7)	111.7(8)
N(2)-C(2)-H(2B)	108.7	O(5)-C(8)-H(8)	109.0
C(1)-C(2)-H(2B)	108.7	C(9)-C(8)-H(8)	109.0
H(2A)-C(2)-H(2B)	107.6	C(7)-C(8)-H(8)	109.0
C(4)-C(3)-N(2)	112.1(8)	C(8)-C(9)-H(9A)	109.5
C(4)-C(3)-H(3A)	109.2	C(8)-C(9)-H(9B)	109.5
N(2)-C(3)-H(3A)	109.2	H(9A)-C(9)-H(9B)	109.5
C(4)-C(3)-H(3B)	109.2	C(8)-C(9)-H(9C)	109.5
N(2)-C(3)-H(3B)	109.2	H(9A)-C(9)-H(9C)	109.5
H(3A)-C(3)-H(3B)	107.9	H(9B)-C(9)-H(9C)	109.5
N(3)-C(4)-C(3)	114.5(9)	C(11)-C(10)-N(1)	110.8(8)
N(3)-C(4)-H(4A)	108.6	C(11)-C(10)-H(10A)	109.5
C(3)-C(4)-H(4A)	108.6	N(1)-C(10)-H(10A)	109.5
N(3)-C(4)-H(4B)	108.6	C(11)-C(10)-H(10B)	109.5
C(3)-C(4)-H(4B)	108.6	N(1)-C(10)-H(10B)	109.5
H(4A)-C(4)-H(4B)	107.6	H(10A)-C(10)-H(10B)	108.1
C(6)-C(5)-N(3)	113.8(11)	O(3)-C(11)-C(10)	106.1(8)
C(6)-C(5)-H(5A)	108.8	O(3)-C(11)-C(12)	110.2(10)
N(3)-C(5)-H(5A)	108.8	C(10)-C(11)-C(12)	112.4(10)
C(6)-C(5)-H(5B)	108.8	O(3)-C(11)-H(11)	109.4
N(3)-C(5)-H(5B)	108.8	C(10)-C(11)-H(11)	109.4
H(5A)-C(5)-H(5B)	107.7	C(12)-C(11)-H(11)	109.4
C(5)-C(6)-N(1)	119.2(10)	C(11)-C(12)-H(12A)	109.5
C(5)-C(6)-H(6A)	107.5	C(11)-C(12)-H(12B)	109.5
N(1)-C(6)-H(6A)	107.5	H(12A)-C(12)-H(12B)	109.5
C(5)-C(6)-H(6B)	107.5	C(11)-C(12)-H(12C)	109.5
N(1)-C(6)-H(6B)	107.5	H(12A)-C(12)-H(12C)	109.5
H(6A)-C(6)-H(6B)	107.0	H(12B)-C(12)-H(12C)	109.5
N(2)-C(7)-C(8)	113.7(7)	C(14)-C(13)-C(18)	120.0
N(2)-C(7)-H(7A)	108.8	C(14)-C(13)-S(1)	117.4(5)
C(8)-C(7)-H(7A)	108.8	C(18)-C(13)-S(1)	122.6(5)
N(2)-C(7)-H(7B)	108.8	C(13)-C(14)-C(15)	120.0

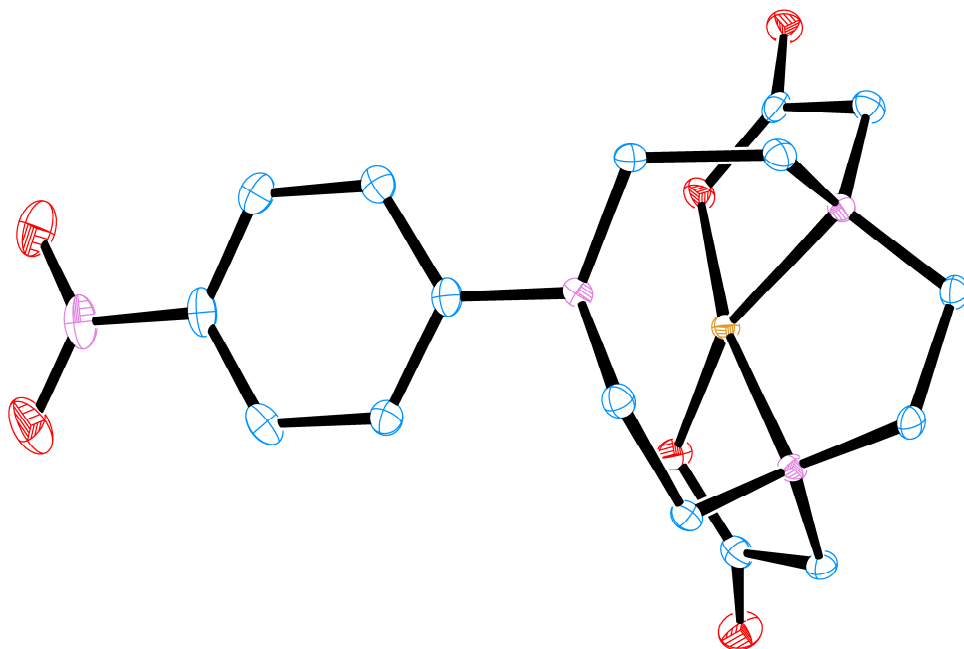
C(13)-C(14)-H(14)	120.0	N(5)-C(22)-H(22B)	108.9
C(15)-C(14)-H(14)	120.0	H(22A)-C(22)-H(22B)	107.7
C(16)-C(15)-C(14)	120.0	N(6)-C(23)-C(22)	116.1(9)
C(16)-C(15)-H(15)	120.0	N(6)-C(23)-H(23A)	108.3
C(14)-C(15)-H(15)	120.0	C(22)-C(23)-H(23A)	108.3
C(15)-C(16)-C(17)	120.0	N(6)-C(23)-H(23B)	108.3
C(15)-C(16)-C(19)	123.8(12)	C(22)-C(23)-H(23B)	108.3
C(17)-C(16)-C(19)	116.0(12)	H(23A)-C(23)-H(23B)	107.4
C(18)-C(17)-C(16)	120.0	C(25)-C(24)-N(6)	117.0(12)
C(18)-C(17)-H(17)	120.0	C(25)-C(24)-H(24A)	108.1
C(16)-C(17)-H(17)	120.0	N(6)-C(24)-H(24A)	108.1
C(17)-C(18)-C(13)	120.0	C(25)-C(24)-H(24B)	108.1
C(17)-C(18)-H(18)	120.0	N(6)-C(24)-H(24B)	108.1
C(13)-C(18)-H(18)	120.0	H(24A)-C(24)-H(24B)	107.3
C(16)-C(19)-H(19A)	109.5	C(24)-C(25)-N(4)	125.5(11)
C(16)-C(19)-H(19B)	109.5	C(24)-C(25)-H(25A)	105.9
H(19A)-C(19)-H(19B)	109.5	N(4)-C(25)-H(25A)	105.9
C(16)-C(19)-H(19C)	109.5	C(24)-C(25)-H(25B)	105.9
H(19A)-C(19)-H(19C)	109.5	N(4)-C(25)-H(25B)	105.9
H(19B)-C(19)-H(19C)	109.5	H(25A)-C(25)-H(25B)	106.3
N(4)-C(20)-C(21)	111.1(8)	N(5)-C(26)-C(27)	111.8(7)
N(4)-C(20)-H(20A)	109.4	N(5)-C(26)-H(26A)	109.3
C(21)-C(20)-H(20A)	109.4	C(27)-C(26)-H(26A)	109.3
N(4)-C(20)-H(20B)	109.4	N(5)-C(26)-H(26B)	109.3
C(21)-C(20)-H(20B)	109.4	C(27)-C(26)-H(26B)	109.3
H(20A)-C(20)-H(20B)	108.0	H(26A)-C(26)-H(26B)	107.9
N(5)-C(21)-C(20)	109.9(8)	C(28)-C(27)-O(10)	111.3(10)
N(5)-C(21)-H(21A)	109.7	C(28)-C(27)-C(26)	111.2(10)
C(20)-C(21)-H(21A)	109.7	O(10)-C(27)-C(26)	107.9(7)
N(5)-C(21)-H(21B)	109.7	C(28)-C(27)-H(27)	108.8
C(20)-C(21)-H(21B)	109.7	O(10)-C(27)-H(27)	108.8
H(21A)-C(21)-H(21B)	108.2	C(26)-C(27)-H(27)	108.8
C(23)-C(22)-N(5)	113.5(9)	C(27)-C(28)-H(28A)	109.5
C(23)-C(22)-H(22A)	108.9	C(27)-C(28)-H(28B)	109.5
N(5)-C(22)-H(22A)	108.9	H(28A)-C(28)-H(28B)	109.5
C(23)-C(22)-H(22B)	108.9	C(27)-C(28)-H(28C)	109.5

H(28A)-C(28)-H(28C)	109.5	C(36)-C(37)-H(37)	120.0
H(28B)-C(28)-H(28C)	109.5	C(32)-C(37)-H(37)	120.0
C(30)-C(29)-N(4)	110.2(8)	C(35)-C(38)-H(38A)	109.5
C(30)-C(29)-H(29A)	109.6	C(35)-C(38)-H(38B)	109.5
N(4)-C(29)-H(29A)	109.6	H(38A)-C(38)-H(38B)	109.5
C(30)-C(29)-H(29B)	109.6	C(35)-C(38)-H(38C)	109.5
N(4)-C(29)-H(29B)	109.6	H(38A)-C(38)-H(38C)	109.5
H(29A)-C(29)-H(29B)	108.1	H(38B)-C(38)-H(38C)	109.5
O(8)-C(30)-C(29)	105.7(9)	C(1)-N(1)-C(10)	110.7(8)
O(8)-C(30)-C(31)	107.8(10)	C(1)-N(1)-C(6)	110.4(9)
C(29)-C(30)-C(31)	113.3(11)	C(10)-N(1)-C(6)	114.6(8)
O(8)-C(30)-H(30)	110.0	C(1)-N(1)-Cu(01)	106.4(6)
C(29)-C(30)-H(30)	110.0	C(10)-N(1)-Cu(01)	105.1(6)
C(31)-C(30)-H(30)	110.0	C(6)-N(1)-Cu(01)	109.2(6)
C(30)-C(31)-H(31A)	109.5	C(2)-N(2)-C(7)	113.8(8)
C(30)-C(31)-H(31B)	109.5	C(2)-N(2)-C(3)	109.0(8)
H(31A)-C(31)-H(31B)	109.5	C(7)-N(2)-C(3)	110.1(7)
C(30)-C(31)-H(31C)	109.5	C(2)-N(2)-Cu(01)	108.2(6)
H(31A)-C(31)-H(31C)	109.5	C(7)-N(2)-Cu(01)	107.6(6)
H(31B)-C(31)-H(31C)	109.5	C(3)-N(2)-Cu(01)	108.1(7)
C(33)-C(32)-C(37)	120.0	C(4)-N(3)-C(5)	120.6(11)
C(33)-C(32)-S(2)	117.7(6)	C(4)-N(3)-S(1)	117.1(7)
C(37)-C(32)-S(2)	122.3(5)	C(5)-N(3)-S(1)	109.1(9)
C(34)-C(33)-C(32)	120.0	C(29)-N(4)-C(20)	110.3(8)
C(34)-C(33)-H(33)	120.0	C(29)-N(4)-C(25)	107.3(9)
C(32)-C(33)-H(33)	120.0	C(20)-N(4)-C(25)	113.4(10)
C(35)-C(34)-C(33)	120.0	C(29)-N(4)-Cu(02)	106.8(6)
C(35)-C(34)-H(34)	120.0	C(20)-N(4)-Cu(02)	107.0(7)
C(33)-C(34)-H(34)	120.0	C(25)-N(4)-Cu(02)	111.9(7)
C(34)-C(35)-C(36)	120.0	C(21)-N(5)-C(22)	108.5(8)
C(34)-C(35)-C(38)	114.6(12)	C(21)-N(5)-C(26)	111.6(7)
C(36)-C(35)-C(38)	125.0(12)	C(22)-N(5)-C(26)	106.7(7)
C(37)-C(36)-C(35)	120.0	C(21)-N(5)-Cu(02)	110.9(6)
C(37)-C(36)-H(36)	120.0	C(22)-N(5)-Cu(02)	110.0(6)
C(35)-C(36)-H(36)	120.0	C(26)-N(5)-Cu(02)	109.1(6)
C(36)-C(37)-C(32)	120.0	C(23)-N(6)-C(24)	117.9(11)

C(23)-N(6)-S(2)	117.1(7)	O(7)-S(2)-C(32)	108.8(6)
C(24)-N(6)-S(2)	113.4(9)	O(6)-S(2)-C(32)	108.3(5)
C(11)-O(3)-Cu(01)	117.3(7)	N(6)-S(2)-C(32)	107.8(5)
Cu(01)#1-O(4)-Cu(01)	129.9(5)	O(3)-Cu(01)-O(4)	90.8(3)
C(30)-O(8)-Cu(02)	116.1(7)	O(3)-Cu(01)-N(1)	83.2(4)
Cu(02)#2-O(9)-Cu(02)	131.0(5)	O(4)-Cu(01)-N(1)	172.0(3)
O(2)-S(1)-O(1)	115.8(7)	O(3)-Cu(01)-N(2)	167.5(3)
O(2)-S(1)-N(3)	113.0(7)	O(4)-Cu(01)-N(2)	101.2(3)
O(1)-S(1)-N(3)	103.6(6)	N(1)-Cu(01)-N(2)	85.2(4)
O(2)-S(1)-C(13)	106.5(6)	O(9)-Cu(02)-O(8)	89.3(3)
O(1)-S(1)-C(13)	111.0(5)	O(9)-Cu(02)-N(4)	170.2(3)
N(3)-S(1)-C(13)	106.6(5)	O(8)-Cu(02)-N(4)	83.3(4)
O(7)-S(2)-O(6)	118.3(9)	O(9)-Cu(02)-N(5)	101.4(3)
O(7)-S(2)-N(6)	107.6(8)	O(8)-Cu(02)-N(5)	166.4(3)
O(6)-S(2)-N(6)	105.7(6)	N(4)-Cu(02)-N(5)	86.9(4)

Symmetry transformations used to generate equivalent atoms:

#1 -x+1,y,-z+2 #2 -x+1,y,-z+3



Ortep plot of CuNPhTACNA₂ - Ellipsoids at 50% probability

Identification code	CuNPhTACNA2	
Empirical formula	C ₁₆ H ₂₀ CuN ₄ O ₆	
Formula weight	427.90	
Temperature	100(2) K	
Wavelength	0.71075 Å	
Crystal system	Monoclinic	
Space group	P21/c	
Unit cell dimensions	a = 16.054(4) Å	α = 90°.
	b = 13.373(3) Å	β = 99.402(3)°.
	c = 7.8011(17) Å	γ = 90°.
Volume	1652.3(7) Å ³	
Z	4	
Density (calculated)	1.720 Mg/m ³	
Absorption coefficient	1.368 mm ⁻¹	
F(000)	884	
Crystal size	0.18 x 0.03 x 0.01 mm ³	

Theta range for data collection	2.99 to 27.49°.
Index ranges	-20<=h<=20, -15<=k<=17, -10<=l<=10
Reflections collected	28242
Independent reflections	3784 [$R_{(int)} = 0.0401$]
Completeness to theta = 27.49°	99.9 %
Absorption correction	Semi-empirical from equivalents
Max. and min. transmission	0.9865 and 0.7909
Refinement method	Full-matrix least-squares on F^2
Data / restraints / parameters	3784 / 0 / 244
Goodness-of-fit on F^2	1.145
Final R indices [$I > 2\sigma(I)$]	R1 = 0.0350, wR2 = 0.0709
R indices (all data)	R1 = 0.0386, wR2 = 0.0721
Largest diff. peak and hole	0.414 and -0.452 e.Å ⁻³

Bond lengths [Å]

C(1)-N(1)	1.489(3)	C(8)-O(1)	1.289(3)
C(1)-C(2)	1.514(3)	C(9)-N(3)	1.485(2)
C(1)-H(1A)	0.9900	C(9)-C(10)	1.532(3)
C(1)-H(1B)	0.9900	C(9)-H(9A)	0.9900
C(2)-N(2)	1.498(2)	C(9)-H(9B)	0.9900
C(2)-H(2A)	0.9900	C(10)-O(4)	1.228(3)
C(2)-H(2B)	0.9900	C(10)-O(3)	1.291(3)
C(3)-N(2)	1.488(3)	C(11)-C(16)	1.407(3)
C(3)-C(4)	1.524(3)	C(11)-C(12)	1.408(3)
C(3)-H(3A)	0.9900	C(11)-N(1)	1.417(3)
C(3)-H(3B)	0.9900	C(12)-C(13)	1.387(3)
C(4)-N(3)	1.498(3)	C(12)-H(12)	0.9500
C(4)-H(4A)	0.9900	C(13)-C(14)	1.385(3)
C(4)-H(4B)	0.9900	C(13)-H(13)	0.9500
C(5)-N(3)	1.488(2)	C(14)-C(15)	1.388(3)
C(5)-C(6)	1.528(3)	C(14)-N(4)	1.460(3)
C(5)-H(5A)	0.9900	C(15)-C(16)	1.380(3)
C(5)-H(5B)	0.9900	C(15)-H(15)	0.9500
C(6)-N(1)	1.489(3)	C(16)-H(16)	0.9500
C(6)-H(6A)	0.9900	N(1)-Cu(1)	2.4464(17)
C(6)-H(6B)	0.9900	N(2)-Cu(1)	2.0195(17)
C(7)-N(2)	1.485(3)	N(3)-Cu(1)	1.9945(18)
C(7)-C(8)	1.525(3)	N(4)-O(6)	1.230(3)
C(7)-H(7A)	0.9900	N(4)-O(5)	1.232(3)
C(7)-H(7B)	0.9900	O(1)-Cu(1)	1.9245(15)
C(8)-O(2)	1.232(3)	O(3)-Cu(1)	1.9323(16)

Bond angles [°]

N(1)-C(1)-C(2)	113.51(17)	H(1A)-C(1)-H(1B)	107.7
N(1)-C(1)-H(1A)	108.9	N(2)-C(2)-C(1)	112.10(17)
C(2)-C(1)-H(1A)	108.9	N(2)-C(2)-H(2A)	109.2
N(1)-C(1)-H(1B)	108.9	C(1)-C(2)-H(2A)	109.2
C(2)-C(1)-H(1B)	108.9	N(2)-C(2)-H(2B)	109.2

C(1)-C(2)-H(2B)	109.2	N(3)-C(9)-H(9A)	109.3
H(2A)-C(2)-H(2B)	107.9	C(10)-C(9)-H(9A)	109.3
N(2)-C(3)-C(4)	109.97(16)	N(3)-C(9)-H(9B)	109.3
N(2)-C(3)-H(3A)	109.7	C(10)-C(9)-H(9B)	109.3
C(4)-C(3)-H(3A)	109.7	H(9A)-C(9)-H(9B)	107.9
N(2)-C(3)-H(3B)	109.7	O(4)-C(10)-O(3)	125.0(2)
C(4)-C(3)-H(3B)	109.7	O(4)-C(10)-C(9)	118.3(2)
H(3A)-C(3)-H(3B)	108.2	O(3)-C(10)-C(9)	116.50(18)
N(3)-C(4)-C(3)	110.25(16)	C(16)-C(11)-C(12)	118.2(2)
N(3)-C(4)-H(4A)	109.6	C(16)-C(11)-N(1)	119.50(19)
C(3)-C(4)-H(4A)	109.6	C(12)-C(11)-N(1)	122.28(19)
N(3)-C(4)-H(4B)	109.6	C(13)-C(12)-C(11)	120.8(2)
C(3)-C(4)-H(4B)	109.6	C(13)-C(12)-H(12)	119.6
H(4A)-C(4)-H(4B)	108.1	C(11)-C(12)-H(12)	119.6
N(3)-C(5)-C(6)	112.65(16)	C(14)-C(13)-C(12)	119.4(2)
N(3)-C(5)-H(5A)	109.1	C(14)-C(13)-H(13)	120.3
C(6)-C(5)-H(5A)	109.1	C(12)-C(13)-H(13)	120.3
N(3)-C(5)-H(5B)	109.1	C(13)-C(14)-C(15)	121.2(2)
C(6)-C(5)-H(5B)	109.1	C(13)-C(14)-N(4)	120.1(2)
H(5A)-C(5)-H(5B)	107.8	C(15)-C(14)-N(4)	118.6(2)
N(1)-C(6)-C(5)	113.22(16)	C(16)-C(15)-C(14)	119.4(2)
N(1)-C(6)-H(6A)	108.9	C(16)-C(15)-H(15)	120.3
C(5)-C(6)-H(6A)	108.9	C(14)-C(15)-H(15)	120.3
N(1)-C(6)-H(6B)	108.9	C(15)-C(16)-C(11)	121.0(2)
C(5)-C(6)-H(6B)	108.9	C(15)-C(16)-H(16)	119.5
H(6A)-C(6)-H(6B)	107.7	C(11)-C(16)-H(16)	119.5
N(2)-C(7)-C(8)	112.40(17)	C(11)-N(1)-C(6)	115.06(16)
N(2)-C(7)-H(7A)	109.1	C(11)-N(1)-C(1)	115.65(17)
C(8)-C(7)-H(7A)	109.1	C(6)-N(1)-C(1)	115.35(16)
N(2)-C(7)-H(7B)	109.1	C(11)-N(1)-Cu(1)	114.69(12)
C(8)-C(7)-H(7B)	109.1	C(6)-N(1)-Cu(1)	100.44(11)
H(7A)-C(7)-H(7B)	107.9	C(1)-N(1)-Cu(1)	92.36(11)
O(2)-C(8)-O(1)	125.0(2)	C(7)-N(2)-C(3)	113.42(16)
O(2)-C(8)-C(7)	117.54(19)	C(7)-N(2)-C(2)	112.43(16)
O(1)-C(8)-C(7)	117.43(18)	C(3)-N(2)-C(2)	111.81(16)
N(3)-C(9)-C(10)	111.71(17)	C(7)-N(2)-Cu(1)	105.66(12)

C(3)-N(2)-Cu(1)	102.12(12)	C(10)-O(3)-Cu(1)	111.56(13)
C(2)-N(2)-Cu(1)	110.72(12)	O(1)-Cu(1)-O(3)	97.69(6)
C(9)-N(3)-C(5)	110.56(16)	O(1)-Cu(1)-N(3)	168.46(7)
C(9)-N(3)-C(4)	112.91(16)	O(3)-Cu(1)-N(3)	86.19(7)
C(5)-N(3)-C(4)	112.23(15)	O(1)-Cu(1)-N(2)	86.37(7)
C(9)-N(3)-Cu(1)	102.87(12)	O(3)-Cu(1)-N(2)	160.42(7)
C(5)-N(3)-Cu(1)	108.44(13)	N(3)-Cu(1)-N(2)	86.46(7)
C(4)-N(3)-Cu(1)	109.33(12)	O(1)-Cu(1)-N(1)	105.66(6)
O(6)-N(4)-O(5)	123.5(2)	O(3)-Cu(1)-N(1)	113.08(6)
O(6)-N(4)-C(14)	117.8(2)	N(3)-Cu(1)-N(1)	82.53(6)
O(5)-N(4)-C(14)	118.7(2)	N(2)-Cu(1)-N(1)	83.88(6)
C(8)-O(1)-Cu(1)	113.93(13)		